USER'S GUIDE

CAMx
COMPREHENSIVE AIR QUALITY MODEL WITH EXTENSIONS

VERSION 4.20

ENVIRON International Corporation
101 Rowland Way, Suite 220
Novato, California 94945-5010
415-899-0700

www.environcorp.com
www.camx.com

June 2005

ACKNOWLEDGMENTS

ENVIRON would like to acknowledge the following groups for their contributions to the development of CAMx:

- The Carnegie-Mellon University, Department of Chemical Engineering, for providing full-science PM algorithms, assistance in incorporating them into CAMx, and testing the implementation;

- The Coordinating Research Council (CRC), for sponsorship of the development, testing, and review of numerous components of the model;

- The Lake Michigan Air Directors Consortium, for sponsorship of the development, testing and review of numerous components of the model, and for providing the new CAMx distribution test case.

- The University of Texas, Center for Energy and Environmental Resources, for assistance in developing and testing the Open-MP multi-processor capability.

- Atmospheric and Environmental Research (AER), for developing the mercury chemistry algorithm.

TABLE OF CONTENTS

TABLES

FIGURES

1. OVERVIEW

The **C**omprehensive **A**ir quality **M**odel with e**x**tensions (CAMx) is an Eulerian photochemical dispersion model that allows for an integrated "one-atmosphere" assessment of gaseous and particulate air pollution (ozone, PM2.5, PM10, air toxics, mercury) over many scales ranging from sub-urban to continental. It is designed to unify all of the technical features required of "state-of-the-science" air quality models into a single system that is computationally efficient, easy to use, and publicly available. The model code has a highly modular and well-documented structure which eases the insertion of new or alternate algorithms and features. The input/output file formats are based on the Urban Airshed Model and are compatible with many existing pre- and post-processing tools.

CAMx simulates the emission, dispersion, chemical reaction, and removal of pollutants in the troposphere by solving the pollutant continuity equation for each chemical species (l) on a system of nested three-dimensional grids. The Eulerian continuity equation describes the time dependency of the average species concentration (c_l) within each grid cell volume as a sum of all of the physical and chemical processes operating on that volume. This equation is expressed mathematically in terrain-following height (z) coordinates:

$$\frac{\partial c_l}{\partial t} = -\nabla_H \cdot V_H c_l + \left[\frac{\partial (c_l \eta)}{\partial z} - c_l \frac{\partial}{\partial z}\left(\frac{\partial h}{\partial t}\right)\right] + \nabla \cdot \rho K \nabla (c_l / \rho)$$

$$+ \left.\frac{\partial c_l}{\partial t}\right|_{Chemistry} + \left.\frac{\partial c_l}{\partial t}\right|_{Emission} + \left.\frac{\partial c_l}{\partial t}\right|_{Removal}$$

where V_H is the horizontal wind vector, η is the net vertical "entrainment rate", h is the layer interface height, ρ is atmospheric density, and K is the turbulent exchange (or diffusion) coefficient. The first term on the right-hand side represents horizontal advection, the second term represents net resolved vertical transport across an arbitrary space- and time-varying height grid, and the third term represents sub-grid scale turbulent diffusion. Chemistry is treated by simultaneously solving a set of reaction equations defined from specific chemical mechanisms. Pollutant removal includes both dry surface uptake (deposition) and wet scavenging by liquid precipitation.

CAMx can perform simulations on three types of cartesian map projections: Universal Transverse Mercator, Rotated Polar Stereographic, and Lambert Conic Conformal. CAMx also offers the option of operating on a curvi-linear geodetic latitude/longitude grid system as well. Furthermore, the vertical grid structure is defined externally, so layer interface heights may be specified as any arbitrary function of space and/or time. This flexibility in defining the horizontal and vertical grid structures allows CAMx to be configured to match the grid of any meteorological model that is used to provide environmental input fields.

In addition to the features it shares with most photochemical grid models, some of the most notable features of CAMx are:

Two-Way Nested Grid Structure: This feature allows CAMx to be run with coarse grid spacing over a wide regional domain in which high spatial resolution is not particularly needed, while within the same run, applying fine grid nests in areas where high resolution is needed.

Flexi-Nesting: CAMx offers the ability for users to arbitrarily introduce and/or remove various nested grids at any point during the course of a simulation. Upon model restart, CAMx automatically diagnoses any changes to the grid system. User's can supply complete information for new grids (emissions, landuse, meteorology) or allow CAMx to interpolate any or all of these inputs from parent grids. Example applications of flexi-nesting include running spin-up days with a single coarse master grid and introducing nests just for episode days, or evaluating sensitivity to grid configuration when designing a model application.

Photochemical and Gas Phase Chemistry Mechanism Options: Users can select among four versions of the Carbon Bond IV (CB-IV) chemical mechanism, or the 1999 version of the SAPRC mechanism. The SAPRC99 mechanism was added as an alternate mechanism because it is chemically up-to-date, has been tested extensively against environmental chamber data, and uses a different approach for VOC lumping than the CB-IV mechanism.

Chemical Kinetics Solver Options: ENVIRON has developed a fast and highly efficient chemistry solver (referred to as the CMC solver) that is based on an "adaptive-hybrid" approach; relative to the standard chemistry solvers for the CB-IV mechanism, this approach results in about a ten-fold speedup in the chemistry solution and an overall model speedup by a factor of 3 to 4. Alternatively, users may select the Implicit-Explicit Hybrid (IEH) chemical solver of Sun, Chock and Winkler (1994). The IEH solver accuracy is comparable to reference methods such as LSODE. The accuracies of the IEH and CMC solvers are very similar during the day with the IEH solver being more accurate than the CMC solver at night. However, the IEH solver is several times slower than the CMC solver. Both solvers may be used to integrate the CB-IV and SAPRC99 mechanisms.

Treatment of Particulate Matter: CAMx features a "one-atmosphere" treatment for ozone and particulate matter (PM) with detailed algorithms for the relevant science processes, including aqueous chemistry (RADM-AQ), inorganic aerosol thermodynamics/partitioning (ISORROPIA), and secondary organic aerosol formation/partitioning (SOAP). The particulate chemistry mechanism utilizes products from the gas-phase photochemistry for production of sulfate, nitrate, condensible organic gases, and chloride. CAMx provides two options for the representation of the particle size distribution: a static two-mode coarse/fine (CF) scheme, and the multi-sectional CMU scheme, which models the size evolution of each aerosol constituent among a number of fixed size sections.

Wet Deposition of Gases and Particles: With the introduction of v4.00, the wet deposition/ scavenging module was dramatically improved to include removal of gases and particles dissolved in cloud water plus scavenging by falling precipitation. Wet deposition is modeled for entire columns of grid cells to account for saturation of sparingly soluble gases. The improved wet deposition requires a new combined cloud/rain file format that must be used when the wet deposition is invoked.

Plume-in-Grid (PiG) Module: CAMx incorporates a PiG feature to model the chemistry and dispersion of large point source NOx plumes; individual sub-grid plume segments are tracked by the Lagrangian module while undergoing dispersion and chemical evolution, until such time as the spatial distribution of their pollutant mass can be adequately represented within the grid model framework.

Ozone Source Apportionment Technology (OSAT): The OSAT and its derivatives (e.g., APCA) allow CAMx to track source region and/or source category contributions to predicted grid cell ozone concentration; thus, for any selected receptor point and time, the model gives a clear picture of the likely distribution of ozone and ozone precursors by source category and/or source region, as well as an indication as to whether the ozone at the selected time and location would more likely respond to upwind NO_x or VOC controls.

Decoupled Direct Method (DDM) for Source Sensitivity of Ozone and Other Species: The DDM calculates sensitivities of all pollutant concentrations to model input parameters. The CAMx implementation tracks first-order sensitivities to emissions, initial conditions and boundary conditions. The primary applications are estimating the impact of changes in input parameters on pollutant concentrations and ranking source regions/source categories as to their importance toward ozone formation. The latter application is similar to the use of OSAT, and results from the DDM and OSAT for source importance are expected to be similar in general, but there are some notable differences. While the DDM requires more resources (memory and CPU time) than OSAT for the same number of source regions/source categories, the DDM can produce information for all chemical species (not just ozone) and is more flexible than OSAT in selecting which parameters to track. Furthermore, sensitivities can be calculated for a wide variety of perturbations, not just the type of perturbations that correspond to OSAT results.

Process Analysis (PA): The PA tool is designed to provide in-depth analyses of the physical and chemical processes in an air quality model. Through PA, one can more fully understand the complex interactions of the different processes, explain simulation results within the context of model formulation, and improve the design of control strategies. Three components of PA are implemented in CAMx: (1) Integrated Processes Rate (IPR) analysis, which provides detailed process rate information for each physical process in CAMx (i.e., advection, diffusion, deposition, emissions, chemistry, etc.) for selected grid cells and selected species; (2) Integrated Reaction Rate (IRR) analysis, which provides detailed reaction rate information for all reactions in the chemical mechanism for selected grid cells; and (3) Chemical Process Analysis (CPA), which is closely related to the IRR method but is designed to be more user friendly and accessible.

Reactive Tracer (RTRAC) Source Apportionment: The RTRAC method provides a flexible approach for tracking the emission, dispersion, deposition, and chemical reaction of multiple gas and particle tracers. The tracers operate in parallel to the CAMx host model. RTRAC can also output locally specific tracer decay rates for input to a separate Gaussian or puff dispersion model for sub-grid scale or "fenceline" dispersion calculations. Potential RTRAC applications include: simulating gaseous and particle air toxic compounds; simulating individual VOC compounds, including reactive decay; simulating source-specific primary emitted inert and reactive compounds.

Horizontal Advection Solver Options: The Area Preserving Flux-Form advection solver of Bott (1989) and the Piecewise Parabolic Method (PPM) of Colella and Woodward (1984) area available in CAMx. These schemes possess high-order accuracy, little numerical diffusion, and are sufficiently quick for applications on very large grids. Either of these solvers may be selected via the CAMx run control file.

Advanced Photolysis Model: The TUV radiative transfer and photolysis model, developed at the National Center of Atmospheric Research (NCAR), is used as a CAMx preprocessor to provide the air quality model with a multi-dimensional lookup table of photolytic rates by surface albedo, total ozone column, haze turbidity, altitude, and zenith angle.

Detailed Cloud Impacts on Photolysis Rates: The model provides an option to adjust photolysis rates for the presence of clouds using the approach developed for the Regional Acid Deposition Model (RADM; Chang et al., 1987). Based upon theoretical calculations from the TUV radiative transfer model, the RADM approach provides a more realistic impact on photolysis rates by accounting for cloud optical depth, rather than just total opaque cloud cover fraction. Besides reducing photolysis below clouds, this option enhances photolytic rates above clouds due to reflection.

Parallel Processing: Multi-processor workstations are widely available and increasingly affordable (e.g., Linux PCs) and multi-processor support is included in CAMx. The approach is to use OpenMP (OMP) compiler directives within the CAMx code since they are widely supported and have no adverse impact on performance for single processor workstations. The chemistry and transport algorithms have been "parallelized" because they are the largest contributors to the CPU time.

1.1 UPDATES IN CAMx VERSION 4.20

CAMx version 4.20 includes the following major updates and additional capabilities over version 4.10s:

Particulate Source Apportionment Technology (PSAT): PSAT provides source-category and geographic source apportionment of modeled PM by individual species or by several species aggregation methods. This new Probing Tool works similarly to OSAT methods for ozone. It works in conjunction with the CF option of Mechanism 4 only.

Restructured PiG Module: The CAMx Plume-in-Grid submodel has been revised to include:

- New puff structure, dynamics, and time-stepping;
- Second-order closure puff spread calculation following SCIPUFF equations;
- A new full photochemical chemistry option called Incremental Reactions for Organics and NOx (IRON) PiG; either CB-IV or SAPRC99 mechanisms.

IRON PiG may be applied to point sources of any kind to simulate full CB-IV or SAPRC99 gas-phase photochemistry. IRON PiG cannot be used in conjunction with OSAT, PSAT, DDM, or PA; it can be used with RTRAC (see below). IRON PiG provides much more interaction with grid chemistry. The GREASD PiG option is retained for use on large NOx point sources and with OSAT.

Expanded RTRAC/PiG Capabilities: RTRAC species can now be carried within IRON PIG puffs. An RTRAC/IRON PiG "sampling grid" capability was added to passively sample surface concentrations of RTRAC species within reactive plume puffs. The sampling grid provides the ability to visualize plume concentrations at any sampling resolution. This is particularly useful at near-source sub-grid scale distances. Sampling grid output is provided at the same output frequency as the computational grid average output files.

Mercury Chemistry: CAMx may now be used to model the chemistry of three mercury species, two gaseous (HG0 and HG2) and one particulate (HGP), via gas and aqueous pathways. The mercury chemistry module requires total PM concentrations, so mercury can only be modeled with Mechanism 4 (CF) by including mercury species among the list of modeled species. All of the rate and equilibrium constants for the mercury mechanism are hard-coded within chemistry module.

Additional Surface/Vegetative Inputs: Optional snow cover, land-ocean, drought stress, and surface roughness maps may now be included within the Albedo/Haze/Ozone (AHO) input file. The AHO file must now be read for inert runs if dry deposition is invoked because several optional parameter fields affect dry deposition rates. Now default drought stress is "0" (unstressed) unless overridden by the input drought stress code. Snow cover impacts dry deposition by forcing season to be "winter with snow", and impacts chemistry by forcing UV albedo to the highest value in the AHO definition. Surface roughness impacts dry deposition and PiG growth rates. Land-ocean map defines chloride concentrations for mercury chemistry.

Mechanism 10: The model now recognizes "Mechanism 10" as a simple way to define your own chemistry mechanism. This option is intended for users to define simple chemical transformations between gas and/or aerosol species. You must develop your own Mechanism 10 subroutine and chemistry parameters file. An example might be a case where the user has only SO_2 emissions from a few sources and wishes to estimate first-order decay to sulfate without the need to employ CB-IV oxidant chemistry.

LSODE: The model now includes LSODE as a chemistry solver option for gas-phase chemistry, in addition to CMC and IEH. It can be used to "benchmark" a simulation to evaluate the performance of CMC or IEH. We do not recommend use of LSODE for typical applications as the model will run MUCH more slowly.

Revised CAMx Control File Format: The CAMx control file has been changed to a Fortran Namelist format. This approach streamlines and improves flexibility in configuring CAMx options, parameters, and I/O filenames. Different namelist "modules" are used to configure the core model and each of the five Probing Tools. A Perl script is available that can translate the old format to the namelist format.

Revised Season Specification: A new latitude- and month-dependent season specification has been incorporated for the dry deposition algorithm. Also, the southern hemisphere is now automatically considered in the season determination. Season was originally set based on date only with no regard to global location. This change should lead to an improved selection of Wesely season-specific surface resistances by location and date.

Revised Internal Surface Roughness Defaults: Surface roughness is now season-dependent for several landuse categories, based on the approach used in EPA's AERMOD plume model. The seasonal change of surface roughness is largest for deciduous forests and agricultural land cover, with minima in the winter and maxima in the summer. This change affects dry deposition and PiG growth rates.

Additional Reactions in Mechanism 4: Seventeen extra inorganic reactions were added to Mechanism 4. These are appropriate for inclusion in any condensed chemical mechanism being used for regional ozone and regional/annual PM, visibility, mercury, and toxics modeling. Tests indicate a general trend for increased regional levels of ozone, but no consistent or significant impacts on PM.

OSAT Updates: The OSAT probing tool has been updated to account for both ozone production and destruction rates in each cell per time step as it apportions ozone change among tracers. Previously, OSAT only considered the net change in ozone in the apportionment algorithm. OSAT results will differ slightly from the original approach.

2. CORE MODEL FORMULATION

This section introduces the basic numerical approach employed in CAMx, and describes the technical formulation of the transport and removal processes. The specific chemical mechanisms and their numerical solvers are discussed in detail in Section 3.

2.1 NUMERICAL APPROACH

The physical representations and the numerical methods used in CAMx for each term of the pollutant continuity equation (described in Section 1) are summarized in Table 2-1. CAMx includes peer-accepted algorithms and component formulations, and its modular framework permits easy substitution of additional and/or updated algorithms in the future.

Table 2-1. Summary of the CAMx modules for key physical processes.

Module	Physical Model	Numerical Method
Horizontal advection/diffusion	Eulerian continuity equation closed by K-theory	Bott or PPM for advection, explicit diffusion
Vertical transport/diffusion	Eulerian continuity equation closed by K-theory	Implicit advection and diffusion
Gas-Phase Chemistry	Carbon Bond IV or SAPRC99 mechanisms	ENVIRON CMC solver, IEH solver, or LSODE
Aerosol Chemistry	Dry and aqueous inorganic and organic chemistry/thermo-dynamics; static 2-mode or evolving multi-section size models	RADM-AQ, ISORROPIA, SOAP
Dry deposition	Separate resistance models for gases and aerosols	Deposition velocity as surface boundary condition for vertical diffusion
Wet deposition	Separate scavenging models for gases and aerosols	Uptake as a function of rainfall rate, cloud water content, gas solubility and diffusivity, PM size

The continuity equation is numerically marched forward in time over a series of time steps. At each step, the continuity equation is replaced by an operator-splitting approach that calculates the separate contribution of each major process (advection, diffusion, chemistry, etc.) to concentration change within each grid cell. The specific equations that are solved individually in the operator-splitting process are shown in order below:

$$\left.\frac{\partial c_l}{\partial t}\right|_{Emission} = m^2 \frac{E_l \Delta t}{\partial x\, \partial y\, \partial z}$$

$$\left.\frac{\partial c_l}{\partial t}\right|_{X\ advection} = -\frac{m^2}{A_{yz}} \frac{\partial}{\partial x}\left(\frac{u A_{yz} c_l}{m}\right)$$

$$\left.\frac{\partial c_l}{\partial t}\right|_{Y\ advection} = -\frac{m^2}{A_{xz}} \frac{\partial}{\partial y}\left(\frac{v A_{xz} c_l}{m}\right)$$

$$\left.\frac{\partial c_l}{\partial t}\right|_{Z\ transport} = \frac{\partial (c_l \eta)}{\partial z} - c_l \frac{\partial}{\partial z}\left(\frac{\partial h}{\partial t}\right)$$

$$\left.\frac{\partial c_l}{\partial t}\right|_{Z\ diffusion} = \frac{\partial}{\partial z}\left[\rho K_v \frac{\partial (c_l/\rho)}{\partial z}\right]$$

$$\left.\frac{\partial c_l}{\partial t}\right|_{XY\ diffusion} = m\left\{\frac{\partial}{\partial x}\left[m\rho K_X \frac{\partial (c_l/\rho)}{\partial x}\right] + \frac{\partial}{\partial y}\left[m\rho K_Y \frac{\partial (c_l/\rho)}{\partial y}\right]\right\}$$

$$\left.\frac{\partial c_l}{\partial t}\right|_{Wet\ Scavenging} = -\Lambda_l c_l$$

$$\left.\frac{\partial c_l}{\partial t}\right|_{Chemistry} = Mechanism - specific\ Reaction\ Equations$$

where c_l is species concentration (μmol/m^3 for gasses, μg/m^3 for aerosols), E_l is the local species emission rate (μmol/s for gasses, μg/s for aerosols), Δt is timestep length (s), u and v are the respective east-west (x) and north-south (y) horizontal wind components (m/s), A_{yz} and A_{xz} are cell cross-sectional areas (m^2) in the y-z and x-z planes, respectively, m is the ratio of the transformed distance on the various map projections to true distance (m=1 for curvi-linear latitude/longitude coordinates), and Λ_l is the wet scavenging rate (s^{-1}). Dry deposition is an important removal mechanism, but it is not explicitly treated as a separate process in the time-splitting approach. Instead, deposition velocities for each species are calculated based on species chemical properties and local meteorological/surface conditions, and used as the lower boundary condition for vertical diffusion. This appropriately couples the surface removal of pollutants through each column of cells via the vertical mixing process.

A master time step for the model is internally determined during the simulation to ensure numerical stability for horizontal advection in the largest and coarsest (master) grid. Time steps typically range from 5-30 minutes for grid cell sizes of 10-50 km, to a minute or less for

small cell sizes of 1-2 km. As a result, transport calculations on nested grids require multiple time steps per master step depending on their grid sizes relative to the master grid spacing. Furthermore, multiple chemistry time steps per transport step are used as necessary to ensure accurate solution of the very numerically stiff chemical reaction equations.

The first process in each time step for a given grid is the injection of emissions from all sources. CAMx then performs horizontal advection, but alternates the order of advection in the *x* and *y* directions each master timestep. This alleviates any potential numerical biases that can develop when the *x/y* advection order is constant. Vertical advection is performed after horizontal advection, followed by vertical diffusion, horizontal diffusion, wet scavenging, and finally chemistry.

Although advection is performed separately in the *x* (east-west), *y* (north-south), and *z* (vertical) directions, the numerical linkage between these components has been developed in a mass consistent fashion to preserve the density field at each time step. This maintains the flexibility to allow many types of meteorological models, and modeling grid resolutions, projections, and layer structures, to characterize transport in CAMx.

2.2 CAMx GRID CONFIGURATION

Grid Cell Arrangement

CAMx carries pollutant concentrations at the center of each grid cell volume, representing the average concentration over the entire cell. Meteorological fields are supplied to the model to quantify the state of the atmosphere in each grid cell for the purposes of calculating transport and chemistry. CAMx internally carries these variables in an arrangement known as an "Arakawa C" grid configuration (Figure 2-1). State variables such as temperature, pressure, water vapor, and cloud water are located at cell center along with pollutant concentration, and represent grid cell average conditions. Wind components and diffusion coefficients are carried at cell interfaces to describe the transfer of mass in and out of each cell face. Note in Figure 2-1, for example, that horizontal wind components *u* and *v* are staggered from each other. This facilitates the solving of the transport equations in "flux form".

Depending upon the source of meteorological data, it is recommended that the user directly provide the gridded horizontal wind fields in the staggered Arakawa C configuration. However, this is not always feasible, and so CAMx offers the option for the user to supply all meteorological variables, including horizontal wind components, at cell center; in this case CAMx internally interpolates the winds to cell interfaces. Note that this leads to a slight smoothing effect on the horizontal wind fields.

Figure 2-1 also describes the horizontal cell indexing convention used in CAMx. Each cell is defined by the index pair (*i,j*), where *i* ranges from 1 to *nx* (the number of cells in the east-west direction), and *j* ranges from 1 to *ny* (the number of cells in the north-south direction). The eastern and northern faces of the cell are indexed (*i,j*), while the western and southern faces are indexed (*i*-1,*j*) and (*i,j*-1), respectively.

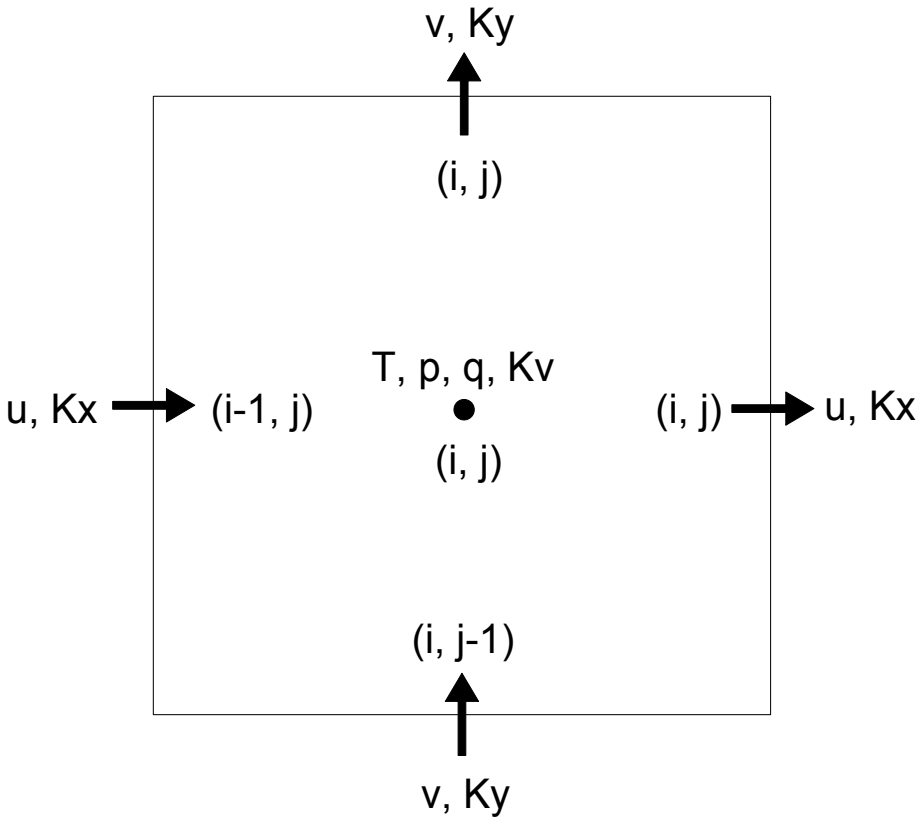

Figure 2-1. A horizontal representation of the Arakawa C variable configuration used in CAMx.

In the vertical, most variables are carried at each layer midpoint (defined as exactly half way between layer interfaces). Again the exceptions are those variables that describe the rate of mass transport across the layer interfaces, which include the vertical diffusion coefficient K_V and the vertical entrainment rate η. These variables are carried in the center of each cell horizontally, but are located at the top of the layer (i.e., the interface) vertically. The indexing convention in the vertical is shown in Figure 2-2, where the top of layer k is referenced as interface k. Index $k=0$ is at the ground.

Grid Nesting

CAMx incorporates two-way grid nesting, which means that pollutant concentration information propagates into and out of all grid nests during model integration. Any number of grid nests can be specified in a single run, while grid spacings and vertical layer structures can vary from one grid nest to another. The nested grid capability of CAMx allows cost-effective application to large regions in which regional transport occurs, yet at the same time providing fine resolution to address small-scale impacts in selected areas.

Each grid nest is defined over a subset of master (coarsest) grid cells. The range of master grid row and column indices that define the coverage of each nested grid must be specified in the run control file. An integer number of nested grid cells must span one master grid cell;

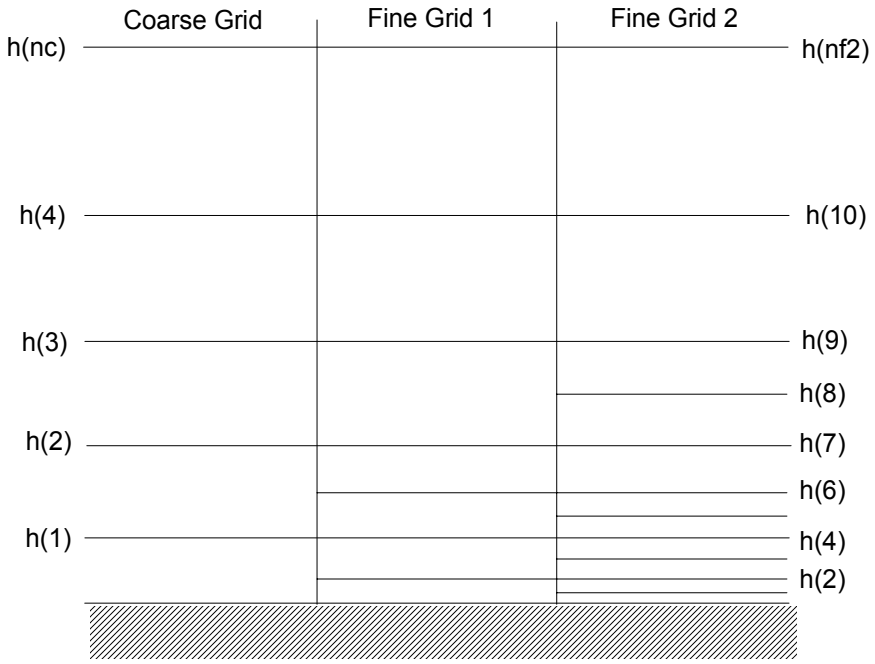

Figure 2-2. A schematic illustration of the CAMx vertical grid indexing convention and vertical nesting. The lowest 2 master (coarse) grid layers are split into 4 layers in nested Fine Grid 1, and the lowest 5 layers of Fine Grid 1 are split into 9 layers in nested Fine Grid 2. Note that the nested grids possess a matching layer interface for every parent grid layer interface.

this number is referred to as a "meshing factor". "Buffer" cells are added around the perimeter of each nested grid to hold boundary conditions. Buffer cells are added automatically within CAMx and should not be specified by the user in the run control file. Allnested grid output files contain data for the entire array of computational and buffer cells; however, buffer cell concentrations are considered invalid and should be ignored. Additionally, all nested grid input files must contain data for the entire array of computational and buffer cells. An example of a horizontal nesting arrangement is shown in Figure 2-3. Here, two telescoping fine grid nests are defined: one with a meshing factor of 2 spanning master grid cells (5,4) to (8,8), and one with a meshing factor of 4 spanning master grid cells (6,6) to (6,7).

Nesting in the vertical is allowed, but only by sub-dividing parent grid layers into a series of finer layers. To maximize flexibility in the vertical grid structure, each parent grid layer may be individually split into a unique set of fine layers, or not split at all. The vertical layer division is defined by the input height/pressure file for each grid. Figure 2-2 displays an example of how layers may be defined for a master grid and two fine grid nests. Vertical nesting is not recommended because it can lead to mass consistency errors (discussed shortly).

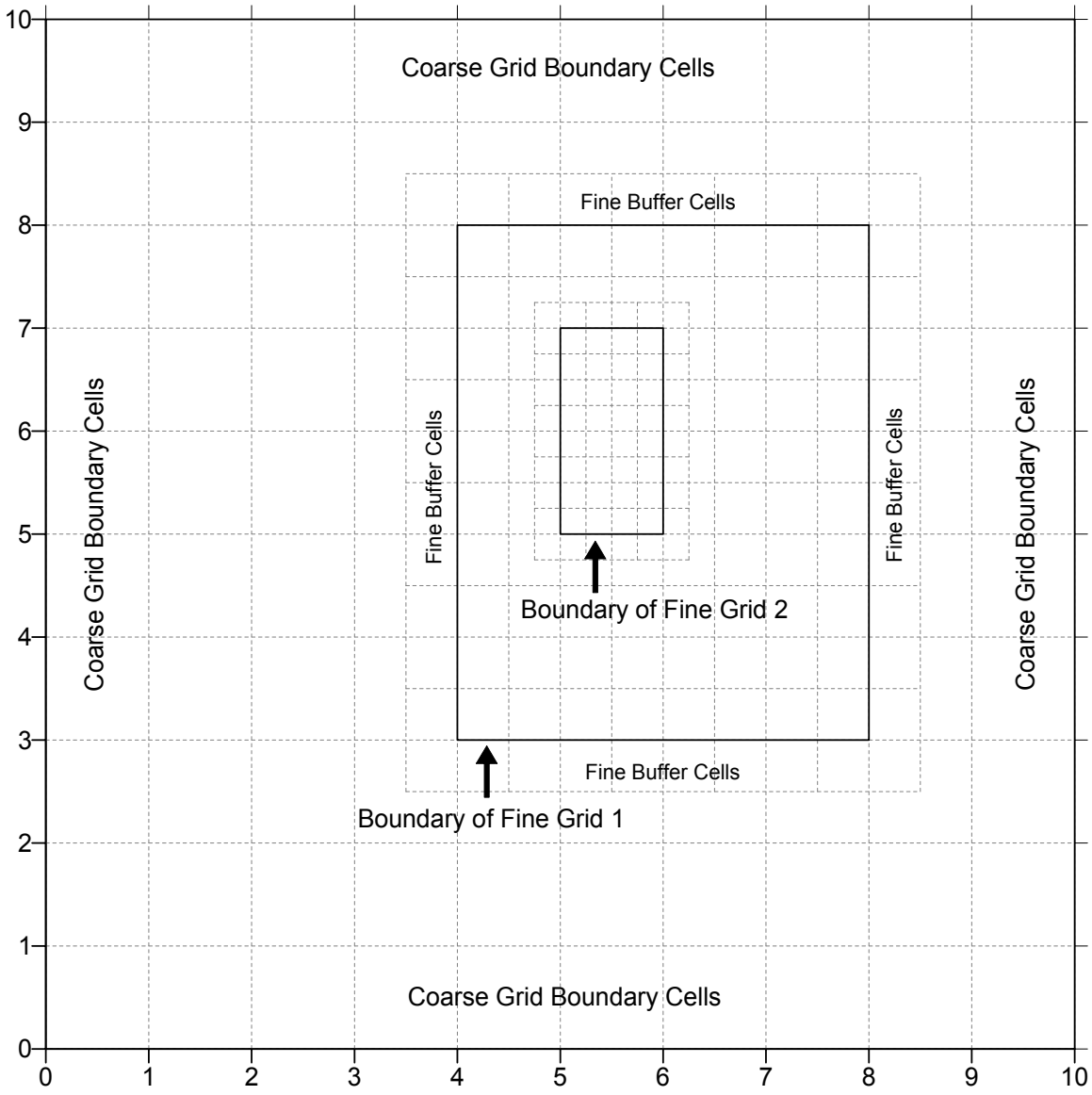

Figure 2-3. An example of horizontal grid nesting, showing two telescoping nested grids within a 10×10 cell master grid. The outer nest contains 10×12 cells, and the inner nest contains 6×10 cells.

Restrictions on specifying the size and resolution of all grid nests include the following:

1) The ratio of master grid cell size to nested grid cell size must be an integer (e.g., a "meshing factor" of 3 means that 3 nested cells span the distance of 1 master cell, resulting in an area of 9 nested cells per master cell);
2) For telescoping grids (a nested grid containing an even finer grid), the cell size of the finest grid must be a common denominator for all parent grids above it (e.g., a 36-12-4 km or 36-12-2 km arrangement is allowed, but a 36-12-9 km is not);
3) The restriction in (2) above does not apply to parallel nested grids of the same generation (e.g., 4 km and 5 km grids can be located in different areas of a master grid provided that the master cell size is some multiple of 20 km);
4) Nested grids cannot overlap, although they may share a common boundary or edge;
5) Nested grids cannot extend into a boundary, or non-modeled, area of the master grid;
6) CAMx is currently configured to allow four "generations" of nests (e.g., four levels of telescoping grids); this can be extended in the code easily if more than four levels of nests are required;
7) The total vertical depth of each nested grid must exactly match the depth of the master grid;
8) Nested grid vertical layers may exactly match the parent grid vertical structure, or the parent grid layers may be individually split into several finer grid layers (defined via the nested grid height/pressure files);
9) A parent grid layer may be unevenly split into any number of finer layers, as long as there is a matching nested grid layer interface at each parent grid layer interface;
10) Nested grids that share a common horizontal boundary must possess equivalent layer structures.

The following Fortran binary I/O files must be provided for the master grid, and optionally provided for each nested grid:

- area emissions;
- fractional landuse distribution;
- height/pressure (defines the layer interface structure);
- horizontal wind components;
- temperatures;
- vertical diffusivities;
- water vapor;
- clouds and rain

Any of these input files may be supplied for each nested grid, or none at all. If any of these files are not supplied for a particular nested grid, CAMx interpolates the missing fields from the parent grid.

The Flexi-Nest option in CAMx allows users to redefine the nested grid configuration at any point in a simulation. Nested grids can be introduced or removed only at the time of a model restart since a new CAMx user control file must be used to redefine the grid configuration. For example, the user may wish to "spin-up" the model using a regional-scale master grid and a single nest over an area of interest for two days. Starting at 6 AM on the third day, the user

might introduce one or more nests within the original nested grid for more detailed analysis. This would require that the model be restarted at 6 AM of the third day with a new control file that defines the position of the two new nests and (optionally) provides any additional input fields for these grids. CAMx will internally reconcile the differences in grid structure between the nested grid restart files and the new user control file, and then interpolate any data fields not supplied to CAMx for the new nests from the parent grid(s).

As just described, flexi-nesting provides flexibility to either provide meteorological and emissions input files for a nested grid or allow CAMx to interpolate data that are not provided from a parent grid. Clearly it is desirable to provide nested grid data whenever possible. However, the ability to interpolate data is useful for testing sensitivity to grid configurations or if it is not possible to run the meteorological model for a grid nest.

2.3 TRANSPORT FUNDAMENTALS

The approach to solving pollutant transport in CAMx provides both mass conservation and mass consistency. Mass conservation refers to the ability to accurately account for all sources and sinks of mass in the model, with no spurious loss or gain of mass during model integration. To be mass conservative, CAMx internally carries concentrations of each species as a density (μmol/m^3 for gases, μg/m^3 for aerosols), and solves the advection equations in flux form. This also serves to simplify mass budget accounting, which is used by the various source apportionment and process analysis options. Gas concentrations are internally converted to volumetric mixing ratio (parts per million, or ppm) for the chemistry and diffusion steps, and when they are written to the average output files.

Mass consistency refers to the model's ability to transport pollutant mass exactly equivalent to the input atmospheric momentum field. For example, a model that is perfectly mass consistent will preserve a unity pollutant mixing ratio field given constant unity boundary and initial conditions and zero sources and sinks. Sources of poor mass consistency in air quality models are typically related to the following (in order of importance):

1) supplying meteorology that is inherently inconsistent, e.g., from an interpolative objective analysis or diagnostic wind model in which wind, temperature, moisture, and pressure fields are all independently developed;
2) spatially interpolating or averaging meteorological model fields, especially *three-dimensional* wind vector fields, to an air quality model grid of different resolution and/or different mapping projection;
3) relying on a nested grid model to internally interpolate coarse grid meteorological parameters to finer grids, especially in cases of varying vertical resolution among the grids;
4) employing numerical techniques within the air quality model that are mass inconsistent, e.g., holding input wind and density fields constant between meteorological update times, assuming non-divergent three-dimensional winds, etc.; and
5) employing different numerical and/or physical methods in the air quality and meteorological models;

It is expected that CAMx users will prepare high quality, mass consistent meteorological fields using advanced prognostic models so as to minimize inconsistencies in the inputs themselves. CAMx operates on the map projections and grid systems employed in several widely used meteorological models (e.g., MM5 and RAMS) so that translation of meteorological data to CAMx requires as little manipulation as possible. The practice of developing meteorological input fields using objective analysis or "diagnostic" approaches is highly discouraged.

However, CAMx provides a very important flexibility that allows the air quality grid to differ from the meteorological grid in terms of projection and/or resolution. This, of course, leads to a potentially large source of mass consistency error as noted in point (2) above, and if nested grids are specified where higher resolution meteorological fields are unavailable, additional error may occur as in point (3). Therefore, adjustments must be made to correct for the external inconsistencies coming into the model. Such adjustments could be applied to the meteorological fields during the interpolation/averaging procedure. However, this approach would not account for internal sources of inconsistency within the air quality model itself (points 3-5 above). Therefore, to account for all sources of error while maintaining flexibility on input requirements and grid configuration, CAMx internally minimizes the sources of mass inconsistency as the model integrates forward in time. As discussed below, the model does this in several ways.

First, the transport equations are written and solved in "flux" form. Gridded meteorological inputs are carried in an "Arakawa C" arrangement (Figure 2-1), which optimizes the calculation of mass flux divergences while ensuring mass conservation. These points are important for the calculations described further below. Solutions based on the alternative "advective" form cannot guarantee mass conservation nor consistency.

Second, CAMx can accept input meteorological fields (horizontal wind components, pressure, temperature, moisture, vertical diffusion coefficients, cloud parameters) for each individual nested grid, if available from a meteorological model. This reduces errors stemming from internal interpolations from parent to nested grids. Input gridded fields of layer heights, temperature, pressure, horizontal winds, water vapor, and vertical diffusivity are then interpolated in time to the unique time steps for each modeling grid.

Third, and most importantly, the grid- and timestep-specific horizontal momentum fields are used to determine a vertical velocity field that balances the local atmospheric continuity equation for the specific grid configuration employed. Since the vertical grid structure is defined via external inputs, layer interface heights may be specified as any arbitrary function of space and/or time. This allows the CAMx vertical grid system to exactly match all or a subset of any meteorological model layer structures, whether they are defined in terms of physical height above ground, normalized height coordinates (i.e., "sigma-z"), or normalized pressure coordinates (i.e., "sigma-p"). Therefore, total vertical transport is the combination of resolved vertical advection and mass exchange across undulating layer interfaces.

The total vertical transport rate is referred to as the local "entrainment rate" η, which is defined as the combination of net vertical velocity w and the local time-rate of change in layer interface heights:

$$\eta = \frac{\partial h}{\partial t} - w$$

To calculate a vertical velocity profile for a given grid column, the atmospheric continuity equation is locally integrated through the depth of the column. Most air quality models perform this integration by assuming an incompressible atmosphere and either a non-divergent wind field ($\nabla\cdot V=0$), or a non-divergent momentum field ($\nabla\cdot \rho V=0$). Both of these approaches presume that the three dimensional divergence components exactly balance to result in a zero net change in local atmospheric density. The non-divergent wind assumption is not valid for model applications spanning a significant fraction of the atmospheric scale height (8 or 9 km). In either case, the presumption of zero density tendency in an air quality model is usually invalid since the externally supplied wind and density fields are often not balanced in the first place (see points 1-3 above). In CAMx, such a density-momentum balance obviously does not exist since a linear rate of temperature, pressure and horizontal wind change is imposed at each time step between meteorological update times.

Thus, the vertical velocity profile at each time step is determined from vertical integration of the divergent incompressible continuity equation

$$\frac{\partial \rho}{\partial t} = -\nabla \cdot \rho V$$

which is

$$\rho w(z) = -\int_0^z \left(\frac{\partial \rho}{\partial t} + \nabla_H \cdot \rho V_H \right) dz$$

where the local time-rate change of atmospheric density ρ in each grid cell is known from the input meteorological fields. In this approach, a vertical velocity profile is constructed that provides a balance between the imposed density tendency and the resolved horizontal momentum divergence in each grid cell at each time step. This vertical velocity is used for subsequent vertical transport calculations for all pollutants.

The fourth way CAMx ensures mass consistency is to calculate the horizontal flux divergence of atmospheric density in a manner that is numerically consistent with the procedure used to horizontally transport pollutants. Atmospheric density is advected in and out of each cell using the same equation as for pollutants:

$$\nabla_H \cdot \rho V_H = \frac{m^2}{A_{yz}} \frac{\partial}{\partial x}\left(\frac{uA_{yz}\rho}{m} \right) + \frac{m^2}{A_{xz}} \frac{\partial}{\partial y}\left(\frac{vA_{xz}\rho}{m} \right)$$

The resulting horizontal advective fluxes include resolved momentum convergence/divergence rates as well as any artificial divergences caused by the horizontal and vertical grid specifications (e.g., spatially varying vertical grid structure, or systematic distortions associated with the map projections). In simple tests in which a uniform pollutant field of unity mixing ratio is transported throughout a single regional grid over several days using actual episodic meteorological inputs, this approach has been shown to provide nearly exact (to 10^{-3}-10^{-4}%) consistency between the density and pollutant fields.

2.4 TRANSPORT ALGORITHMS

Horizontal advection is performed using the area preserving flux-form advection solver of Bott (1989) or the Piecewise Parabolic Method (PPM) of Colella and Woodward (1984) as implemented by Odman and Ingram (1993). The Bott and PPM schemes were incorporated into CAMx because they provide increased accuracy, less numerical diffusion, and equivalent execution speed compared to the original Smolarkiewicz (1983) scheme (Bott is slightly faster while PPM is slightly slower). The Smolarkiewicz scheme is no longer available in CAMx. When used in other modeling platforms, the Bott and PPM algorithms have produced significant differences in ozone predictions from the Smolarkiewicz algorithm. This is a result of the drastically reduced level of numerical diffusion associated with these approaches when used with the same level of explicit horizontal diffusion. As discussed by Yamartino (2000) the latest advection solvers reduce numerical diffusion to the point where modelers need to be concerned about including appropriate levels of explicit horizontal diffusion. Currently, there is very little information on the appropriate level of horizontal diffusion for Eulerian grid models. We see this issue becoming increasingly important as more accurate advection solvers (such as PPM and Bott) are utilized in grid models. This issue is not limited to CAMx.

Horizontal diffusion coefficients are determined within CAMx using a deformation approach based on the methods of Smagorinsky (1963):

$$K_{X/Y} = K_o + \frac{\Delta x \Delta y}{4\sqrt{2}} \left[\left(\frac{\partial u}{\partial y} + \frac{\partial v}{\partial x} \right)^2 + \left(\frac{\partial u}{\partial x} - \frac{\partial v}{\partial y} \right)^2 \right]^{1/2}$$

Separate diffusivity components are generated for fluxes in the x- and y-directions since K_X and K_Y are calculated for separate cell faces in the Arakawa C grid arrangement. The value of K_0 is specified according to the approach in MM5 (Anthes and Warner, 1978):

$$K_0 = 3 \times 10^{-3} \frac{\Delta x \Delta y}{\Delta t}$$

A maximum value of $K_{X/Y}$ is set to maintain numerical stability for the given grid-specific timestep. Explicit simultaneous two-dimensional horizontal diffusion is calculated through a simple flux-divergence calculation after all horizontal advection and vertical transport/diffusion are completed.

Vertical transport and diffusion are separately solved using an implicit integration approach after horizontal advection is completed. The simultaneous fully implicit calculations require the inversion of a tri-diagonal matrix. Since the implicit scheme is absolutely stable, only one vertical advection solution step is necessary per driving time step. Explicit approaches require potentially many sub-steps (on the order of 10-100) to maintain a stable solution, which introduces the potential for excessive numerical diffusion. Whereas the vertical advection step is implicitly solved in a single step, the vertical diffusion is implicitly solved over potentially several sub-steps, depending upon the magnitude of the vertical diffusivity relative to the vertical layer depths (we use a minimum 5 minute sub-step, or the grid time step, whichever is smaller). This ensures non-local diffusive coupling among all layers that exhibit high diffusivity, especially for long driving time steps on coarser grids that would otherwise only experience mixing between adjacent layers during a single implicit step. Gridded vertical

diffusion coefficients must be supplied to the model for the master grid via input file; the user may optionally supply vertical diffusion coefficients for any or all nested grids.

2.5 POLLUTANT REMOVAL

Trace gases and small particles are removed from the atmosphere via deposition to the surface. Dry deposition refers to the direct sedimentation and/or diffusion of material to various terrestrial surfaces and uptake into biota. Wet deposition refers to the uptake of material via chemical absorption (gases) or nucleation/impaction (particles) into cloud water, and the subsequent transfer to the Earth's surface by precipitation. The efficiency with which wet and dry deposition processes can remove pollutants from the air depends on the physical and chemical properties of the pollutants, local meteorological conditions, the type of surface on which they are being deposited, and on the frequency, duration, and intensity of precipitation events.

Removal by Precipitation

Wet deposition is an important removal process for particles. Particles act as cloud condensation nuclei; the cloud droplets grow and collect into sufficiently large sizes to fall as precipitation. A fraction of particles that are subsequently entrained into the cloud, and that exist within sub-cloud layers, are scavenged by liquid precipitation via impaction. The rates of nucleation and impaction depend upon cloud type (e.g., prolonged stratiform vs. vigorous convective development), rainfall rate, and particle size distribution.

Wet deposition is an important removal process for relatively soluble gaseous pollutants and this occurs through the following series of steps:

- Mixing of trace gas and condensed water in common air space;
- Absorption of gas molecules by water droplets;
- Possible aqueous-phase reactions of the pollutant within water droplets;
- Precipitation of droplets to the earth's surface;
- Diffusion of ambient gases into falling precipitation.

It is important to note that each of the above steps may be reversible, so that the overall wet deposition rate depends on the net results of the forward and backward processes at each step.

The rate at which the first and fourth steps proceed depends on the frequency and nature of cloud formation and precipitation events. For example, mid-latitude cyclonic storm events (e.g., winter storms) will result in different deposition rates than convective precipitation events such as summertime thunderstorms. The rates at which the second, third, and fifth steps proceed depend on the extent to which the pollutant in question dissolves in water and its overall reaction rate once in solution. Cloud water droplets can absorb gases from the air up the limit of their solubility in water. For many pollutants this solubility far exceeds the amount of pollutant present in the air so that the distribution of the pollutant between the air and water droplets is determined by the Henry's Law constant, which is defined as the ratio of

pollutant concentrations in the liquid-phase to the gas-phase at equilibrium. High values for the Henry's law constant (greater than about 10,000 M/atm) indicate a strong tendency to dissolve in water droplets, whereas low values (less than about 100 M/atm) indicate a tendency to remain in the air (Seinfeld and Pandis, 1998). Equilibrium between concentrations of pollutants in the air and in water droplets is usually established on time scales of minutes, so equilibrium conditions can generally be assumed to exist in the atmosphere.

If a pollutant partitions significantly into water droplets it can be removed by wet deposition when it rains. Averaged globally, highly soluble gases that are removed efficiently by wet deposition (e.g., nitric acid) are estimated to have lifetimes due to rainout of about 5 days (Warneck, 1989). Clearly, on regional or local scales, lifetimes against wet deposition will depend upon the frequency and intensity of rainout events. Gases that are removed less efficiently by wet deposition will have longer lifetimes. For example, the corresponding global average lifetime of formaldehyde against rainout is estimated to be 14 days (Warneck, 1989).

The wet scavenging of pollutants by liquid precipitation is improved in CAMx with the introduction of the new full-science PM chemistry package. The basic model implemented in CAMx is a scavenging approach in which the local rate of concentration change $\partial c/\partial t$ within or below a precipitating cloud depends on a scavenging coefficient Λ:

$$\frac{\partial c}{\partial t} = -\Lambda c$$

The scavenging coefficient is determined separately for gases and particulates, based upon relation ships described by Seinfeld and Pandis (1998). For gasses, two components are calculated: (1) the uptake of ambient gas concentration into falling precipitation, which can occur within and below clouds; and (2) the collection by precipitation of cloud droplets that contain dissolved gas species. For particles, separate in-cloud and below-cloud scavenging coefficients are determined. Within clouds, all aerosol mass is assumed to exist in cloud droplets (all particles are activated as condensation nuclei), so scavenging is due to the efficient collection of cloud droplets by precipitation. Below clouds, dry particles are scavenged by falling precipitation with an efficiency that is dependent upon particle size. Each of these processes are described below.

The following general assumptions are made in this scavenging model:

1) Only liquid cloud water and precipitation are effective at removing pollutants;
2) Rain drops and cloud droplets are each represented by a single mean size; rain drop size is an empirical function of rainfall intensity;
3) Within clouds, dissolved pollutants in liquid cloud water droplets and are in equilibrium with ambient concentrations according to Henry's Law;
4) Cloud water acidity is non-evolving and is set to a representative cloud pH as established by the model's list of Henry's Law equilibrium constants for each species (pH ~ 5);
5) All gas species behave as ideal gases;
6) All PM species and sizes are hygroscopic and internally mixed;

7) All in-cloud PM mass exists in cloud water (i.e., no "dry" aerosols exist in the interstitial air between cloud droplets), so in-cloud scavenging results from scavenging of cloud droplets by falling precipitation.

Wet Scavenging of Ambient Gases

Wet scavenging of gases occurs within and below precipitating clouds. Below the cloud, the total gas concentration in a given grid cell is subject to precipitation scavenging. Within a cloudy cell, the total gas concentration must first be partitioned into an aqueous fraction c_{aq} within cloud water and the remaining gaseous fraction c_g within the interstitial air; this split is determined by Henry's Law thereby assuming that a steady-state equilibrium exists between the two.

The Henry's Law constant for a given gas species k_0 (M/atm) specifies the ratio of pollutant mass in aqueous solution (M or mol/l_{h2o}) to its equilibrium partial pressure (atm). This constant is adjusted for temperature T (K) and converted to a dimensionless molar ratio:

$$H = k_0 R T \exp\left[A\left(\frac{1}{298} - \frac{1}{T} \right) \right]$$

where R is the ideal gas constant (8.206×10^{-2} l·atm/mol K), and A is the temperature dependence factor (K). The aqueous concentration (mass per volume of water) can thus be determined from the equilibrium gas concentration (mass per volume of air),

$$c_{aq} = H c_g$$

Given the relatively short residence times of falling rain drops through a given grid cell, aqueous equilibrium between ambient gas and precipitation water cannot be assumed and so the transfer of ambient gas into precipitation is explicitly calculated. The rate of transfer W of a gas to a water drop is

$$W = K_c \left(H c_g - c_{aq} \right)$$

where K_c is the mass transfer coefficient.

For a falling rain drop with speed v_d (m/s) and diameter d_d (m), the mass transfer coefficient is given by

$$K_c = \frac{D_g}{d_d}\left[2 + 0.6\left(\frac{v_d d_d}{\nu} \right)^{1/2} \left(\frac{\nu}{D_g} \right)^{1/3} \right]$$

where D_g and ν are the molecular diffusivity of the gas species and air, respectively.

The mean raindrop diameter and fall speed are taken from the empirical estimates of Scott (1978). The drop diameter is related to rainfall rate P (mm/hr), and the fall speed relationship has been modified to better agree with data provided by Seinfeld and Pandis (1998):

$$d_d = 9.0\times10^{-4} P^{0.21}$$

$$v_d = 3100\, d_d$$

The rate of c_{aq} increase can be represented by a mass balance with the rate of transport to the drop:

$$\frac{1}{6}\pi d_d^3 \frac{dc_{aq}}{dt} = \pi d_d^2 W$$

The expression for W is substituted into the equation above, rearranged, and expressed in terms of rainfall velocity. Then assuming that through a given model layer the ambient gas concentration, pH, and raindrop size is constant, and specifying c_{aq}^0 at the top of the layer, integration through a layer depth Δz (m) is performed. After falling through the layer each drop will have scavenged a species mass m_{aq} equal to

$$m_{aq} = \frac{1}{6}\pi d_d^3 \left(H c_g - c_{aq}^0\right)\left[1 - \exp\left(-\frac{6K_c\Delta z}{d_d v_d H}\right)\right]$$

Multiplying this mass by the number density of falling raindrops (N_d, m^{-3}) yields the gas concentration scavenged by all drops falling through the layer. The number density can be expressed in terms of rainfall rate, fall velocity, and drop size:

$$N_d = \frac{2.8\times10^{-7} P}{\pi d_d^3 v_d / 6}$$

Finally, to obtain a gas-phase scavenging rate, the mass equation above is multiplied by N_d, and divided by the total ambient concentration c and by the time it takes for rain to fall through the layer depth:

$$\Lambda_g = \frac{2.8\times10^{-7} P}{c\,\Delta z}\left(H c_g - c_{aq}^0\right)\left[1 - \exp\left(-\frac{6K_c\Delta z}{d_d v_d H}\right)\right]$$

For below-cloud scavenging, c_g in the difference term is replaced with c so that all ambient gas is subject to scavenging.

Wet Scavenging of Gases Dissolved in Cloud Water

The fraction of gases present in cloud water can be removed by precipitation via collection/ impaction. As a raindrop falls, it sweeps a cylindrical volume per unit time equal to

$$V = \frac{\pi}{4}\left(d_d + d_c\right)^2 v_d$$

where d_c is the size of cloud droplets. This implies that the motion of cloud droplets is insignificant compared to the raindrop fall speed. Due to aerodynamic perturbations of air flow around the falling drop, a collection efficiency is applied, i.e., the fraction of cloud

droplets within the collection volume that are scavenged by precipitation. For large raindrops with sizes greater than 0.5 mm and droplets 10-20 μm, we take this efficiency to be 0.9 (Seinfeld and Pandis, 1998). Also, we further assert that $(d_d + d_c)^2 \sim d_d^2$. Assuming then that a monodisperse distribution of rain drops are falling through a monodisperse distribution of cloud water droplets, the scavenging coefficient for rain collecting cloud water is

$$\Lambda_c = \frac{\pi}{4} d_d^2 \, v_d \, E \, N_d$$

where E is the collection efficiency (0.9) and N_d is the rain drop number density described earlier. Substituting the relationship between N_d and rainfall parameters, then

$$\Lambda_c = 4.2 \times 10^{-7} \frac{E \, P}{d_d}$$

The cloud water scavenging coefficient is scaled by the ratio of aqueous concentration to total grid cell concentration to achieve the aqueous-phase scavenging coefficient:

$$\Lambda_a = \Lambda_c \frac{c_{aq} \, L_c}{c \, \rho_w}$$

Within cloud layers, the gas-phase and aqueous-phase scavenging coefficients are added to provide the total in-cloud scavenging rate for gases, $\Lambda = \Lambda_c + \Lambda_a$.

Wet Scavenging of In-cloud Aerosols

All aerosols within cloudy layers are assumed to be in cloud water. Therefore, the scavenging coefficient for aqueous aerosols is exactly the same as for the scavenging of cloud droplets: $\Lambda = \Lambda_c$.

Wet Scavenging of Dry Particles

Wet scavenging of dry particles only occurs below precipitating clouds. We use the same scavenging coefficient as derived for the collection of cloud droplets:

$$\Lambda_c = 4.2 \times 10^{-7} \frac{E \, P}{d_d}$$

In this case, however, the collection efficiency E is a function of particle size d_p, and is given by Seinfeld and Pandis (1998) as

$$E(d_p) = \frac{4}{R_e S_c}\left(1 + 0.4 \, R_e^{1/2} \, S_c^{1/3} + 0.16 \, R_e^{1/2} \, S_c^{1/2}\right)$$

$$+ \; 4\phi\left[\frac{\mu}{\mu_w} + \phi\left(1 + 2 \, R_e^{1/2}\right)\right]$$

$$+ \left(\frac{S_t - S^*}{S_t - S^* + 2/3}\right)^{3/2}$$

where μ and μ_w are the kinematic viscosity of air (1.8×10^{-5} kg/ms) and water (10^{-3} kg/ms), respectively, $\phi = d_p/d_d$ is the ratio of particle size to rain drop size, R_e is the Reynolds number for the rain drop, S_c is the Schmidt number for the collected particle, and S_t is the Stokes number of the collected particle. The Reynolds number is given by

$$R_e = \frac{D_d v_d}{2\nu}$$

while the Schmidt number is

$$S_c = \frac{\nu}{D_p}$$

where D_p is the particle Brownian diffusivity:

$$D_p = \frac{kTC}{3\pi\mu d_p}$$

Here, k is the Boltzman constant (1.38×10^{-23} J/K) and C is the Cunningham correction factor for small particles:

$$C = 1 + \frac{2\lambda}{d_p}\left[1.257 + 0.4\exp\left(-\frac{0.55 d_p}{\lambda}\right)\right]$$

and where λ is the mean free path of air (6.5×10^{-8} m). The Stokes number is given by

$$S_t = \frac{v_d d_p^2 \rho_p C}{9\mu d_d}$$

where ρ_p is the particle density. The S^* parameter is given by

$$S^* = \frac{1.2 + \ln(1+R_e)/12}{1+\ln(1+R_e)}$$

Dry Deposition

For many compounds, dry deposition can be as important as wet deposition as a removal process. Due to the difficulty of making direct measurements of dry deposition and the need for a suitable model parameterization, dry deposition is often treated as a first-order removal mechanism, where the flux of a pollutant to the surface is the product of a characteristic deposition velocity and its concentration in the "surface layer" (i.e., the lowest model layer). Deposition velocities are derived from models that account for the reactivity, solubility, and diffusivity of gases, the sizes of particles, local meteorological conditions, and surface characteristics. The factors affecting deposition are discussed in more detail below.

For a given species, particle size, and grid cell, CAMx determines a deposition velocity for each landuse type in that cell and then linearly combines them according to the fractional distribution of landuse. The deposition flux is used as the lower boundary condition in the vertical diffusion algorithm. Aerosol size spectra and species-dependent properties needed for

the deposition velocity calculations are externally supplied to CAMx for all pollutant species via the chemistry parameters file; gridded landuse is supplied to the master grid and optionally any nested fine grids; the season is determined by the simulation date.

Movement of material along a path from the atmosphere, through any plant canopy, and onto the various plant and ground surfaces within and below the canopy is typically modeled by analogy to an electrical circuit. Resistances in serial and parallel arrangements are used to represent the relative ease with which material moves through different portions of the deposition pathway. Each branch of the circuit represents a different path by which material may be deposited. For example, gaseous pollutants may transfer through the lowest layers of the atmosphere partially into a plant canopy, through the stomatal openings on plant leaves and into the plant mesophyll tissue. Alternatively, the material may travel all the way through the plant canopy and deposit on the ground surface.

Dry Deposition of Gases

Wesely (1989) has developed a resistance model that incorporates the major elements described above. Deposition velocity v_d is calculated from three primary resistances r (s/m) in series:

$$V_d = \frac{1}{r_a + r_b + r_s}$$

The aerodynamic resistance r_a represents bulk transport through the lowest model layer by turbulent diffusion, and operates equivalently for all gases and small particles. The magnitude of this resistance depends on the intensity of turbulent motion, which in turn depends on solar insolation, wind speed, surface roughness, and near-surface temperature lapse rate. In CAMx it is calculated from

$$r_a = \frac{1}{k\,u_*}\left[\ln\left(\frac{1}{z_o}\right) - \phi_h\right]$$

where u_* is friction velocity (m/s), k is von Karman's constant, z is the lowest model layer midpoint height (m), z_0 is the surface roughness length (m), and ϕ_h is a stability correction term. The surface layer parameterization of Louis (1979) is used to supply friction velocity and stability correction as a function of input surface meteorology and roughness length. By default, roughness length is internally assigned according to season and the input gridded distribution of landuse type based on values used in AERMOD (EPA, 1998). However, the user may override this default by explicitly providing gridded roughness fields via the albedo/haze/ozone file as described in Section 5. In general, aerodynamic resistance is at a minimum on warm, sunny days with strong mixing due to surface heating and mechanical turbulence, and at a maximum on cool, calm nights when turbulent mixing is suppressed.

The quasi-laminar sublayer (or boundary) resistance r_b represents molecular diffusion through the thin layer of air directly in contact with the particular surface to which material is being deposited. It is usually assumed to depend only on the molecular diffusivity of each pollutant species, and is given by

$$r_b = \frac{2 S_c^{2/3}}{k u_*}$$

where S_c is the Schmidt number, or the ratio of air viscosity to species molecular diffusivity.

Over land, surface resistance r_s is further expressed as several more serial and parallel resistances that depend upon the physical and chemical properties of the surface in question:

$$r_s = \frac{1}{\frac{1}{r_{st} + r_m} + \frac{1}{r_{uc}} + \frac{1}{r_{dc} + r_{cl}} + \frac{1}{r_{ac} + r_{gs}}}$$

where the first serial resistance set represents the pathway into the stomatal and mesophyllic portions of active plants, the second is the pathway into the upper canopy, the third is the pathway into the lower canopy, and the fourth is the pathway to the ground surface. Many of these resistances are season- and landuse-dependent, and are built into Wesely's model; some in turn are adjusted within CAMx for solar insolation, moisture stress, and surface wetness (by default, vegetation is assumed to be unstressed, but several degrees of moisture stress can be introduced to the model through the gridded albedo/haze/ozone input file as described in Section 5). A few other resistances have been developed by Wesely for SO_2 and ozone, and so are scaled for each gaseous species based on the following pollutant properties:

- Molecular diffusivity;
- Henry's law solubility;
- Chemical reactivity toward oxidation of biological substances.

This allows the resistance approach to be used to estimate deposition velocities for a wide range of gaseous pollutants.

Over water, the surface resistance is based on some improvements adopted by Kumar et al. (1996) in UAM-AERO, following Sehmel (1980):

$$r_s = \frac{1}{3.9 \times 10^{-5} H T_S u_*}$$

where T_s is surface temperature (K).

The surface resistance for strong acids such as nitric and hydrochloric acid are set to zero given their strong rates of update by biota and other surfaces. The species for which surface resistance is to be zeroed are defined in the CAMx chemistry parameters file.

Dry Deposition of Aerosols

Surface deposition of particles occurs via diffusion, impaction, and/or gravitational settling. Particle size is the dominant variable controlling these processes. The resistance approach of Slinn and Slinn (1980), as implemented in UAM-AERO (Kumar et al., 1996), has been

adopted in CAMx. Particle deposition velocity for a given aerosol size is calculated using the following resistance equation:

$$v_d = v_{sed} + \frac{1}{r_a + r_b + r_a r_b v_{sed}}$$

where v_{sed} is the gravitational settling (or sedimentation) velocity. This velocity is dependent on aerosol size and density:

$$v_{sed} = \frac{D^2 g C \rho_p}{18 \nu}$$

where D is the log-mean particle diameter (m) of a given size section, ρ_p is particle density (g/m^3), g is gravitational acceleration, and ν is the viscosity of air. The factor C is the Cunningham correction for small particles, as described earlier for wet scavenging of particles.

Aerodynamic resistance r_a is identical to the value used for gaseous dry deposition. Resistance to diffusion through the quasi-laminar sub-layer layer depends on aerosol Brownian diffusion and inertial impaction. Particles are assumed to remain on a surface once they impact, so resuspension effects are ignored. Boundary resistance r_b is given by

$$r_b = \frac{1}{u_* \left(S_c^{-2/3} + 10^{-3/S_t} \right)}$$

The stokes number S_t is calculated from

$$S_t = \frac{v_{sed} u_*^2}{\nu g}$$

Specification of Season for Dry Deposition

The Wesely (1989) deposition algorithm specifies the various surface resistances by land cover type for five seasons:

- Spring
- Summer
- Fall
- Winter
- Winter with snow-cover

CAMx internally defines a season map to determine four of these five seasons by month and latitude (Table 2-2). Five latitude bands exist in each hemisphere:

- Tropical $< 20°$
- Sub-tropical 20° to 35°
- Temperate 35° to 50°

- Cool 50° to 75°
- Polar > 75°

The seasons in the Northern and Southern hemispheres are offset by six months. This offset does not cause any discontinuity at the equator because all 12 months are defined as summer in the tropical band at the equator. This season map is generalized and may not be ideal for all locations. The season map is coded into data statements in the "`chmdat.f`" subroutine and could be changed to better suit a specific region.

Table 2-2. Relationships between season and month/latitude used in the CAMx dry deposition algorithm. Exception: seasons for the area within 50N-75N and 15W-15E are internally set to those of latitude band 35-50 to account for regions of Europe in which the climate is influenced by the Gulf Stream.

Month		Latitude Band				
Northern Hemisphere	Southern Hemisphere	< 20° Tropical	20° - 35° Sub-tropical	35° - 50° Temperate	50° - 75° Cool	> 75° Polar
Jan	Jul	Summer	winter	winter	winter	winter
Feb	Aug	Summer	spring	winter	winter	winter
Mar	Sep	Summer	spring	spring	winter	winter
Apr	Oct	Summer	spring	spring	spring	winter
May	Nov	Summer	summer	spring	spring	winter
Jun	Dec	Summer	summer	summer	summer	spring
Jul	Jan	Summer	summer	summer	summer	summer
Aug	Feb	Summer	summer	summer	summer	fall
Sep	Mar	Summer	summer	fall	fall	winter
Oct	Apr	Summer	fall	fall	fall	winter
Nov	May	Summer	fall	fall	winter	winter
Dec	Jun	summer	fall	winter	winter	winter

Specifying Snow-Cover

The season map shown in Table 2-2 does not specify any snow-cover because snow-cover is quite variable in space and time. Instead, CAMx provides a way of explicitly specifying which grid cells are snow-covered during the simulation. An optional snow-cover data field was added to the albedo/haze/ozone column (AHO) file; this allows the snow-cover to vary spatially and temporally during a simulation (see Section 5). The snow-cover input is a binary value where 1 signifies that the grid cell is snow-covered. Snow-covered grid cells are assigned the Wesely (1989) surface resistances for winter with snow-cover, regardless of the season. Snow cover also impacts photolysis rates (see Section 3).

Snow-cover data can be developed in several ways:

- Spatially interpolated snow-cover observations;
- Analyses of snow-cover data included in existing metrological data sets, such as the NCEP Eta Data Assimilation System (EDAS);
- Analyses of climatological snow-cover based on surface reflectivity data from the Total Ozone mapping Spectrometer (TOMS).

3. CHEMISTRY MECHANISMS

The photochemical mechanisms supported in CAMx are based on Carbon Bond version 4 (CB4; Gery et. al., 1989) and SAPRC99 (Carter, 2000). There are five specific mechanisms currently supported for CAMx, along with a plug-in that allows a simple user-defined chemical mechanism to be employed (referred to as "Mechanism 10"). These are listed in Table 3-1.

Table 3-1. Chemistry mechanisms currently implemented in CAMx.

Mechanism ID	Description
2	CB4 (Gery et al., 1989) gas-phase chemistry with revised radical-radical termination reactions that are necessary for regional modeling. 91 reactions and 36 species (24 state gasses and 12 radicals).
3	Mechanism 2 with updated isoprene chemistry based on Carter (1996) as implemented for the Ozone Transport Assessment Group (OTAG) by Whitten et.al., (1996). 96 reactions and 37 species (25 state gasses and 12 radicals).
1	Mechanism 3 with reactive chlorine chemistry (Tanaka et al., 2000). 110 reactions and 48 species (34 state gasses and 14 radicals).
4	Mechanism 3 expanded to include aerosol and mercury chemistry, including: secondary organic aerosol formation from condensable gasses, aqueous PM chemistry, inorganic PM thermodynamics, aerosol size evolution, and several additional inorganic reactions appropriate for regional modeling. 117 reactions and up to 67 species (37 state gasses, up to 18 state particulates, and 12 radicals).
5	The fixed parameter version of the SAPRC99 gas-phase mechanism (Carter, 2000). 211 reactions and 74 species (56 state gasses and 18 radicals).
10	A user-defined simple chemistry mechanism can be developed for any gas and/or particulate species, which is defined by a "Mechanism 10" parameters file and solved within a user-supplied subroutine called "`chem10.f`."

3.1 GAS-PHASE CHEMISTRY

Two versions of the "standard" CB4 mechanism are included in CAMx, labeled Mechanisms 2 and 3. The choice between 2 and 3 depends upon whether the user wishes to use the original CB4 isoprene chemistry or the newer Carter "one product" isoprene chemistry (Carter, 1996). Compared to the original isoprene chemistry, the Carter chemistry is generally less reactive at low to medium VOC/NO_x ratios, but under NO_x-limited conditions may produce more ozone because it has weaker NO_x removal pathways. Most users who don't need to simulate aerosols choose Mechanism 3 because it was established as the "default" mechanism in the US during the OTAG modeling. Mechanism 1 extends the CB4 by adding reactive chlorine chemistry (Cl_2, Cl and ClO reactions) to Mechanism 3 (Tanaka et al., 2000). Mechanism 4 includes aerosol (and optionally mercury) chemistry and is described in detail in Section 3.2.

Mechanism 5 is the SAPRC99 chemistry adapted for photochemical grid modeling by selecting a specific "fixed parameter" lumping scheme (Carter, 2000). The SAPRC99 mechanism was added as an alternate mechanism because it is chemically up-to-date, has been tested extensively against environmental chamber data, and uses a different approach for VOC lumping than the CB4 mechanism.

Mechanisms 1 through 5 are all balanced for nitrogen conservation so that predicted NO_Y can be calculated as the sum of nitrogen containing species. A listing of the species and reactions in Mechanism 3 (CB4), Mechanism 5 (SAPRC99), and the additional chlorine compounds and reactions in Mechanism 1, are provided in Tables 3-2 through 3-8, respectively.

The selection of which mechanism to employ in a given CAMx application is provided by a "chemistry parameters" input file. This file defines the number of gas and aerosol species, the number of reactions for the mechanism, lists the species by name with associated physio-chemical properties, lists the reaction rate constants and temperature dependencies for each reaction, and defines which reactions are photolytic. Chemistry parameters files for Mechanisms 1 through 5 are provided with CAMx. See Section 5 for additional information on the format and usage of these files.

Photolysis Rates

The rates of atmospheric photolysis reactions depend upon solar irradiance and therefore are sensitive to the amount of solar radiation transmitted through the atmosphere as well as reflected from the earth's surface (albedo). Photolysis rates are derived for each grid cell assuming clear sky conditions as a function of five parameters: solar zenith angle, altitude, total ozone column, surface albedo, and atmospheric turbidity. The rates are taken from a large lookup table that spans the range of conditions for each of the five dimensions. This table may be developed using the accompanying TUV photolysis preprocessor (Madronich; 1993, 2002). The CAMx version of TUV is modified to output information in a format directly compatible with CAMx for either the CB4 or SAPRC99 chemical mechanisms. See Sections 5 and 11 for more information on developing photolysis inputs.

Table 3-2. Reactions and rate constants for the CB4 mechanism (Mechanism 3).

Reaction Number	Reactants	Products	k_{298}^{1} (ppm^{-n} min^{-1})
1	NO2	NO + O	Photolysis
2	O	O3	4.323E+06
3	O3 + NO	NO2	2.664E+01
4	O + NO2	NO	1.375E+04
5	O + NO2	NO3	2.309E+03
6	O + NO	NO2	2.438E+03
7	NO2 + O3	NO3	4.731E-02
8	O3	O	Photolysis
9	O3	O1D	Photolysis
10	O1D	O	4.250E+10
11	O1D + H2O	2 OH	3.260E+05
12	O3 + OH	HO2	1.000E+02
13	O3 + HO2	OH	2.999E+00
14	NO3	0.89 NO2 + 0.89 O + 0.11 NO	Photolysis
15	NO3 + NO	2 NO2	4.417E+04
16	NO3 + NO2	NO + NO2	5.901E-01
17	NO3 + NO2	N2O5	1.853E+03
18	N2O5 + H2O	2 HNO3	1.900E-06
19	N2O5	NO3 + NO2	2.776E+00
20	NO + NO	2 NO2	1.539E-04
21	NO + NO2 + H2O	2 HONO	1.600E-11
22	NO + OH	HONO	9.799E+03
23	HONO	NO + OH	Photolysis
24	OH + HONO	NO2	9.770E+03
25	HONO + HONO	NO + NO2	1.500E-05
26	NO2 + OH	HNO3	1.682E+04
27	OH + HNO3	NO3	2.179E+02
28	HO2 + NO	OH + NO2	1.227E+04
29	HO2 + NO2	PNA	0.000E+00
30	PNA	HO2 + NO2	0.000E+00
31	OH + PNA	NO2	0.000E+00
32	HO2 + HO2	H2O2	4.144E+03
33	HO2 + HO2 + H2O	H2O2	2.181E-01
34	H2O2	2 OH	Photolysis
35	OH + H2O2	HO2	2.520E+03
36	OH + CO	HO2	3.220E+02
37	FORM + OH	HO2 + CO	1.500E+04
38	FORM	2 HO2 + CO	Photolysis
39	FORM	CO	Photolysis
40	FORM + O	OH + HO2 + CO	2.370E+02
41	FORM + NO3	HNO3 + HO2 + CO	9.300E-01
42	ALD2 + O	C2O3 + OH	6.360E+02
43	ALD2 + OH	C2O3	2.400E+04
44	ALD2 + NO3	C2O3 + HNO3	3.700E+00
45	ALD2	FORM + 2 HO2 + CO + XO2	Photolysis
46	C2O3 + NO	FORM + NO2 + HO2 + XO2	2.820E+04
47	C2O3 + NO2	PAN	1.370E+04
48	PAN	C2O3 + NO2	2.540E-02
49	C2O3 + C2O3	2 FORM + 2 XO2 + 2 HO2	3.700E+03
50	C2O3 + HO2	0.79 FORM + 0.79 XO2 + 0.79 HO2 + 0.79 OH	9.600E+03
51[2]	OH	FORM + XO2 + HO2	2.100E+01
52	PAR + OH	0.87 XO2 + 0.13 XO2N + 0.11 HO2 + 0.11 ALD2 - 0.11 PAR + 0.76 ROR	1.203E+03
53	ROR	0.96 XO2 + 1.1 ALD2 + 0.94 HO2 - 2.1 PAR + 0.04 XO2N	1.371E+05
54	ROR	HO2	9.545E+04
55	ROR + NO2	NTR	2.200E+04
56	O + OLE	0.63 ALD2 + 0.38 HO2 + 0.28 XO2 + 0.3 CO + 0.2 FORM + 0.02 XO2N + 0.22 PAR + 0.2 OH	5.920E+03
57	OH + OLE	FORM + ALD2 - PAR + XO2 + HO2	4.200E+04
58	O3 + OLE	0.5 ALD2 + 0.74 FORM + 0.22 XO2 + 0.1 OH + 0.33 CO + 0.44 HO2 - PAR	1.800E-02
59	NO3 + OLE	0.91 XO2 + FORM + 0.09 XO2N + ALD2 + NO2 - PAR	1.135E+01
60	O + ETH	FORM + 1.7 HO2 + CO + 0.7 XO2 + 0.3 OH	1.080E+03
61	OH + ETH	XO2 + 1.56 FORM + 0.22 ALD2 + HO2	1.192E+04
62	O3 + ETH	FORM + 0.42 CO + 0.12 HO2	2.700E-03
63	TOL + OH	0.44 HO2 + 0.08 XO2 + 0.36 CRES + 0.56 TO2	9.150E+03
64	TO2 + NO	0.9 NO2 + 0.9 HO2 + 0.9 OPEN + 0.1 NTR	1.200E+04
65	TO2	CRES + HO2	2.500E+02

Reaction Number	Reactants	Products	k_{298}[1] (ppm^{-n} min^{-1})
66	OH + CRES	0.4 CRO + 0.6 XO2 + 0.6 HO2 + 0.3 OPEN	6.100E+04
67	CRES + NO3	CRO + HNO3	3.250E+04
68	CRO + NO2	NTR	2.000E+04
69	OPEN	C2O3 + HO2 + CO	Photolysis
70	OPEN + OH	XO2 + 2 CO + 2 HO2 + C2O3 + FORM	4.400E+04
71	OPEN + O3	0.03 ALD2 + 0.62 C2O3 + 0.7 FORM + 0.03 XO2 + 0.69 CO + 0.08 OH + 0.76 HO2 + 0.2 MGLY	1.500E-02
72	OH + XYL	0.7 HO2 + 0.5 XO2 + 0.2 CRES + 0.8 MGLY + 1.1 PAR + 0.3 TO2	3.620E+04
73	OH + MGLY	XO2 + C2O3	2.600E+04
74	MGLY	C2O3 + HO2 + CO	Photolysis
75	O + ISOP	0.75 ISPD + 0.5 FORM + 0.25 XO2 + 0.25 HO2 + 0.25 C2O3 + 0.25 PAR	5.320E+04
76	OH + ISOP	0.912 ISPD + 0.629 FORM + 0.991 XO2 + 0.912 HO2 + 0.088 XO2N	1.476E+05
77	O3 + ISOP	0.65 ISPD + 0.6 FORM + 0.2 XO2 + 0.066 HO2 + 0.266 OH + 0.2 C2O3 + 0.15 ALD2 + 0.35 PAR + 0.066 CO	1.900E-02
78	NO3 + ISOP	0.2 ISPD + 0.8 NTR + XO2 + 0.8 HO2 + 0.2 NO2 + 0.8 ALD2 + 2.4 PAR	9.960E+02
79	XO2 + NO	NO2	1.200E+04
80	XO2 + XO2		2.000E+03
81	XO2N + NO	NTR	1.200E+04
82	SO2 + OH	SULF + HO2	1.110E+03
83	SO2	SULF	8.167E-05
84	MEOH + OH	FORM + HO2	1.600E+03
85	ETOH + OH	HO2 + ALD2	4.300E+03
86	XO2 + HO2		8.900E+03
87	XO2N + HO2		8.900E+03
88	XO2N + XO2N		2.000E+03
89	XO2 + XO2N		4.000E+03
90	OH + HO2		1.626E+05
91	CRO		2.778E-04
92	OH + ISPD	1.565 PAR + 0.167 FORM + 0.713 XO2 + 0.503 HO2 + 0.334 CO + 0.168 MGLY + 0.273 ALD2 + 0.498 C2O3	4.967E+04
93	O3 + ISPD	0.114 C2O3 + 0.15 FORM + 0.85 MGLY + 0.154 HO2 + 0.268 OH + 0.064 XO2 + 0.02 ALD2 + 0.36 PAR + 0.225 CO	1.050E-02
94	NO3 + ISPD	0.357 ALD2 + 0.282 FORM + 1.282 PAR + 0.925 HO2 + 0.643 CO + 0.85 NTR + 0.075 C2O3 + 0.075 XO2 + 0.15 HNO3	1.478E+00
95	ISPD	0.333 CO + 0.067 ALD2 + 0.9 FORM + 0.832 PAR + 1.033 HO2 + 0.7 XO2 + 0.967 C2O3	Photolysis
96	NO2 + ISOP	0.2 ISPD + 0.8 NTR + XO2 + 0.8 HO2 + 0.2 NO + 0.8 ALD2 + 2.4 PAR	2.200E-04

Notes:

[1] Rate constants are shown for 298 K and 1 atmosphere in units of ppm and minutes. See the CAMx chemistry parameters file (Section 5) for the temperature and pressure dependencies.

[2] Reaction 51 implicitly assumes 1.85 ppm of methane in the rate constant.

Table 3-3. Species in the CB4 mechanism (Mechanism 3).

SpeciesName	Description
NO2	Nitrogen dioxide
NO	Nitric oxide
O	Oxygen atom in the O^3(P) electronic state
O3	Ozone
NO3	Nitrate radical
O1D	Oxygen atom in the O^1(D) electronic state
OH	Hydroxyl radical
HO2	Hydroperoxy radical
N2O5	Dinitrogen pentoxide
HNO3	Nitric acid
HONO	Nitrous acid
PNA	Peroxynitric acid (HNO_4)
H2O2	Hydrogen peroxide
CO	Carbon monoxide
FORM	Formaldehyde
ALD2	Higher aldehyde (based on acetaldehyde)
C2O3	Acylperoxy radical (based on acetylperoxy)
XO2	NO to NO2 conversion from alkylperoxy (RO_2) radical
PAN	Peroxyacyl nitrate (based on peroxyacetyl nitrate)
PAR	Paraffin carbon bond (C-C)
XO2N	NO to organic nitrate conversion from alkylperoxy (RO_2) radical
ROR	Secondary alkoxy radical
NTR	Organic nitrate (RNO_3)
OLE	Olefin carbon bond (C=C)
ETH	Ethene
TOL	Toluene and other monoalkyl aromatics
CRES	Cresol and higher molecular weight phenols
TO2	Toluene-hydroxyl radical adduct
OPEN	Aromatic ring opening product
CRO	Methylphenoxy radical
MGLY	Methylglyoxal and other aromatic products
XYL	Xylene and other polyalkyl aromatics
ISOP	Isoprene
ISPD	Isoprene product (lumped methacrolein, methyl vinyl ketone, etc.)
SO2	Sulfur dioxide
SULF	Sulfuric acid (gaseous)
MEOH	Methanol
ETOH	Ethanol

Table 3-4. Reactions and rate constants for the SAPRC99 mechanism (Mechanism 5).

Reaction Number	Reactants	Products	k_{298}[1] (ppm^{-n} min^{-1})
1	NO2	NO + O	Photolysis
2	O + O2 + M	O3 + M	2.106E-05
3	O + O3	2O2	1.176E+01
4	O + NO + M	NO2 + M	3.679E-03
5	O + NO2	NO + O2	1.436E+04
6	O + NO2	NO3	2.691E+03
7	O3 + NO	NO2 + O2	2.683E+01
8	O3 + NO2	O2 + NO3	5.204E-02
9	NO + NO3	2NO2	3.850E+04
10	NO + NO + O2	2NO2	7.109E-10
11	NO2 + NO3	N2O5	2.269E+03
12	N2O5	NO2 + NO3	3.169E+00
13	N2O5 + H2O	2HNO3	3.842E-07
14	NO2 + NO3	NO + NO2 + O2	9.693E-01
15	NO3	NO + O2	Photolysis
16	NO3	NO2 + O	Photolysis
17	O3	O + O2	Photolysis
18	O3	O1D + O2	Photolysis
19	O1D + H2O	2OH	3.251E+05
20	O1D + M	O + M	4.250E+04
21	OH + NO	HONO	1.095E+04
22	HONO	OH + NO	Photolysis
23	HONO	HO2 + NO2	Photolysis
24	OH + HONO	NO2	9.553E+03
25	OH + NO2	HNO3	1.327E+04
26	OH + NO3	HO2 + NO2	2.956E+04
27	OH + HNO3	NO3 + H2O	2.176E+02
28	HNO3	OH + NO2	Photolysis
29	OH + CO	HO2	3.082E+02
30	OH + O3	HO2	9.798E+01
31	HO2 + NO	OH + NO2	1.244E+04
32	HO2 + NO2	HNO4	0.000E+00
33	HNO4	HO2 + NO2	0.000E+00
34	HNO4	0.61HO2 + 0.61NO2 + 0.39OH + 0.39NO3	Photolysis
35	HNO4 + OH	NO2	0.000E+00
36	HO2 + O3	OH	2.764E+00
37	HO2 + HO2	HO2H + O2	4.237E+03
38	HO2 + HO2 + H2O	HO2H + O2 + H2O	2.349E-01
39	NO3 + HO2	0.8OH + 0.8NO2 + 0.2HNO3	5.911E+03
40	NO3 + NO3	2NO2 + O2	3.375E-01
41	HO2H	2OH	Photolysis
42	HO2H + OH	HO2	2.505E+03
43	OH + HO2		1.642E+05
44	OH + SO2	HO2 + SULF	1.444E+03
45	OH + H2	HO2	9.902E+00
46	CXO2 + NO	NO2 + HCHO + HO2	1.076E+04
47	CXO2 + HO2	COOH + O2	7.693E+03
48	CXO2 + NO3	HCHO + HO2 + NO2	1.921E+03
49	CXO2 + CXO2	MEOH + HCHO + O2	3.916E+02
50	CXO2 + CXO2	2HCHO + 2HO2	1.581E+02
51	RO2R + NO	NO2 + HO2	1.335E+04
52	RO2R + HO2	ROOH	2.201E+04
53	RO2R + NO3	NO2 + O2 + HO2	3.399E+03
54	RO2R + CXO2	HO2 + 0.75HCHO + 0.25MEOH	2.956E+02
55	RO2R + RO2R	HO2	5.172E+01
56	R2O2 + NO	NO2	1.335E+04
57	R2O2 + HO2	HO2	2.201E+04
58	R2O2 + NO3	NO2	3.399E+03
59	R2O2 + CXO2	CXO2	2.956E+02
60	R2O2 + RO2R	RO2R	5.172E+01
61	R2O2 + R2O2		5.172E+01
62	RO2N + NO	RNO3	1.335E+04
63	RO2N + HO2	ROOH	2.201E+04
64	RO2N + CXO2	HO2 + 0.25MEOH + 0.5MEK + 0.5PROD + 0.75HCHO	2.956E+02
65	RO2N + NO3	NO2 + O2 + HO2 + MEK	3.399E+03

Reaction Number	Reactants	Products	k_{298}[1] (ppm^{-n} min^{-1})
66	RO2N + RO2R	HO2 + 0.5MEK + 0.5PROD	5.172E+01
67	RO2N + R2O2	RO2N	5.172E+01
68	RO2N + RO2N	MEK + HO2 + PROD	5.172E+01
69	CCO3 + NO2	PAN	1.549E+04
70	PAN	CCO3 + NO2	3.123E-02
71	CCO3 + NO	CXO2 + NO2	3.153E+04
72	CCO3 + HO2	0.75CO3H + 0.25CO2H + 0.25O3	2.084E+04
73	CCO3 + NO3	CXO2 + NO2	5.911E+03
74	CCO3 + CXO2	CO2H + HCHO	1.425E+04
75	CCO3 + RO2R	CO2H	1.108E+04
76	CCO3 + R2O2	CCO3	1.108E+04
77	CCO3 + RO2N	CO2H + PROD	1.108E+04
78	CCO3 + CCO3	2CXO2	2.296E+04
79	RCO3 + NO2	PAN2	1.784E+04
80	PAN2	RCO3 + NO2	2.661E-02
81	RCO3 + NO	NO2 + CCHO + RO2R	4.134E+04
82	RCO3 + HO2	0.75RC3H + 0.25RC2H + 0.25O3	2.084E+04
83	RCO3 + NO3	NO2 + CCHO + RO2R	5.911E+03
84	RCO3 + CXO2	RC2H + HCHO	1.425E+04
85	RCO3 + RO2R	RC2H	1.108E+04
86	RCO3 + R2O2	RCO3	1.108E+04
87	RCO3 + RO2N	RC2H + PROD	1.108E+04
88	RCO3 + CCO3	CXO2 + CCHO + RO2R	2.296E+04
89	RCO3 + RCO3	2CCHO + 2RO2R	2.296E+04
90	BZCO + NO2	PBZN	2.025E+04
91	PBZN	BZCO + NO2	1.873E-02
92	BZCO + NO	NO2 + BZO + R2O2	4.134E+04
93	BZCO + HO2	0.75RC3H + 0.25RC2H + 0.25O3	2.084E+04
94	BZCO + NO3	NO2 + BZO + R2O2	5.911E+03
95	BZCO + CXO2	RC2H + HCHO	1.425E+04
96	BZCO + RO2R	RC2H	1.108E+04
97	BZCO + R2O2	BZCO	1.108E+04
98	BZCO + RO2N	RC2H + PROD	1.108E+04
99	BZCO + CCO3	CXO2 + BZO + R2O2	2.296E+04
100	BZCO + RCO3	CCHO + RO2R + BZO + R2O2	2.296E+04
101	BZCO + BZCO	2BZO + 2R2O2	2.296E+04
102	MCO3 + NO2	MPAN	1.784E+04
103	MPAN	MCO3 + NO2	2.127E-02
104	MCO3 + NO	NO2 + HCHO + CCO3	4.134E+04
105	MCO3 + HO2	0.75RC3H + 0.25RC2H + 0.25O3	2.084E+04
106	MCO3 + NO3	NO2 + HCHO + CCO3	5.911E+03
107	MCO3 + CXO2	RC2H + HCHO	1.425E+04
108	MCO3 + RO2R	RC2H	1.108E+04
109	MCO3 + R2O2	MCO3	1.108E+04
110	MCO3 + RO2N	2RC2H	1.108E+04
111	MCO3 + CCO3	CXO2 + HCHO + CCO3	2.296E+04
112	MCO3 + RCO3	HCHO + CCO3 + CCHO + RO2R	2.296E+04
113	MCO3 + BZCO	HCHO + CCO3 + BZO + R2O2	2.296E+04
114	MCO3 + MCO3	2HCHO + 2CCO3	2.296E+04
115	TBUO + NO2	RNO3	3.547E+04
116	TBUO	ACET + CXO2	5.923E+04
117	BZO + NO2	NPHE	5.622E+04
118	BZO + HO2	PHEN	2.201E+04
119	BZO	PHEN	6.000E-02
120	BZNO + NO2	2XN	5.622E+04
121	BZNO + HO2	NPHE	2.201E+04
122	BZNO	NPHE	6.000E-02
123	HCHO	2HO2 + CO	Photolysis
124	HCHO	CO	Photolysis
125	HCHO + OH	HO2 + CO	1.360E+04
126	HCHO + HO2	HCO3	1.167E+02
127	HCO3	HO2 + HCHO	9.060E+03
128	HCO3 + NO	HC2H + NO2 + HO2	1.076E+04
129	HCHO + NO3	HNO3 + HO2 + CO	8.481E-01
130	CCHO + OH	CCO3	2.342E+04
131	CCHO	CO + HO2 + CXO2	Photolysis
132	CCHO + NO3	HNO3 + CCO3	4.029E+00
133	RCHO + OH	0.034RO2R + 0.001RO2N + 0.965RCO3 + 0.034CO + 0.034CCHO	2.956E+04

Reaction Number	Reactants	Products	k_{298}[1] (ppm^{-n} min^{-1})
134	RCHO	CCHO + RO2R + CO + HO2	Photolysis
135	RCHO + NO3	HNO3 + RCO3	5.423E+00
136	ACET + OH	HCHO + CCO3 + R2O2	2.841E+02
137	ACET	CCO3 + CXO2	Photolysis
138	MEK + OH	0.37RO2R + 0.042RO2N + 0.616R2O2 + 0.492CCO3 + 0.096RCO3 + 0.115HCHO + 0.482CCHO + 0.37RCHO	1.742E+03
139	MEK	CCO3 + CCHO + RO2R	Photolysis
140	MEOH + OH	HCHO + HO2	1.351E+03
141	COOH + OH	0.35HCHO + 0.35OH + 0.65CXO2	8.114E+03
142	COOH	HCHO + HO2 + OH	Photolysis
143	ROOH + OH	RCHO + 0.34RO2R + 0.66OH	1.626E+04
144	ROOH	RCHO + HO2 + OH	Photolysis
145	GLY	2CO + 2HO2	Photolysis
146	GLY	HCHO + CO	Photolysis
147	GLY + OH	0.63HO2 + 1.26CO + 0.37RCO3	1.626E+04
148	GLY + NO3	HNO3 + 0.63HO2 + 1.26CO + 0.37RCO3	1.425E+00
149	MGLY	HO2 + CO + CCO3	Photolysis
150	MGLY + OH	CO + CCO3	2.217E+04
151	MGLY + NO3	HNO3 + CO + CCO3	3.586E+00
152	BACL	2CCO3	Photolysis
153	PHEN + OH	0.24BZO + 0.76RO2R + 0.23GLY	3.887E+04
154	PHEN + NO3	HNO3 + BZO	5.586E+03
155	CRES + OH	0.24BZO + 0.76RO2R + 0.23MGLY	6.207E+04
156	CRES + NO3	HNO3 + BZO	2.025E+04
157	NPHE + NO3	HNO3 + BZNO	5.586E+03
158	BALD + OH	BZCO	1.906E+04
159	BALD		Photolysis
160	BALD + NO3	HNO3 + BZCO	3.869E+00
161	METH + OH	0.5RO2R + 0.416CO + 0.084HCHO + 0.416MEK + 0.084MGLY + 0.5MCO3	4.964E+04
162	METH + O3	0.008HO2 + 0.1RO2R + 0.208OH + 0.1RCO3 + 0.45CO + 0.2HCHO + 0.9MGLY + 0.333HC2H	1.671E-03
163	METH + NO3	0.5HNO3 + 0.5RO2R + 0.5CO + 0.5MCO3 + 0.5XN	6.764E+00
164	METH + O	RCHO	9.369E+03
165	METH	0.34HO2 + 0.33RO2R + 0.33OH + 0.67CCO3 + 0.67CO + 0.67HCHO + 0.33MCO3	Photolysis
166	MVK + OH	0.3RO2R + 0.025RO2N + 0.675R2O2 + 0.675CCO3 + 0.3HCHO + 0.675RCHO + 0.3MGLY	2.797E+04
167	MVK + O3	0.064HO2 + 0.05RO2R + 0.164OH + 0.05RCO3 + 0.475CO + 0.1HCHO + 0.95MGLY + 0.351HC2H	6.768E-03
168	MVK + O	0.45RCHO + 0.55MEK	6.384E+03
169	MVK	0.3CXO2 + 0.7CO + 0.7PROD + 0.3MCO3	Photolysis
170	ISPD + OH	0.67RO2R + 0.041RO2N + 0.289MCO3 + 0.336CO + 0.055HCHO + 0.129CCHO + 0.013RCHO + 0.15MEK + 0.332PROD + 0.15GLY + 0.174MGLY	9.147E+04
171	ISPD + O3	0.4HO2 + 0.048RO2R + 0.048RCO3 + 0.285OH + 0.498CO + 0.125HCHO + 0.047CCHO + 0.21MEK + 0.023GLY + 0.742MGLY + 0.1HC2H + 0.372RC2H	6.177E-03
172	ISPD + NO3	0.799RO2R + 0.051RO2N + 0.15MCO3 + 0.572CO + 0.15HNO3 + 0.227HCHO + 0.218RCHO + 0.008MGLY + 0.572RNO3 + 0.278XN	1.478E+02
173	ISPD	1.233HO2 + 0.467CCO3 + 0.3RCO3 + 1.233CO + 0.3HCHO + 0.467CCHO + 0.233MEK	Photolysis
174	PROD + OH	0.379HO2 + 0.473RO2R + 0.07RO2N + 0.029CCO3 + 0.049RCO3 + 0.213HCHO + 0.084CCHO + 0.558RCHO + 0.115MEK + 0.329PROD	2.217E+04
175	PROD	0.96RO2R + 0.04RO2N + 0.515R2O2 + 0.667CCO3 + 0.333RCO3 + 0.506HCHO + 0.246CCHO + 0.71RCHO	Photolysis
176	RNO3 + OH	0.338NO2 + 0.113HO2 + 0.376RO2R + 0.173RO2N + 0.596R2O2 + 0.01HCHO + 0.439CCHO + 0.213RCHO + 0.006ACET + 0.177MEK + 0.048PROD + 0.31RNO3 + 0.352XN	1.153E+04
177	RNO3	NO2 + 0.341HO2 + 0.564RO2R + 0.095RO2N + 0.152R2O2 + 0.134HCHO + 0.431CCHO + 0.147RCHO + 0.02ACET + 0.243MEK + 0.435PROD	Photolysis
178	DCB1 + OH	RCHO + RO2R + CO	7.389E+04
179	DCB1 + O3	1.5HO2 + 0.5OH + 1.5CO + GLY	2.956E-03
180	DCB2 + OH	R2O2 + RCHO + CCO3	7.389E+04
181	DCB2	RO2R + 0.5CCO3 + 0.5HO2 + CO + R2O2 + 0.5GLY + 0.5MGLY	Photolysis
182	DCB3 + OH	R2O2 + RCHO + CCO3	7.389E+04
183	DCB3	RO2R + 0.5CCO3 + 0.5HO2 + CO + R2O2 + 0.5GLY + 0.5MGLY	Photolysis

Reaction Number	Reactants	Products	k_{298}[1] (ppm^{-n} min^{-1})
184	CH4 + OH	CXO2	9.405E+00
185	ETHE + OH	RO2R + 1.61HCHO + 0.195CCHO	1.259E+04
186	ETHE + O3	0.12OH + 0.12HO2 + 0.5CO + HCHO + 0.37HC2H	2.347E-03
187	ETHE + NO3	RO2R + RCHO + XN	3.023E-01
188	ETHE + O	0.5HO2 + 0.2RO2R + 0.3CXO2 + 0.491CO + 0.191HCHO + 0.25CCHO + 0.009GLY	1.077E+03
189	ISOP + OH	0.907RO2R + 0.093RO2N + 0.079R2O2 + 0.624HCHO + 0.23METH + 0.32MVK + 0.357ISPD	1.451E+05
190	ISOP + O3	0.266OH + 0.066RO2R + 0.008RO2N + 0.126R2O2 + 0.192MCO3 + 0.275CO + 0.592HCHO + 0.1PROD + 0.39METH + 0.16MVK + 0.204HC2H + 0.15RC2H	1.898E-02
191	ISOP + NO3	0.187NO2 + 0.749RO2R + 0.064RO2N + 0.187R2O2 + 0.936ISPD + 0.813RNO3	9.962E+02
192	ISOP + O	0.01RO2N + 0.24R2O2 + 0.25CXO2 + 0.24MCO3 + 0.24HCHO + 0.75PROD	5.320E+04
193	TERP + OH	0.75RO2R + 0.25RO2N + 0.5R2O2 + 0.276HCHO + 0.474RCHO + 0.276PROD	1.222E+05
194	TERP + O3	0.567OH + 0.033HO2 + 0.031RO2R + 0.18RO2N + 0.729R2O2 + 0.123CCO3 + 0.201RCO3 + 0.157CO + 0.235HCHO + 0.205RCHO + 0.13ACET + 0.276PROD + 0.001GLY + 0.031BACL + 0.103HC2H + 0.189RC2H	1.014E-01
195	TERP + NO3	0.474NO2 + 0.276RO2R + 0.25RO2N + 0.75R2O2 + 0.474RCHO + 0.276RNO3 + 0.25XN	9.718E+03
196	TERP + O	0.147RCHO + 0.853PROD	4.832E+04
197	ALK1 + OH	RO2R + CCHO	3.754E+02
198	ALK2 + OH	0.246OH + 0.121HO2 + 0.612RO2R + 0.021RO2N + 0.16CO + 0.039HCHO + 0.155RCHO + 0.417ACET + 0.248GLY + 0.121HC2H	1.533E+03
199	ALK3 + OH	0.695RO2R + 0.07RO2N + 0.559R2O2 + 0.236TBUO + 0.026HCHO + 0.445CCHO + 0.122RCHO + 0.024ACET + 0.332MEK	3.516E+03
200	ALK4 + OH	0.835RO2R + 0.143RO2N + 0.936R2O2 + 0.011CXO2 + 0.011CCO3 + 0.002CO + 0.024HCHO + 0.455CCHO + 0.244RCHO + 0.452ACET + 0.11MEK + 0.125PROD	6.488E+03
201	ALK5 + OH	0.653RO2R + 0.347RO2N + 0.948R2O2 + 0.026HCHO + 0.099CCHO + 0.204RCHO + 0.072ACET + 0.089MEK + 0.417PROD	1.378E+04
202	ARO1 + OH	0.224HO2 + 0.765RO2R + 0.011RO2N + 0.055PROD + 0.118GLY + 0.119MGLY + 0.017PHEN + 0.207CRES + 0.059BALD + 0.491DCB1 + 0.108DCB2 + 0.051DCB3	8.796E+03
203	ARO2 + OH	0.187HO2 + 0.804RO2R + 0.009RO2N + 0.097GLY + 0.287MGLY + 0.087BACL + 0.187CRES + 0.05BALD + 0.561DCB1 + 0.099DCB2 + 0.093DCB3	3.901E+04
204	OLE1 + OH	0.91RO2R + 0.09RO2N + 0.205R2O2 + 0.732HCHO + 0.294CCHO + 0.497RCHO + 0.005ACET + 0.119PROD	4.772E+04
205	OLE1 + O3	0.155OH + 0.056HO2 + 0.022RO2R + 0.001RO2N + 0.076CXO2 + 0.345CO + 0.5HCHO + 0.154CCHO + 0.363RCHO + 0.001ACET + 0.215PROD + 0.185HC2H + 0.05CO2H + 0.119RC2H	1.574E-02
206	OLE1 + NO3	0.824RO2R + 0.176RO2N + 0.488R2O2 + 0.009CCHO + 0.037RCHO + 0.024ACET + 0.511RNO3 + 0.489XN	1.863E+01
207	OLE1 + O	0.45RCHO + 0.437MEK + 0.113PROD	7.211E+03
208	OLE2 + OH	0.918RO2R + 0.082RO2N + 0.001R2O2 + 0.244HCHO + 0.732CCHO + 0.511RCHO + 0.127ACET + 0.072MEK + 0.061BALD + 0.025METH + 0.025ISPD	9.342E+04
209	OLE2 + O3	0.378OH + 0.003HO2 + 0.033RO2R + 0.002RO2N + 0.137R2O2 + 0.197CXO2 + 0.137CCO3 + 0.006RCO3 + 0.265CO + 0.269HCHO + 0.456CCHO + 0.305RCHO + 0.045ACET + 0.026MEK + 0.006PROD + 0.042BALD + 0.026METH + 0.073HC2H + 0.129CO2H + 0.303RC2H	1.577E-01
210	OLE2 + NO3	0.391NO2 + 0.442RO2R + 0.136RO2N + 0.711R2O2 + 0.03CXO2 + 0.079HCHO + 0.507CCHO + 0.151RCHO + 0.102ACET + 0.001MEK + 0.015BALD + 0.048MVK + 0.321RNO3 + 0.288XN	1.073E+03
211	OLE2 + O	0.013HO2 + 0.012RO2R + 0.001RO2N + 0.012CO + 0.069RCHO + 0.659MEK + 0.259PROD + 0.012METH	3.089E+04

Notes:

[1] Rate constants are shown for 298 K and 1 atmosphere in units of ppm and minutes. See the CAMx chemistry parameters file for the temperature and pressure dependencies (Section 5).

Table 3-5. Species in the SAPRC99 mechanism (Mechanism 5).

Species Name	Description
NO2	Nitrogen dioxide
NO	Nitric oxide
O	Ozone
O3	Oxygen atom in the O^3(P) electronic state
NO3	Nitrate radical
N2O5	Dinitrogen pentoxide
HNO3	Nitric acid
O1D	Oxygen atom in the O^1(D) electronic state
OH	Hydroxyl radical
HONO	Nitrous acid
HO2	Hydroperoxy radical
CO	Carbon monoxide
HNO4	Peroxynitric acid
HO2H	Hydrogen peroxide
SO2	Sulfur dioxide
SULF	Sulfuric acid (gaseous)
CXO2	Methylperoxy radical
HCHO	Formaldehyde
COOH	Formic acid
MEOH	Methanol
RO2R	Organic peroxy radical converting NO to NO2 with HO2 production
ROOH	Organic hydroperoxide
R2O2	Organic peroxy radical converting NO to NO2
RO2N	Organic peroxy radical converting NO to organic nitrate
RNO3	Organic nitrate
MEK	Methylethyl ketone
PROD	Organic product
CCO3	Acetylperoxy radical
PAN	Peroxyacetyl nitrate
CO3H	Peroxyacetic acid
CO2H	Acetic acid
RCO3	Higher acylperoxy radical (based on propylperoxy)
PAN2	Higher peroxyacetyl nitrate (based on peroxypropyl nitrate)
CCHO	Acetaldehyde
RC3H	Higher percarboxylic acid
RC2H	Higher carboxylic acid
BZCO	Peroxybenxoyl radical
PBZN	Peroxybenzoyl nitrate
BZO	Phenoxy radical
MCO3	Peroxyacyl radical from methacrolein
MPAN	PAN compound from methacrolein
TBUO	Tertiary-butoxy radical
ACET	Acetone
NPHE	Nitrophenol
PHEN	Phenol
BZNO	Nitrophenol reaction product
XN	Other nitrogen containing product
HCO3	Adduct from HO2 plus formaldehyde
HC2H	Formic acid
RCHO	Higher aldehyde (based on propionaldehyde)
GLY	Glyoxal
MGLY	Methylglyoxal
BACL	Biacetyl
CRES	Cresol

Species Name	Description
BALD	Benzaldehyde
METH	Methacrolein
MVK	Methylvinyl ketone
ISPD	Isoprene product
DCB1	Aromatic ring opening dicarbonyl product
DCB2	Aromatic ring opening dicarbonyl product
DCB3	Aromatic ring opening dicarbonyl product
ETHE	Ethene
ISOP	Isoprene
TERP	Terpene
ALK1	Lumped alkane 1
ALK2	Lumped alkane 2
ALK3	Lumped alkane 3
ALK4	Lumped alkane 4
ALK5	Lumped alkane 5
ARO1	Lumped aromatic 1
ARO2	Lumped aromatic 2
OLE1	Lumped olefin 1
OLE2	Lumped olefin 2

Table 3-6. Properties of VOC species in the SAPRC99 mechanism: average carbon numbers, molecular weights and k_{OH} values ($ppm^{-1}min^{-1}$).

Species	Molecular Weight	Carbon Number	Average k_{OH}[1]
ALK1	46.81	1.88	375
ALK2	47.02	2.65	1,533
ALK3	57.72	2.92	3,516
ALK4	73.23	4.36	6,488
ALK5	106.97	6.42	13,784
ETHE	28.05	2	
OLE1	61.68	3.99	47,720
OLE2	79.05	5.67	93,422
ISOP	68.12	5	
TERP	136.24	10	122,170
ARO1	100.47	7.27	8,796
ARO2	113.93	8.58	39,013
HCHO	30.03	1	
CCHO	44.05	2	
RCHO	67.32	3.66	
BALD	108.21	7.15	
ACET	58.08	3	
MEK	72.82	4.03	
PRD2	106.44	6.48	
MEOH	32.04	1	
GLY	58.04	2	
MGLY	72.06	3	
BACL	101.31	6.37	
PHEN	94.11	6	
CRES	115.38	7.52	
MACR	56.06	3	
MVK	112.17	7	
IPRD	70.45	4.03	

Notes:

[1] k_{OH} values are given to assist in assigning VOC species to SAPRC99 lumped species.

Table 3-7. Reactions and rate constants for the CB4/chlorine mechanism.

Reaction Number	Reactants	Products	k_{298}[1] (ppm^{-n} min^{-1})
97	CL2	2 CL	Photolysis
98	HOCL	OH + CL	Photolysis
99	CL + O3	CLO + O2	1.779E+04
100	CLO + NO	CL + NO2	2.449E+04
101	CLO + HO2	HOCL + O2	7.314E+03
102	CL + PAR	HCL + 0.87 XO2 + 0.13 XO2N + 0.11 RCHO + 0.76 ROR - 0.11 PAR	9.383E+04
103	CL + OLE	FMCL + RCHO + 2 XO2 + HO2 - PAR	8.400E+05
104[2]	CL	HCL + XO2 + FORM + HO2	2.816E+02
105	CL + ETH	FORM + 2 XO2 + FMCL + HO2	1.502E+05
106	CL + ISOP	0.15 HCL + XO2 + HO2 + 0.28 ICL1	6.642E+05
107	OH + ICL1	ICL2	2.804E+04
108	CL + BUTA	XO2 + HO2 + 0.7 BCL1	6.199E+05
109	OH + BCL1	BCL2	5.314E+04
110	CLO + CLO	0.3 CL2 + 1.4 CL	2.410E+01

Notes:

[1] Rate constants are shown for 298 K and 1 atmosphere in units of ppm and minutes; see the CAMx "Mechanism 1" chemistry parameters file for the temperature and pressure dependencies.

[2] Reaction 104 implicitly assumes 1.85 ppm of methane in the rate constant.

Table 3-8. Species added for the CB4/chlorine mechanism.

Species Name	Description
CL2	Molecular chlorine
HOCL	Hypochlorous acid
CL	Chlorine atom
CLO	Chlorine monoxide
ICL1	Unique product of CL + isoprene reaction
ICL2	Reaction product of ICL1
BUTA	1,3-Butadiene
BCL1	Unique product of CL + 1,3-butadiene reaction
BCL2	Reaction product of BCL1

Effects of Clouds

Photolysis rates can be significantly affected by the presence of clouds. CAMx treats the impact of clouds on photolysis based upon the RADM approach (Chang, et al., 1987). This approach requires information on cloud optical depth for each cell. Optical depth is used to scale down photolysis rates for layers within or below clouds to account for UV attenuation, or to scale up the rates for layers above clouds to account for UV reflection. The older UAM-V approach for scaling photolysis rates is no longer supported since CAMx version 4.00.

The adjustment to clear-sky photolysis rates is given by

$$J = \left[1 + F_c\left(A_c - 1\right)\right] J_{clear}$$

where A_c is the vertical cloud attenuation factor. This factor is calculated separately for above clouds and within/below clouds:

$$A_c = 1 + \left(1 - t_r\right)\cos\varphi, \qquad \textit{above cloud layer}$$
$$A_c = 1.6\, t_r \cos\varphi, \qquad \textit{within / below cloud layer}$$

where φ is solar zenith angle ($\leq 60°$) and t_r is the energy transmission coefficient for normally incident light. For zenith angles greater than 60°, values for A_c at $\varphi = 60°$ are used. The expression for the energy transmission coefficient is derived from delta-Eddington theory and is given by

$$t_r = \frac{5 - e^{-t}}{4 + 3\tau\left(1 - f\right)}$$

where f is a scattering phase function asymmetry factor, given by Chang et al. (1987) as 0.86, and τ is total cloud optical depth above the current grid cell to the top of the troposphere. For optically thin clouds ($\tau < 5$), no adjustment is made to the photolysis rates. Gridded cloud optical depth fields are provided in the CAMx cloud/rain file. Optical depth can be approximated by

$$\tau = \frac{3 L \Delta z_c}{2 \rho_w r}$$

where L is the mean cloud liquid water in the cell (g/m^3), Δz_c is the cloud depth in the cell, ρ_w is the density of liquid water (10^6 g/m^3), and r is the mean cloud drop radius (10^{-5} m).

Effects of Surface Albedo

Photolysis rates also depend the amount of solar radiation reflected from the earth's surface (albedo). The CAMx albedo/haze/ozone column (AHO) input file specifies the UV albedo for each grid cell. The UV-albedo generally is calculated from land cover data using characteristic values by land cover type as shown in Table 5-5. This approach results in UV albedos that fall in the range 0.04 to 0.08 and are constant in time, because the land cover data are constant in time. Analyses of reflected UV radiation recorded in TOMS satellite data

(Herman and Celarier, 1997) report similar UV albedo values in the range 0.02-0.08 for surfaces not covered by snow.

Snow is much more reflective than other types of surfaces and so snow cover will enhance the rates of photolysis reactions. Since most photolysis reactions depend upon ultra-violet radiation it is important to characterize the effect of snow cover on UV albedo. Measurements of the UV albedo for Antarctic snow report values of 0.96 to 0.98 over a wide range of snow grain sizes and solar zenith angles. However, these high values should be considered an upper limit to the reflectivity of snow-covered surfaces at the scale of grid cells because snow may not cover all surface features (e.g., in forests and urban areas) and because the snow may be dirty. For areas with snow cover, TOMS climatology shows surface albedos spanning a wide range of values from 0.2 to nearly 1.0. Potential reasons for this wide range of values include coarse resolution (1° latitude by 1.25° longitude) such that snow-covered and snow-free surfaces are combined, differences between rough and smooth land cover types (e.g., forest vs. open range land), and differences between clean and dirty snow.

CAMx assigns the highest albedo value included in the AHO and photolysis rate input files for snow covered grid cells. The AHO and photolysis rate input files classify grid cells to one of five albedo ranges. When providing snow-cover data to CAMx, the fifth (highest) albedo range should be assigned a value representative of snow and the lower four albedo ranges should represent surfaces without snow-cover. We recommend a UV albedo of 0.5 for snow-covered surfaces because this is in the middle of the range reported by Herman and Celarier (1997) and because grid cells should be defined as snow-covered if the fractional cover is greater than 0.5.

Gas-Phase Chemistry Solvers

Numerically integrating (solving) the time evolution of the gas phase chemistry is typically the most "expensive" part of a photochemical grid model simulation for ozone (aerosol phase chemistry is even more expensive but the discussion that follows is for gas-phase simulation of ozone). For example, in the EPA UAM, the gas-phase chemistry consumes about 85% of the model CPU time. Thus, the efficiency of the chemistry solver is the dominant factor in determining the overall efficiency of a grid model. The most accurate solution methods available are the "Gear" type implicit solvers (Gear, 1971) such as LSODE (Hindmarsh, 1983). Gear solvers are stable when applied to "stiff" problems, such as gas phase chemistry, but they are impractically slow for grid model applications. Sun et al. (1994) developed an implicit-explicit hybrid (IEH) method based on LSODE that is accurate and moderately fast. Chock et al. (1994) evaluated several other widely used numerical methods against LSODE and IEH, but found that none of the methods that were faster than IEH were very accurate. Consequently, a new chemistry solver was developed for CAMx with two objectives: (1) increased efficiency and (2) increased flexibility (see the discussion of flexibility under chemical mechanism compiler, below).

Three chemistry solver options are available in CAMx, the IEH solver of Sun et al. (1994), the CMC fast solver, and LSODE. The CMC fast solver is about three times faster than the IEH solver. Solutions from the IEH and CMC solvers are very similar for daytime conditions, but differ at night. The accuracy of the CMC fast solver is an improvement over

many commonly used solvers (e.g., the QSSA solver; Hesstvedt et al., 1978) and is adequate for all CAMx applications. The availability of the IEH solver option provides a way for User's to evaluate the CMC solver performance and provides an alternative for User's who choose to accept longer run-times.

The CMC fast chemistry solver uses a hybrid numerical approach to solve the gas-phase chemistry. The fastest reacting species (the radicals) are solved using the steady state approximation, i.e., it is assumed that their concentrations are fully equilibrated, and determined by, the slower reacting (state) species. This is a good approximation for the radicals because their chemical lifetimes are very short compared to the model timesteps. The solution for the radicals uses a semi-implicit numerical method that accurately accounts for the strong couplings between radical species concentrations. Radicals are not transported by the model advection because their lifetimes are so short that transport is negligible.[1] The radicals are re-calculated at equilibrium with the remaining (state) species each time chemistry is performed. The state species are divided into two groups: fast state species with chemical lifetimes of seconds to a few minutes, and slow state species with longer chemical lifetimes. The fast state species are solved using a second order implicit Runge-Kutta method (see, for example, Lambert, 1973) and the slow state species are solved explicitly. If necessary, chemistry time steps are sub-divided for the solution of the fast state species to obtain an accurate solution. The solutions for the radicals and slow state species are continually updated to remain synchronous with the solution of the fast state species.

The species NO, NO_2, and O_3 are always considered fast state species. PAN is either considered fast or slow depending upon whether it's concentration is greater or less than 1% of NO_2, respectively. Since the number of fast species is variable based on the chemical condition, this method is referred to as an "adaptive hybrid method" (Guthrie et al., 1995).

The accuracy of the CMC solver has been evaluated in a box model by comparison to results for a Gear solver (the Gear solver results are considered an accurate benchmark, as discussed above). The Gear solver used was LSODE. Results are shown in Figure 3-1 and 3-2 for two representative conditions:

1) An initial VOC:NO_X ratio of 3:1 with no emissions

2) An initial VOC:NO_X ratio of 14:1 with subsequent continuous emissions of VOC and NO_X also at a 14:1 ratio.

In both figures, the lines show the Gear solver result and the symbols show the CMC solver result. Results are shown for several key species that also represent the three groups of species used in the CMC solver: steady state, fast state and slow state species. NO, NO_2, and O_3 are important for ozone modeling and are treated as fast state species by the CMC solver; OH is equally important and is treated as a steady state species; FORM and ALD2 are important sources of radicals and are treated as slow state species by the CMC solver. Agreement for all species is excellent in both tests.

[1] NO_3 is an exception to this because the mass of NO_3 may be significant. The mass of nitrogen in NO_3 and N_2O_5 is transported using the counter species NXOY.

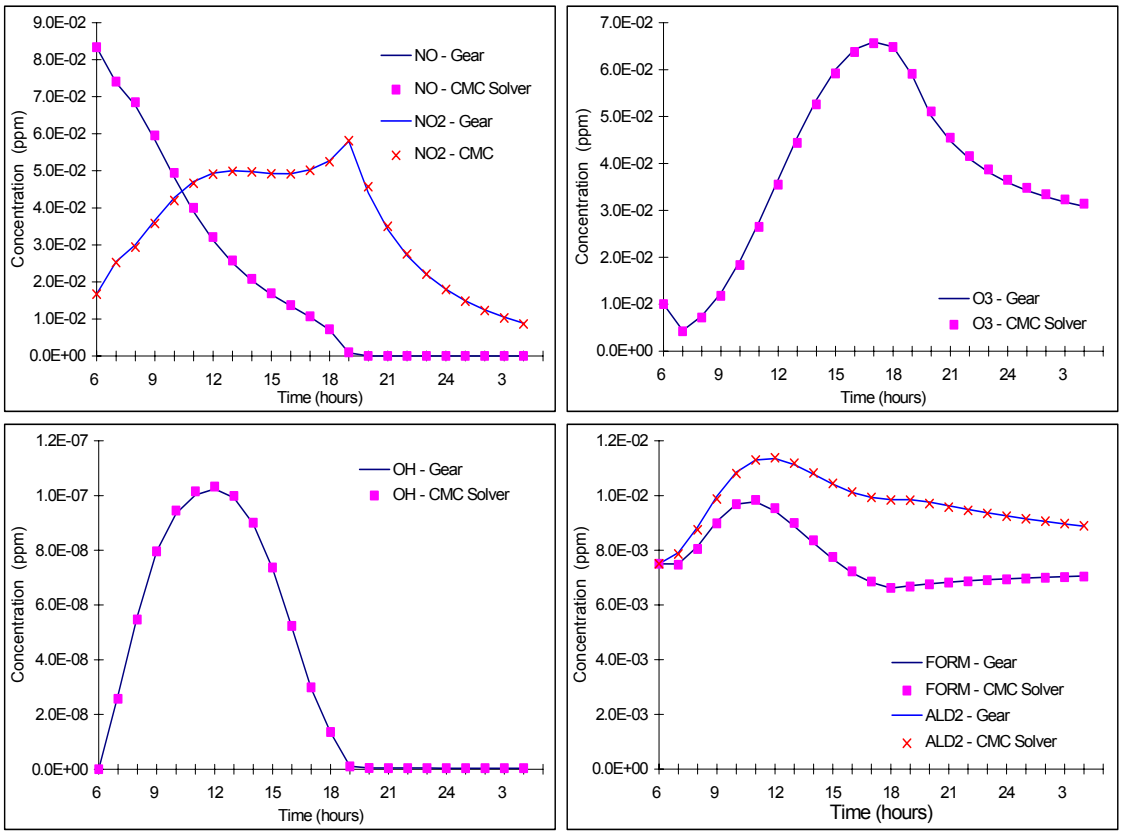

Figure 3-1. Comparison of CMC solver and Gear solver (LSODE) results for VOC:NOx ratio of 3:1 with no emissions.

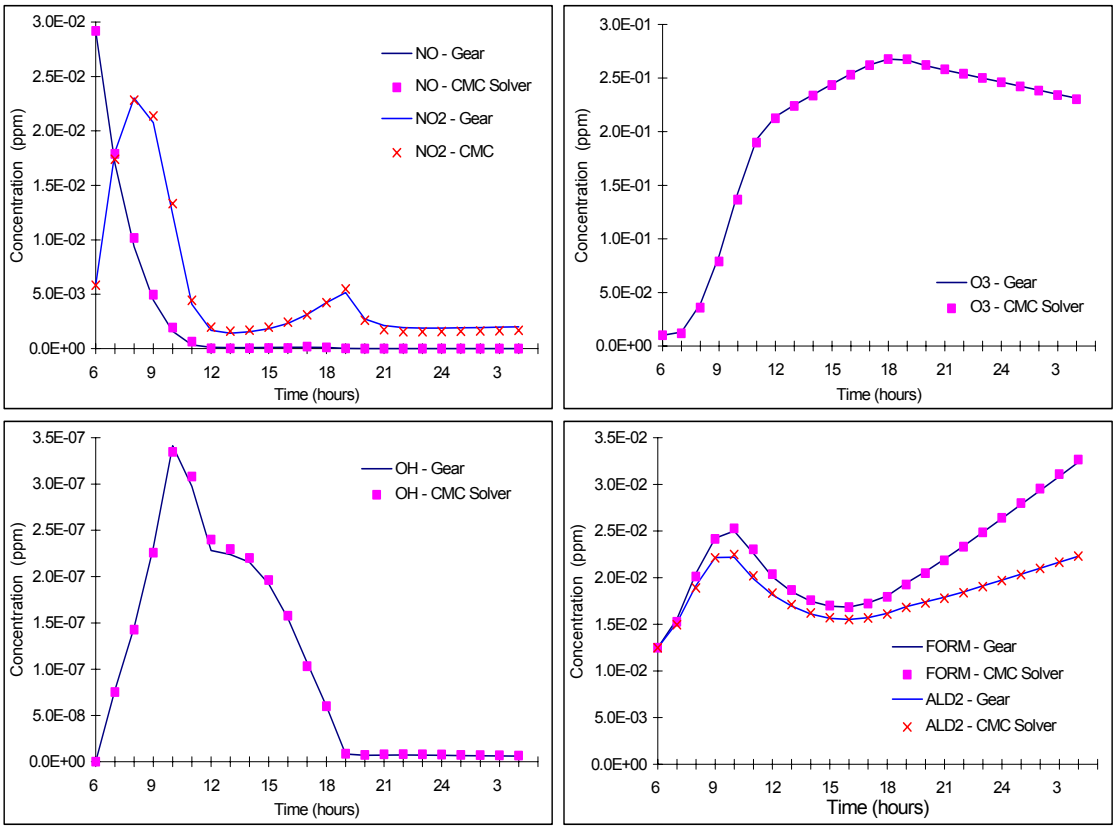

Figure 3-2. Comparison of CMC solver and Gear solver (LSODE) results for VOC:NOx ratio of 14:1 with continuous emissions.

Chemical Mechanism Compiler

A practical limitation of many chemistry solvers for photochemical grid models has been that the solver is coded by hand for a single mechanism. This means that any non-trivial change to the mechanism requires time consuming manual re-coding of the solver followed by careful testing to assure that the re-coding is free of errors. In contrast, the CAMx chemistry solver is prepared by a pre-processor program called the Chemical Mechanism Compiler (CMC). The CMC reads an ASCII file that lists the reactions for the mechanism and then prepares FORTRAN subroutines that are ready to be linked into the CAMx chemistry solver. This automation means that changes to the mechanism can be made quickly and with a high degree of confidence that they are correctly implemented. Another advantage of this design is that several mechanisms can be implemented in the model in parallel allowing the user to switch between mechanisms simply by changing a model input (the CHEMPARAM file, discussed in Section 5). The CMC pre-processor is not supplied with CAMx, so users interested in using mechanisms other than those supplied with the model should contact ENVIRON.

3.2 AEROSOL CHEMISTRY

CAMx includes model structures to treat aerosol chemistry. Aerosol processes are currently linked to the CB4 gas-phase chemical mechanism and are selected by choosing Mechanism 4 (Table 3-1). Aerosol processes will be linked to SAPRC99 in a future release. Mechanism 4 provides two options for treating aerosol size distributions: the CF scheme and CMU scheme. The CF scheme divides the size distribution into two static modes (coarse and fine). Primary species are modeled as fine and/or coarse particles, while all secondary species are modeled as fine particles. The CMU scheme employs a sectional approach that dynamically models the size evolution of each aerosol constituent among a number of fixed size sections. The user defines the number of size sections and their size ranges in the chemistry parameters file (Section 5). Aerosol water is explicitly treated in both CF and CMU options; it affects aerosol size and density.

The gas-phase chemistry for Mechanism 4 is based on Mechanism 3 with the following extensions:

1) A biogenic olefin species (OLE2) is added to represent terpenes. To use the OLE2 species, prepare your biogenic emissions the same way as for Mechanism 3 but rename the CB4 OLE emissions (representing terpenes) to OLE2.
2) Five condensable organic gas species (CG1- CG5) are added as secondary organic aerosol (SOA) precursors. CG1-CG3 and CG5 are formed from anthropogenic VOCs and CG4 is formed from terpenes (OLE2).
3) Ammonia is added as a precursor for inorganic aerosol.
4) Hydrogen chloride (HCl) is added as a product of acidified sea salt aerosol.
5) Seventeen additional inorganic chemistry reactions are added that are most important for regional/annual ozone, PM, mercury and toxics modeling.
6) Rate expressions for gas-phase reactions 26, 36, 51 and 82 are updated to explicitly include pressure dependence.

7) The rate for reaction 83 is set to zero. This reaction was used in the UAM to represent heterogeneous SO_2 to sulfate conversion but now should be set to zero because aqueous chemistry is explicitly handled.
8) The rate for reaction 18 ($N_2O_5 + H_2O -> 2\ HO_3$) is reduced to a value that is consistent with just the known gas-phase processes (Mentel, Bleilebens and Wahner, 1996). There is evidence for a heterogeneous pathway to this reaction, but there continues to be considerable uncertainty in how to model the heterogeneous pathway.

The gas-phase photochemistry in Mechanism 4 forms aerosol precursors via the OH initiated oxidation of SO_2 to sulfate, production of nitric acid, and formation of condensible organic gasses. These aerosol precursors are supplied to either the CF or CMU version of the aerosol chemistry algorithm, both of which operate on a unique aerosol "coupling" time step that is defined within the Mechanism 4 chemistry parameters file (see Section 5). By default, the aerosol coupling time step is 15 minutes, and this is used for all grids in a simulation regardless of the grid-specific driving time step. The CF and CMU aerosol chemistry algorithms both perform the following three processes:

1) Aqueous sulfate and nitrate formation in resolved cloud water using the RADM aqueous chemistry algorithm (Chang et al., 1987).
2) Partitioning of condensible organic gases (CG1-CG5) to secondary organic aerosols (SOA1-SOA5) to form a condensed "organic solution phase" using a semi-volatile, equilibrium scheme called SOAP (Strader et al., 1999).
3) Partitioning of inorganic aerosol constituents (sulfate, nitrate, ammonium, sodium, and chloride) between the gas and particle phases using the ISORROPIA thermodynamic module (Nenes et al., 1998, 1999).

The aqueous chemistry does not treat sub-grid scale clouds; clouds are assumed to either occupy the entirety of a grid cell volume, or be completely absent from it. Cloudy grid cells are determined by cloud liquid water contents above a threshold of 0.05 g/m^3.

The yields and properties of the condensible organic gases (CGs) are shown in Table 3-9. The CG yields are expressed as ppm of aerosol precursor formed per ppm of VOC reacted so that CG concentrations follow the CAMx convention for gasses and are in ppm. The secondary organic aerosols (SOAs) formed from the CGs are in units of $\mu g/m^3$ as are all other aerosol species.

Table 3-10 shows the aerosol species that can be run with the CF scheme. Note that certain species must be present for this scheme (as shown by the X for "Mandatory Species") as they are intimately tied to the gas-phase chemistry. The other species are optional (meaning that they can be removed from the chemistry parameters input file), except that both sodium and chloride must always be present together if they are to be run (i.e., one cannot be present without the other). If sodium and chloride are not modeled then default background values are used within CAMx.

In the CMU scheme, CRST is used to identify all primary inert material, which replaces the CF species of FPRM, FCRS, CPRM, and CCRS in Table 3-10. Individual aerosol species names specify both the constituent and the size section using the following naming convention, e.g., PSO4_1 refers to particle sulfate in the section 1.

Table 3-9. Properties of condensable organic gasses (CG1 – CG5) that are precursors to secondary organic aerosols (SOA1 – SOA5).

CB4 VOC Precursor	Condensable Gas Species	Aerosol Yield (ppm/ppm)	Saturation Concentration ($\mu g\ m^{-3}$ at 281.5 K)	Heat of vaporization ($J\ mole^{-1}$)	Molecular Weight ($g\ mole^{-1}$)
PAR	CG3	0.0024	0.007	0	150
TOL	CG1	0.07	0.023	156250	150
TOL	CG2	0.137	0.674	156250	150
XYL	CG1	0.044	0.023	156250	150
XYL	CG2	0.192	0.674	156250	150
CRES	CG5	0.036	0.007	0	150
OLE2	CG4	0.136	0.008	0	180

Table 3-10. List of PM species carried by CAMx Mechanism 4 (CF).

Internal Label	Name	Mandatory Species
PSO4	Sulfate	X
PNO3	Particulate Nitrate	X
PNH4	Particulate Ammonium	X
PH2O	Aerosol Water Content	X
SOA1-5	Five Secondary Organic Aerosols	X
NA	Sodium	
PCL	Particulate Chloride	
POA	Primary Organic Aerosol	
PEC	Primary Elemental Carbon	
FPRM	Fine Other Primary (<2.5 µm)	
FCRS	Fine Crustal (<2.5 µm)	
CPRM	Coarse Other Primary	
CCRS	Coarse Crustal	

The use of the underscore character to separate the constituent and section is compatible with using PAVE for post-processing because PAVE does not interpret the underscore as part of a formula. The CMU scheme requires that the complete list of all aerosol species be present in the chemistry parameters file (i.e., none of the specific aerosol species are optional).

Alternatively, only the gas-phase chemistry portion of Mechanism 4 may be run by simply omitting the entire list of aerosol species in the chemistry parameters file (see Section 5).

Aerosol Sectional Approach

Unlike the CF scheme, where each species is represented by a single particle size, the CMU scheme institutes an additional step to distribute the bulk aerosol concentrations from the aqueous/aerosol chemistry modules into each size bin.

For inorganic aerosol species, ISORROPIA yields the bulk aerosol composition at equilibrium. The aerosol size distribution is then determined by distributing the change in aerosol mass during the time step into each size bin using a weighting factor (Pandis et al., 1993). The fraction $f_{i,k}$ of total flux of species i between gas and aerosol phases that condenses onto or evaporates from an aerosol size section k is given by,

$$f_{i,k} = \frac{2\pi N_k d_k D_i \left(c_i - c_i^{eq}\right)/\left(\beta_k + 1\right)}{\sum_k 2\pi N_k d_k D_i \left(c_i - c_i^{eq}\right)/\left(\beta_k + 1\right)},$$

where N_k and d_k are the number and mean diameter of particles in the section k, respectively, D_i, c_i, and c_i^{eq} are the diffusivity, bulk gas-phase concentration, and equilibrium concentration at the particle surface of species i, respectively, $\beta_k = 2\lambda/ad_k$, λ is the mean free path of air, and a is the accommodation coefficient (Pandis et al., 1993). Assuming that c_i^{eq} is independent of particle size, the fraction is reduced to,

$$f_{i,k} = \frac{N_k d_k/\left(\beta_k + 1\right)}{\sum_k N_k d_k/\left(\beta_k + 1\right)} = f_k .$$

The above weighting factor then depends on the surface area only.

For organic aerosols, SOAP calculates the bulk equilibrium composition. Using the pseudo-ideal solution assumption (Strader et al., 1999), the effect of chemical composition of the particle can be incorporated into the weighting factor:

$$f_{i,k} = \frac{N_k d_k \left(c_i - x_{i,k} c_i^*\right)/\left(\beta_k + 1\right)}{\sum_k N_k d_k \left(c_i - x_{i,k} c_i^*\right)/\left(\beta_k + 1\right)} .$$

where $x_{i,k}$ is the mole fraction of species i in the section k and c_i^* is the effective saturation concentration of species i. Since the fraction determines the composition of each size section, the above equation should be solved iteratively at each time step. Assuming that the chemical composition changes slowly during a time step, however, the mole fractions can be approximated with those from the previous time step (Koo et al., 2003).

For cloud/fog droplets, RADM is used to calculate sulfate and nitrate formation in the bulk aqueous phase. The added mass is then distributed into each size bin by a weighting factor which is based on the size-resolved aqueous chemistry model simulation results (Fahey and Pandis, 2001).

In addition, mathematical descriptions of nucleation and coagulation have been added to the CMU scheme. The nucleation model employs the nucleation rate parameterization proposed by Russell et al. (1994). The model assumes a linear sulfuric acid vapor concentration variation for the given time step of the aerosol module based on the initially available sulfuric acid and assigns all the nucleated mass to the first section of the distribution. The coagulation

rate of the aerosol particles is modeled according to Seinfeld and Pandis (1998). A high-resolution distribution is used for the coagulation calculations by subdividing each section of the original distribution into 3 additional sections.

Additional Inorganic Reactions

CAMx v4.20 introduces 17 additional inorganic chemistry reactions to Mechanism 4 (Table 3-11). The added reactions are *unimportant* for smog chamber conditions (high NOx levels, 1-day experiments, room temperature and pressure) but potentially important for regional and annual modeling conditions (lower NOx levels, multi-day simulations, low temperatures and pressures). Hence, the new inorganic reactions improve the science in the mechanism without creating inconsistency with the evaluation of the CB4 against smog chamber data. They are appropriate for inclusion in any condensed chemical mechanism being used for regional ozone and regional/annual PM, visibility, mercury, and toxics modeling.

Table 3-11. Reactions added in CAMx Mechanism 4, noting those that are included in SAPRC99.

Number	Reaction	Included in SAPRC99
101	O1D + H2 = OH + HO2	
102	OH + H2 = HO2	Yes
103	OH + O = HO2	
104	OH + OH = O	
105	OH + OH = H2O2	
106	HO2 + O = OH	
107	H2O2 + O = OH + HO2	
108	NO3 + O = NO2	
109	NO3 + OH = HO2 + NO2	Yes
110	NO3 + HO2 = HNO3	Yes
111	NO3 + O3 = NO2	
112	NO3 + NO3 = 2 NO2	Yes
113	PAN = C2O3 + NO2	
114	HNO3 = OH + NO2	Yes
115	N2O5 = NO2 + NO3	
116	NTR = NO2 + XO2	Yes
117	PNA = 0.61 HO2 + 0.61 NO + 0.39 OH + 0.39 NO2	Yes

The extended inorganic reactions are summarized as follows:

- Reactions of molecular hydrogen (101 and 102) are somewhat important to odd-hydrogen (OH and HO_2) for very dry conditions in the upper troposphere. Including hydrogen allows the air quality impacts of hydrogen as an alternative fuel to be evaluated. Currently, hydrogen is included in CAMx with a constant atmospheric concentration of 0.6 ppm (Novelli et al, 1999).
- Odd-oxygen reactions (103 to 107) may be important for pristine conditions such as the upper troposphere. Including these reactions provides a more complete description of

hydroxyl radical (OH) chemistry in the upper troposphere to improve modeling for persistent air toxics and mercury.

- Additional NO_3 radical reactions (108 to 112) improve nighttime chemistry. The NO_3 radical is the main driver for atmospheric chemistry at night and including additional NO_3 removal reactions improves the calculation of nighttime destruction rates for several types of reactive hydrocarbons (e.g., aldehydes, olefins) and for NOx (via NO_3 and N_2O_5 reactions).
- NOx recycling reactions (113 to 117) improve the representation of the fate of NOx over multi-day timescales. These are all photolysis reactions that occur quite slowly in the troposphere. Reactions 113, 115 and 117 are only important for very cold conditions such as the upper troposphere where corresponding thermal decomposition reactions are slow. Reactions 114 and 116, photolysis of nitric acid and organic nitrates, are important to regional ozone and oxidant chemistry in the lower troposphere (Zaveri and Peters, 1999). These "NOx recycling reactions" slowly recycle nitrogen from an inactive form (NOz) to an active form (NOx).

The impacts of these additional inorganic reactions were evaluated using three LADCO/ MRPO modeling databases. Overall, the updated mechanism increased regional levels of ozone, improving model performance, yet did not significantly change PM concentrations. The higher regional ozone is due to the NOx recycling reactions, specifically the photolysis of organic nitrates and nitric acid that are included in other mechanisms such as SAPRC99 (Carter, 2000) and CBM-Z (Zaveri and Peters, 1999). The effect of these NOx recycling reactions partially explains why SAPRC99 tends to predict higher regional ozone than CB4. Zaveri and Peters (1999) also concluded that including photolysis of organic nitrates would increase regional ozone predictions.

The impacts of the additional reactions on PM are highlighted below:

- PM nitrate and sulfate was higher in summer, consistent with slightly higher oxidant levels that slightly accelerate the oxidation of NOx and SO_2;
- Adding the NOx recycling reactions that convert a small amount of nitric acid back to NOx did not reduce PM nitrate. This is because only a small amount of nitric acid is recycled and the change in oxidant levels is the dominant effect.
- PM ammonium increased slightly along with the PM sulfate and nitrate increases.
- Changes in PM sulfate/nitrate/ammonium were smaller in winter than summer because oxidant production is much less active in winter. In winter, oxidant levels are determined mainly by tropospheric background (i.e., CAMx boundary conditions) rather than photochemistry within CAMx.
- There were small decreases in SOA – the chemical reaction updates did not alter any reactions that produce SOA so differences must be due to differences in the oxidants that trigger SOA formation, possibly small spatial and/or temporal shifts.

3.3 MERCURY CHEMISTRY

Mercury exists in the atmosphere as elemental mercury, Hg(0), and oxidized mercury, Hg(II) (Schroeder and Munthe, 1998). Hg(II) can be inorganic (e.g., mercuric chloride, $HgCl_2$) or organic (e.g., methyl mercury, MeHg). It can also be present as particulate mercury (e.g.,

mercuric oxide, HgO, or mercury sulfide, HgS). In the global atmosphere, Hg(0) is the dominant form. Hg(II) typically constitutes a few percent of total mercury and is predominantly in the gas phase. MeHg concentrations in the atmosphere are negligible, about a factor of 10 to 30 lower than Hg(II) concentrations, based on analysis of precipitation samples conducted by Frontier Geosciences, Inc. (e.g., Seigneur et al., 1998). However, Hg(II) becomes methylated in water bodies, where it can bioaccumulate in the food chain. Hg(0) is sparingly soluble and is not removed significantly by wet deposition; its dry deposition velocity is also believed to be low. As a result, Hg(0) has a long atmospheric lifetime, on the order of several months, that is governed by its oxidation to Hg(II). On the other hand, Hg(II) is quite soluble; it is consequently removed rapidly by wet and dry deposition processes. Particulate mercury, Hg(p), is mostly present in the fine fraction of particulate matter ($PM_{2.5}$), although some Hg(p) may be present in coarse PM (e.g., Landis and Keeler, 2002).

Known transformations among inorganic mercury species include the gas-phase oxidation of Hg(0) to Hg(II), the aqueous-phase oxidation of Hg(0) to Hg(II), the aqueous-phase reduction of Hg(II) to Hg(0), various aqueous-phase equilibria of Hg(II) species and the aqueous-phase adsorption of Hg(II) to PM. The inorganic mercury chemistry modules implemented in CAMx are based on our current knowledge of these transformations. However, it should be noted that our knowledge of mercury chemistry continues to evolve as new laboratory data become available, and the Hg chemical kinetic mechanisms in CAMx and other models that treat the atmospheric fate of mercury will need to be revised accordingly.

Below, we provide additional details on the gas- and aqueous-phase mercury chemistry mechanisms implemented in CAMx, and the implementation approach.

Gas-Phase Chemistry

The gas-phase transformations include the oxidation of Hg(0) to Hg(II) by ozone (O_3) (Hall, 1995), hydrogen chloride (HCl) (Hall and Bloom, 1993), hydrogen peroxide (H_2O_2) (Tokos et al., 1998), molecular chlorine (Cl_2) (Ariya et al., 2002), and hydroxyl radicals (OH) (Sommar et al., 2001):

$$Hg(0)\,(g) + O_3\,(g) \rightarrow Hg(II)\,(g),\ k = 3 \times 10^{-20}\ cm^3\ molec^{-1}s^{-1}$$
$$Hg(0)\,(g) + HCl\,(g) \rightarrow HgCl_2\,(g),\ k = 1 \times 10^{-19}\ cm^3\ molec^{-1}s^{-1}$$
$$Hg(0)\,(g) + H_2O_2\,(g) \rightarrow Hg(OH)_2\,(g),\ k = 8.5 \times 10^{-19}\ cm^3\ molec^{-1}s^{-1}$$
$$Hg(0)\,(g) + Cl_2\,(g) \rightarrow HgCl_2\,(g),\ k = 2.6 \times 10^{-18}\ cm^3\ molec^{-1}s^{-1}$$
$$Hg(0)\,(g) + OH\,(g) \rightarrow Hg(OH)_2\,(g),\ k = 8 \times 10^{-14}\ cm^3\ molec^{-1}s^{-1}$$

The reaction rate constants provided above are for temperatures in the range of 20 to 25°C; no temperature dependence information is available.

Aqueous-Phase Chemistry

The aqueous-phase chemistry includes the reduction of Hg(II) to Hg(0) via reaction with hydroperoxy radicals (HO_2) and by the formation of the sulfite complexes (at low HCl concentrations), $HgSO_3$ and $Hg(SO_3)_2^{2-}$, as well as the oxidation of Hg(0) to Hg(II) by dissolved O_3, OH, and Cl_2. Adsorption of Hg(II) species on atmospheric particulate matter (PM) is simulated using an adsorption coefficient ($K = 34$ L g^{-1}) recommended by Seigneur et al. (1998). The relevant reactions are listed below. Note that the gas-liquid equilibria and ionic equilibria of the non-mercury species (e.g., SO_2, O_3) involved in the mercury aqueous-phase chemistry are not shown here, since they are identical to those in the other CAMx mechansims.

Gas-liquid Equilibria

$Hg(0)\,(g) \Leftrightarrow Hg(0)\,(aq)$, $K = 0.11$ M atm^{-1}, Sanemasa, 1975; Clever et al., 1985
$HgCl_2\,(g) \Leftrightarrow HgCl_2\,(aq)$, $K = 1.4 \times 10^6$ M atm^{-1}, Lindqvist and Rodhe, 1985
$Hg(OH)_2\,(g) \Leftrightarrow Hg(OH)_2\,(aq)$, $K = 1.2 \times 10^4$ M atm^{-1}, Lindqvist and Rodhe, 1985

The Henry's Law constants listed above are for temperatures in the range of 20 to 25°C. Temperature dependence information is available for the Hg(0) Henry's Law constant but the validity of this information for temperatures below 0°C is not established.

Aqueous-phase Equilibria

$HgCl_2\,(aq) \Leftrightarrow Hg^{2+} + 2Cl^-$, $K = 10^{-14}$ M^2, Sillen and Martel, 1964
$Hg(OH)_2\,(aq) \Leftrightarrow Hg^{2+} + 2OH^-$, $K = 10^{-22}$ M^2, Sillen and Martel, 1964
$Hg^{2+} + SO_3^{2-} \Leftrightarrow HgSO_3$, $K = 2.1 \times 10^{13}$ M^{-1}, van Loon et al., 2001
$HgSO_3 + SO_3^{2-} \Leftrightarrow Hg(SO_3)_2^{2-}$, $K = 1 \times 10^{10}$ M^{-1}, van Loon et al., 2001

Adsorption of Hg(II) on PM

$Hg(II)\,(aq) \Leftrightarrow H(II)\,(p)$, $K = 34$ L g^{-1}, Seigneur et al., 1998

Aqueous-phase Kinetics

$Hg(0)\,(aq) + O_3\,(aq) \rightarrow Hg^{2+}$, $k = 4.7 \times 10^7$ $M^{-1}s^{-1}$, Munthe, 1992
$Hg(0)\,(aq) + OH\,(aq) \rightarrow Hg^{2+}$, $k = 2 \times 10^9$ $M^{-1}s^{-1}$, Lin and Pehkonen, 1997
$HgSO_3\,(aq) \rightarrow Hg(0)\,(aq)$, $k = 0.0106$ s^{-1}, van Loon et al., 2000
$Hg(II)\,(aq) + HO_2\,(aq) \rightarrow Hg(0)\,(aq)$, $k = 1.7 \times 10^4$ $M^{-1}s^{-1}$, Pehkonen and Lin, 1998
$Hg(0)\,(aq) + HOCl\,(aq) \rightarrow Hg^{2+}$, $k = 2.09 \times 10^6$ $M^{-1}s^{-1}$, Lin and Pehkonen, 1998
$Hg(0)\,(aq) + OCl^- \rightarrow Hg^{2+}$, $k = 1.99 \times 10^6$ $M^{-1}s^{-1}$, Lin and Pehkonen, 1998

In the last two reactions listed above, HOCl and OCl^- come from the dissolution and subsequent dissociation of molecular chlorine (Cl_2). Note that Hg(II) (aq) refers to all divalent Hg species in solution (i.e., Hg^{2+} + $HgCl_2(aq)$ + $Hg(OH)_2(aq)$ + $HgSO_3$ + $Hg(SO_3)_2^{2-}$).

The rate constants listed for the aqueous-phase kinetics are for temperatures in the range of 20 to 25°C. Temperature dependence information is available for the $HgSO_3$ reduction reaction.

As mentioned previously, the gas- and aqueous-phase Hg transformations presented above represent the current state of the science (Ryaboshapko et al., 2002; Seigneur et al., 2001a, 2003a), but our knowledge of mercury chemistry continues to evolve. For example, Gardfeldt and Johnson (2003) have recently challenged the aqueous-phase reduction of Hg(II) to Hg(0) by dissolved HO_2, suggesting that this pathway is unimportant. There also seems to be some circumstantial evidence of reduction of Hg(II) to Hg(0) in power plant plumes from various experimental studies that is not accounted for in current treatments of Hg chemistry (e.g., Edgerton et al., 2001; Seigneur et al., 2001b). Additional details are provided in a recent scoping study for mercury deposition conducted for the Midwest Regional Planning Organization by Seigneur et al. (2003b).

Implementation Approach

The approach used to implement the mercury transformation pathways, discussed above, into CAMx is based on the assumption that the mercury species concentrations are much smaller than those of the species with which they react. Thus, the concentrations of the non-mercury species can be assumed to be constant during the mercury chemistry calculations and analytical solutions are available for both the gas-phase and aqueous-phase conversions.

The mercury chemistry discussed in the previous sections requires the concentrations of the following non-mercury species: O_3, H_2O_2, OH, SO_2, HO_2, Cl_2, HCl, and atmospheric particulate matter (PM). The concentrations of most of these species are available from CAMx. However, Cl_2 and HCl are not explicitly simulated because the emissions data required to model these species are generally inadequate or unavailable. Thus, we specify typical vertical profiles of HCl and Cl_2 concentrations. The Cl_2 concentrations are prescribed to be non-zero over oceans and zero elsewhere. Also, daytime Cl_2 concentrations are lower than nighttime values to account for the fact that Cl_2 is photolyzed during the day. The zenith angle is used for the determination of night/day. A 2-D array of integer values (1 if ocean, 0 if not) is used to determine if the grid column is predominantly over ocean. This array is initialized at the beginning of the simulation from an input file and is specific for the modeling domain and grid.

The mercury aqueous-phase chemistry module also requires the specification of cloud liquid water content (LWC) and cloudwater pH. Both these variables are available from CAMx – the mercury aqueous-phase chemistry module is invoked after the CAMx PM aqueous-phase chemistry calculations are performed, so the cloudwater pH has already been calculated. Note that the PM aqueous-phase module (based on the RADM aqueous-phase chemistry module that is also used in Models-3/CMAQ) does not explicitly simulate the cloud chemistry of OH and HO_2 radicals. The concentrations of these radicals can be reduced by their heterogeneous

chemistry within clouds (e.g., Jacob, 2000; Jaegle et al., 2001). In the CAMx implementation, we account for this by reducing the concentrations of OH and HO_2 radicals by factors of 2 and 10, respectively.

Chemistry Parameters for Mercury

The mercury chemistry module requires total PM concentrations, so mercury can only be modeled in conjunction with PM chemistry. In CAMx, PM chemistry is modeled using Mechanism 4. Mercury chemistry is selected by invoking Mechanism 4 and including mercury species among the list of modeled species. The CAMx mercury species names are:

HG0 – elemental gaseous mercury, or Hg(0)
HG2 – reactive gaseous mercury, or Hg(II)
HGP – primary particulate mercury, or Hg(P)

CAMx requires that all three or none of these species be included in a simulation. Therefore, mercury chemistry is not required for PM modeling, but if mercury chemistry is selected then all three mercury species must be modeled. All of the rate constants and equilibrium constants for the mercury chemistry module are hard-coded and so no mercury reaction rate data are included in the chemistry parameters input file (see Section 5). This is similar to the RADM aqueous chemistry and ISORROPIA inorganic aerosol equilibrium modules.

Several physical properties of the mercury species must be specified on the chemistry parameters file (see Figure 5-2a). The physical properties specified for the gas species (Henry's Law, molecular diffusivity, surface reactivity) influence the deposition characteristics. The Henry constant for HG2 is assumed to be similar to that of HNO_3 because these two gases have similar solubility. The HG2 species represents $HgCl_2$ and $Hg(OH)_2$. The Henry constant for the former is 1.4E+06 M atm-1 and for the latter it is 1.2E+04 M atm^{-1}. The Henry constant used for HNO_3 is 2.0E+05 M atm^{-1} and is within this range. No temperature dependence is assumed for the HG2 Henry constant because there is no information available to determine this. The molecular diffusivity ratio for HG2 was calculated as the average for $HgCl_2$ and $Hg(OH)_2$. The surface reactivity parameter is set to zero for strong acids, such as HNO_3, that have a strong tendency to stick to surfaces. Setting the surface reactivity to zero overrides the surface resistance calculated in the Wesely (1989) deposition algorithm and forces the surface resistance to zero. The reactivity parameter for HG2 is set to 1 so that surface resistance will be calculated based on the Henry constant using Wesely's algorithm.

The dry deposition of HG0 is set to zero by choosing a very low Henry constant (similar to CO). This is based on the assumption that background emissions and dry deposition of HG0 balance each other over the modeling domain. This assumption is justified by the fact that the atmospheric lifetime of HG0 (about 1 year) greatly exceeds its residence time (days to weeks) within a regional modeling domain. Since background emissions of HG0 are not included in the mercury emissions inventory, this means that the dry deposition of HG0 should be ignored. In CAMx, setting a Henry constant of smaller the 1.0E-08 M atm^{-1} results in zero dry and wet deposition for the species. The HG0 Henry constant is set to 1.0E-10 M atm^{-1}.

3.4 SIMPLE CHEMISTRY VIA MECHANISM 10

CAMx offers 5 different chemical mechanisms for ozone and particulate matter modeling. However, the minimum level of chemistry is the CB4 mechanism for ozone with 36 species and 91 reactions. Using CB4 requires significant effort to prepare all of the input data, particularly with regard to emissions. There are many cases when air pollution problems could be investigated with a much simpler chemistry scheme. An example of this would include modeling SO_2 from a few specific sources over a relatively small region, and treating conversion to sulfate by assuming a representative decay rate. An approach was necessary to provide a simple and flexible scheme that can be used for modeling chemical reactions other than the ozone or secondary PM reactions treated by the full-science mechanisms.

The new simple chemistry scheme is selected by specifying a mechanism ID of 10 in the chemistry parameters input file. The specific chemical reactions to be modeled must be set in the subroutine `chem10.f`, which resides in the main source code directory. The user must modify this subroutine to implement whatever reactions are desired. Follow the guidelines for implementing reactions that are included in the subroutine. This approach requires some knowledge from the user, but also provides complete flexibility in implementing reactions.

The simple chemistry has been tested using a modeling database for primary PM species in Cairo, Egypt (Mr. Usama Faramawy, personal communication, Egyptian Environmental Affairs Agency). Results of the tests are shown in Figures 3-3 and 3-4. A simple chemical reaction was implemented where the species PMT decayed to PM2 with a first-order rate constant of 10% per hour. These species were selected because PMT has high emissions and PM2 has low emissions. This modeling is not intended to represent any actual chemical reactions for PM species in Cairo, but rather is just a hypothetical testing scenario. The expected result is that the chemical reaction will lower the concentration of PMT and raise the concentration of PM2. Figure 3-3 shows the expected result, that the PMT concentration is lowered by the reaction. The reduction in PMT becomes proportionately greater at longer downwind distances because there has been more time for reaction to take place. Figure 3-4 shows the complementary increase in PM2 due to chemical production.

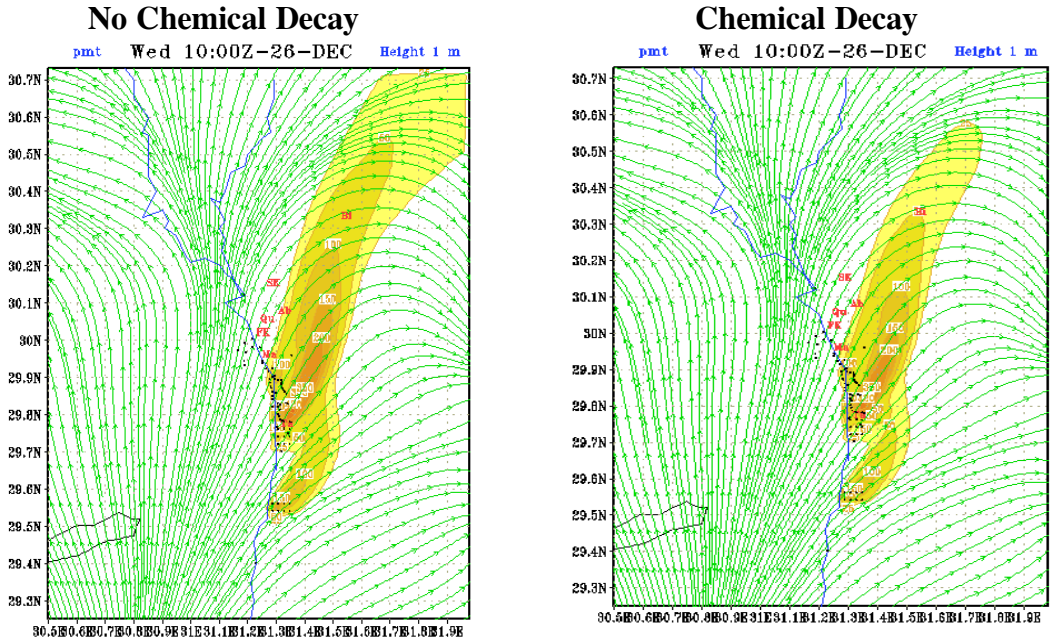

Figure 3-3. Impact of chemical decay on the concentration of the donor species PMT.

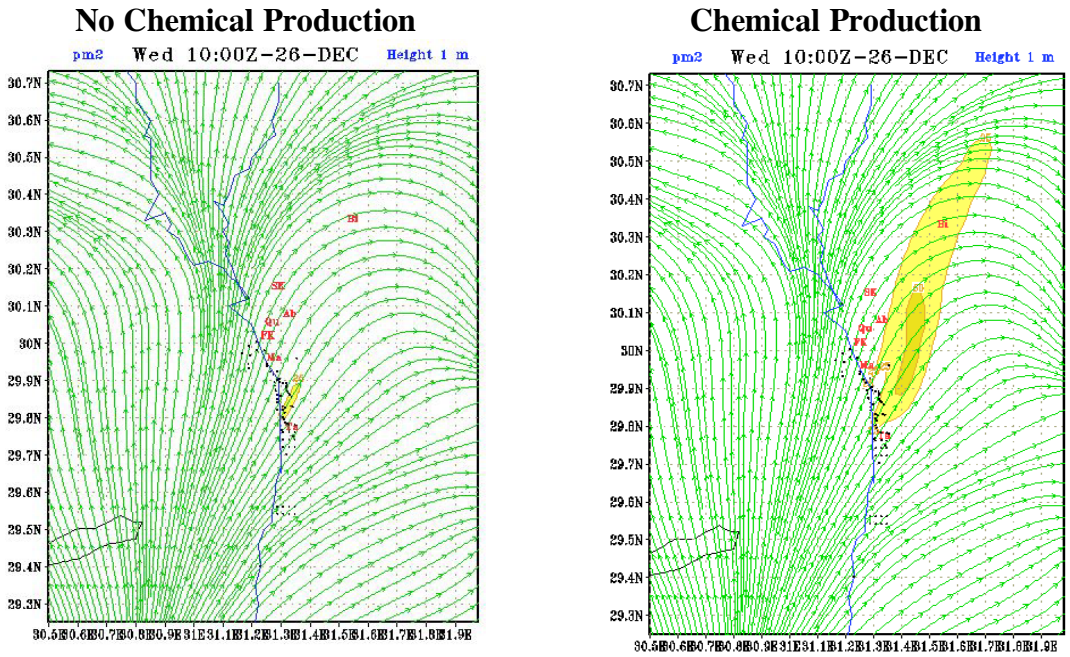

Figure 3-4. Impact of chemical production on the concentration of the recipient species PM2.

4. PLUME-IN-GRID SUBMODEL

Practical and theoretical considerations suggest that the lower limit on horizontal grid spacing is about 1000 meters for Eulerian air quality models such as CAMx. However, finer resolution may be needed to adequately simulate chemistry within concentrated point source plumes that are much smaller than the grid spacing. To deal with such subgrid scale processes, many state-of-the-science Eulerian models contain a Plume-in-Grid sub-model that tracks individual plume segments (or puffs) in a Lagrangian sense, accounting for dispersion and chemical evolution, until such time as puff mass can be adequately represented within the larger grid model framework. It is important to understand that the inclusion of a Lagrangian puff model within an Eulerian grid model is a forced construct. The formulations of the two modeling approaches are fundamentally different and there is no theoretically "correct" methodology. This explains the variety of methods that have been developed through the years.

Two CAMx Plume-in-Grid (PiG) approaches are available that provide different levels of chemical complexity. Both approaches share common design features for puff initialization, basic puff structure, transport, and growth. They deviate in their chemical complexity, certain structural details, and how/when they transfer mass from puffs to grid cells. This section details the structure and functionality of both options.

The first (and original) PiG approach is aimed at treating the near-source chemical evolution of large NO_x point sources when just a few inorganic gas-phase reactions are operative. The method is called the Greatly Reduced Execution and Simplified Dynamics (GREASD) PiG, and it is much faster and structurally simpler than other approaches. The streamlining employed in this version was based upon our experiences in developing, utilizing, and studying the responses of more detailed PiG algorithms for large NOx plumes. The GREASD PiG model works with the Ozone Source Apportionment Technology (OSAT). This is possible because of the simplified approach used in GREASD PiG and because compatibility with OSAT was an explicit design objective. GREASD PiG does not include any PM treatment.

The second (and newest) approach treats the full suite of gas-phase photochemistry for all types of point sources and so by necessity incorporates much more complexity than the first. This CAMx plume treatment is called the Incremental Reactions for Organics and NOx (IRON) PiG. Chemical processes are simulated within each plume segment using an "incremental chemistry" approach, whereby puffs carry the incremental contributions of the puff relative to the grid concentrations. Incremental puff concentrations can be positive or negative, depending upon the species and stage of plume evolution. A similar chemistry approach is used in the SCICHEM Lagrangian model (EPRI, 2000). The approach lends itself to incorporating chemistry for particulates as well. However, the incremental chemistry technique, along with the puff-grid mass transfer constructs, are sufficiently complex as to prohibit the implementation of source apportionment Probing Tools within IRON PiG.

4.1 CAMx PiG FORMULATION

Basic Puff Structure and Diffusive Growth

Both GREASD and IRON PiG sub-models share a common basic structure and growth algorithm. A stream of plume segments (puffs) is released from a designated point source. Each puff possesses a longitudinal length and directional orientation defined by the separation of a leading and a trailing point. Initial separation of these points is determined by the wind vector at final plume rise, and each point is then subsequently and independently transported through the gridded wind fields. Like other puff models, the shape of each puff is characterized by a spread tensor, which is defined from a set of Gaussian standard deviations (so-called "sigmas") along the three spatial axes (σ_x, σ_y, σ_z). Diffusive growth is defined by the growth in these sigma values.

We have developed an explicit solution approach for puff growth that shares SCICHEM theory and concepts (EPRI, 2000), but includes some simplifications. SCICHEM solves predictive spatial moment equations with second-order closure that relate the evolution of the puff spread tensor ($\sigma_{ij}=\sigma_i\times\sigma_j$) to resolved mean shears and turbulent velocity statistics. The Reynolds-averaged second-moment transport equation is given as

$$\frac{d\sigma_{ij}}{dt} = \sigma_{ik}\frac{\partial \overline{u}_j}{\partial x_k} + \sigma_{jk}\frac{\partial \overline{u}_i}{\partial x_k} + \frac{\left\langle x_i' \overline{u_j' c'} \right\rangle}{Q} + \frac{\left\langle x_j' \overline{u_i' c'} \right\rangle}{Q}$$

where $\overline{u}$ is the mean wind vector component, the primed values represent turbulent fluctuations from the mean, and the angle brackets denote integrals over space. The Reynolds averaging process always introduces higher-order fluctuation correlations, and this is given by the turbulent flux moments $\left\langle x'\overline{u'c'}\right\rangle$, where $\overline{u'c'}$ represents the turbulent flux of concentration. It is these last two diffusion terms that SCICHEM solves in it's second-order closer scheme.

For sub-puff scale turbulence, SCICHEM employs the restriction that the only off-diagonal component of $\left\langle x'\overline{u'c'}\right\rangle$ to be considered is the symmetric horizontal term ($i=x$, $j=y$), and then only for the large-scale (meso to synoptic) contribution to puff deformation when puff scale reaches such dimensions. In CAMx, we ignore this off-diagonal flux moment term altogether since puff mass is ultimately introduced to the grid when puff size is at the grid scale (1-50 km in practically all applications), and thus puffs never reach spatial scales at which this term becomes important. SCICHEM also makes the assumption that the horizontal turbulence is isotropic, $\left\langle x'\overline{u'c'}\right\rangle = \left\langle y'\overline{v'c'}\right\rangle$. This results in a single diffusivity equation for both x and y directions, and a single diffusivity for the z direction:

$$K_x = K_y = \frac{\left\langle y'\overline{v'c'}\right\rangle}{Q}$$

$$K_z = \frac{\left\langle z'\overline{w'c'}\right\rangle}{Q}$$

In our approach for CAMx, we have adopted the SCICHEM second-order tendency equations to model the time-evolution of puff turbulent flux moments (represented by diffusivities $K_x = K_y$ and K_z) and their contribution to the evolution of puff spread (represented by the diagonal components of the puff spread tensor, $\sigma_x^2 = \sigma_y^2$ and σ_z^2). Note that we ignore the off-diagonal contributions to puff spread, since they are unnecessary in the context of the CAMx PiG. Puff spread is defined for puff depth (σ_z) and puff width (σ_y); the latter is also added to the longitudinal length to allow for diffusive growth along the puff centerline. We account for the effects of wind shears in the evolution of lateral spread, but assume that the evolution of vertical spread is solely the result of turbulent fluxes.

The resulting two Reynolds-averaged second-moment transport equations for CAMx PiG are:

$$\frac{d\sigma_z^2}{dt} = 2K_z$$

$$\frac{d\sigma_y^2}{dt} = 2\sigma_y^2 D + 2\sigma_y\sigma_z\left(\frac{du}{dz}^2 + \frac{dv}{dz}^2\right)^{1/2} + 2K_y$$

where D is deformation of horizontal wind (see Section 2).

The SCICHEM tendency equation for the horizontal turbulent flux moment is

$$\frac{d}{dt}\left\langle y'\overline{v'c'}\right\rangle = Qq^2 - A\frac{q}{\Lambda}\left\langle y'\overline{v'c'}\right\rangle$$

where $A = 0.75$, $q^2 = \overline{v'v'}$, and Λ is the horizontal turbulent length scale. Separate equations are given for two different boundary layer turbulence scales (shear- and buoyancy-produced), such that

$$\left\langle y'\overline{v'c'}\right\rangle = \left\langle y'\overline{v'c'}\right\rangle_{shear} + \left\langle y'\overline{v'c'}\right\rangle_{buoyancy}$$

Within the surface-based boundary layer, the horizontal velocity variance is given by

$$q_{buoyancy}^2 = 0.13\,w_*^2\left[1 + 1.5\exp\left(z/z_i\right)\right]$$

$$q_{shear}^2 = 2.5u_*^2\left(1 - z/z_i\right)$$

where u_* is the friction velocity, w_* is the convective velocity scale, z is height above the surface, and z_i is the height of the surface-based boundary layer. The horizontal turbulent length scale is given by

$$\frac{1}{\Lambda_{shear}^2} = \frac{1}{\left(0.3\,z_i\right)^2} + \frac{1}{\left(0.65\,z\right)^2}$$

$$\Lambda_{buoyancy} = 0.3\,z_i$$

In the stable boundary layer, only the shear components of q^2 and Λ are applied. Above the boundary layer, SCICHEM applies rough approximations for the velocity variance and turbulent length scale: $q^2 = 0.25$ m^2/s^2, and $\Lambda = 1000$ m.

The SCICHEM tendency equation for the vertical turbulent flux moment is

$$\frac{d}{dt}\left\langle z'\overline{w'c'}\right\rangle = A\frac{q_v}{\Lambda_v}\left(QK_z^{eq} - \left\langle z'\overline{w'c'}\right\rangle\right)$$

where $q_v^2 = \overline{w'w'}$, Λ_v is the vertical turbulent length scale, and K_z^{eq} is the equilibrium diffusivity. Whereas a specific equation for K_z^{eq} is formulated for SCICHEM, we have chosen to specify the value of this parameter from the gridded fields of vertical diffusivity in CAMx. Again SCICHEM gives separate equations for shear- and buoyancy-produced turbulence scales.

Within the surface-based boundary layer, the vertical velocity variance is given by

$$q_v^2\Big|_{shear} = 1.5u_*^2\left(1 - z/z_i\right)$$

$$q_v^2\Big|_{buoyancy} = 1.1w_*^2\left(z/z_i\right)^{2/3}\left(1.05 - z/z_i\right)$$

The vertical turbulent length scale for both shear and buoyancy is equal to Λ_{shear} given above for horizontal length scale. Above the boundary layer, SCICHEM again applies rough approximations for the velocity variance and turbulent length scale: $q_v^2 = 0.01$ m^2/s^2, and $\Lambda_v = 10$ m.

The external variables needed by IRON PiG to complete the dispersion calculations include z_i, u_* and w_*. All of these are available from an internal module in CAMx that calculates these boundary layer similarity theory parameters. Thus, no additional parameters are needed to be input to the model.

Puff Transport

A fresh set of new puffs are released from all PiG point sources within the modeling domain for the duration of the smallest time step among the master and all nested grids. The length of each puff is determined by the combination of the mean total wind speed at the height of final plume rise and time step. Limits are placed on maximum extruded length based on half the finest resolution in the given simulation. If winds and time-steps are such that the maximum allowed length is violated, then several puffs are extruded from a given stack per time step. The orientation of the puff length is along the total wind vector. Total puff volume is determined by stack volumetric flow rate in conjunction with growth due to turbulent entrainment following the SCICHEM approach. Initial σ_y and σ_z are explicitly calculated from this entrainment calculation.

Effects of wind divergence on plume deformation are treated in an explicit manner within the CAMx PiG using a "chained puff" approach. Points at the leading and trailing edges of the

puff centerline are individually transported through the gridded wind fields, which directly accounts for puff stretching and changes to centerline orientation due to deforming shears. Since IRON PiG puffs can extend over multiple layers, layer density-weighted average wind components are determined for each endpoint based on the vertical coverage of the puff, and these are used for advection of those points. GREASD PiG puffs are not allowed to expand beyond the depth of the layer in which the center point resides, so only the single layer wind components are used to advect the end points.

The "chain" aspect means that at least initially (as puffs are extruded from the stack) the trailing point of a puff emitted at time t will be the leading point of a puff emitted at time $t+dt$. However, as the puffs are advected downstream, the leading point of one puff will deviate from the trailing point the puff behind it due to evolving puff size and wind fields. Puff volume is conserved in convergent/divergent wind fields. Puff endpoints may move closer together or further apart, in wind fields that are slowing or accelerating downstream. We compute puff end-point separation changes and then adjust puff widths and depths to maintain constant puff volume. The change in computed puff endpoint spacing defines puff length tendencies, then puff depth tendencies are computed from grid-resolved vertical wind shear (dw/dz), and finally we determine the puff width tendencies required to conserve puff volume.

The official "position" of each puff is defined by the center point of each puff between the endpoints. This position defines which grid domain and grid cell the puff resides for the calculation of diffusion and chemistry. This definition holds even if the puff is sufficiently long that the endpoints are in different grid cells (or even different grid domains if near a domain boundary). With our definition for termination when horizontal area approaches grid cell area, the extents of the puff length should not extend across more than two grid cells.

4.2 GREASD PiG

The GREASD PiG is designed for large NOx point sources, where the chemistry is applicable only for early plume life with the intention of simply aging the NOx to mitigate the chemical effects of emitting fresh point source NO directly from the stack to the modeling grid. Therefore, it does not include any VOC chemistry, and so it cannot be used for VOC sources. Also, the physical constructs developed for GREASD PiG force the puffs to transfer their mass to the grid before full photochemical processing can develop.

For chemical calculations, a uniform mass distribution is assumed throughout the entire puff (i.e., concentration equals puff mass divided by puff volume). The total cross-sectional width and depth both extend $\pm 1.5\sigma$ from puff centerline. The limits of $\pm 1.5\sigma$ result in a two-dimensional average concentration that about equals the uniformly mixed concentration assumption. The total longitudinal length is the distance between the puff endpoints $\pm 1.5\sigma_y$. Total volume is calculated using the formula for an ellipsoid.

The GREASD PiG approach recognizes that the most important chemistry within young NO_x-rich point source plumes can be adequately represented by three pathways:

1) NO-NO termolecular reaction producing NO_2;

2) NO_x-O_3 equilibrium via titration; and
3) nitric acid formation via separate nighttime and daytime pathways.

This allows for only four species to be carried within each puff: NO, NO_2, O_3, and HNO_3. Only ozone is entrained during the life of the puff, and all NO_x originates from initial emissions. As ozone is depleted, through any of the reactions described above, the depleted ozone mass is immediately removed from the host grid cell, thereby removing the need to track incremental (puff – grid cell) ozone concentrations. The objective for GREASD PiG is to transfer plume mass to the grid system at about the time when organic chemistry starts to become important. Organic chemistry should be handled on the grid because interactions between multiple sources become important at this point. Kumar and Russell (1996) found that a PiG model with simplified inorganic chemistry produced results that were very similar to full chemistry.

There are two schools of thought regarding the appropriate times at which to transfer puff mass into the host model grid system. The first primarily focuses on the physical size of puffs relative to grid cells. It is assumed that once puffs are large enough to be adequately resolved by a grid, their mass should be added to the host cell. The two principle problems associated with this approach are deciding what the appropriate size criteria are to be, and how to distribute puff mass into the grid system. Almost always, puffs are super-resolved in the vertical long before their widths become commensurate with grid widths. The second school focuses on the chemical maturity of the puffs (Gillani and Pleim, 1996), and the potential performance effects of dumping immature plume mixtures into a grid system. The main problem seen with this approach relates to how chemically mature plume mixtures may be identified within an ever-evolving puff relative to an ever-evolving grid chemistry. Puffs may reach a stage of chemical maturity after very long simulation periods (say 24 hours), however it is unrealistic to assume that puffs will maintain physical coherence over such a long period given the cumulative effects of wind shears and mixing gradients. In summary, neither of the above approaches is completely satisfactory and we strongly believe that further research is needed to develop new approaches to PiG modeling that adequately address both chemical maturity and physical size considerations.

Given the reduced inorganic chemistry of the GREASD PiG, the puff dumping criteria in CAMx is based upon the first approach described above that suggests that puffs should dump when adequately resolved by the grid. However, the GREASD approach acknowledges the problem of super-resolving puffs vertically by employing the following methodology. Each puff is allowed to grow unchecked until its depth, defined by $\pm 1.5\sigma_z$, spans the depth of the current host cell. At this point, the puff is considered to be vertically resolved, and is limited to its current size. Puff NO_x and nitric acid masses are "leaked" from the puff in subsequent time steps at a rate that is linked to its Gaussian shape and the rate at which σ_y and σ_z continue to grow given the current cell conditions. For a puff just reaching this state, the rate of mass leakage is small as the tails of the Gaussian distribution are leaked. As this puff ages further, the rate of leakage increases as the central portion of the Gaussian distribution grows outwards toward the fixed puff edge.

Once the remaining puff NO_x mass leads to a grid concentration increment of 0.1 ppb or less, or it reaches a user-specified maximum age (usually 12-24 hours) all remaining mass is leaked to the host cell and the puff is terminated. However, in an effort to prohibit the potential

sudden introduction of significant NO_x mass to the grid in a single time step, the age-limited puffs undergo increased artificial leakage over a period of about 1-1.5 hours (depending on time step and puff size).

4.3 IRON PiG

The IRON PiG model incorporates several technical advancements. The primary goal was to include a more complete treatment of chemistry in point source pollutant plumes, while secondarily improving puff-grid mass exchange and adding additional features central for treating toxic pollutants not normally carried by the standard CAMx chemical mechanisms. Several approaches have been developed to treat photochemistry within point source plume models. One of the more elegant methodologies is the incremental chemistry idea embodied in the SCICHEM model (EPRI, 2000). However, we found that the implementation of incremental chemistry in SCICHEM is very complex, especially in its handling of the chemistry of overlapping puffs. In adopting this innovative approach for the IRON PiG, it was necessary to reformulate the physical and chemical configuration of the PiG puffs, and to utilize an accurate numerical solution approach based on the LSODE chemical solver.

The Concept of Incremental Chemistry

For a second-order reaction between puff species *A* and *B*, the total reaction rate is the following:

$$R_T = k(P_A)(P_B) \tag{1}$$

where P_A and P_B are the total puff concentrations of each species. The total puff concentrations can be expressed as the sum of the background and puff perturbation concentrations in:

$$P_A = (c_A + C_A)$$

$$P_B = (c_B + C_B)$$

where *C* is the ambient concentration and *c* is the puff increment concentration. Thus the reaction rate is found to be:

$$R_T = k(c_A + C_A)(c_B + C_B)$$

or

$$R_T = k(c_A c_B + C_A c_B + c_A C_B + C_A C_B)$$

If we subtract the rate of change of the background,

$$R_{Ambient} = C_A C_B \tag{2}$$

by assuming that it is explicitly and separately treated by the grid model, we obtain the reaction rate for the puff increments:

$$R_P = k\left(c_A c_B + C_A c_B + c_A C_B\right) \quad (3)$$

Equation 3 is the basis of SCICHEM incremental chemical kinetic solver. One problem with this approach is the mixed terms, $C_A c_B$ and $c_A C_B$. Most chemical solver packages are designed to solve rate equations for total concentration, as in Equation 1. Thus, for the IRON PiG we developed an alternative numerical solution scheme for puff perturbation chemistry. We note that the CAMx chemical solver can be independently applied to the rate equation for total puff concentrations, Equation 1, and to the rate equation for ambient concentrations, Equation 2. By subtraction of the two solutions, we obtain the solution to rate Equation 3. This requires no modification to, and is obviously completely self-consistent with, the CAMx chemical solvers. Once the incremental puff reaction rates are obtained they are applied to the incremental puff mass to calculate the new (adjusted for chemistry) incremental concentrations. These new puff increments are subsequently advected and dispersed by the transport portions of the PiG code.

Puff Constructs For Incremental Chemistry

The IRON PiG sub-model includes three new constructs designed specifically to facilitate the incremental chemistry approach:

- Treatments to handle puff-grid information exchange for puffs spanning multiple model layers;
- The concept of "virtual dumping" to handle the chemical impacts of large puffs that can overlap other puffs within a given grid column;
- The concept of multiple puff "reactor" cells to account for the chemical effects of concentration distributions within each puff.

Each of these are described below.

Puff Layer Spanning

The IRON PiG is designed to chemically processes point source plume mass within streams of puffs until such time that each puff can be adequately resolved on the *horizontal* grid. Unlike the GREASD PiG approach, where the vertical layer structure dictates puff leaking and ultimately termination, the approach in IRON PiG leads to the necessity that puffs be allowed to vertically span multiple grid model layers before they reach horizontal grid scales. This introduces technical implications for defining "background" concentrations and ambient conditions for puff chemistry, as well as for transferring plume incremental mass to the grid. The solution employed in IRON PiG is to:

1) Assume that the vertical distribution of puff concentration is always uniform;
2) Distribute puff mass transfer (via "leaking" and "dumping") to the grid according to the puff fractional coverage across each model layer and by density-weighting; and

3) Determine mean background concentrations and other ambient conditions (e.g., temperature, humidity, etc.) over the puff vertical span via similar fractional layer-density weighting.

IRON PiG puffs are considered to be elliptical in the horizontal, with the minor axis spanning the cross-wind puff width (defined as $\pm 1.5\sigma_y$), and the major axis spanning the along-wind puff length (defined as length $\pm 1.5\sigma_y$ on each end). This is similar to GREASD PiG. However, given the complications associated with multiple layer spanning and mass-weighting of ambient inputs and dumped mass, IRON puffs are rectangular and uniform in the vertical, with total puff depth defined as $\pm 1.5\sigma_z$.

Horizontally, the mean background concentration and ambient conditions are taken from the single host grid column containing each puff center point, even if the puff is large and/or spans a horizontal cell interface.

Puff Overlap and the Idea of Virtual Dumping

The chemical effects of puff overlap were considered to be an important attribute of IRON PiG. However, we wished to maintain a relatively simple approach, while appropriately accounting for the largest probable effects. We assume that the largest effect is the condition in which older expansive puffs span significant fractions of their host grid cell, thereby potentially overlapping all other puffs contained within the same cell. Instead of geometrically determining fractional overlap puff-by-puff, we instead introduce a process that we refer to as "virtual dumping."

For a given grid column, the mass from all puffs determined to be "sufficiently" large are temporarily dumped to the column, distributed according to each puff's vertical layer span, and added together along with the pre-existing grid concentrations. This process is referred to as a "virtual dump" of puff mass to the grid column. The criteria to determine a "sufficiently" large puff is the same that initiates puff mass leaking to the grid (as described below). In this approach, all large puffs contribute to the background chemistry step for other puffs occupying the same grid column. Double-counting of chemistry is avoided by not including a puff's contribution to the background while it's specific background and incremental chemical calculations are performed.

Multiple Puff Reactors

Accounting for full chemistry potentially introduces significant non-linear effects that are highly dependent upon the distribution of pollutant mass within each puff. Especially for ozone, aircraft flights through power plant plumes have often recorded wide concentration variations relative to ambient conditions: within the plume core where NOx remains concentrated, ozone is often depressed and follows NO-NO_2-ozone equilibrium, whereas on plume fringes where NOx is dilute and mixes with ambient VOC, ozone concentrations can exhibit concentration maxima. Past models have accounted for cross-plume chemistry variations through the use of reactors, with approaches ranging from multiple rectangular slabs to concentric shells.

In IRON PiG, the user may select multiple reactors as well to sub-divide the puff. Any number of reactors may be chosen (the default is 1). Multiple reactors simply divide the total puff volume evenly, and the initial mass assignments for newly emitted puffs are made using the standard error function that results in an initial Gaussian-like mass/concentration distribution among the reactors. This provides a mechanism for simulating the differing chemical processing that takes place in various concentration regimes. As the purpose of the reactors is merely to represent the range of photochemical conditions that are likely to occur at various locations within the puff as it undergoes differential shearing and mixing, there is no particular physical orientation assigned to these reactors with respect to each other or to the puff as a whole. Thus, there is no communication (i.e., diffusional mass exchange) between the reactors. The same background concentration chemistry applies to all reactors of a given puff. When puff mass is leaked or dumped, all reactors shed the same relative fraction of mass.

In summary, chemistry is solved for each IRON puff "reactor" in three steps:

1) The layer-mean background (grid + overlapping puff) concentrations and environmental conditions over the volume occupied by the puff are stored and then chemically updated via the LSODE gas-phase chemistry mechanism;
2) The pre-updated mean background concentrations are added to the puff increments and the total concentrations are chemically updated; and
3) The updated results from step 1 are subtracted from the updated results of step 2 to provide the updated incremental concentrations.

An important consequence of this approach is that the incremental puff mass may be positive or negative. For example, a high-NOx puff that is destroying ambient ozone will have negative ozone increments. The puff increments are subsequently advected and dispersed by the transport portions of the IRON PiG code. Note that the updated background concentrations, which include "virtual dumps" of mass from large puffs, are used for reference only in the puff incremental chemistry algorithm; the actual grid concentrations are updated in the grid chemistry routine.

IRON Puff Dumping and PiG Rendering

Mass transfer from puff to grid can happen in two ways: slowly, termed "leaking", or suddenly, termed "dumping." As described earlier, all mass is transferred to the vertical grid structure in a density-weighted fashion according to each puff's fractional layer coverage. The process of leaking ensures that puff mass is transferred to the grid continuously, rather than in discrete lumps of pollutants with very different concentrations than those in the grid. Sudden dumping can cause unphysical numerical shocks in the grid and can lead to unrealistic gridded concentration patterns that appear as "bullseyes". The idea behind puff leakage is to account for turbulent shearing of mass from the main plume and its subsequent dispersion to the grid scale. This rate of transfer should be directly proportional to the puff size relative to the grid scale.

Puff leakage is controlled by comparing the horizontal area of a puff to a specified leakage parameter, defined as a fraction of horizontal grid cell area. When a puff is first emitted there is no leakage. As the puff grows in volume the concentrations within the reactors are reduced accordingly by dilution. When the puff area exceeds the leakage onset parameter, a fraction of the mass in each puff reactor is transferred to the grid. This fraction is determined by the relative exceedance of the leakage parameter; initial leakage is slow as the exceedance is relatively small, but leakage rates grow as the puff continues to grow beyond the leakage parameter.

Like GREASD PiG, the reduced mass from leakage is compensated by a reduced effective volume, so that concentrations are not artificially diluted by leakage (an essential chemical imperative). Thus, two distinct volumes are tracked: the actual volume (defined by the puff spread sigmas) and the effective volume. While these are identical before leakage, they obviously deviate after leakage is initiated, and thereafter the relative deformation of the actual puff volume (via diffusion, shearing, etc.) is used to scale the deformation of effective puff volume.

Eventually the horizontal span of the puff will exceed the grid cell area, and the remaining mass is then dumped all at once to the grid. However, because of the combination of photochemical processing and leakage, by the time a puff dumps the potential for producing numerical shocks is much reduced. Furthermore, if the puff exceeds a user-defined maximum age, puff mass is transferred to the grid at the rate of 10% per timestep (as in GREASD PiG).

While the mass confined to the puffs at any given time has not yet affected the grid concentrations, it will eventually, so it can be somewhat misleading not to include it in visualizations of a model simulation. The puff mass can be optionally incorporated into the model average output files for visualization purposes (referred to as "PiG rendering"). Rendering employs a "virtual dump" of the puff masses into the average concentration array each time step. As described for chemistry, virtual puff mass is added as an increment over the entire grid column according to fractional layer-density weighting over puff depth, thus diluting it's concentrations relative to that within the puff. The actual puff mass remains within the puffs over the course of their lifetimes. It should be noted that this visualization is available for 3-D average output files, and can produce some rather startling effects in output displays, including very narrow virtual plumes, or streaks, representing mass moving through the grid in sub-grid puffs, but not subject to grid-scale eddy diffusion.

4.4 PiG CONFIGURATION

Invoking the CAMx PiG sub-model is controlled by keywords in the CAMx control file (`CAMx.in`), as described in Section 5. The choices are:

```
PiG_Submodel  = 'NONE',
PiG_Submodel  = 'GREASD',
PiG_Submodel  = 'IRON',
```

Several new parameters have been added with the introduction of IRON PiG. It is important to note that all PiG configuration parameters exist in the CAMx Fortran parameters file

(./Inc/camx.prm), as described in Section 11. PiG parameters are grouped together and briefly described at the end of that file. By effectively configuring the PiG submodel in the code, the default PiG configuration (as recommended by the model developers) is preset within the model distribution and alleviates the need for users to select settings on their own. The default values are shown below:

```
parameter ( GRESPIG = 1 )
parameter ( IRONPIG = 2 )
parameter ( MXRECTR = 1 )
parameter ( FLEAK = .25 )
parameter ( LEAKON = .FALSE. )
parameter ( LVISPIG = .TRUE. )
parameter ( OVERLAP = .FALSE. )
parameter ( DXYMAX = 0. )
parameter ( AGEMAX = 18.*3600. )
```

Users should exercise thoughtful consideration when altering these default values; the GRESPIG and IRONPIG flags cannot be changed, as these tell the program which version of PiG the user has selected. A description of each of the remaining parameters are provided below, along with guidance in setting values.

Guidance on the Use of CAMx PiG

PiG Flag

The PiG flag controls whether the PiG option is to be invoked in a CAMx simulation, and whether the emissions are treated with the GREASD or IRON options. If this flag is switched from NONE to GREASD or IRON on a model restart, CAMx expects an existing PiG file to exist from which to reinitialize the PiG module, and will stop if this file cannot be found. If this flag is switched to NONE on a model restart, CAMx will continue the simulation without PiG, but all mass contained in puffs at the end of the previous run will be lost.

- Guidance:
  - Invoke GREASD or IRON PiG for all simulation days, or none at all.
  - GREASD PiG should be invoked for large NOx point sources only, since it does not provide any organic chemistry. It can be run in conjunction with the OSAT, DDM, and PA Probing Tools.
  - IRON PiG can be invoked for any point sources to treat gas-phase chemical evolution using CB-IV or SAPRC99 mechanisms. This option uses the expensive LSODE chemistry solver exclusively, so users will notice a significant impact on run time, particularly if many (~thousands) puffs are to be carried and/or puffs are configured with many puff reactor cells (see below). IRON PiG does not currently treat particulate chemistry. It can be run in conjunction with the RTRAC Probing Tool. It does not support OSAT, DDM, or PA.

Number of IRON PiG Reactors

MXRECTR sets the number of IRON puff reactors; when greater than 1, each puff is separated into that number of reactor cells and primary emissions are apportioned among them using a Gaussian distribution. Since chemistry is performed for each individual reactor cell (both background and puff+background), this parameter can affect the speed of chemical computations in the IRON PiG; it is not used in GREASD PiG. We have not seen a significant sensitivity to values greater than 1, but testing for each application is warranted.

- Guidance:
  - Use the default of 1 for initial simulations, but test the sensitivity to this parameter for each unique application.

Leakage Parameters

FLEAK, LEAKON, and DXYMAX together control IRON puff leakage to the computational grid and ultimately puff termination. When LEAKON is true, FLEAK and DXYMAX control when puffs begin to leak portions of reactor mass to the grid along their trajectory. When LEAKON is false, no leaking is performed and puffs maintain all of their mass until they reach sizes for termination, at which point all mass is directly introduced to the grid at that point. DXYMAX sets the maximum dimension that puff size will be compared to for leaking and termination; when it is zero, puff size will be compared to grid area, but when it is non-zero, puff size will be compared to the value of DXYMAX. FLEAK is the relative fraction of horizontal puff area to cell area ,or DXYMAX, above which leaking will begin and continue until sufficient mass is shed and the puff is terminated. In the example above, IRON puffs will begin to leak mass when they reach 25% of the host grid cell's area. These parameters have no impact on GREASD PiG.

- Guidance: If LEAKON is set to true, maintain FLEAK at the default value of 0.25. Then test model sensitivity to different values of FLEAK and/or DXYMAX.

Overlap Flag

OVERLAP controls whether puff overlap is to be treated in the background chemistry step. As stated earlier, puffs only overlap if they meet the size criteria for leaking; all puffs smaller than this size do not overlap any other puffs in the same grid cell.

- Guidance: We recommend that the OVERLAP flag remain set to the default value of "false".

Virtual Puff Rendering

LVISPIG is a flag that turns on IRON puff "rendering" to the computational grid average concentrations. When it is false, the chemical effects of puff mass are not seen on the output average files until they either begin to leak mass to the grid and/or they are terminated and

their mass is entirely introduced to the computation grid. This is always the case for GREASD PiG. However, when the flag is true, all IRON puff mass that resides in each grid column is summed, apportioned vertically to each grid cell according to puff vertical extent (via density and layer-depth weighting), converted to concentrations, and added to the average gridded concentrations for output. This process is referred to as rendering since the effects of all puff mass can be readily visualized in the CAMx output.

- Guidance: This option has no impact on the actual CAMx chemical solution. However, output average concentration files will be affected by puff rendering, and therefore could impact graphics of CAMx results and model performance measures.

Maximum Puff Age

AGEMAX is the age limit for all PiG puffs (IRON and GREASD). When puffs reach this age limit, they are terminated and all of their mass is transferred to the host grid.

The assumption of a stream of coherent puffs becomes less valid with time as horizontal and vertical wind shears increase plume spread. At some point the plume mass is better resolved on the grid than within puffs. In CAMx the rate of puff expansion most often determines this transfer of mass, and the maximum puff age provides a safety check to ensure that puffs do not persist for unrealistic times in stable environments. The maximum puff age should be set long enough to allow puffs to persist overnight, but a lifetime of longer than a day is probably not realistic.

- Guidance: limit puff age to 12-24 hours – we find that 18 hours works best since it will allow puffs emitted in the late afternoon to last through the night and into the following morning. The purpose is to restrict growth-limited puffs to terminate over night simply as a result of age constraints. Twelve hours is seen to be too short in this regard; puffs usually do not reach 24 hours of age before being terminated by grid constraints.

Elevated Point Source Emissions File

Selecting the individual elevated point sources to receive the PiG treatment is accomplished by setting their stack diameters negative within the header (time-invariant point list) section of the CAMx input point source file. CAMx will run correctly with these negative diameters even if the PiG algorithm is not invoked. CAMx preprocessors exist to ease the procedure of ranking elevated point sources by emission rate and flagging the sources that the user wishes to treat.

While this process is straightforward, the user must carefully consider certain issues since incorrectly preparing these input files can lead to confusing and erroneous model results and study conclusions. This section provides guidance on how to use the PiG algorithm effectively and how to prepare input files that make sense. The most difficult aspect of setting up the PiG algorithm is ensuring that the elevated point source emission files are consistent from day to day. This is where some users have made mistakes in the past, and so this aspect is discussed in detail below.

In practice, the process of flagging sources for PiG treatment can be complicated. Often, separate point source files are prepared for different days (e.g., weekday and weekend) or for different scenarios (e.g., base case and emission control scenarios). These separate point source files may not have the same number of sources, and/or sources may not be in the same order. The PiG algorithm must necessarily make assumptions about the list of PiG sources once it is invoked for a given multi-day simulation (an important issue here is keeping track of source locations for source attribution within OSAT). The primary assumption is that ***the positions of PiG sources within the point source file do not change from day to day***. In other words, if the 5th source is flagged for PiG on the first simulation day, then the 5th source will receive PiG treatment on all subsequent days. Therefore, the 5th source must be the same source on each simulation day. This degree of consistency can be hard to achieve when source lists vary between days or emission scenarios, as described above. CAMx provides runtime error messages when inconsistencies in PiG point sources are found on a model restart.

The best approach to correctly prepare point source files for the PiG treatment is to build a "master" point source list containing the union of all point sources to be modeled for all days of a given scenario. Then rank and select point sources from this list. This ensures the same order for every day of the simulation, and each day-specific point source file is then reconfigured with this master list. Depending on the application, it may also be helpful to rearrange the master point source list such that all PiG sources are listed first and in the same order on each day, followed by all other sources in any order. This could facilitate any subsequent processing of the point source files (say, for various emission scenarios) since the first *n* sources are always known to be PiG sources. When preparing a different emissions scenario, either: (1) build a completely new "master" point source file and completely reselect PiG sources; or (2), use the base case master list with various points controlled or zeroed ***but no sources removed or added***. Building new point source files for various scenarios and then assuming the same point source number and order for the purposes of flagging PiG sources is usually a bad idea, since the sources thought to be selected are not, while others are. Again, the key is to run the model with an invariant point source list.

- Guidance: build a "master" point source file that is the union of all point sources to be modeled, then rank and select point sources from this list. Also, rearrange the point source file such that all PiG sources are listed first and appear in the same order on each day, followed by all other sources. In the case of a control scenario, either: (1) build a completely new "master" point source file and completely reselect PiG sources; or (2), use the base case master list with various points controlled or zeroed ***but no sources removed or added***.

5. CORE MODEL INPUT/OUTPUT STRUCTURES

CAMx requires inputs to describe photochemical conditions, surface characteristics, initial/boundary conditions, emission rates, and various meteorological fields over the entire modeling domain. Table 5-1 summarizes the input data requirements of CAMx. Preparing this information requires several preprocessing steps to translate "raw" emissions, meteorological, air quality and other data into final input files for CAMx. We expect that most CAMx applications will utilize output from a prognostic meteorological model that can generate all of the required time varying three-dimensional meteorological fields. Most CAMx I/O file formats are compatible with those of the UAM genre, which allows the user to employ widely available software designed specifically for these formats to develop the input files or to postprocess and visualize the output files.

Table 5-1. Data requirements of CAMx.

DATA CLASS	DATA TYPES
Meteorology *Supplied by a Meteorological Model*	• 3-Dimensional Gridded Fields: - Vertical Grid Structure - Horizontal Wind Components - Temperature - Pressure - Water Vapor - Vertical Diffusivity - Clouds/Rainfall
Air Quality *Obtained from Measured Ambient Data*	• Gridded Initial Concentrations • Gridded Boundary Concentrations • Time/space Constant Top Concentrations
Emissions *Supplied by an Emissions Model*	• Elevated Point Sources • Combined Gridded Sources - Low-level Point - Mobile - Area/Non-road Mobile - Biogenic
Geographic *Developed from Landuse/Landcover Maps, Drought Index Maps, Modeled or Satellite-derived Snow Cover*	• Gridded Surface Characteristics - Land Use/Vegetative Cover - UV Albedo - Snow Cover - Land/Water Mask - Roughness Length - Drought Stress
Photolysis *Derived from Satellite Measurements and Radiative Transfer Models*	• Atmospheric Radiative Properties - Gridded Haze Opacity Codes - Gridded Ozone Column Codes - Photolysis Rates Lookup Table

CAMx produces gridded time-averaged concentration output files; the user selects the time interval (usually hourly), the species to be output, and whether the output contains just surface layer fields or entire three-dimensional fields. An average output file is written for the master grid, and a separate file is written containing all fine grid nests together. Deposition fields for

the same user-selected species are also written to output files with the same structure as the surface layer concentration files. Gridded instantaneous fields of all species are assumed to be used for restarts only, and so only the last two hours of the simulation are written to these files. Commonly available graphical output visualization and animation software such as PAVE can be used to view CAMx output files. The CAMx Probing Tool options provide their own information in separate output files that can be viewed directly or further post-processed for detailed analysis. Diagnostic output files include three files that track computer resources, echo input selections, provide mass budget and diagnostic summaries, and provide error/warning messages.

5.1 CAMx RUN CONTROL FILE

CAMx reads a text (ASCII) run control file named "`CAMx.in`" that must exist locally in the directory from which the model is run. This file is in the Fortran "namelist" format, and contains all user-specified control parameters for a given simulation, including model configuration, option-specific inputs, and I/O filenames. The run control file must contain the primary namelist module labeled "`&CAMx_Control`", which provides all of the information to configure and run the core model. Additional namelist modules may be provided in the run control file to configure and run the various CAMx Probing Tools. These optional namelists are ignored if none of the Probing Tools are selected in the primary namelist.

Each record in the CAMx control file contains a variable name that is explicitly set to a numerical, logical, or character value. The variable names are used by the program directly, and therefore cannot be changed without source code modifications. Character strings must be enclosed by single quotes, and all variable assignments must be delimited with commas. The order of the records may be arranged in any fashion that the user prefers. Any number of comment statements may be included anywhere within the namelists, provided that they do not interrupt "`variable_name = value,`" assignments. The "`!`" characater is the Fortran namelist comment delimiter.

Certain variables are multi-dimension arrays; the user may provide a comma-delimited list of values to fill the array or assign values to specific array elements. Certain other variables are optional or associated with option flags; these do not need to appear in the namelist if their associated options are not invoked, and they will be ignored if they remain in the file. If the user does not provide necessary inputs, the model will stop with a descriptive error message. We suggest that users start with the `CAMx.in` template that is provided with the source code. Alternatively, for those that are updating from previous version of CAMx, a conversion program is available to translate the original flat text control file formats to the namelist format (see Section 11).

A detailed description of the run control file variables necessary to run the core model are provided below. The order of the variables follow the template available with the source code. The Probing Tools require separate additional namelist modules in the run control file, and their contents vary among the various options. The specific run control information needed for each of these options is provided in Sections 6 through 10.

Description of the CAMx Run Control File

&CAMx_Control	Label for the primary namelist module that configures the core model; it must begin in column 2
&	Flag ending a namelist module; it must be in column 2
Run_Message	60-character simulation message, written to output files to label the run

Model Clock Control

Time_Zone	Integer time zone (0=UTC, 5=EST, 6=CST, 7=MST, 8=PST)
Restart	Logical model restart flag (TRUE=read restart file, FALSE=read initial conditions file)
Start_Date_Hour	Integer array start time (YYYY, MM, DD, HHmm)
End_Date_Hour	Integer array end time (YYYY, MM, DD, HHmm)
Maximum_Timestep	Real maximum allowable timestep (minutes)
Met_Input_Frequency	Real input frequency of environmental fields (minutes)
Ems_Input_Frequency	Real input frequency of emissions (minutes)
Output_Frequency	Real output frequency (minutes)

Map Projection Parameters

Map_Projection	Character mapping projection keyword (LAMBERT, POLAR, UTM, LATLON)
UTM_Zone	Integer UTM zone
POLAR_Longitude_Pole	Real longitude of projection pole (degrees, west<0)
POLAR_Latitude_Pole	Real latitude of projection pole (degrees, south<0)
LAMBERT_Center_Longitude	Real central longitude of modeling domain (degrees, west<0)
LAMBERT_Center_Latitude	Real central latitude of modeling domain (degrees, south<0)
LAMBERT_True_Latitude1	Real first true latitude of projection (degrees, south<0)
LAMBERT_True_Latitude2	Real second true latitude of projection (degrees, south<0)

Parameters For The Master (First) Grid

Number_of_Grids	Integer number of grids in simulation
Master_Origin_XCoord	Real x-coordinate of domain southwest corner (km, or degrees for LATLON)
Master_Origin_YCoord	Real y-coordinate of domain southwest corner (km, or degrees for LATLON)
Master_Cell_XSize	Real cell size in x (km, or degrees for LATLON)
Master_Cell_Ysize	Real cell size in y (km, or degrees for LATLON)
Master_Grid_Columns	Integer number of master grid columns (E-W grid cells)
Master_Grid_Rows	Integer number of master grid rows (N-S grid cells)
Number_of_Layers	Integer array (by grid) number of grid layers

Parameters For The Nested Grids

Nest_Meshing_Factor	Integer array (by grid) nested grid cell size relative to master grid
Nest_Beg_I_Index	Integer array (by grid) master grid column containing western edge of nest
Nest_End_I_Index	Integer array (by grid) master grid column containing eastern edge of nest
Nest_Beg_J_Index	Integer array (by grid) master grid row containing southern edge of nest
Nest_End_J_Index	Integer array (by grid) master grid row containing northern edge of nest

Model Options

Diagnostic_Error_Check	Logical model startup diagnostic flag (TRUE=stops before first timestep indicating successful model initialization, FALSE=continues with simulation after model initialization)
Advection_Solver	Character horizontal advection solver keyword (PPM, BOTT)
Chemistry_Solver	Character chemistry solver keyword (CMC, IEH, LSODE)

PiG_Submodel	Character PiG submodel keyword (NONE, GREASD, IRON)
Probing_Tool	Character Probing Tool keyword (NONE, OSAT, GOAT, APCA, DDM, PA, RTRAC)
Chemistry	Logical chemistry flag (TRUE=chemistry on, FALSE=chemistry off)
Dry_Deposition	Logical dry deposition flag (TRUE=deposition on, FALSE=deposition off)
Wet_Deposition	Logical wet deposition flag (TRUE=deposition on, FALSE=deposition off)
Staggered_Winds	Logical staggered input wind field flag (TRUE=winds are input at cell interfaces, FALSE=winds are input at cell midpoints)
Gridded_Emissions	Logical gridded emissions flag (TRUE=gridded emissions will be used, FALSE=gridded emissions will be ignored)
Point_Emissions	Logical elevated point source flag (TRUE=point emissions will be used, FALSE=point emissions will be ignored)
Ignore_Emission_Dates	Logical date-insensitive emission flag (TRUE=dates on emission files will be ignored, FALSE=dates on emission files will be checked against simulation date)

Output Specifications

Root_Output_Name	Character root output path/filename (see Table 5-2 for description of file suffixes)
Average_Output_3D	Logical 3-D average output file flag (TRUE=output full 3-D concentration fields, FALSE=output surface layer concentration fields)
HDF_Format_Output	Logical HDF average output format flag (TRUE=output additional HDF format files, FALSE=do not output HDF format files)[1]
HDF_File_Root	Character HDF root output path/filename
Number_of_Output_Species	Integer number of species to be written to average and deposition output files

[1] Note that currently the HDF output option temporarily produces RAMS "VFM" formatted files to support certain ENVIRON projects. The HDF format will become available in a later version release. The format of the VFM files are not discussed further in this document.

Output_Species_Names	Character array (by output species) species names to be written to average and deposition output files

Input Files

Chemistry_Parameters	Character input chemistry parameters path/filename
Photolyis_Rates	Character input photolysis rates path/filename (optional according to Chemistry flag and Chemistry_Parameters file)
Initial_Conditions	Character input master grid initial conditions path/filename (ignored if Restart=TRUE)
Boundary_Conditions	Character input master grid boundary conditions path/filename
Top_Concentrations	Character input master grid top boundary conditions path/filename
Albedo_Haze_Ozone	Character input albedo/haze/ozone column path/filename (ignored if Chemistry=FALSE and Dry_Deposition=FALSE)
Point_Sources	Character input elevated point source emissions path/filename (ignored if Point_Emissions=FALSE)
Master_Grid_Restart	Character input master grid restart path/filename (ignored if Restart=FALSE)
Nested_Grid_Restart	Character input nested grid restart path/filename (ignored if Restart=FALSE or Number_of_Grids=1)
PiG_Restart	Character input PiG restart path/filename (ignored if Restart=FALSE or PiG_Submodel=FALSE)
Landuse_Grid	Character array (by grid) input landuse path/filename (ignored if Dry_Deposition=FALSE and PiG_Submodel=NONE, optional for nested grids)
ZP_Grid	Character array (by grid) input height/pressure path/filename (optional for nested grids)
Wind_Grid	Character array (by grid) input wind path/filename (optional for nested grids)
Temp_Grid	Character array (by grid) input temperature path/filename (optional for nested grids)

Vapor_Grid	Character array (by grid) input water vapor path/filename (ignored if Chemistry=FALSE and Dry_Deposition=FALSE and Wet_Deposition=FALSE, optional for nested grids)
Cloud_Grid	Character array (by grid) input cloud/rain path/filename (required if Wet_Deposition=FALSE, otherwise optional, optional for nested grids)
Kv_Grid	Character array (by grid) input vertical diffusivity path/filename (optional for nested grids)
Emiss_Grid	Character array (by grid) input gridded emissions path/filename (ignored if Gridded_Emissions=FALSE, optional for nested grids)

The user specifies a "root" path and filename that will be used for all CAMx core model output files. The model appends suffixes to these root names according to the file type generated. The relationship between CAMx file types is shown in Table 5-2. The user specifies the simulation start/end year, month, day, and hour; the model uses julian dates internally. All times must be given in military format (e.g., 1:30 PM must be given as 1330). The simulation time zone must match the time zone in which the emission and environmental inputs are developed, usually the most central time zone in the domain.

The grid projection may be selected as Cartesian (fixed physical distance coordinates on a flat plane) or curvi-linear geodetic (following the curved surface of the Earth). The Cartesian options include Universal Transverse Mercator (UTM), Lambert Conic Conformal (LAMBERT), and Rotated Polar Stereographic (POLAR). The geodetic option performs the simulation on a latitude/longitude grid (LATLON). All gridded input files must be defined on the grid projection specified for the CAMx simulation.

The user has the option of selecting among the Bott or Piecewise Parabolic Method horizontal advection solvers by specifying "BOTT" or "PPM" as keywords in the run control file. The user also has the option to use the CMC, IEH, or LSODE chemistry solvers for gas-phase chemistry by specifying these respective keywords. The description of PiG submodel is provided in Section 4.

A subset of species may be output to the average concentration output files; see the description of output file formats later in this section. The definition of nested grids is specified in the CAMx.in file in terms of the range of master grid cells that each nested grid spans (see Section 2). If CAMx cannot find or open a non-blank filename provided in the run control file, the model will stop with an error. CAMx will accept blank filenames for only those files that are optional.

Table 5-2. CAMx output file suffixes and their corresponding file types.

Suffix	CAMx File Type
.out	Simulation tracking file (CPU, input files read, error/warning messages)
.diag	Simulation diagnostic file (repeat of run control inputs, PiG diagnostics, miscellaneous diagnostic output)
.mass	Mass budget file for subsequent postprocessing
.inst.1	Master grid binary instantaneous concentration file for last odd simulation hour (used for restarts)
.inst.2	Master grid binary instantaneous concentration file for last even simulation hour (used for restarts)
.finst.1	Nested grid binary instantaneous concentration file for last odd simulation hour (used for restarts)
.finst.2	Nested grid binary instantaneous concentration file for last even simulation hour (used for restarts)
.avrg	Master grid binary average concentration file; optionally contains 2-D layer 1 concentration field or full 3-D concentration field
.favrg	Nested grid binary average concentration file; optionally contains 2-D layer 1 concentration field or full 3-D concentration field
.depn	Master grid binary deposition file
.fdepn	Nested grid binary deposition file
.PiG	PiG submodel file (used for restarts)

On computer platforms running Unix or Linux the generation of the run control file is most easily accomplished in the job script that actually runs the model; Figure 5-1 shows an example of a CAMx job script that builds a "`CAMx.in`" file and runs the model for each day to be simulated. Alternatively, the run control file could be written separately with a name specific to a given simulation, then linked or copied to the standard "`CAMx.in`" filename before the model is executed at a command line or in a job script.

```
#!/bin/csh
#
set EXEC      = "/models/camx/src.v4.20/CAMx.mrpo.36.12.linux"
#
set RUN     = "v4.20.mrpo.36.12.mech4"
set INPUT   = "test_run/inputs"
set MET     = "test_run/inputs/met"
set EMIS    = "test_run/emiss"
set PTSRCE  = "test_run/ptsrce"
set OUTPUT  = "test_run/outputs/$RUN"
#
mkdir -p $OUTPUT
set RESTART = "NO"
foreach today (13.164 14.165)
set JUL = $today:e
set CAL = $today:r
set YESTERDAY = `echo $CAL | awk '{printf("%2.2d",$1-1)}'`
#
if( ${RESTART} == "NO" ) then
        set RESTART = "false"
else
        set RESTART = "true"
endif
#
#  --- Create the input file (always called CAMx.in) ---
#
cat << ieof > CAMx.in
!--------------------------------------------------------------------------
 &CAMx_Control

 Run_Message = 'CAMx 4.20 test case - Mech 4CF - MRPO 36/12 June ${CAL},2002',

!--- Model clock control ---

 Time_Zone        = 5,                ! (0=UTC,5=EST,6=CST,7=MST,8=PST)
 Restart          = .${RESTART}.,
 Start_Date_Hour  = 2002,06,${CAL},0000,   ! (YYYY,MM,DD,HHHH)
 End_Date_Hour    = 2002,06,${CAL},2400,   ! (YYYY,MM,DD,HHHH)

 Maximum_Timestep    = 15.,           ! minutes
 Met_Input_Frequency = 60.,           ! minutes
 Ems_Input_Frequency = 60.,           ! minutes
 Output_Frequency    = 60.,           ! minutes

!--- Map projection parameters ---

 Map_Projection           = 'LAMBERT', ! (LAMBERT,POLAR,UTM,LATLON)
 UTM_Zone                 = 0,
 POLAR_Longitude_Pole     = 0.,       ! deg (west<0,south<0)
 POLAR_Latitude_Pole      = 0.,       ! deg (west<0,south<0)
 LAMBERT_Center_Longitude = -97.,     ! deg (west<0,south<0)
 LAMBERT_Center_Latitude  =  40.,     ! deg (west<0,south<0)
 LAMBERT_True_Latitude1   =  45.,     ! deg (west<0,south<0)
 LAMBERT_True_Latitude2   =  33.,     ! deg (west<0,south<0)
```

Figure 5-1. A sample CAMx job script that generates a "CAMx.in" file and runs the model.

```
!--- Parameters for the master (first) grid ---

 Number_of_Grids      = 2,
 Master_Origin_XCoord = -900.,         ! km or deg, SW corner of cell(1,1)
 Master_Origin_YCoord = -1620.,        ! km or deg, SW corner of cell(1,1)
 Master_Cell_XSize    = 36.,           ! km or deg
 Master_Cell_YSize    = 36.,           ! km or deg
 Master_Grid_Columns  = 97,
 Master_Grid_Rows     = 90,
 Number_of_Layers(1)  = 14,

!--- Parameters for the second grid ---

 Nest_Meshing_Factor(2) = 3,           ! Relative to master grid
 Nest_Beg_I_Index(2)    = 31,          ! Relative to master grid
 Nest_End_I_Index(2)    = 69,          ! Relative to master grid
 Nest_Beg_J_Index(2)    = 29,          ! Relative to master grid
 Nest_End_J_Index(2)    = 72,          ! Relative to master grid
 Number_of_Layers(2)    = 14,

!--- Model options ---

 Diagnostic_Error_Check = .false.,   ! True = will stop after 1st timestep
 Advection_Solver       = 'PPM',     ! (PPM,BOTT)
 Chemistry_Solver       = 'CMC',     ! (CMC,IEH,LSODE)
 PiG_Submodel           = 'None',    ! (None,GREASD,IRON)
 Probing_Tool           = 'None',    ! (None,OSAT,PSAT,GOAT,APCA,DDM,PA,RTRAC)
 Chemistry              = .true.,
 Dry_Deposition         = .true.,
 Wet_Deposition         = .true.,
 Staggered_Winds        = .true.,
 Gridded_Emissions      = .true.,
 Point_Emissions        = .true.,
 Ignore_Emission_Dates  = .true.,

!--- Output specifications ---

 Root_Output_Name         = '$OUTPUT/camx.$RUN.200206${CAL}',
 Average_Output_3D        = .false.,
 HDF_Format_Output        = .false.,
 HDF_File_Root            = ' ',
 Number_of_Output_Species = 20,
 Output_Species_Names(1)  = 'NO',
 Output_Species_Names(2)  = 'NO2',
 Output_Species_Names(3)  = 'O3',
 Output_Species_Names(4)  = 'SO2',
 Output_Species_Names(5)  = 'H2O2',
 Output_Species_Names(6)  = 'HNO3',
 Output_Species_Names(7)  = 'NH3',
 Output_Species_Names(8)  = 'PNO3',
 Output_Species_Names(9)  = 'PSO4',
 Output_Species_Names(10) = 'PNH4',
 Output_Species_Names(11) = 'POA',
 Output_Species_Names(12) = 'PEC',
 Output_Species_Names(13) = 'FPRM',
```

Figure 5-1. (continued).

```
 Output_Species_Names(14) = 'CPRM',
 Output_Species_Names(15) = 'CCRS',
 Output_Species_Names(16) = 'FCRS',
 Output_Species_Names(17) = 'SOA1',
 Output_Species_Names(18) = 'SOA2',
 Output_Species_Names(19) = 'SOA3',
 Output_Species_Names(20) = 'SOA4',

!--- Input files ---

 Chemistry_Parameters = '$INPUT/CAMx4.2.chemparam.4_CF',
 Photolyis_Rates      = '$INPUT/rate.2002${JUL}.do.mech3',
 Initial_Conditions   = '$INPUT/init.2002.4rpos.36.14.m3profile.ld.camx',
 Boundary_Conditions  = '$INPUT/bndr.2002.4rpos.36.14.m3profile.ld.camx',
 Top_Concentrations   = '$INPUT/topc.2002.4rpos.36.14.m3profile.ld.camx',
 Albedo_Haze_Ozone    = '$INPUT/ahoz.2002${JUL}.4rpos.36.ld',
 Point_Sources        = '$PTSRCE/ptsr.2002${JUL}.4rpos.NR.baseF.ld.camx',
 Master_Grid_Restart  = '$OUTPUT/camx.$RUN.200206${YESTERDAY}.inst.2',
 Nested_Grid_Restart  = '$OUTPUT/camx.$RUN.200206${YESTERDAY}.finst.2',
 PiG_Restart          = ' ',

 Landuse_Grid(1) = '$INPUT/surf.4rpos.36.ld.bin',
 Landuse_Grid(2) = '$INPUT/surf.mrpo.12.ld.bin',
 ZP_Grid(1)      = '$MET/pres.2002${JUL}.4rpos.36.14.mm5.ld.camx',
 ZP_Grid(2)      = '$MET/pres.2002${JUL}.mrpo.12.14.mm5.ld.camx',
 Wind_Grid(1)    = '$MET/wind.2002${JUL}.4rpos.36.14.mm5.ld.camx',
 Wind_Grid(2)    = '$MET/wind.2002${JUL}.mrpo.12.14.mm5.ld.camx',
 Temp_Grid(1)    = '$MET/temp.2002${JUL}.4rpos.36.14.mm5.ld.camx',
 Temp_Grid(2)    = '$MET/temp.2002${JUL}.mrpo.12.14.mm5.ld.camx',
 Vapor_Grid(1)   = '$MET/wvap.2002${JUL}.4rpos.36.14.mm5.ld.camx',
 Vapor_Grid(2)   = '$MET/wvap.2002${JUL}.mrpo.12.14.mm5.ld.camx',
 Cloud_Grid(1)   = '$MET/clra.2002${JUL}.4rpos.36.14.mm5.ld.camx',
 Cloud_Grid(2)   = '$MET/clra.2002${JUL}.mrpo.12.14.mm5.ld.camx',
 Kv_Grid(1)      = '$MET/vdif.2002${JUL}.4rpos.36.14.mm5.ld.camx.OB70',
 Kv_Grid(2)      = '$MET/vdif.2002${JUL}.mrpo.12.14.mm5.ld.camx.OB70',
 Emiss_Grid(1)   = '$EMIS/lamb.2002${JUL}.4rpos.36.baseF.ld.camx',
 Emiss_Grid(2)   = '$EMIS/lamb.2002${JUL}.mrpo.12.baseF.ld.camx',

 &
!------------------------------------------------------------------------------
ieof
$EXEC
date
end
```

Figure 5-1. (concluded).

5.2 CAMx CHEMISTRY PARAMETERS FILE

Chemistry parameters are provided in a text (ASCII) file that provides chemical information for the simulation and selects which mechanism is to be used. The chemistry parameters file format is unique to CAMx; the formats are defined in Table 5-3, and samples are given in Figure 5-2. Some records in this file are labeled (columns 1-20) to indicate the type of information to supply on that line (starting in column 21). For records that are not labeled, data start in column 1. Some chemistry parameter records are optional, depending upon the logical flags indicated for such records, and are shown in Table 5-3 by a check in the third column; if the indicated option is not invoked these records should not appear in the file. The first record of the chemistry parameters file must contain the string "VERSION 4.2", which indicates that this file is compatible with CAMx version 4.20.

If the chemistry flag is set "true" on the `CAMx.in` file, CAMx checks that certain properties of the selected mechanism are consistent with parameters supplied on the input file (e.g., number of reactions, photolysis reactions and species). If any discrepancies are found, they are reported in the output message file and the simulation is halted. The user may also specify an inert simulation by setting the chemistry flag to "false". In this case, any number of arbitrarily named species may be listed, and chemistry reaction parameters are read but not used. The lower bound values specified in the chemistry parameter file are used to specify initial and/or boundary conditions for species that are omitted from the initial and/or boundary condition files. The Henry's Law, diffusion, reactivity, and surface resistance scaling parameters for gasses are used for dry deposition calculations (Wesley, 1989). Aerosol density and diameters are used for both wet and dry deposition calculations.

The chemistry parameters file controls how photolysis rates are calculated in CAMx. So-called "primary" photolysis rates are input to CAMx via the photolysis rates file. The primary photolysis reactions are identified by number in the chemistry parameters file and the photolysis rates file must match this declaration. So-called "secondary" photolysis rates are set by scaling factors to one of the primary reactions. Clearly, this approach requires at least one primary photolysis reaction.

CAMx supports several equations for specifying rate constants, as shown in Table 5-4a. The type of equation being used for each reaction is identified by the second parameter specified for each reaction – a number between 1 and 7 (Table 5-3). The number of additional parameters required depends upon the expression type and varies between 2 and 13, as shown in Table 5-4b. Currently, the CBM-IV mechanisms implemented in CAMx (Table 3-1) use expression types 1 and 2, whereas the SAPRC99 mechanism uses types 1, 3, 4, 6 and 7. Expression type 4 allows for a complete description of dependencies on temperature and pressure; background information on Troe expressions may be found in the NASA and IUPAC rate constant compilations (NASA, 1997; IUPAC, 1992).

Rate constants can be specified in molecular units (e.g., cm^3 $molecule^{-1}$ s^{-1}) or ppm units (e.g., ppm^{-1} min^{-1}). All the rate constants must be in a single units system; CAMx will determine which units system is being used from the magnitude of the rate constants. Diagnostic information on the rate constants and units system is output by CAMx at run-time.

Table 5-3. Description of the CAMx chemistry parameters file. The record labels exist in columns 1-20, and where given, the input data for that record start in column 21. The format denoted "list" indicates a free-format list of numbers (comma or space-delimited).

Record Label (columns 1-20)	Record Optional	Format	Description
CAMx version		A	Model version keyword (VERSION4.2)
Mechanism ID		list	ID number of chemical mechanism (see Table 3-1) Keyword for aerosol scheme (CF or CMU)[1]
Description		A	Message record to describe this file
No of gas species		list	Number of gas species (NGAS ≥ 1)
No of aero species		list	Number of aerosol species (NAERO ≥0) Aerosol chemistry timestep (min) (**if NAERO>0**) Number of size bins (NBIN ≥ 1) (**if NAERO>0**)[2] Aerosol diameter (μm) for NBIN+1 cut points (**if NAERO>0**)
No of reactions		list	Number of reactions (NREACT ≥ 0)
Prim photo rxns		list	Number of primary photolysis reactions (NPHOT1 ≥ 0) List of primary photolysis reaction ID numbers (must match the photolysis rates input file)
No of sec photo rxn		list	Number of secondary photolysis reactions (NPHOT2 ≥ 0)
ID, prim ID, scale	√	list	***If NPHOT>0*, repeat this record for each secondary photolysis reaction** ID number of the secondary photolysis reaction ID number of the primary photolysis reaction used for scaling Secondary reaction scale factor
Species Records			Heading
Gas Spec ...			Heading
		5X, A10, E10.0, E10.0, F10.0, F10.0, F10.0 F10.0	Repeat this record for each gas species (start in column 1) Gas species name Lower bound concentration (ppm) Henry's law constant (M/atm) Henry's law temperature dependence (K) Molecular diffusivity ratio Wesley's reactivity parameter Surface resistance scaling factor for strong acids (0-1)

Table 5-3. Description of the CAMx chemistry parameters file. The record labels exist in columns 1-20, and where given, the input data for that record start in column 21. The format denoted "list" indicates a free-format list of numbers (comma or space-delimited).

Record Label (columns 1-20)	Record Optional	Format	Description
`Aero Spec ...`	√		Heading (***if NAERO>0***)
	√	5X, A10, E10.0, F10.0	***If NAERO>0*, repeat this record for each aerosol species** (start in column 1) Aerosol species name Lower bound concentration ($\mu g/m^3$) Species density (g/cm^3)
`Reaction Records`	√		Heading (***if NREACT>0***)
`Rxn Typ Param ...`	√		Heading (***if NREACT>0***)
	√	list	***If NREACT>0*, repeat this record for each gas-phase reaction** (start in column 1) Reaction ID number Rate constant expression ID number (1-7, as shown in Table 5-4) Rate constant parameters (depending on expression type in Table 5-4). For reactions identified as photolysis reactions above, the rate constant is not used and is customarily set to zero.

[1] Used only for Mechanism 4: CF = Coarse/Fine scheme; CMU = multi-sectional scheme.
[2] For the CF scheme, NBIN *must be set to 2*, and the user specifies the coarse/fine size ranges.

```
CAMx Version       |VERSION4.2
Mechanism ID       |4 CF
Description        |Mech3 plus aerosols, static 2-mode size model
No of gas species  |37
No of aero species |18 15.0 2 0.039 2.5 10.0
No of reactions    |100
Prim photo rxns    |6 1 38 39 9 45 95
No of sec photo rxn|6
ID, prim ID, scale | 8  1  0.053
                   |14  1 33.9
                   |23  1  0.1975
                   |34 39  0.189
                   |69 38  9.04
                   |74 38  9.64
Species Records
     Gas Spec   lower bnd     H-law   T-fact    Diffrat  Reactvty    Rscale
  1  NO          1.00E-15  1.90e-03    -1480.      1.29       0.0        1.
  2  NO2         1.00E-09  1.00e-02    -2516.      1.60       0.1        1.
  3  O3          1.00E-09  1.10e-02    -2415.      1.63       1.0        1.
  4  PAN         1.00E-09  3.60e+00    -5910.      2.59       0.1        1.
  5  NXOY        1.00E-12  3.20e+04    -8706.      2.45       0.1        0.
  6  OLE         1.00E-09  5.00e-03        0.      1.80       0.0        1.
  7  PAR         1.00E-04  1.00e-03        0.      2.00       0.0        1.
  8  TOL         1.00E-09  1.20e+00        0.      2.26       0.0        1.
  9  XYL         1.00E-09  1.40e+00        0.      2.43       0.0        1.
 10  FORM        1.00E-09  6.30e+03    -6492.      1.29       0.0        1.
 11  ALD2        1.00E-09  6.30e+03    -6492.      1.56       0.0        1.
 12  ETH         1.00E-09  1.00e-02        0.      1.25       0.0        1.
 13  CRES        1.00E-09  2.70e+03    -6492.      2.45       0.0        1.
 14  MGLY        1.00E-09  2.70e+03    -6492.      2.00       0.0        1.
 15  OPEN        1.00E-12  2.70e+03    -6492.      2.47       0.0        1.
 16  PNA         1.00E-09  2.00e+04    -5910.      2.09       0.0        1.
 17  CO          1.00E-04  1.00e-10        0.      1.25       0.0        1.
 18  HONO        1.00E-09  5.90e+01    -4781.      1.62       0.1        1.
 19  H2O2        1.00E-09  7.40e+04    -6643.      1.37       1.0        1.
 20  HNO3        1.00E-09  2.00e+05    -8707.      1.87       0.0        0.
 21  ISOP        1.00E-09  1.00e-02        0.      1.94       0.0        1.
 22  MEOH        1.00E-09  2.20e+02    -4932.      1.33       0.0        1.
 23  ETOH        1.00E-09  2.20e+02    -4932.      1.60       0.0        1.
 24  ISPD        1.00E-09  6.30e+03    -6492.      1.97       0.0        1.
 25  NTR         1.00E-09  9.40e+03    -8706.      2.72       0.0        1.
 26  SO2         1.00E-09  1.00e+05    -3156.      1.89       0.0        1.
 27  SULF        1.00E-12  1.00e+10        0.      1.00       0.0        0.
 28  NH3         1.00E-09  2.00e+04    -3400.      0.97       0.0        1.
 29  HCL         1.00E-12  1.00e+05        0.      1.42       0.0        0.
 30  OLE2        1.00E-12  5.00e-03        0.      1.80       0.0        1.
 31  CG1         1.00E-12  2.70e+03    -6492.      2.50       0.0        1.
 32  CG2         1.00E-12  2.70e+03    -6492.      2.50       0.0        1.
 33  CG3         1.00E-12  2.70e+03    -6492.      2.50       0.0        1.
 34  CG4         1.00E-12  2.70e+03    -6492.      2.50       0.0        1.
 35  CG5         1.00E-12  2.70e+03    -6492.      2.50       0.0        1.
 36  HG0         1.00E-12  1.00e-10        0.      3.34       0.0        1.
 37  HG2         1.00E-12  2.00e+05        0.      3.76       0.0        1.
     Aero Spec  lower bnd   Density
  1  PNO3        1.00E-09       1.5
  2  PSO4        1.00E-09       1.5
  3  PNH4        1.00E-09       1.5
  4  POA         1.00E-09       1.0
  5  SOA1        1.00E-09       1.0
  6  SOA2        1.00E-09       1.0
  7  SOA3        1.00E-09       1.0
  8  SOA4        1.00E-09       1.0
```

Figure 5-2a. Example CAMx chemistry parameters file for Mechanism 4 (CF scheme), including the mercury species HG0, HG2, and HGP.

```
  9  SOA5         1.00E-09       1.0
 10  PEC          1.00E-09       2.0
 11  FPRM         1.00E-09       3.0
 12  FCRS         1.00E-09       3.0
 13  CPRM         1.00E-09       3.0
 14  CCRS         1.00E-09       3.0
 15  NA           1.00E-09       2.0
 16  PCL          1.00E-09       2.0
 17  PH2O         1.00E-09       1.0
 18  HGP          1.00E-12       2.0
Reaction Records
Rxn Typ Order Parameters (1 to 12, depending upon Typ)
1    1  1    0.0000E+00
2    2  2    4.3233E+06   -1.1750E+03
3    2  2    2.6640E+01    1.3700E+03
4    1  2    1.3750E+04
5    2  2    2.3090E+03   -6.8700E+02
6    2  2    2.4380E+03   -6.0200E+02
7    2  2    4.7310E-02    2.4500E+03
8    1  1    0.0000E+00
9    1  1    0.0000E+00
10   2  2    4.2500E+10   -3.9000E+02
11   1  2    3.2600E+05
12   2  2    1.0000E+02    9.4000E+02
13   2  2    2.9990E+00    5.8000E+02
14   1  1    0.0000E+00
15   2  2    4.4167E+04   -2.5000E+02
16   2  2    5.9010E-01    1.2300E+03
17   2  2    1.8530E+03   -2.5600E+02
18   1  2    3.8400E-07
19   2  1    2.7760E+00    1.0897E+04
20   2  2    1.5390E-04   -5.3000E+02
21   1  3    1.6000E-11
22   2  2    9.7990E+03   -8.0600E+02
23   1  1    0.0000E+00
24   1  2    9.7700E+03
25   1  2    1.5000E-05
26   4  2    9.4640E-02    0.0000E+00 -3.2000E+00  3.0000E+02  3.5470E+04
 0.0000E+00 -1.3000E+00  3.0000E+02  6.0000E-01  1.0000E+00
27   2  2    2.1790E+02   -1.0000E+03
28   2  2    1.2270E+04   -2.4000E+02
29   1  2    0.0000E+00
30   1  1    0.0000E+00
31   1  1    0.0000E+00
32   2  2    4.1440E+03   -1.1500E+03
33   2  3    2.1810E-01   -5.8000E+03
34   1  1    0.0000E+00
35   2  2    2.5200E+03    1.8700E+02
36   7  2    2.2170E+02    0.0000E+00  0.0000E+00  3.0000E+02  1.3300E-04
 0.0000E+00  0.0000E+00  3.0000E+02
37   1  2    1.5000E+04
38   1  1    0.0000E+00
39   1  1    0.0000E+00
40   2  2    2.3700E+02    1.5500E+03
41   1  2    9.3000E-01
42   2  2    6.3600E+02    9.8600E+02
43   2  2    2.4000E+04   -2.5000E+02
44   1  2    3.7000E+00
45   1  1    0.0000E+00
46   2  2    2.8200E+04    1.8000E+02
47   2  2    1.3700E+04   -3.8000E+02
48   2  1    2.5400E-02    1.3500E+04
49   1  2    3.7000E+03
```

Figure 5-2a. (continued).

```
50   1  2    9.6000E+03
51   2  2    1.6290E+01    1.7750E+03
52   1  2    1.2030E+03
53   2  1    1.3710E+05    8.0000E+03
54   1  1    9.5450E+04
55   1  2    2.2000E+04
56   2  2    5.9200E+03    3.2400E+02
57   2  2    4.2000E+04   -5.0400E+02
58   2  2    1.8000E-02    2.1050E+03
59   1  2    1.1350E+01
60   2  2    1.0800E+03    7.9200E+02
61   2  2    1.1920E+04   -4.1100E+02
62   2  2    2.7000E-03    2.6330E+03
63   2  2    9.1500E+03   -3.2200E+02
64   1  2    1.2000E+04
65   1  1    2.5000E+02
66   1  2    6.1000E+04
67   1  2    3.2500E+04
68   1  2    2.0000E+04
69   1  1    0.0000E+00
70   1  2    4.4000E+04
71   2  2    1.5000E-02    5.0000E+02
72   2  2    3.6200E+04   -1.1600E+02
73   1  2    2.6000E+04
74   1  1    0.0000E+00
75   1  2    5.3200E+04
76   1  2    1.4760E+05
77   1  2    1.9000E-02
78   1  2    9.9600E+02
79   1  2    1.2000E+04
80   2  2    2.0000E+03   -1.3000E+03
81   1  2    1.2000E+04
82   4  2    1.0910E-02    0.0000E+00 -3.3000E+00  3.0000E+02  2.2170E+03
 0.0000E+00  0.0000E+00  3.0000E+02  6.0000E-01  1.0000E+00
83   1  1    0.0000E+00
84   1  2    1.6000E+03
85   2  2    4.3000E+03   -1.7600E+02
86   2  2    8.9000E+03   -1.3000E+03
87   2  2    8.9000E+03   -1.3000E+03
88   2  2    2.0000E+03   -1.3000E+03
89   2  2    4.0000E+03   -1.3000E+03
90   2  2    1.6260E+05   -2.5000E+02
91   1  1    2.7778E-04
92   1  2    4.9667E+04
93   1  2    1.0500E-02
94   1  2    1.4780E+00
95   1  1    0.0000E+00
96   1  2    2.2000E-04
97   2  2    5.9200E+03    3.2400E+02
98   2  2    4.2000E+04   -5.0400E+02
99   2  2    1.8000E-02    2.1050E+03
100  1  2    1.1350E+01
```

Figure 5-2a. (concluded).

```
CAMx Version        |VERSION4.2
Mechanism ID        |0
Description         |inert test
No of gas species   |1
No of aero species  |0
No of reactions     |0
Prim photo rxns     |0
No of sec photo rxn|0
Species Records
    Gas Spec    lower bnd      H-law    T-fact     Diffrat  Reactvty
 1  TRACER       1.00E-09  1.00e-10         0.       1.00       0.0
```

Figure 5-2b. Example inert chemistry parameters file (requires chemistry flag to be set false- see the description of the CAMx control file).

Table 5-4a. Rate constant expression types supported in CAMx and order of expression parameters for the chemistry parameters file.

Expression Type	Description	Expression
1	Constant	$k = k_{298}$
2	UAM (Arrhenius expression)	$k = k_{298} \exp\left[E_a \left(\frac{1}{298} - \frac{1}{T} \right) \right]$
3	General temperature dependence	$k = A\left(\frac{T}{T_R} \right)^B \exp\left[\frac{-E_a}{T} \right]$
4	Troe-type temperature and pressure dependence	$k = \left[\frac{k^o[M]}{1 + k^o[M]/k^\infty} \right] F^G$ $k^o = A\left(\frac{T}{T_R} \right)^B \exp\left[\frac{-E_a}{T} \right]$ $k^\infty = A'\left(\frac{T}{T_R'} \right)^{B'} \exp\left[\frac{-E_a'}{T} \right]$ $G = \left[1 + \left(\frac{\log(k^o[M]/k^\infty)}{n} \right)^{-2} \right]^{-1}$
5	Equilibrium with a previously defined reaction (k_{ref})	$k = k_{ref} A\left(\frac{T}{T_R} \right)^B \exp\left[\frac{-E_a}{T} \right]$
6	Lindemann - Hinshelwood as used for OH + HNO3	$k = k^o + \frac{k_3[M]}{1 + k_3[M]/k_2}$
7	Simple pressure dependence used for OH + CO	$k = k_1 + k_2\,[M]$

Table 5-4b. Order of parameters in chemistry parameter file for CAMx rate constant expressions. Use ppm/minute units for A and Kelvin for E_a and T_R.

Expression Type		Parameters											
	1[1]	2	3	4	5	6	7	8	9	10	11	12	13
1	O	k_{298}											
2	O	k_{298}	E_a										
3	O	A	E_a	B	T_R								
4	O	A	E_a	B	T_R	A'	E_a'	B'	T_R'	F	n		
5	O	k_{ref}	A	E_a	B	T_R							
6	O	A^o	$E_a{}^o$	B^o	$T_R{}^o$	A^2	$E_a{}^2$	B^2	$T_R{}^2$	A^3	$E_a{}^3$	B^3	$T_R{}^3$
7	O	A^1	$E_a{}^1$	B^1	$T_R{}^1$	A^2	$E_a{}^2$	B^2	$T_R{}^2$				

[1] O is the order of the reaction.

5.3 PHOTOLYSIS RATES FILE

The rates for the primary photolysis reactions are supplied via the photolysis rates file in units of minute^{-1}. This file must be supplied if chemistry is invoked, and it is essentially a large look-up table that provides the photolysis rates in five dimensions, including variations over solar zenith angle, height above ground, ultraviolet (UV) albedo of the ground, atmospheric turbidity, and total ozone column density. This table can be generated using the TUV radiative transfer model as a preprocessor, which can be configured by the user for the range of conditions expected during a specific CAMx application. Therefore, the user must supply the number of intervals (or "classes") and associated values in each of the five dimensions. Typically, TUV is run for a matrix of 11 heights, 10 solar zenith angles, 5 ozone column values, 5 albedo values, and 3 turbidity values.

```
Loop from 1 to nozn ozone column intervals:
    Loop from 1 to nalb UV albedo intervals:
        Loop from 1 to nhaz haze turbidity intervals:
            ozcl,albcl,hazcl                    (12X,f7.3,8X,f7.3,11X,f7.3)
            Loop from 1 to nalt altitudes above ground:
                height                          (*)
                Loop from 1 to nphot photolysis reactions:
                    (pk(n),n=1,nsol)            (1X,10F12.0)
```

The photolysis rates file is a readable text (ASCII) format and it has the following structure:

where the variables in the photolysis rates file have the following definitions:

`ozcl` Ozone column value for the current interval (Dobson units)

`albcl` UV albedo value for the current interval (unitless)

`hazcl`	Haze turbidity value for the current interval (unitless)
`height`	Altitude (km)
`pk`	Photolysis rates (min^{-1}) for *nsol* solar zenith angles

Figure 5-3 presents an example of a photolysis rates file for the first several panels of data.

5.4 ALBEDO/HAZE/OZONE FILE

This file (commonly condensed to ALHZOZ or AHO) contains the spatial and temporal distribution of surface UV albedo, ozone column density, and turbidity for a specific CAMx domain and episode. These parameters are essential for photochemical simulations as they determine the spatial and temporal variation of photolysis rates. Therefore, this file must be supplied if chemistry is invoked. Additionally, the AHO file may also provide optional fields of snow cover, land/ocean mask, drought stress codes, and surface roughness.

The mandatory time-invariant UV albedo, and optional time-invariant land/ocean mask, drought stress, and surface roughness fields, must be supplied for each cell of the master grid, and optionally any nested grids. The mandatory time-varying ozone and turbidity fields, and the optional time-varying snow cover field, are supplied for the master grid only; CAMx internally assigns master cell values to all nested grids cells for these three fields. The time-invariant fields must be located at the top of the file (below some definition records), followed by all time-varying fields.

Instead of supplying the actual values of these parameters, the file contains the respective "codes" for each interval (or class). For ozone column, UV albedo, and turbidity, the classes must exactly coincide with the values specified in preparing the photolysis rates file. For example, if 5 ozone column classes are specified in TUV, then the ozone column map in the ALHZOZ file must consist of a distribution of integers ranging from 1 to 5 and the value ranges of those 5 classes must match the value ranges used in TUV.

The optional surface roughness field allows the user to override the default surface roughness that is set internally in CAMx according to season and the input landuse file. This effects dry deposition and PiG puff growth rates. If roughness is provided, the ALHZOZ header must include the definition of the surface roughness classes. CAMx is configured to read 9 roughness classes, and their definitions must range between the limits of 1×10^{-5} and 20 m, otherwise CAMx will stop with an error message.

Class interval definitions are not needed for land/ocean mask, drought stress, or snow cover. The land/ocean mask is used for Hg chemistry and defines chloride concentrations; it is simply a map of 0 (land) and 1 (ocean). Drought stress indices coincide with the Palmer Drought Index (PDI) and range from 0 to 5 (corresponding to PDI values 0 [normal] to –5 [severe drought]). Drought stress impacts dry deposition calculations for non-water landuse categories. Snow cover is simply a map of 0 (no snow) and 1(snow); if snow exists, the season is overridden to "winter with snow". This impacts surface roughness, surface resistances for dry deposition, and chemistry by setting UV albedo to the maximum class.

```
O3 Column =0.285  Albedo =0.040  Haze O.D. =0.000
  0.000 = Current altitude in km
   4.562E-01   4.526E-01   4.416E-01   4.224E-01   3.934E-01   3.516E-01   2.921E-01   2.065E-01   1.148E-01   3.074E-02
   1.670E-03   1.643E-03   1.563E-03   1.427E-03   1.236E-03   9.889E-04   6.936E-04   3.747E-04   1.502E-04   2.570E-05
   2.211E-03   2.186E-03   2.107E-03   1.973E-03   1.776E-03   1.506E-03   1.152E-03   7.108E-04   3.352E-04   7.560E-05
   2.078E-03   2.007E-03   1.801E-03   1.485E-03   1.097E-03   6.925E-04   3.382E-04   1.034E-04   2.201E-05   2.056E-06
   3.131E-04   3.058E-04   2.841E-04   2.491E-04   2.027E-04   1.482E-04   9.100E-05   4.015E-05   1.264E-05   1.517E-06
   8.728E-05   8.638E-05   8.364E-05   7.891E-05   7.189E-05   6.212E-05   4.892E-05   3.166E-05   1.580E-05   3.934E-06
  0.150 = Current altitude in km
   4.866E-01   4.830E-01   4.717E-01   4.521E-01   4.223E-01   3.794E-01   3.179E-01   2.284E-01   1.308E-01   3.760E-02
   1.855E-03   1.827E-03   1.742E-03   1.598E-03   1.394E-03   1.130E-03   8.102E-04   4.566E-04   1.956E-04   3.701E-05
   2.443E-03   2.416E-03   2.334E-03   2.193E-03   1.986E-03   1.701E-03   1.322E-03   8.415E-04   4.159E-04   1.000E-04
   2.327E-03   2.249E-03   2.024E-03   1.677E-03   1.250E-03   8.008E-04   4.035E-04   1.337E-04   3.383E-05   4.166E-06
   3.489E-04   3.410E-04   3.177E-04   2.799E-04   2.297E-04   1.704E-04   1.075E-04   5.024E-05   1.755E-05   2.556E-06
   9.553E-05   9.460E-05   9.176E-05   8.684E-05   7.952E-05   6.928E-05   5.530E-05   3.672E-05   1.910E-05   5.068E-06
  0.360 = Current altitude in km
   5.050E-01   5.013E-01   4.900E-01   4.702E-01   4.402E-01   3.968E-01   3.343E-01   2.426E-01   1.412E-01   4.171E-02
   1.974E-03   1.945E-03   1.857E-03   1.708E-03   1.497E-03   1.222E-03   8.862E-04   5.096E-04   2.245E-04   4.415E-05
   2.587E-03   2.560E-03   2.477E-03   2.333E-03   2.120E-03   1.826E-03   1.432E-03   9.258E-04   4.673E-04   1.152E-04
   2.494E-03   2.411E-03   2.174E-03   1.806E-03   1.353E-03   8.740E-04   4.474E-04   1.536E-04   4.129E-05   5.492E-06
   3.722E-04   3.640E-04   3.396E-04   3.002E-04   2.475E-04   1.851E-04   1.183E-04   5.679E-05   2.067E-05   3.210E-06
   1.006E-04   9.970E-05   9.681E-05   9.180E-05   8.433E-05   7.382E-05   5.940E-05   3.999E-05   2.122E-05   5.763E-06
  0.640 = Current altitude in km
   5.230E-01   5.193E-01   5.080E-01   4.882E-01   4.581E-01   4.143E-01   3.510E-01   2.574E-01   1.520E-01   4.577E-02
   2.092E-03   2.062E-03   1.972E-03   1.819E-03   1.601E-03   1.315E-03   9.632E-04   5.633E-04   2.535E-04   5.126E-05
   2.731E-03   2.703E-03   2.618E-03   2.471E-03   2.254E-03   1.951E-03   1.544E-03   1.011E-03   5.191E-04   1.304E-04
   2.664E-03   2.577E-03   2.327E-03   1.939E-03   1.459E-03   9.497E-04   4.928E-04   1.738E-04   4.872E-05   6.809E-06
   3.958E-04   3.872E-04   3.618E-04   3.207E-04   2.656E-04   2.000E-04   1.294E-04   6.343E-05   2.378E-05   3.860E-06
   1.057E-04   1.047E-04   1.018E-04   9.672E-05   8.912E-05   7.839E-05   6.354E-05   4.331E-05   2.336E-05   6.448E-06
  0.980 = Current altitude in km
   5.409E-01   5.373E-01   5.260E-01   5.062E-01   4.760E-01   4.321E-01   3.682E-01   2.727E-01   1.635E-01   4.989E-02
   2.210E-03   2.179E-03   2.087E-03   1.930E-03   1.705E-03   1.409E-03   1.041E-03   6.178E-04   2.827E-04   5.837E-05
   2.873E-03   2.845E-03   2.758E-03   2.609E-03   2.387E-03   2.077E-03   1.656E-03   1.099E-03   5.718E-04   1.454E-04
   2.837E-03   2.746E-03   2.483E-03   2.074E-03   1.567E-03   1.028E-03   5.396E-04   1.944E-04   5.611E-05   8.121E-06
   4.195E-04   4.106E-04   3.842E-04   3.414E-04   2.840E-04   2.152E-04   1.407E-04   7.017E-05   2.689E-05   4.509E-06
   1.107E-04   1.097E-04   1.068E-04   1.016E-04   9.392E-05   8.299E-05   6.775E-05   4.673E-05   2.556E-05   7.133E-06
  1.380 = Current altitude in km
   5.593E-01   5.556E-01   5.444E-01   5.247E-01   4.947E-01   4.507E-01   3.863E-01   2.892E-01   1.760E-01   5.427E-02
   2.329E-03   2.298E-03   2.203E-03   2.042E-03   1.811E-03   1.505E-03   1.122E-03   6.743E-04   3.128E-04   6.563E-05
   3.016E-03   2.988E-03   2.900E-03   2.749E-03   2.524E-03   2.207E-03   1.773E-03   1.190E-03   6.270E-04   1.609E-04
   3.015E-03   2.920E-03   2.644E-03   2.215E-03   1.681E-03   1.109E-03   5.887E-04   2.158E-04   6.364E-05   9.454E-06
   4.437E-04   4.345E-04   4.071E-04   3.627E-04   3.029E-04   2.310E-04   1.524E-04   7.716E-05   3.009E-05   5.169E-06
   1.157E-04   1.148E-04   1.118E-04   1.066E-04   9.883E-05   8.772E-05   7.213E-05   5.031E-05   2.789E-05   7.835E-06
  1.840 = Current altitude in km
   5.782E-01   5.746E-01   5.635E-01   5.440E-01   5.141E-01   4.702E-01   4.056E-01   3.069E-01   1.897E-01   5.904E-02
   2.451E-03   2.419E-03   2.322E-03   2.157E-03   1.920E-03   1.605E-03   1.206E-03   7.338E-04   3.445E-04   7.312E-05
   3.162E-03   3.133E-03   3.045E-03   2.892E-03   2.664E-03   2.341E-03   1.894E-03   1.286E-03   6.856E-04   1.769E-04
   3.200E-03   3.101E-03   2.811E-03   2.361E-03   1.799E-03   1.196E-03   6.407E-04   2.385E-04   7.141E-05   1.082E-05
   4.685E-04   4.589E-04   4.307E-04   3.846E-04   3.224E-04   2.473E-04   1.647E-04   8.451E-05   3.341E-05   5.848E-06
   1.209E-04   1.199E-04   1.169E-04   1.117E-04   1.039E-04   9.263E-05   7.671E-05   5.412E-05   3.039E-05   8.570E-06
  2.350 = Current altitude in km
   5.974E-01   5.939E-01   5.829E-01   5.636E-01   5.340E-01   4.904E-01   4.257E-01   3.258E-01   2.046E-01   6.425E-02
   2.572E-03   2.540E-03   2.441E-03   2.273E-03   2.031E-03   1.706E-03   1.292E-03   7.955E-04   3.775E-04   8.077E-05
   3.307E-03   3.278E-03   3.190E-03   3.036E-03   2.805E-03   2.477E-03   2.019E-03   1.386E-03   7.476E-04   1.934E-04
   3.389E-03   3.285E-03   2.983E-03   2.512E-03   1.922E-03   1.285E-03   6.952E-04   2.622E-04   7.936E-05   1.221E-05
   4.934E-04   4.836E-04   4.544E-04   4.068E-04   3.424E-04   2.641E-04   1.774E-04   9.214E-05   3.685E-05   6.538E-06
   1.261E-04   1.251E-04   1.221E-04   1.169E-04   1.090E-04   9.763E-05   8.142E-05   5.811E-05   3.305E-05   9.333E-06
  2.910 = Current altitude in km
   6.169E-01   6.134E-01   6.026E-01   5.836E-01   5.543E-01   5.111E-01   4.466E-01   3.458E-01   2.209E-01   7.003E-02
   2.694E-03   2.661E-03   2.561E-03   2.390E-03   2.143E-03   1.810E-03   1.382E-03   8.602E-04   4.124E-04   8.867E-05
   3.452E-03   3.423E-03   3.335E-03   3.180E-03   2.948E-03   2.615E-03   2.148E-03   1.492E-03   8.140E-04   2.106E-04
   3.582E-03   3.474E-03   3.159E-03   2.667E-03   2.049E-03   1.379E-03   7.528E-04   2.874E-04   8.761E-05   1.363E-05
   5.187E-04   5.086E-04   4.786E-04   4.294E-04   3.628E-04   2.814E-04   1.906E-04   1.002E-04   4.045E-05   7.246E-06
   1.312E-04   1.303E-04   1.273E-04   1.221E-04   1.142E-04   1.027E-04   8.630E-05   6.231E-05   3.593E-05   1.014E-05
  3.530 = Current altitude in km
   6.368E-01   6.334E-01   6.228E-01   6.041E-01   5.754E-01   5.328E-01   4.687E-01   3.673E-01   2.389E-01   7.670E-02
   2.818E-03   2.784E-03   2.683E-03   2.510E-03   2.258E-03   1.917E-03   1.476E-03   9.296E-04   4.505E-04   9.704E-05
   3.599E-03   3.571E-03   3.482E-03   3.328E-03   3.094E-03   2.759E-03   2.283E-03   1.605E-03   8.871E-04   2.291E-04
   3.783E-03   3.670E-03   3.343E-03   2.830E-03   2.184E-03   1.478E-03   8.148E-04   3.147E-04   9.644E-05   1.512E-05
   5.446E-04   5.343E-04   5.034E-04   4.528E-04   3.840E-04   2.996E-04   2.046E-04   1.088E-04   4.434E-05   7.989E-06
   1.365E-04   1.355E-04   1.326E-04   1.274E-04   1.195E-04   1.080E-04   9.142E-05   6.681E-05   3.911E-05   1.103E-05
  4.210 = Current altitude in km
   6.569E-01   6.536E-01   6.433E-01   6.250E-01   5.969E-01   5.550E-01   4.917E-01   3.902E-01   2.588E-01   8.447E-02
   2.943E-03   2.909E-03   2.807E-03   2.632E-03   2.376E-03   2.029E-03   1.574E-03   1.004E-03   4.925E-04   1.060E-04
   3.747E-03   3.719E-03   3.631E-03   3.477E-03   3.243E-03   2.906E-03   2.424E-03   1.725E-03   9.679E-04   2.493E-04
   3.992E-03   3.875E-03   3.534E-03   3.000E-03   2.325E-03   1.585E-03   8.818E-04   3.447E-04   1.060E-04   1.668E-05
   5.711E-04   5.605E-04   5.289E-04   4.769E-04   4.060E-04   3.186E-04   2.195E-04   1.181E-04   4.859E-05   8.775E-06
   1.417E-04   1.408E-04   1.379E-04   1.327E-04   1.249E-04   1.135E-04   9.674E-05   7.161E-05   4.262E-05   1.202E-05
 O3 Column =0.285  Albedo =0.040  Haze O.D. =0.094
  0.000 = Current altitude in km
   4.655E-01   4.615E-01   4.493E-01   4.279E-01   3.958E-01   3.499E-01   2.855E-01   1.957E-01   1.048E-01   2.871E-02
   1.688E-03   1.660E-03   1.576E-03   1.435E-03   1.237E-03   9.833E-04   6.824E-04   3.626E-04   1.414E-04   2.142E-05
   2.240E-03   2.212E-03   2.129E-03   1.987E-03   1.780E-03   1.498E-03   1.132E-03   6.858E-04   3.159E-04   6.495E-05
   2.098E-03   2.025E-03   1.815E-03   1.492E-03   1.098E-03   6.883E-04   3.334E-04   1.009E-04   2.101E-05   1.716E-06
   3.162E-04   3.086E-04   2.863E-04   2.503E-04   2.029E-04   1.473E-04   8.961E-05   3.896E-05   1.193E-05   1.254E-06
   8.857E-05   8.761E-05   8.467E-05   7.961E-05   7.213E-05   6.180E-05   4.802E-05   3.042E-05   1.483E-05   3.488E-06
  0.150 = Current altitude in km
   5.004E-01   4.963E-01   4.839E-01   4.623E-01   4.296E-01   3.828E-01   3.163E-01   2.220E-01   1.237E-01   3.1E-02
   1.870E-03   1.841E-03   1.752E-03   1.604E-03   1.394E-03   1.123E-03   7.976E-04   4.424E-04   1.847E-04   3.188E-05
   2.473E-03   2.445E-03   2.359E-03   2.211E-03   1.994E-03   1.697E-03   1.306E-03   8.179E-04   3.956E-04   8.840E-05
   2.338E-03   2.259E-03   2.030E-03   1.677E-03   1.245E-03   7.929E-04   3.960E-04   1.294E-04   3.180E-05   3.572E-06
   3.509E-04   3.428E-04   3.189E-04   2.803E-04   2.292E-04   1.690E-04   1.056E-04   4.859E-05   1.651E-05   2.187E-06
   9.713E-05   9.614E-05   9.312E-05   8.789E-05   8.013E-05   6.934E-05   5.476E-05   3.574E-05   1.823E-05   4.615E-06
```

Figure 5-3. Example of the first several panels of lookup data in the photolysis rates input file.

Only one map of codes per grid is present in the ALHZOZ file for the time-invariant fields (UV albedo, land/water mask, drought stress, and surface roughness); these fields can be provided in any order. For time-varying fields (ozone column, turbidity, and snow cover) multiple maps of these codes may be provided for arbitrary time intervals, unique to each field, to span the entire simulation period. It is not necessary that the time spans of the ozone, turbidity, and snow cover maps match; for example, six maps of ozone column may be supplied for a six day simulation along with only one map for turbidity and snow cover covering the same time span.

The ALHZOZ file is a readable text (ASCII) format and it has the following structure:

`text`	(A)	
`alname,(albcl(n),n=1,nalb)`	(A10,5F10.0)	
`hzname,(hazcl(n),n=1,nhaz)`	(A10,3F10.0)	
`ozname,(ozncl(n),n=1,nozn)`	(A10,5F10.0)	
`rlname,(ruflen(n),n=1,nruf)`	(A10,9f10.0)	-- Optional
`loname`	(A10)	-- Optional
`drname`	(A10)	-- Optional
`swname`	(A10)	-- Optional
`alname,igrd,nx,ny`	(A10,3I10)	
Loop from *ny* grid rows to 1		
`(jalb(i,j),i=1,nx)`	(9999I1)	
`alname,igrd,nx,ny`	(A10,3I10)	
`rlname,igrd,nx,ny`	(A10,3I10)	
Loop from *ny* grid rows to 1		
`(jruf(i,j),i=1,nx)`	(9999I1)	
`rlname,igrd,nx,ny`	(A10,3I10)	
`loname,igrd,nx,ny`	(A10,3I10)	
Loop from *ny* grid rows to 1		
`(jocn(i,j),i=1,nx)`	(999I1)	-- Optional
`loname,igrd,nx,ny`	(A10,3I10)	
`drname,igrd,nx,ny`	(A10,3I10)	
Loop from *ny* grid rows to 1		
`(jdrt(i,j),i=1,nx)`	(999I1)	
`drname,igrd,nx,ny`	(A10,3I10)	
`name,idt1,tim1,idt2,tim2`	(A10,I10,F10.0,I10,F10.0)	
Loop from *ny* master grid rows to 1		
`(jozn(i,j),i=1,nx)` or	(9999I1)	
`(jhaz(i,j),i=1,nx)` or	(9999I1)	
`(jsno(i,j),i=1,nx)`	(9999I1)	-- Optional
	(*name* determines if *jozn, jhaz,* or *jsno* is read)	

where the variables in the ALHZOZ file have the following definitions:

`text`	Text identifying file and any messages
`alname`	Text string "ALBEDO"
`albcl`	UV albedo (unitless) for each of *nalb* albedo values
`hzname`	Text string "HAZE"

`hazcl`	Haze turbidity (unitless) for each of *nhaz* haze values
`ozname`	Text string "OZONE COL"
`ozncl`	Ozone column (Dobson units) for each of *nozn* ozone values
`rlname`	Text string "ROUGHNESS"
`ruflen`	Roughness length (m) for each of *nruf* roughness values
`loname`	Text string "OCEAN"
`drname`	Text string "DROUGHT"
`swname`	Text string "SNOW"
`igrd`	Grid index (1 = master grid, 2+=nested grid, 0 = end of data)
`nx`	Number of grid columns for this grid index
`ny`	Number of grid rows for this grid index
`jalb`	Grid *igrd,* row *j* albedo codes for *nx* grid columns
`jruf`	Grid *igrd,* row *j* roughness codes for *nx* grid columns
`jocn`	Grid *igrd,* row *j* land/ocean codes for *nx* grid columns
`jdrt`	Grid *igrd,* row *j* drought codes for *nx* grid columns
`name`	Text string "OZONE COL", "HAZE", or "SNOW"
`idt1`	Beginning date (YYMMDD or YYJJJ) of time span
`tim1`	Beginning hour (HHMM) of time span
`idt2`	Ending date of time span
`tim2`	Ending hour of time span
`jozn`	Master grid row *j* ozone column codes for *nx* master grid columns
`jhaz`	Master grid row *j* haze codes for *nx* master grid columns
`jsno`	Master grid row *j* snow codes for *nx* master grid columns

An example of a small ALHZOZ file is given in Figure 5-4.

5.5 TOP CONCENTRATION FILE

The top concentration file contains the time- and space-invariant species concentrations that are assumed to exist above the top boundary of the entire modeling grid. Top concentrations may be specified for a sub-set of the total number of modeled species. For those species not supplied in the top concentration file, CAMx assumes the "lower bound" values specified in the chemistry parameters file. Only one top concentration file must be developed for the entire domain, and it must contain a concentration value for at least one species. The concentrations are assumed to be valid for the duration of the simulation (although separate top concentration files could be supplied for each individual day modeled as long as CAMx is run separately for each day).

The top concentration file is a readable text (ASCII) format and it has the following structure:

Loop from 1 to *nspec* species:	
`name,caloft`	(a10,f10.7)

```
Sample AHO file with all optional fields
ALBEDO        0.0400    0.0500    0.0600    0.0700    0.0800
HAZE          0.0000    0.0940    0.3950
OZONE COL     0.2850    0.3150    0.3450    0.3750    0.4050
ROUGHNESS     0.0010    0.0100    0.0200    0.0500    0.1000    0.2000    0.5000 …
OCEAN
DROUGHT
SNOW
ALBEDO              1         64         10
22222222222222222221111111112222222222222222223333333333333333
22222222222222222222222221111111112222222222222222333333333333
22222222222222222222222111111111112222222222222222233333333333
22222222222222222222222211111111111222222222222222223333333333
22222222222222222222222221111111111122222222222222222222223333
22222222222222222222222211111111111112222222222222222222222222
22222222222222222222222111111111111111222222222222222222222222
22222222222222222222221111111111111111222222222222222222222222
22222222222222222222211111112222222221111111122222222222222222
22222222222222222222211111111222222221111111112222222222222222
22222222222222222222211111111122222221111111111222222222222222
ALBEDO              2         24         15
212111211111111111112222
222122222211111111111112
222222222222211111111111
222222222222111111111111
222222222211111111111111
222222222111111111111111
222222222111111111111111
222222222111111111111111
222222222112222221111111
222222211112222221111111
222222211122222221111111
222222211122222221111111
222222211122222221111111
222222211112222221111111
222222211112222221111111
ALBEDO              0          0          0
ROUGHNESS           1         64         10
444444444433333333337777777773333333333333333322222222222222222
444444444444433333333333337777777773333333333333333222222222222
444444444444443333333333377777777777733333333333333322222222222
444444444444444333333333337777777777733333333333333333333332222
444444444444443333333333777777777777733333333333333333333333333
444444444444443333333377777777777777733333333333333333333333333
444444444443333333333777777777777777733333333333333333333333333
444444444433333333337777777773333333377777777733333333333333333
444444444333333333333777777777733333333377777777773333333332222
ROUGHNESS           0          0          0
OCEAN               1         64         10
000000000000000000001111111110000000000000000000000000000000000
000000000000000000000000001111111110000000000000000000000000000
000000000000000000000000011111111111100000000000000000000000000
000000000000000000000000001111111111110000000000000000000000000
000000000000000000000001111111111111110000000000000000000000000
000000000000000000000011111111111111110000000000000000000000000
000000000000000000000111111100000000111111110000000000000000000
000000000000000000001111111100000000111111110000000000000000000
000000000000000000001111111110000000011111111100000000000000000
OCEAN               0          0          0
```

Figure 5-4. Example of the structure of a 2-grid abedo/haze/ozone input file showing panels for all mandatory and optional fields.

```
DROUGHT
22222222222222222222222222222222222222222211111111111111111111
22222222222222222222222222222222222222222222211111111111111111
22222222222222222222222222222222222222222222222211111111111111
22222222222222222222222222222222222222222222222222211111111111
22222222222222222222222222222222222222222222222222222211111111
22222222222222222222222222222222222222222222222222222222211111
22222222222222222222222222222222222222222222222222222222222111
22222222222222222222222222222222222222222222222222222222222222
22222222222222222222222222222222222222222222222222222222222222
22222222222222222222222222222222222222222222222222222222222222
22222222222222222222222222222222222222222222222222222222222222
DROUGHT            0         0         0
HAZE          950707      0.00    950718   2400.00
22222222222222222222222222222222222222222222222222222222222222
22222222222222222222222222222222222222222222222222222222222222
22222222222222222222222222222222222222222222222222222222222222
22222222222222222222222222222222222222222222222222222222222222
22222222222222222222222222222222222222222222222222222222222222
22222222222222222222222222222222222222222222222222222222222222
22222222222222222222222222222222222222222222222222222222222222
22222222222222222222222222222222222222222222222222222222222222
22222222222222222222222222222222222222222222222222222222222222
22222222222222222222222222222222222222222222222222222222222222
OZONE COL     950707      0.00    950718   2400.00
33333333333333333333333333333333333333333333333333333333333333
33333333333333333333333333333333333333333333333333333333333333
22222222222233333333333333333333333333333333333333333333333333
22222222222222333333333333333333333333333333333333333333333333
22222222222222333333333333333333333333333333333333333333333333
22222222222222333333333333333333333333333333333333333333333333
22222222222222333333333333333333333333333333333333333333333333
22222222222222333333333333333333333333333333333333333333333333
22222222222222333333333333333333333333333333333333333333333333
22222222222222333333333333333333333333333333333333333333333333
22222222222222222222233333333333333333333333333333333333333333
SNOW          950707      0.00    950718   2400.00
00000000000000000000000000000000000000000000000000000000000000
00000000000000000000000000000000000000000000000000000000000000
00000000000000000000000000000000000000000000000000000000000000
00000000000000000000000000000000000000000000000000000000000000
00000000000000000000000000000000000000000000000000000000000000
00000000000000000000000000000000000000000000000000000000000000
00000000000000000000000000000000000000000000000000000000000000
00000000000000000000000000000000000000000000000000000000000000
00000000000000000000000000000000000000000000000000000000000000
00000000000000000000000000000000000000000000000000000000000000
```

Figure 5-4. (concluded).

where the variables in the top concentration file have the following definitions:

`name`	Species *l* name (following the convention in the chemistry parameters file)
`caloft`	Species *l* concentration aloft (ppm for gases, $\mu g/m^3$ for aerosols)

An example top concentration file is shown below:

```
NO          .000000049
NO2         .000085550
O3          .034630000
OLE         .000000000
PAR         .003078000
TOL         .000006043
XYL         .000000000
HCHO        .001068000
ALD2        .000105100
ETH         .000005315
PAN         .000038340
CO          .099540000
HNO2        .000000728
H2O2        .002263000
HNO3        .001525000
ISOP        .000000000
```

5.6 FORTRAN BINARY INPUT FILES

Options for Format of Fortran Binary Input/Output Files

CAMx reads and writes many 3-D, time resolved files that can require significant disk storage. Therefore, these files are written as Fortran unformatted binary to minimize storage requirements. Furthermore, all CAMx binary I/O is written in the IEEE "big_endian" standard to maximize platform portability. Most UNIX workstations internally represent binary data as big_endian; however, Digital Equipment Corporation (DEC) Alpha workstations and Linux PCs use a reversed format by default, referred to as "little_endian". Compiler options are available in the CAMx Makefile (which compiles the source code and "makes" an executable application) so that CAMx compiled on DEC and PC machines will be able to read and write IEEE big_endian binary I/O files. More information on this topic is provided in Section 11.

Meteorological Input Files

Landuse File

The Fortran binary landuse input file contains time-invariant two-dimensional gridded fields of landuse distribution. This file must be developed for the master grid, and optionally any of

the nested fine grids, if either dry deposition or the PiG submodel is invoked. The fractional distribution of 11 landuse categories are supplied for each grid cell. These are used to define surface resistances for dry deposition calculations and to set default surface roughness lengths. These landuse categories follow the UAM-IV conventions (EPA, 1990), and are described in Table 5-5. The landuse file has the following structure:

```
(((fland(i,j,k),i=1,nx),j=1,ny),k=1,11)
```

where the variables in the landuse file have the following definitions:

`fland` Fractional landuse distribution for *nx* grid columns, *ny* grid rows, and 11 landuse categories

Table 5-5. CAMx landuse categories and the default surface roughness values (m) assigned to each category by season. Winter is defined for conditions where there is snow present; winter months with no snow are assigned to the Fall category. Roughness for water is taken as the maximum of the baseline value given in the table, and the function $z_0 = 2\times10^{-6} w^{2.5}$, where *w* is surface wind speed (m/s). The listed UV albedo values can be used to assign UV albedo from landuse data in preparing the albedo/haze/ozone (AHO) input file.

Category Number	Land Cover Category	Surface Roughness (meters)				UV Albedo
		Spring	Summer	Fall	Winter	
1	Urban	1.00	1.00	1.00	1.00	0.08
2	Agricultural	0.03	0.20	0.05	0.01	0.05
3	Rangeland	0.05	0.10	0.01	0.001	0.05
4	Deciduous forest	1.00	1.30	0.80	0.50	0.05
5	Coniferous forest, wetland	1.30	1.30	1.30	1.30	0.05
6	Mixed forest*	1.15	1.30	1.05	0.90	0.05
7	Water	0.0001	0.0001	0.0001	0.0001	0.04
8	Barren land	0.002	0.002	0.002	0.002	0.08
9	Non-forested wetlands	0.20	0.20	0.20	0.05	0.05
10	Mixed agricultural/range*	0.04	0.15	0.03	0.006	0.05
11	Rocky (with low shrubs)	0.30	0.30	0.30	0.15	0.05

* Roughness for these categories is taken to be the average of their components.

Height/Pressure File

The Fortran binary height/pressure input file contains three-dimensional gridded fields of layer interface heights and layer-average pressure. This file must be developed for the master grid and optionally any fine grid nest specified for a given simulation. The layer interface heights define the vertical grid structure for each grid, as well as the vertical nesting structure for fine grid nests. For this reason, vertical nesting is not allowed when flexi-nesting is used. The layer interface heights may be specified to vary in space and/or time (e.g., to follow the layer

structure of meteorological models), or they may be set to a constant field. The pressure field is used for transport, plume rise, PiG, dry deposition, and chemistry calculations.

The height/pressure file has the following structure, where the following records are repeated for each update time:

```
Loop from 1 to nlay layers:
   hour,idate,((height(i,j,k),i=1,nx),j=1,ny)
   hour,idate,((press(i,j,k),i=1,nx),j=1,ny)
```

The variables in the height/pressure file have the following definitions:

`hour`	Simulation time (HHMM: 1300.0 is 1:00 PM)
`idate`	Simulation date (YYMMDD or YYJJJ)
`height`	Layer *k* interface height (m AGL) for *nx* grid columns, and *ny* grid rows
`press`	Layer *k* pressure (mb) for *nx* grid columns, and *ny* grid rows

CAMx time-interpolates the height and pressure arrays to each model timestep for each grid, and so the model requires that data be available on file for an additional update time at the end of the simulation. For example, in the case of hourly fields, a 24-hour simulation requires 25 input fields on file.

Wind File

The Fortran binary wind file contains three-dimensional gridded fields of layer average horizontal (*u* and *v*) wind components. This file must be developed for the master grid and optionally any of the fine grid nests. CAMx allows the user to optionally supply these components at cell center, in which case the model will interpolate the components to their respective positions on cell interfaces, or the user may supply these components directly on the Arakawa C configuration (recommended). In any case, the user must supply a full $nx \times ny \times nz$ array of wind values for each component (even though for the Arakawa C configuration in CAMx, only $(nx-1) \times (ny-1)$ values are used in the horizontal). Wind fields are used for transport, plume rise, PiG, and dry deposition calculations.

The wind file has the following structure, where the following records are repeated for each update time:

```
hour,idate
Loop from 1 to nlay layers:
   ((uwind(i,j,k),i=1,nx),j=1,ny)
   ((vwind(i,j,k),i=1,nx),j=1,ny)
((dummy,i=1,nx),j=1,ny)
```

The variables in the wind file have the following definitions:

`hour`	Simulation time (HHMM: 1300.0 is 1:00 PM)
`idate`	Simulation date (YYMMDD or YYJJJ)

`uwind`	Layer *k* *u*-component (east-west) wind (m/s) for *nx* grid columns, and *ny* grid rows
`vwind`	Layer *k* *v*-component (north-south) wind (m/s) for *nx* grid columns, and *ny* grid rows
`dummy`	Dummy array

CAMx time-interpolates the wind components to each model timestep for each grid, and so the model requires that data be available on file for an additional update time at the end of the simulation. For example, in the case of hourly fields, a 24-hour simulation requires 25 input fields on file.

Temperature File

The Fortran binary temperature file contains three-dimensional gridded fields of layer average temperature and two-dimensional gridded fields of surface temperature. This file must be developed for the master grid and optionally any of the fine grid nests. The three-dimensional temperature fields are used for transport, plume rise, PiG, dry and wet deposition and chemistry calculations, while the surface temperatures are used for dry deposition calculations.

The temperature file has the following structure, where the following records are repeated for each update time:

```
hour,idate,((temps(i,j),i=1,nx),j=1,ny)
Loop from 1 to nlay layers:
   hour,idate,((temp(i,j,k),i=1,nx),j=1,ny)
```

The variables in the temperature file have the following definitions:

`hour`	Simulation time (HHMM: 1300.0 is 1:00 PM)
`idate`	Simulation date (YYMMDD or YYJJJ)
`temps`	Surface temperature (K) for *nx* grid columns, and *ny* grid rows
`temp`	Layer *k* temperature (K) for *nx* grid columns, and *ny* grid rows

CAMx time-interpolates the temperature to each model timestep for each grid, and so the model requires that data be available on file for an additional update time at the end of the simulation. For example, in the case of hourly fields, a 24-hour simulation requires 25 input fields on file.

Water Vapor File

The Fortran binary water vapor file contains three-dimensional gridded fields of layer average water vapor concentration. This file must be developed for the master grid, and optionally any fine grid nests, if chemistry, dry deposition, and/or wet deposition are invoked. The three-dimensional water vapor fields are used for dry and wet deposition and chemistry calculations.

The water vapor file has the following structure, where the following record is repeated for each update time:

```
Loop from 1 to nlay layers:
   hour,idate,((water(i,j,k),i=1,nx),j=1,ny)
```

The variables in the water vapor file have the following definitions:

`hour`	Simulation time (HHMM: 1300.0 is 1:00 PM)
`idate`	Simulation date (YYMMDD or YYJJJ)
`water`	Layer *k* water vapor concentration (ppm) for *nx* grid columns and *ny* grid rows

CAMx time-interpolates the water vapor to each model timestep for each grid, and so the model requires that data be available on file for an additional update time at the end of the simulation. For example, in the case of hourly fields, a 24-hour simulation requires 25 input fields on file.

Cloud/Rain File

The Fortran binary cloud/rain file contains three-dimensional gridded fields of cloud parameters to be used for chemistry and wet/dry deposition calculations. Note that rainfall rate is not explicitly provided to the model; instead, it is internally calculated from the precipitation water content provided on the cloud/rain file. This file must be developed for the master grid, and optionally any fine grid nests, if chemistry, dry, and/or wet deposition are invoked. CAMx incorporates the RADM approach of Chang et al. (1987) to treat the impacts of cloud cover on photolysis rates. This approach requires information on cloud optical depth and liquid water content to scale down photolysis rates for layers within or below clouds to account for UV attenuation, or to scale up the rates for layers above clouds to account for UV reflection.

The cloud/rain file contains a header record to define the file:

```
cldhdr,nxcl,nycl,nzcl
```

The remainder of the file has the following structure, where the following records are repeated for each update time:

```
hour,idate
Loop from 1 to nz layers:
   ((cwater(i,j,k),i=1,nx),j=1,ny)
   ((pwater(i,j,k),i=1,nx),j=1,ny)
   ((cldod(i,j,k),i=1,nx),j=1,ny)
```

The variables on the cloud/rain file have the following definitions:

`cldhdr`	Text string "CAMX CLOUD_RAIN"
`nxcl`	Number of master grid columns
`nycl`	Number of master grid rows
`nzcl`	Number of master grid layers
`hour`	Simulation time (HHMM: 1300.0 is 1:00 PM)
`idate`	Simulation date (YYMMDD or YYJJJ)
`cwater`	Layer *k* cloud water content (g/m^3) for *nx* grid columns, and *ny* grid rows
`pwater`	Layer *k* precipitation water content (g/m^3) for *nx* grid columns, and *ny* grid rows
`cldod`	Layer *k* total integrated column cloud optical depth (dimensionless) for *nx* grid columns, and *ny* grid rows

Vertical Diffusivity File

The Fortran binary vertical diffusivity file contains three-dimensional gridded fields of layer-interface vertical diffusivity (i.e., turbulent exchange or diffusion coefficients). This file must be developed for the master grid, and optionally any fine grid nests. The three-dimensional diffusivity fields are used for vertical diffusion and PiG puff growth calculations.

The vertical diffusivity file has the following structure, where the following records are repeated for each update time:

Loop from 1 to *nz* layers:

```
hour,idate,((rkv(i,j,k),i=1,nx),j=1,ny)
```

The variables on the vertical diffusivity file have the following definitions:

`hour`	Simulation time (HHMM: 1300.0 is 1:00 PM)
`idate`	Simulation date (YYMMDD or YYJJJ)
`rkv`	Layer *k* interface diffusivity (m^2/s) for *nx* grid columns, and *ny* grid rows

CAMx time-interpolates the diffusivity to each model timestep for each grid, and so the model requires that data be available on file for an additional update time at the end of the simulation. For example, in the case of hourly fields, a 24-hour simulation requires 25 input fields on file.

Initial Conditions File

The Fortran binary initial conditions file contains three-dimensional gridded concentration fields on the master grid. Initial concentration fields may be specified for a sub-set of the total number of modeled species. The format of this file follows that defined for UAM-IV concentration files (EPA, 1990) so that pre-existing software may be used to develop these input files. An initial condition file must be developed for the master grid, and contain

concentration fields for at least one species. For those species not on the initial condition file, CAMx sets up uniform fields using the "lower bound" values specified in the chemistry parameters file. CAMx then interpolates all master grid initial conditions to each fine grid nest at the start of the simulation.

The initial conditions file contains a set of time-invariant header records, followed by a set of data records that contain time- and species-specific gridded concentration fields. The time span of concentration data must contain the start time/date of the simulation.

The header portion of the initial conditions file contains four records with the following structure:

```
name,note,ione,nspec,ibdate,btime,iedate,etime
rdum,rdum,iutm,xorg,yorg,delx,dely,nx,ny,nz,idum,idum,rdum,rdum,rdum
ione,ione,nx,ny
(mspec(l),l=1,nspec)
```

The time-variant portion of the initial conditions file has the following structure, where the following records are repeated for each update time:

```
ibdate,btime,iedate,etime
Loop from 1 to nspec species:
    Loop from 1 to nz layers:
        ione,mspec(l),((conc(i,j,k,l),i=1,nx),j=1,ny)
```

The variables on the initial conditions file have the following definitions:

name	Text string "AIRQUALITY" (character*4(10) array)
note	Text string containing file description (character*4(60) array)
ione	Dummy variable = 1
nspec	Number of species on file
ibdate	Beginning date (YYJJJ)
btime	Beginning hour (HH)
iedate	Ending date (YYJJJ)
etime	Ending hour (HH)
rdum	Dummy real variable
iutm	UTM zone (ignored for other projections)
xorg	Grid x-origin at southwest corner of domain (m or degrees longitude)
yorg	Grid y-origin at southwest corner of domain (m or degrees latitude)
delx	Cell size in x-direction (m or degrees longitude)
dely	Cell size in y-direction (m or degrees longitude)
nx	Number of grid columns
ny	Number of grid rows
nz	Number of layers
idum	Dummy integer variable
mspec	Species names for *nspec* species (character*4(10,nspec) array)

conc	Species *l*, layer *k* initial concentrations (ppm for gases, $\mu g/m^3$ for aerosols) for *nx* grid columns and *ny* grid rows

Lateral Boundary Conditions File

The Fortran binary lateral boundary conditions file contains two-dimensional gridded concentration fields on the lateral faces of the master grid boundary. Boundary concentration fields may be specified for a sub-set of the total number of modeled species. However, if a boundary concentration is specified for a given species, it must be supplied for all four boundaries. This file also defines any non-modeled portions of the master grid (i.e., a non-uniform boundary may be specified). The format of this file follows that defined for UAM-IV (EPA, 1990) so that pre-existing software may be used to develop these input files. The user should refer to the UAM-IV User's Guide for more information on specifying non-uniform boundaries. A boundary concentration file must be developed for the master grid, and contain concentration fields for at least one species. For those species not on the boundary conditions file, CAMx sets up uniform fields using the "lower bound" values specified in the chemistry parameters file.

The boundary file contains a set of time-invariant header records, followed by a set of data records that contain the time- and species-varying gridded boundary concentration fields. The time span of each set of boundary data records may be set arbitrarily; e.g., a set of boundary conditions may be specified for a six hour span, followed by a set spanning just an hour.

The header portion of the boundary conditions file contains eight records with the following structure:

```
name,note,ione,nspec,ibdate,btime,iedate,etime
rdum,rdum,iutm,xorg,yorg,delx,dely,nx,ny,nz,idum,idum,rdum,rdum,rdum
ione,ione,nx,ny
(mspec(l),l=1,nspec)
Loop from 1 to 4 boundaries:
   ione,iedge,ncell,(icell(n),idum,idum,idum,n=1,ncell)
```

The time-variant portion of the boundary conditions file has the following structure, where the following records are repeated for each update time:

```
ibdate,btime,iedate,etime
Loop from 1 to nspec species:
   Loop from 1 to 4 boundaries:
      ione,mspec(l),iedge,((bc(i,k,iedge,l),k=1,nz),i=1,ncell)
```

The variables that are unique to the boundary conditions file have the following definitions:

name	Text string "BOUNDARY" (character*4(10) array)
note	Text string containing file description (character*4(60) array)
iedge	Boundary edge number (1=west, 2=east, 3=south, 4=north)
ncell	Number of rows or columns on this edge

icell	Index of first cell modeled (edges 1,3), or last cell modeled (edges 2,4): if=0, this row/column is omitted from the simulation
bc	Species *l*, edge *iedge* boundary concentrations (ppm for gases, $\mu g/m^3$ for aerosols) for *ncell* grid rows/columns, and *nz* layers

See the section describing the initial conditions file for a full list of variable definitions common to all UAM-IV type files.

Elevated Point Source File

The Fortran binary elevated point source emissions file contains stack parameters and emission rates for all elevated point sources, and for all emitted species, to be modeled. The format of this file follows that defined for UAM-IV (EPA, 1990) so that pre-existing emission pre-processing software may be used to develop these input files. If elevated point sources are to be modeled, only one point source emissions file must be developed for the entire modeling domain. The point source file also flags the individual stacks to be treated by the CAMx PiG sub-model by setting the stack diameter as a negative value. The file offers the ability to optionally specify the effective plume height for each point source and to bypass the internal plume rise calculation.

The point source emissions file contains a set of time-invariant header records, followed by a set of data records that contain the time- and species-varying point source emissions data. The time span of each set of emission data records may be set arbitrarily; e.g., a set of point emissions may be specified for a six hour span, followed by a set spanning just an hour.

The header portion of the elevated point source file contain 5+*nstk* records with the following structure:

```
name,note,ione,nspec,ibdate,btime,iedate,etime
rdum,rdum,iutm,xorg,yorg,delx,dely,nx,ny,nz,idum,idum,rdum,rdum,rdum
ione,ione,nx,ny
(mspec(l),l=1,nspec)
ione,nstk
(xstk(n),ystk(n),hstk(n),dstk(n),tstk(n),vstk(n),n=1,nstk)
```

The time-variant portion of the elevated point source file has the following structure, where the following records are repeated for each update time:

```
ibdate,btime,iedate,etime
ione,nstk
(idum,idum,kcell(n),flow(n),plmht(n),n=1,nstk)
Loop from 1 to nspec species:
   ione,mspec(l),(ptems(n,l),n=1,nstk)
```

The variables that are unique to the elevated point source file have the following definitions:

name	Text string "PTSOURCE" (character*4(10) array)
note	Text string containing file description (character*4(60) array)

`nstk`	Number of point sources
`xstk`	Stack x-coordinate (m or degrees longitude) for *nstk* point sources
`ystk`	Stack y-coordinate (m or degrees latitude) for *nstk* point sources
`hstk`	Stack height (m) for *nstk* point sources
`dstk`	Stack diameter (m, negative if PiG source) for *nstk* point sources
`tstk`	Stack exit temperature (K) for *nstk* point sources
`vstk`	Stack exit velocity (m/hr) for *nstk* point sources
`kcell`	Ignored, except as flag for OSAT point source override, for *nstk* point sources
`flow`	Stack flow rate (m^3/hr) for *nstk* point sources
`plmht`	Effective plume height override (m, a negative value replaces the internal plume rise calculation) for *nstk* point sources
`ptems`	Species *l* point emission rate (mol/time period for gasses, g/time period for aerosols) for *nstk* point sources. Note that the emissions time period (the denominator for the emissions rate) is normally, but not necessarily, 1 hour.

See the section describing the initial conditions file for a full list of variable definitions common to all UAM-IV type files.

Gridded Emissions File

The Fortran binary emissions file contains two-dimensional gridded fields of low-level (i.e., surface) emission rates for all emitted species to be modeled. The format of this file follows that defined for UAM-IV (EPA, 1990) so that pre-existing emission pre-processing software may be used to develop these input files. If gridded emissions are to be modeled, a gridded emissions file must be developed for the master grid and optionally any nested fine grids.

The gridded emissions file contains a set of time-invariant header records, followed by a set of data records that contain the time- and species-varying gridded emission fields. The time span of each set of emission data records may be set arbitrarily; e.g., a set of emissions may be specified for a six hour span, followed by a set spanning just an hour.

The header portion of the gridded emissions file contain four records with the following structure:

```
name,note,ione,nspec,ibdate,btime,iedate,etime
rdum,rdum,iutm,xorg,yorg,delx,dely,nx,ny,nz,idum,idum,rdum,rdum,rdum
ione,ione,nx,ny
(mspec(l),l=1,nspec)
```

The time-variant portion of the initial conditions file has the following structure, where the following records are repeated for each update time:

```
ibdate,btime,iedate,etime
Loop from 1 to nspec species:
   ione,mspec(l),((emiss(i,j,l),i=1,nx),j=1,ny)
```

The time-span of the emissions record must match the input frequency of the emissions as specified in the CAMx.in file.

The variables that are unique to the gridded emission file have the following definitions:

`name`	Text string "EMISSIONS" (character*4(10) array)
`note`	Text string containing file description (character*4(60) array)
`emiss`	Species *l* gridded emission rate (mol/time period for gases, g/time period for aerosols) for *nx* grid columns and *ny* grid rows. Note that the emissions time period (the denominator for the emissions rate) is normally, but not necessarily, 1 hour.

See the section describing the initial conditions file for a full list of variable definitions common to all UAM-IV type files.

5.7 FORTRAN BINARY OUTPUT FILES

Master and nested grid instantaneous files contain full three-dimensional fields of all species modeled, while the master and nested grid average and deposition files contain only those species specified in the run control file. For flexibility, CAMx offers the option to write full three-dimensional average concentration fields, or just surface layer two-dimensional fields (see the "3-D average file" option in the CAMx control file). It is permissible to change the number of species on the average file, or change between 2-D and 3-D average files, from one CAMx simulation period to the next (provided the periods are configured as separate CAMx runs). As the instantaneous concentration files are used for CAMx restarts, the model only writes instantaneous fields for the latest two simulation hours. The instant file labeled "1" receives instantaneous fields for the latest odd hour, and the file labeled "2" receives instantaneous fields for the latest even hour. PiG output files are unique to CAMx, and are used primarily for model restarts. The PiG file contains all information carried by the sub-model for all simulation hours; therefore, there is sufficient information in the PiG file for subsequent postprocessing and analysis.

Master (Coarse) Grid Output Files

The master (or "coarse") grid Fortran binary output average, instantaneous, and deposition files have the same format, which is identical to the initial concentration file format described earlier. There are three differences between the output concentration files and the input initial concentration files. First, the file name given in the file description header record is "AVERAGE" for the average output file, "INSTANT" for the instantaneous output file, and "AIRQUALITY" for the input initial concentration file. Second, the "note" in the file description header record of the output concentration files is the message supplied in the first line of the CAMx run control file whereas the "note" in the air quality file is set as part of the

input file preparation. Third, the species lists can be different among the files: the output instantaneous file contains all species modeled (as specified in the chemistry parameters file), the average output file contains only the species specified in the run control file, and the input initial concentration file may contain any subset of modeled species as determined when that file is prepared.

Two other differences exist between the average and instantaneous output files. As noted above, the average file may contain only surface-level fields or the entire three-dimensional fields, as selected by the user. Also, gas concentration fields are output as ppm in average files, but as μmol/m^3 in instantaneous files (aerosols are in μg/m^3 in both files). Because of these differences, and because average files usually do not contain all modeled species, CAMx does not allow the average output concentration file to be used for simulation restarts.

The output deposition file is identical in format to the two-dimensional surface-level output average concentration file. The file name given on the first record of the deposition file is "AVERAGE" so that software such as PAVE will recognize the format for plotting (it will not recognize any other name, such as "DEPOSITION", and therefore will not read the file). However, the output deposition file differs from the output average concentration file in one important way. The species list is identical to the list on the average concentration output files, except that four parameters are output for each species:

species_DV	Two-dimensional dry deposition velocity field for *species* (m/s)
species_DD	Two-dimensional dry deposited mass field for *species* (mol/ha for gasses, g/ha for aerosols)
species_WD	Two-dimensional wet deposited mass field for *species* (mol/ha for gasses, g/ha for aerosols)
species_LC	Two-dimensional precipitation liquid concentration for *species* (mol/l for gasses, g/l for aerosols)

Nested (Fine) Grid Output Files

The nested (or "fine") grid Fortran binary output average, instantaneous, and deposition files have the same format. Output fields for all nested grids are contained together in these files, as opposed to separate files for each grid. All grid definition parameters given in these files are referenced relative to the master grid, so specific absolute information about grid cell size or projection coordinates for each nested grid must be determined from master grid parameters. Again, the only potential difference between average and instantaneous concentration output file formats are the number of layers and species. If the user utilizes the Flexi-nesting capability of CAMx, then the gridded fields output to the nested fine grid files will change according to how nests are altered, added, and/or removed during the course of a simulation.

The header portion of the nested grid output files contain 3+*nnest* records with the following structure:

```
message
nnest,nspec
(mspec(l),l=1,nspec)
Loop from 1 to nnest grid nests
   ibeg,jbeg,iend,jend,mesh,ione,nx,ny,nz,iparnt,ilevel
```

The time-variant portion of the nested grid output files have the following structure, where the following records are repeated for each output time:

```
time,idate
Loop from 1 to nnest grid nests
    Loop from 1 to nspec species:
        Loop from 1 to nz layers:
            ((conc(i,j,k,l),i=1,nx),j=1,ny)
```

The variables on the nested grid output concentration files have the following definitions:

`message`	Text string containing file description (character*60)
`nnest`	Number of fine grid nests on file
`nspec`	Number of species on file
`mspec`	Species names for *nspec* species
`ibeg`	Grid *n* x-direction starting index of grid (master grid cell)
`jbeg`	Grid *n* y-direction starting index of grid (master grid cell)
`iend`	Grid *n* x-direction ending index of grid (master grid cell)
`jend`	Grid *n* y-direction ending index of grid (master grid cell)
`mesh`	Grid *n* meshing factor (number of nested cells per master)
`ione`	Dummy integer = 1
`nx`	Grid *n* number of grid rows
`ny`	Grid *n* number of grid columns
`nz`	Grid *n* number of layers
`iparnt`	Grid *n's* parent grid (grid index within which this fine grid is nested; 0 = master grid)
`ilevel`	Grid *n's* grid level (depth at which this grid is nested; 1=master grid is parent)
`time`	Time of output (HHMM); ending hour for average output
`idate`	Date of output (YYJJJ)
`conc`	Grid *n*, species *l*, layer *k* concentrations (ppm for average gasses, μg/m^3 for average aerosols, μmol/m^3 for instantaneous gas species) for *nx* grid columns, and *ny* grid rows

The nested grid output deposition file is identical in format to the two-dimensional surface-level output average concentration file. As described above for the master grid output file, the species list is identical to the list on the average concentration output file, except that four parameters are output for each species.

PiG Restart File

When the PiG option is invoked, CAMx outputs all puff parameters each hour for model restart capabilities. This file is Fortran binary and is analogous to the instantaneous gridded concentration output files in that it represents a "snapshot" of data at the top of each hour. The file contains information for each puff, including grid location, cell location, size specifications, age, and mass of each of the chemical species carried. While this file contains PiG information for the entire simulation, it would be of limited use for certain analyses such as plotting puff trajectories. This is because the instantaneous nature of the data, and the dynamic memory allocation utilized in the PiG submodel, leads to insufficient information to identify and track individual puffs hour to hour. However, a PiG postprocessing utility is available that generates the hourly spatial distribution (as represented in the grid system) of all puff mass emitted from a user-selected set of PiG point sources, which can be displayed using PAVE.

The time-invariant header portion of both GREASD and IRON PiG restart files contains two records with the following structure:

```
nsrc
(idpsrc(n),xsrc(n),ysrc(n),hsrc(n),dsrc(n),tsrc(n),vsrc(n),n=1,nsrc)
```

The variables on the PiG restart header records have the following definitions:

`nsrc`	Number of point sources receiving PiG treatment
`idpsrc`	Point source number in elevated point source file
`xsrc`	Stack x-coordinate (m or degrees longitude) of *nsrc* PiG point sources
`ysrc`	Stack y-coordinate (m or degrees latitude) of *nsrc* PiG point sources
`hsrc`	Stack height (m) of *nsrc* PiG point sources
`dsrc`	Stack diameter (m) of *nsrc* PiG point sources
`tsrc`	Stack exit temperature (K) of *nsrc* PiG point sources
`vsrc`	Stack exit velocity (m/hr) of *nsrc* PiG point sources

These data are simply a list of PiG point source stack parameters. This allows CAMx to compare the list of PiG sources in the restart file with the PiG sources read from the input point source file to ensure that the two lists exactly agree.

The time-variant portion of the GREASD PiG restart file contains two records with the following structure, and these are repeated for each output time:

```
idatpig,timpig,npig
(ingrd(n),idpig(n),xpigf(n),xpigb(n),ypigf(n),ypigb(n),zpig(n),
&     axisy(n),axisz(n),sigy(n),sigz(n),htfms(n),htfmb(n),vtfms(n),
&     vtfmb(n),agepigf(n),agepigb(n),fmspig(n),
&     (puffmass(i,n),i=1,4),n=1,npig)
```

The variables on the GREASD PiG restart file have the following definitions:

`idatpig`	Date of output (YYJJJ)

timpig	Time of output (HHMM)
npig	Number of PiG puffs active at this output time
ingrd	Grid index for *npig* puffs
idpig	Point source index for *npig* puffs
xpigf	x-coordinate of puff front (km from master grid origin) for *npig* puffs
xpigb	x-coordinate of puff back (km from master grid origin) for *npig* puffs
ypigf	y-coordinate of puff front (km from master grid origin) for *npig* puffs
ypigb	y-coordinate of puff back (km from master grid origin) for *npig* puffs
zpig	Puff height (m AGL) for *npig* puffs
axisy	Puff lateral width (m) for *npig* puffs
axisz	Puff vertical depth (m) for *npig* puffs
sigy	Puff Gaussian lateral dimension (m) for *npig* puffs
sigz	Puff Gaussian vertical dimension (m) for *npig* puffs
htfms	Puff horizontal turbulent flux moment, shear (m^2/s)
htfmb	Puff horizontal turbulent flux moment, buoyancy (m^2/s)
vtfms	Puff vertical turbulent flux moment, shear (m^2/s)
vtfmb	Puff vertical turbulent flux moment, buoyancy (m^2/s)
agepigf	Puff front age since release (s) for *npig* puffs
agepigb	Puff back age since release (s) for *npig* puffs
fmspig	Puff volume parameter (unitless) for *npig* puffs
puffmass	Puff mass (μmol) for 4 species and *npig* puffs

The time-variant portion of the IRON PiG restart file contains two records with the following structure, and these are repeated for each output time:

```
idatpig,timpig,npig,nreactr
(ingrd(n),idpig(n),xpigf(n),xpigb(n),ypigf(n),ypigb(n),zpig(n),
&     axisy(n),axisz(n),sigy(n),sigz(n),pufftop(n),puffbot(n),
&     htfms(n),htfmb(n),vtfms(n),vtfmb(n),agepigf(n),agepigb(n),fmspig(n),
&     ((puffrad(i,nr,n),i=1,nrad),nr=1,nreactr),
&     ((puffpol(i,nr,n),i=1,nspec),nr=1,nreactr),n=1,npig
```

Most of the variables on the IRON PiG restart file have the same definitions as those on the GREASD PiG file. The variables that are unique to IRON PiG include the following:

nreactr	Number of chemical reactors in each puff
pufftop	Puff top height (m AGL) for *npig* puffs
puffbot	Puff bottom height (m AGL) for *npig* puffs
puffrad	Puff first-guess radical concentrations (ppm) for *nrad* species, *nreactr* reactors, and *npig* puffs
puffpol	Puff pollutant mass (μmol) for *nspec* species, *nreactr* reactors, and *npig* puffs

6. OZONE SOURCE APPORTIONMENT TECHNOLOGY

6.1 INTRODUCTION

Photochemical grid models are used to develop NO_x and/or VOC emission reduction strategies to attain ozone air quality objectives. Traditionally, the development of an ozone attainment strategy involves iteration through many photochemical grid model scenarios to identify what pollutants, source categories and source regions should be controlled. It is impractical to analyze every potential control strategy and so there is potential for implementing controls on sources that contribute little to the high ozone levels or, conversely, not controlling sources that do contribute.

ENVIRON developed an ozone source attribution approach that has become known as the "Ozone Source Apportionment Technology", or OSAT (Yarwood et al., 1996). This method was originally implemented in the Urban Airshed Model (UAM) and was then built into CAMx[1]. OSAT provides a method for estimating the contributions of multiple source areas, categories, and pollutant types to ozone formation in a single model run. OSAT also includes a methodology for diagnosing the temporal relationships between ozone and emissions from groups of sources. The capabilities of OSAT are summarized below along with an assessment of the strengths and limitations of the approach.

The main challenges in developing and implementing a methodology to track the spatial and temporal relationships between separate groups of emission sources and ozone formation are:

- Accounting not only for the presence of ozone precursors from a given source region at a given receptor location, but also accurately estimating the cumulative contribution to ozone production of those precursors while they were en-route to the receptor.

- Insuring compatibility with the underlying air quality model formulation so that derived source-receptor relationships will be consistent with model response to emission changes.

- Providing sufficient spatial and temporal resolution while managing, within practical constraints, the computer resources required to run the software tool.

OSAT uses multiple tracer species to track the fate of ozone precursor emissions (VOC and NO_x) and the ozone formation caused by these emissions within a simulation. The tracers operate as spectators to the normal CAMx calculations so that the underlying CAMx predicted relationships between emission groups (sources) and ozone concentrations at specific locations (receptors) are not perturbed. Tracers of this type are conventionally referred to as "passive tracers," however it is important to realize that the tracers in the OSAT track the effects of chemical reaction, transport, diffusion, emissions and deposition within CAMx. In

[1] Note that with the release of CAMx v4.20, the formulation of the Ozone Source Apportionment Technology differs slightly from earlier versions in that it accounts for the fact that ozone production and destruction occur simultaneously as it apportions ozone change among tracers. Previously, OSAT only considered the net change in ozone in the apportionment algorithm. The approach is described later in this section.

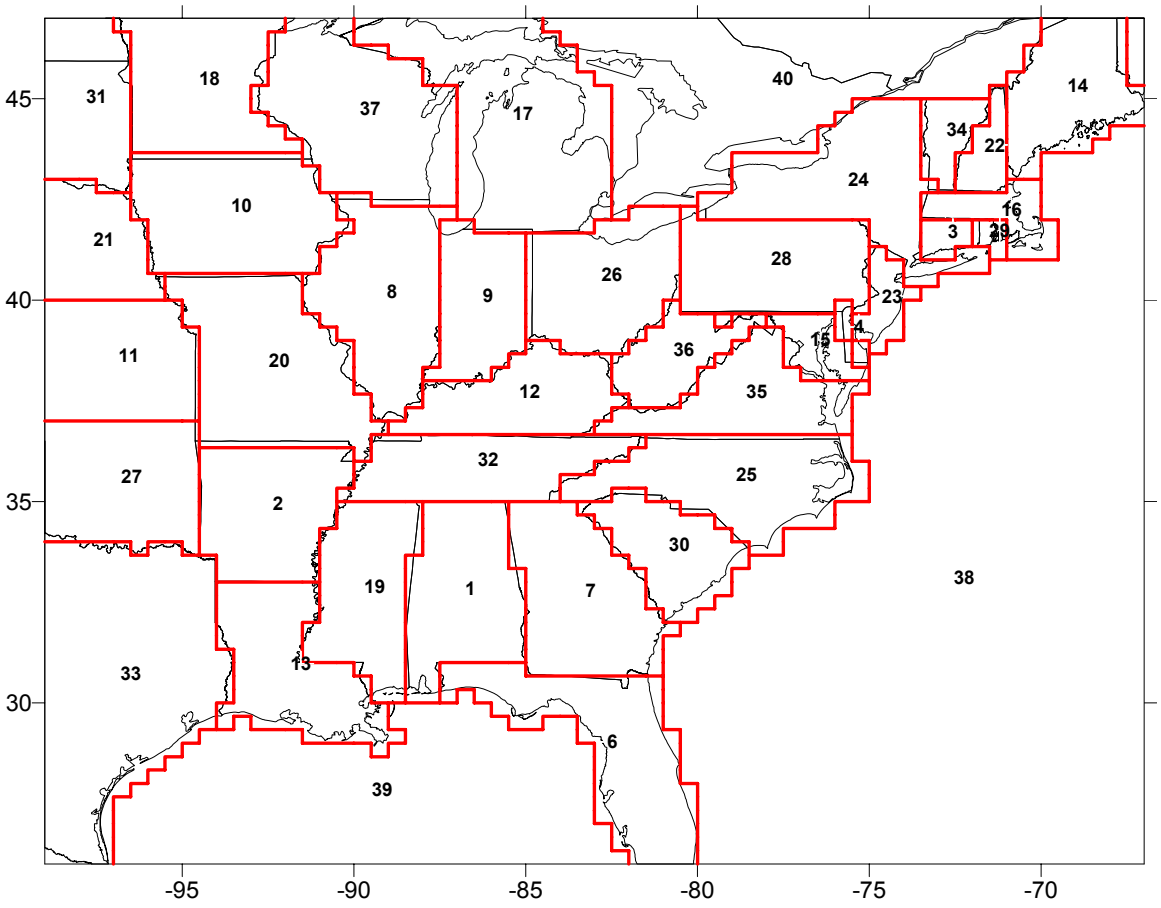

Figure 6-1. Example of the sub-division of a CAMx domain into separate areas for geographic source apportionment.

recognition of this, they are described here as "ozone reaction tracers." The ozone reaction tracers allow ozone formation from multiple "source groupings" to be tracked simultaneously within a single simulation. A source grouping can be defined in terms of geographical area and/or emission category. Figure 6-1 provides an example of the way that a CAMx domain can be sub-divided into multiple source areas – 40 in this example. Also, the emission inventory could be sub-divided into several source categories – two emission categories over 40 source regions would produce 80 separate source groupings. So that all sources of ozone precursors are accounted, the CAMx boundary conditions and initial conditions are always tracked as separate source groupings.

The methodology is designed so that all ozone and precursor concentrations are attributed among the selected source groupings at all times. Thus, for all receptor locations and times, the ozone (or ozone precursor concentrations) predicted by CAMx are attributed among the source groupings selected for OSAT. The methodology also estimates the fractions of ozone arriving at the receptor that were formed en-route under VOC- or NOx-limited conditions. This information indicates how ozone concentrations at the receptor will respond to reductions in VOC and NOx precursor emissions.

In addition to using ozone reaction tracers to apportion ozone formation, the OSAT uses separate families of timing tracers to allow source-receptor transport times to be estimated. Unique timing tracers are released from each geographical area selected for ozone source apportionment. Thus, if the ozone formation tracers show that emissions from a given source area contributed to ozone at any receptor of interest, the timing tracers can then be used to estimate the time at which the emissions were released. This provides a way of investigating temporal features of the source-receptor relationships and even developing temporally targeted control strategies.

An example display of the type of ozone source apportionment information available from OSAT is shown in Figure 6-2. The figure shows information for the location of the region wide maximum hourly average ozone concentration (the hourly peak) for an example OSAT run (this run had 17 geographical source areas and a single emission group). Summary information for scenario and receptor is shown in the center. At top left, a bar chart shows how the total amount of ozone was attributed between initial conditions, boundary conditions and emissions, with the emissions contribution being divided between ozone formed under VOC and NO_x limited conditions. At top right, a pie chart shows the relative ozone contributions from initial conditions, boundary conditions and emissions, with the emissions contributions broken out by numbered geographical source areas. Only the source areas with the largest ozone contribution are shown, the remaining source areas are lumped together under "All Others." At bottom, there is a tabular summary of ozone contributions underlying the charts at the top. The tabular summary also shows the estimated release times for the emissions from different source areas impacting the receptor (under the "Time Emitted" column). The release times are estimated using the timing tracers. The timing tracers are also used to estimate whether there is more than one significant source-receptor pathway between each source area and the receptor, i.e. if timing tracers of different ages from the same source area are present at the receptor it is likely that recirculation of emissions is occurring. The display shown in Figure 6-2 is only one of many ways in which OSAT results can be displayed to gain insight into ozone source-receptor relationships predicted by CAMx. Figure 6-2 is shown here to illustrate the types of information available. Displays like Figure 6-2 are generated using post-processing software described later in this section.

An important feature of the ozone reaction tracer approach used in OSAT is that the normal CAMx calculations are not perturbed; thus, OSAT estimates the same ozone and precursor concentrations as CAMx. Further, since the same inputs are used for meteorology, emissions etc., and the same numerical methods are employed throughout the model, the source-receptor relationships developed by OSAT inherently have a high degree of consistency with those present in CAMx. The level of consistency between the source-receptor relationships developed by OSAT and CAMx is limited by three factors:

- The completeness of the conceptual methodology underlying the source apportionments;
- The limitations of the numerical methods employed by CAMx; and
- The non-linear nature of the ozone formation process.

The completeness of the source apportionment methodology was analyzed by performing a series of evaluations of OSAT results against UAM sensitivity tests (Yarwood et al., 1996). These tests showed that the OSAT performed well in predicting both the spatial area of

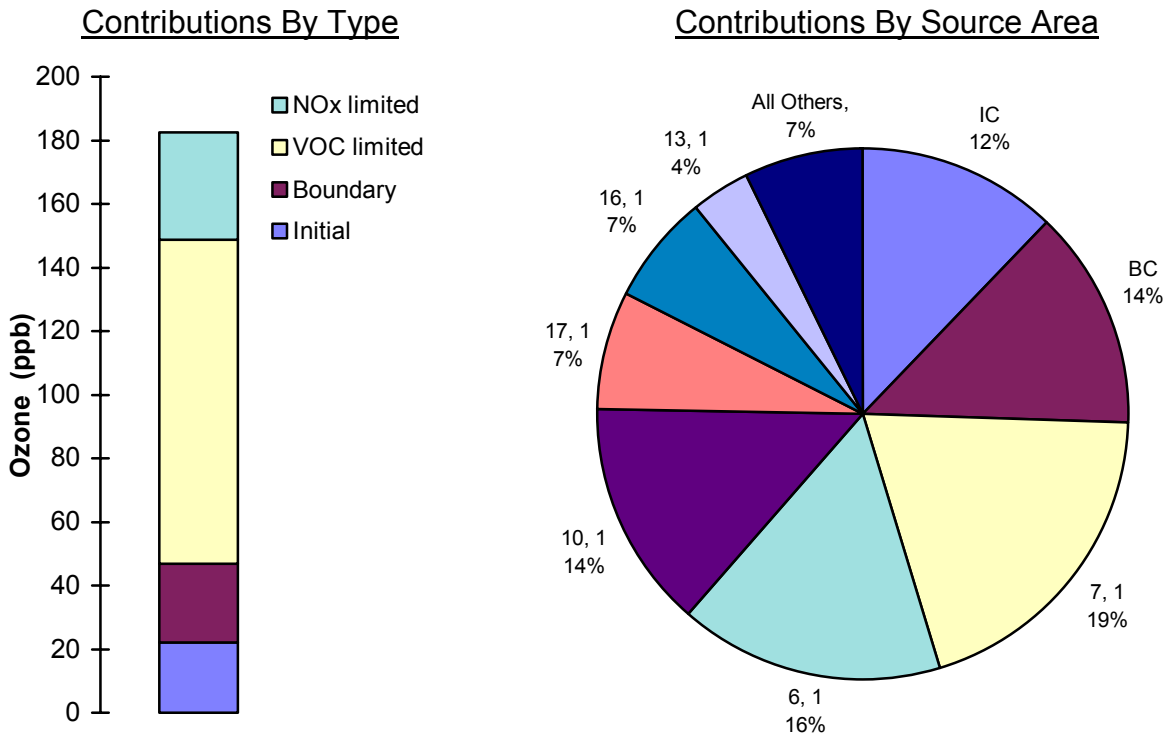

Receptor	**=**	**HourlyPeak**		
Time	**=**	**16**	**To**	**17**
Date	**=**	**8/28/87**		
Scenario	**=**	**Evaluation Test**		
Total Ozone	**=**	**183**	**ppb**	

Detailed Ozone Apportionment

Source Area	*Emission Group*	*Percent Ozone from NOx*	*VOC*	*Total*	*Time Emitted*	*Recirculation Likely*
IC				12%		
BC				14%		
7	1	3%	17%	20%	8/28 5 am	No
6	1	4%	13%	16%	8/28 6 am	No
10	1	7%	7%	14%	8/28 7 am	No
17	1	1%	6%	7%	8/27 1 pm	No
16	1	1%	6%	7%	8/27 6 am	No
13	1	2%	1%	4%	8/28 2 pm	No
All Others				7%		

Figure 6-2. Example display of ozone source apportionment information provided by OSAT for a run with 17 source areas and 1 emission group.

impacts of emissions from given source regions and the relative contributions of separate emission regions/groups to ozone. OSAT cannot overcome numerical limitations inherent to CAMx (as well as other grid models). The UAM evaluation tests referred to above suggested that a potential serious numerical limitation was the Smolarkeiwicz horizontal advection solver (Smolarkeiwicz, 1983). As discussed below, the non-linear numerical limitations of advection algorithms were addressed in the OSAT design, and we believe that they probably pose greater problems for the use of CAMx in conventional control strategy evaluations than for OSAT (Yarwood et al., 1996). This issue was one of the primary reasons for incorporating the Bott (1989) and PPM (Colella and Woodward, 1984) advection algorithms into CAMx and redesigning the three-dimensional transport scheme to be more mass consistent[2]. Further, the tracer transport routines were modified to directly use the advective fluxes diagnosed by the regular model advection solvers to minimize inconsistencies between tracers and regular model species.

The biggest limitation of this, or any other, ozone source apportionment approach likely results from the third factor mentioned above: namely, the non-linear nature of the chemical interactions between emissions from different source groupings. This means that as soon as the emission inventory is perturbed, the source receptor relationships begin to change. Thus, OSAT can only estimate the contribution to ozone from a specific source grouping under the current emissions scenario. It cannot directly quantify the ozone reductions that will result from an emission control strategy because the CAMx response may well be non-linear with the magnitude of the control applied (e.g. 20 percent or 60 percent control) and the presence/absence of other simultaneous controls on other source groupings.

However, this fundamental truth of photochemical modeling does not limit the usefulness of OSAT: arguably it increases its usefulness. At any rate, it suggests the following approach to control strategy development with OSAT. For the base CAMx scenario, OSAT could be used to identify specific source groupings for which ozone reductions from emissions controls would be maximized. Just as important, OSAT will identify source groupings for which emissions controls are not effective at reducing ozone concentrations. The most effective and feasible control measures identified in this way can be applied to the emission inventory, leading to a revised CAMx scenario with different (lower) emissions. If additional controls are needed, OSAT could be applied again to identify the most effective control measures under the new conditions. Development of the control plan will still proceed by an iterative process, but OSAT can be used to guide the process to develop (and justify) more refined, better targeted and more cost-effective ozone control strategies.

6.2 OSAT FORMULATION

CAMx has been extended to accommodate extra tracer species needed to perform ozone source apportionment. For each user-specified source grouping (geographical area/emissions category) there are two distinct types of tracer species, "timing tracers" and "ozone reaction tracers." The timing tracers are used to track the temporal relationships between precursor emissions and ozone formation. The ozone reaction tracers track the fate of ozone precursors (NO_x and VOC) emissions from each source grouping plus the ozone formation attributed to

[2] The Smolarkiewicz advection routine is no longer available in CAMx.

those emissions. The methodology requires that all ozone precursors be tracked so that all contributions to ozone can be accounted for, thus ozone and precursors originating from the model boundary and initial concentrations are also tracked as separate source groupings (however, no timing tracers are allocated to the initial or boundary conditions). The following sub-sections describe the methodologies employed for the timing and ozone reaction tracers.

Timing Tracers

There are two types of "timing" tracers called inert and decay-companion tracers. Inert and decay-companion tracers are used in tandem to identify the age of emissions from any source area. Timing tracers are emitted into every surface grid cell at a constant rate. Timing tracers have unique names that identify the source area in which they were released. After release, the decay-companion tracers decay exponentially with a constant lifetime. Since the inert and decay-companion tracers are affected identically by transport and diffusion, differences in predicted concentrations between the two are due only to the first-order decay of the decay-companion tracer. The presence of inert tracer from a given source area (A) at a receptor (B) indicates that a transport pathway exists from A to B. The amount of tracer decay that has occurred since release (i.e. the ratio of the decay companion tracer to its matched inert tracer) can be used to calculate the transport time from A to B and therefore the time period during which emissions at source area A can potentially impact receptor B.

To resolve ambiguities in timing calculations that could result from wind flow reversals (e.g., land/sea breezes) or other recirculation patterns, new sets of inert and decay-companion tracers can be released at user specified time periods. When a new set of timing tracers (i.e. one pair for each source area) is released, emissions of the previous set cease. Old timing tracers are still carried in the model to track emissions from those source areas and time period as they age. Thus, as a simulation progresses the number of timing tracers being carried increases as new sets are released. The names of timing tracer species identify the species type and source area/time period in which the tracer was released:

$I_{i,t}$ = Inert timing tracer for region *i* and time period *t*. Emitted at a constant rate during that time period.

$D_{i,t}$ = Decay companion timing tracer for region *i* and time period *t*. Emitted at a constant rate during that time period. Decays exponentially with a constant lifetime of 12 hours after release.

This method is more computationally efficient than the simpler alternative of releasing non-decaying tracers many short time periods, since the latter approach would rapidly lead to an impossibly large number of tracers.

Ozone Reaction Tracers

The second category of tracers are called "ozone-reaction" tracers. There are four ozone-reaction tracers per source area to account for the contributions of emissions of separate source areas to the complex process of the ozone formation activity. It is important to recall

that the mass of NOx or VOC from a given source area that may be present at a given receptor at a selected hour is often not particularly relevant to the amount of ozone present there at that time. Rather, it is the contribution to ozone formation activity of source areas' NOx and VOC emissions en-route to a receptor that must be determined. The ozone-reaction tracers are designed to integrate these en-route contributions to ozone production/destruction activity.

Ozone formation involves both NOx and VOCs, and the NOx and VOCs participating in ozone formation in any particular grid cell/time step may have originated from different source groupings. The ozone formation process can be controlled more by the availability of VOCs or NOx, depending upon the relative abundance of both precursors, and ozone formation is described either as VOC limited or NOx limited, respectively. When ozone production at a given location and time is NOx limited it makes sense to attribute ozone production to source groupings based on their contributions to the local NOx and similarly to allocate based on VOC contributions when ozone formation is VOC limited. Consequently, separate tracers are used to track ozone formation occurring under NOx and VOC limited conditions. The criterion used to determine whether ozone formation is occurring under locally NOx or VOC limited conditions is described in detail in a separate section below.

The four types of ozone-reaction tracers that are tracked for each source grouping (i.e., geographic area/source category, boundary conditions or initial conditions) are explained below. The name of each tracer uniquely identifies the source grouping it represents:

N_i = NOx tracer for source grouping i. Emitted with the same spatial and temporal distribution as NOx emissions for source grouping i. Decays with local dNO_x/dt for each grid cell/time step.

V_i = VOC tracer for source grouping i. Emitted with the same spatial and temporal distribution as VOC emissions for source grouping i. Decays with local $dVOC/dt$ for each grid cell/time step. Note that VOC tracers are defined as single carbon species, so their concentrations are numerically equal in ppb and ppbC units.

$O3V_i$ = Tracer of ozone formation under VOC limited conditions attributed to source grouping i. If ozone formation is determined to be VOC-limited for a given grid cell/time step, $O3V_i$ is formed in proportion to local dO_3/dt in proportion weighted by the distribution of VOC precursors (V_i).

$O3N_i$ = Tracer of ozone formation under NOx limited conditions attributed to source grouping i. If ozone formation is determined to be NOx-limited for a given grid cell/time step, $O3N_i$ is formed in proportion to local dO_3/dt in proportion weighted by the distribution of NOx precursors (N_i).

Mass Consistency with CAMx

The ozone reaction tracer methodology was designed to be inherently mass consistent with CAMx. In other words, the sums of the NOx, VOC and ozone tracers should remain consistent with their standard CAMx counterparts as follows:

$$\sum N_i = NO + NO_2$$

$$\sum V_i = \sum CB4\ VOCs$$

$$O3 = \sum O3V_i + \sum O3N_i$$

The validity of these relationships was evaluated and it was found that the chemistry, emissions, deposition, horizontal diffusion, and vertical transport/diffusion algorithms maintained mass consistency on an overall and cell by cell basis. However, it was found that the horizontal advection algorithms inherently maintained mass consistency on an overall basis, but not a cell by cell basis. Accordingly, the horizontal advection algorithm for the ozone reaction tracers was modified as described below to maintain mass consistency.

Emissions

The tracer families, N_i and V_i, track NOx and VOC emissions from each source grouping to allow attribution of ozone formation as it occurs throughout CAMx. The rates of emission of the N_i and V_i tracers are set equal to the total NOx and VOC emissions in the inventory for a source grouping, respectively. For the V_i tracers, the emissions are set equal on a ppmC basis. For the initial condition (IC) source grouping, the N_{IC} and V_{IC} tracers are initialized from the CAMx initial concentration fields and receive no more mass input after the start of the simulation. For the boundary condition (BC) source grouping, the fluxes of NOx and VOC entering CAMx from the boundaries are effectively interpreted as emissions of the N_{BC} and V_{BC} tracers at the model boundaries. Unlike emission source groupings, boundary and initial conditions also introduce ozone directly into CAMx. Since there is no way of determining whether the ozone in the boundary and initial conditions was formed under VOC or NOx limited conditions, this ozone is divided equally between O3N and O3V tracers. However, subsequent ozone formation within CAMx from boundary and initial condition VOCs and NOx is allocated to O3V and O3N tracers on the basis of whether ozone formation occurred under VOC or NOx limited conditions (discussed below).

Deposition

The N_i, V_i, $O3N_i$ and $O3V_i$ tracers are deposited at rates determined by the standard CAMx deposition calculation on a surface grid cell by grid cell basis. For NOx, the deposition velocity for each tracer N_i [$V_d(N_i)$] is set equal to the concentration weighted average of the deposition velocities for NO and NO_2:

$$V_d(N_i) = \frac{NO \times V_D(NO) + NO_2 \times V_D(NO_2)}{NO + NO_2} \qquad (1)$$

Similarly, the deposition velocity for each tracer V_i is set equal to the concentration weighted average of the deposition velocities for the CBM-IV VOC species (the concentration weighting

is performed on a ppmC basis). The deposition velocity for the O3N and O3V tracers is set equal to the ozone deposition velocity.

Transport and Diffusion

Originally, the N_i, V_i, $O3N_i$ and $O3V_i$ tracers were transported and diffused by the CAMx algorithms. As mentioned above, testing of OSAT showed that the original CAMx horizontal advection routine (Smolarkiewicz, 1983) did not accurately preserve the spatial relationships between ozone reaction tracers and their corresponding CAMx species (i.e., between the sum of the O3V and O3N species and CAMx O_3). The distortion in any one model time-step was small, but the distortion built up over time to unacceptable levels. The discrepancies arising from the Smolarkiewicz algorithm were not surprising in light of the well known limitations of the Smolarkiewicz algorithm (Odman et al., 1996; Chock and Winkler, 1994).

The preferred solution to this problem was to use an alternative, more accurate, numerical algorithm to solve the horizontal advection. This is one reason why the Bott (1989) and PPM (Collella and Woodward, 1984) approaches were included as options in CAMx. However, both Smolarkiewicz and Bott routines are "flux-corrected", meaning that non-linear adjustment are internally made to the advective fluxes to reduce numerical diffusion. Indeed, all three algorithms are non-linearly dependent upon the gradients of the advecting material, which can differ substantially between the standard model species and each of the OSAT tracers. This results in OSAT predictions that differ from the standard CAMx concentrations.

Such an outcome was inconsistent with the objectives in developing OSAT, so an alternative approach was adopted. As the horizontal transport operation is carried out for all CAMx species, the individual advective fluxes for ozone and each NO_x and VOC species are reported by the advection algorithm. The individual NO_x and VOC fluxes are combined (and weighted by carbon number for VOC), as are the individual concentrations of these species before advection. The bulk NO_x, VOC, and ozone advective fluxes are then normalized by the weighted mean concentrations, and then these normalized fluxes are used to advect each tracer species directly, rather than sending the tracers through the advection algorithms. This approach has significantly improved consistency between tracer and regular model concentrations.

The OSAT tracers are sent to the standard CAMx routines for vertical advection, vertical diffusion, and horizontal diffusion. Since small deviations sometimes occur between the OSAT tracer concentrations and the regular CAMx species (due to numerical limitations), the ozone reaction tracer concentrations are renormalized after transport to be consistent with the standard CAMx concentration fields. The renormalization is applied in the same subroutine as chemical change because this is computationally efficient.

Chemical Change

The N_i tracer mass in each grid cell at each time step decays according to the chemical change in the CAMx predicted NOx (ΔNOx) weighted by the tracer contribution to the total of NOx tracers from all source groupings:

$$N_i = N_i + \Delta NO_x \times \frac{N_i}{\sum N_i} \qquad (2)$$

The V_i tracer mass in each grid cell at each time step decays according to the chemical change in the CAMx predicted VOC (ΔVOC) weighted by the tracer contribution to the total of VOC tracers from all source groupings. However, because the reactivity of VOCs from different source groupings can be different, a weighting factor based on the OH-reactivity of each V tracer (kOH_i) is also introduced. The kOH_i for each source grouping is calculated at the start of each simulation period (typically one day) by averaging the OH rate constants of the speciated VOC emissions for each source grouping. The V tracer mass in each grid cell at each time step decays at a rate determined by the following equation:

$$V_i = V_i + \Delta VOC \times \frac{V_i \times kOH_i}{\sum (V_i \times kOH_i)} \qquad (3)$$

The O3N and O3V tracers for each source grouping accumulate a weighted fraction of the ozone production activity (PO_3) and ozone destruction activity (DO_3) that occurs in each grid cell at each time step. The process of apportioning PO_3 and DO_3 across O3N and O3V tracers occurs as follows:

1. Determine whether the local (grid cell/time step) ozone production process is NO_x or VOC limited. As described in detail below, the determination is based on the ratio of the local HNO_3 and H_2O_2 production rates. If the H_2O_2/HNO_3 production ratio is greater than 1/3 during a time step, then ozone formation is NO_x limited. If this ratio is less than or equal to 1/3, then ozone formation is VOC limited.

2. For allocating ozone production under conditions determined to be:

   (a) NO_x limited: allocate PO_3 across O3N tracers

   $$O3N_i = O3N_i + PO_3 \times \frac{N_i}{\sum N_i} \qquad (4)$$

   (b) VOC limited: allocate PO_3 across O3v tracers accounting for reactivity

   $$O3V_i = O3V_i + PO_3 \times \frac{V_i \times kOH_i}{\sum V_i \times kOH_i} \qquad (5)$$

3. For ozone destruction, allocate across all ozone tracers.

   $$O3X_i = O3X_i + DO_3 \times \frac{X_i}{\sum X_i} \qquad (6)$$

   where X = N and V.

This is the algorithm used for OSAT. The GOAT and APCA methods use different algorithms for allocating ozone production, as described below.

Accounting for Ozone Destruction Reactions in OSAT

The original OSAT algorithm (i.e., CAMx v4.11s and earlier) allocated chemical change to ozone tracers based on the total change in ozone (ΔO_3) across a call to the gas-phase chemistry solver. A positive ΔO_3 was equated to ozone production and ozone tracers were incremented according to the OSAT, APCA or GOAT rules for apportioning ozone production. A negative ΔO_3 was equated to ozone destruction and the destruction was distributed equally among all ozone tracers. However, ozone production and destruction mechanisms operate simultaneously within the chemical mechanism (e.g., CB4) and so the net change in ozone is the balance of production and destruction. For example, VOC oxidation can drive photochemical ozone production at the same time that O_3 + VOC reactions directly consume ozone, and these processes may lead to a net increase or decrease in ozone depending mainly upon availability of NOx and sunlight. OSAT has been modified to explicitly track several ozone destruction mechanisms as follows:

1. O_3 + VOC reactions since these remove ozone;
2. $O(^3P)$ + VOC reactions since these effectively remove ozone;
3. $O(^1D)$ + H_2O reaction since this effectively removes ozone;
4. HOx + O_3 reactions that do not re-form ozone.

Ozone production is then calculated from the difference between ΔO_3 and total ozone destruction ($PO3 = \Delta O_3 - DO3$). The OSAT ozone tracers are adjusted first for ozone destruction (applied to all tracers) and second for ozone production (applied using the OSAT, APCA or GOAT rules).

The amount of ozone destruction is calculated using integrated reaction rates obtained from the Process Analysis (PA) Probing Tool; see Section 9. It is easy to account for processes 1-3 using PA since the ozone destroyed is simply the integrated rates of the reactions involved. Process 4 is less easy to identify but is very important as an ozone destruction mechanism in low NOx (rural) environments. Therefore, accounting for process 4 is important to understanding long range ozone transport.

The main reaction pathways between ozone and HOx (OH and HO_2) are shown in Figure 6-3. Ozone reacts directly with both with OH and HO_2:

$$O_3 + OH \rightarrow O_2 + HO_2 \qquad (7)$$
$$O_3 + HO_2 \rightarrow 2\ O_2 + OH \qquad (8)$$

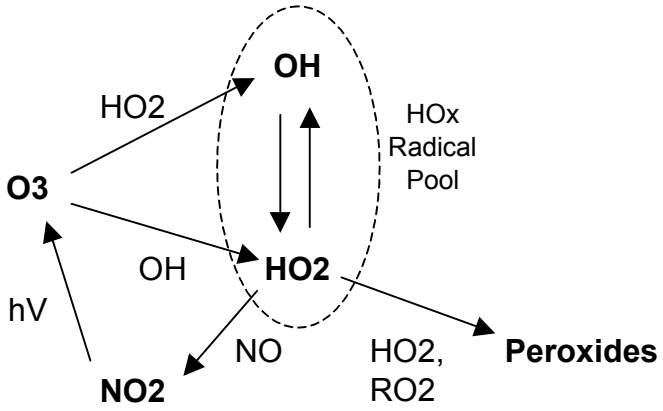

Figure 6-3. Daytime reactions of ozone with HOx (OH and HO_2) showing potential for reformation of ozone or ozone destruction via peroxide formation.

Since OH and HO_2 radicals inter-convert rapidly during the daytime they can be viewed as a radical pool, called HOx. During the daytime, there are two main sinks for HOx:

(1) *propagation* by reaction with NO, which reforms ozone:

$$\begin{aligned} &NO + HO_2 \rightarrow NO_2 + OH \\ &NO_2 + h\nu \rightarrow NO + O(^3P) \\ &O(^3P) + O_2 \rightarrow O_3 \\ \text{Net:}\quad &HO_2 + O_2 + h\nu \rightarrow O_3 + OH \end{aligned}$$

(2) *termination* by reaction with HO_2 or RO_2 to form peroxides and other organic products, which prevents HOx from propagating to reform ozone:

$$\begin{aligned} &HO_2 + HO_2 \rightarrow H_2O_2 + O_2 \\ &HO_2 + RO_2 \rightarrow ROOH + O_2 \\ &RO_2 + RO_2 \rightarrow \text{organic products} + O_2 \end{aligned}$$

In the revised OSAT algorithms, the ozone destruction rate due to O_3 + HOx reactions is estimated as:

$$O_3\ Destruction\ Rate \quad = \quad Rate_{(O_3 + HOx)} \times \left(\frac{Rate_{(HO_2\ term)}}{Rate_{(HO_2 + NO)} + Rate_{(HO_2\ term)}} \right)$$

This equation is the rate of O_3 + HOx reaction (i.e., the rates of [7] plus [8]) multiplied by a branching ratio that estimates the fraction of O_3 + HOx reactions that result in loss of ozone.

Ozone destruction due to the $O_3 + NO \rightarrow NO_2 + O_2$ titration reaction is explicitly excluded from the accounting of ozone destruction because it is hard to disentangle its role in ozone destruction and production. Under high NOx (ozone titration) conditions and at night this

reaction becomes clearly an ozone destruction pathway, and in these situations ΔO_3 becomes negative and ozone destruction due to the O_3 + NO reaction is accounted for. Under most daytime conditions, this reaction is part of the O_3, NO, NO_2 photo-stationary state and ozone can be reformed again when NO_2 photolyzes so this reaction is not clearly an ozone destruction pathway.

Distinguishing VOC-Limited from NOx-Limited Ozone Formation

The classic trajectory model EKMA diagram can be used to distinguish VOC-limited from NOx-limited trajectories and develop a classification based on initial VOC-to-NOx ratio. However, this approach classifies VOC- or NOx-limited behavior based on response the of the peak ozone, which is the net response from several hours of photochemistry. In reality, many of the trajectories start out VOC-limited and become NOx-limited during the course of the day essentially because the NOx is depleted more rapidly than the VOC. For OSAT, a more fundamental indicator of the instantaneous state of ozone formation with regard to VOC- or NOx-limitation is required.

The sensitivity of ozone formation to VOCs and NOx at any given time is attributable to the fate of radicals. The radical pool is often referred to as odd-hydrogen (HOx) and is most usefully considered as the sum of OH, HO_2 and RO_2 radicals. When NOx is plentiful, the main radical termination (i.e., HOx removal) pathway is nitric acid formation, i.e.:

$$OH + NO_2 (+M) \rightarrow HNO_3 (+M) \qquad (9)$$

Under these conditions, ozone formation is limited by the rate at which radicals can be formed, which is generally described as the VOC-limited condition. Thus nitric acid (HNO_3) production is indicative of plentiful NOx and VOC-limited ozone formation.

When NOx is scarce, radical-radical reactions dominate HOx removal, e.g.:

$$HO_2 + HO_2 (+M) \rightarrow H_2O_2 + O_2 (+M) \qquad (10)$$

$$HO_2 + RO_2 \rightarrow ROOH + O_2 \qquad (11)$$

Under these conditions, ozone formation is limited by the availability of NO to react with HO_2 and RO_2 radicals, which is described as the NOx-limited condition. HO_2 and RO_2 radicals that do not react with NO participate in peroxide formation. Thus, peroxide formation (H_2O_2 = hydrogen peroxide, or ROOH = organic hydroperoxides) is indicative of scarce NOx and NOx-limited ozone formation.

Sillman (1995) has exploited this situation to develop useful indicators of VOC vs. NOx limited ozone formation based on the ratio of peroxide production to nitric acid production. Sillman proposed that the transition between these conditions occurs when:

$$(P_{H2O2} + P_{ROOH}) / P_{HNO3} = 0.5 \qquad (12)$$

The production rates of nitric acid (P_{HNO3}) and hydrogen peroxide (P_{H2O2}) in each CAMx grid cell at each time step are readily accessible, but the production rate of organic peroxides (P_{ROOH}) is not readily accessible because the CB4 mechanism does not explicitly track these species. The balance between P_{ROOH} and P_{H2O2} depends upon the relative production of HO_2 and RO_2 radicals, and Sillman suggests that it is not highly variable within/across simulations. Accordingly, he proposes that equation (12) is equivalent to a transition point of:

$$P_{H2O2} / P_{HNO3} = 0.35 \qquad (13)$$

In other words, when this ratio exceeds 0.35 ozone formation is NOx-limited, and when this ratio is less than 0.35 ozone formation is VOC-limited.

Evaluation of Sillman's P_{H2O2}/P_{HNO3} Indicator

Equation (13) was evaluated as an indicator of VOC vs. NOx-limited ozone formation for several trajectory model scenarios using the CB4 mechanism as implemented in the UAM.[3] The ozone concentration for a scenario with an initial VOC/NOx ratio of 10 (0.3 ppmC of VOC, 30 ppb of NOx) is shown in Figure 6-4. Also plotted, against the right axis, is the ratio P_{H2O2}/P_{HNO3}.

Sillman's proposed P_{H2O2}/P_{HNO3} transition point of 0.35 is shown by the dashed line. Before about 12 noon, P_{H2O2}/P_{HNO3} is less than 0.35 indicating VOC-limited ozone formation, whereas from about 12 noon to 7 PM P_{H2O2}/P_{HNO3} exceeds 0.35 indicating NOx-limited ozone formation. After 7 PM, P_{H2O2}/P_{HNO3} falls below 0.35 again, but this is after the ozone peak when ozone is decreasing and the concepts of VOC and NOx-limitation are no longer relevant.

In summary, the P_{H2O2}/P_{HNO3} indicator suggested a transition from VOC to NOx-limited ozone formation at about noon. To investigate whether this prediction is corroborated by responses to emission controls, the trajectory model scenario was re-run with 30 percent reductions in initial concentrations and emissions of VOC and NOx (Figure 6-5). Figure 6-5 shows that NOx controls started to be effective at about noon whereas VOC controls had maximum effect before noon. This finding is even clearer in Figure 6-6, which shows the difference in ozone (control-base) for the reduced VOC and NOx cases. Thus, the response of ozone to reducing VOC and NOx was found to be consistent with the prediction of the P_{H2O2}/P_{HNO3} indicator.

The evaluation described above and shown in Figures 6-4 and 6-6 was repeated for two more scenarios with different base VOC/NOx ratios. The results for a base VOC/NOx ratio of 20 (0.3 ppmC of VOC, 15 ppb of NOx) are shown in Figure 6-7, and for a base VOC/NOx ratio of 5 (0.15 ppmC of VOC, 15 ppb of NOx) are shown in Figure 6-8. For a base VOC/NOx ratio of 20 Figure 6-7a shows that the transition from VOC to NOx-limited ozone formation is predicted to occur at about 9:30 AM. Figure 6-7b shows that this is confirmed by the response to VOC and NOx controls. For a base VOC/NOx ratio of 5, Figure 6-8a shows that

[3] The scenarios begin at sunrise at 6 a.m. with 10 ppb of O_3 plus initial VOCs and NOx. There is no dilution, and 5 percent of the initial VOCs and NOx are added in each hour as emissions.

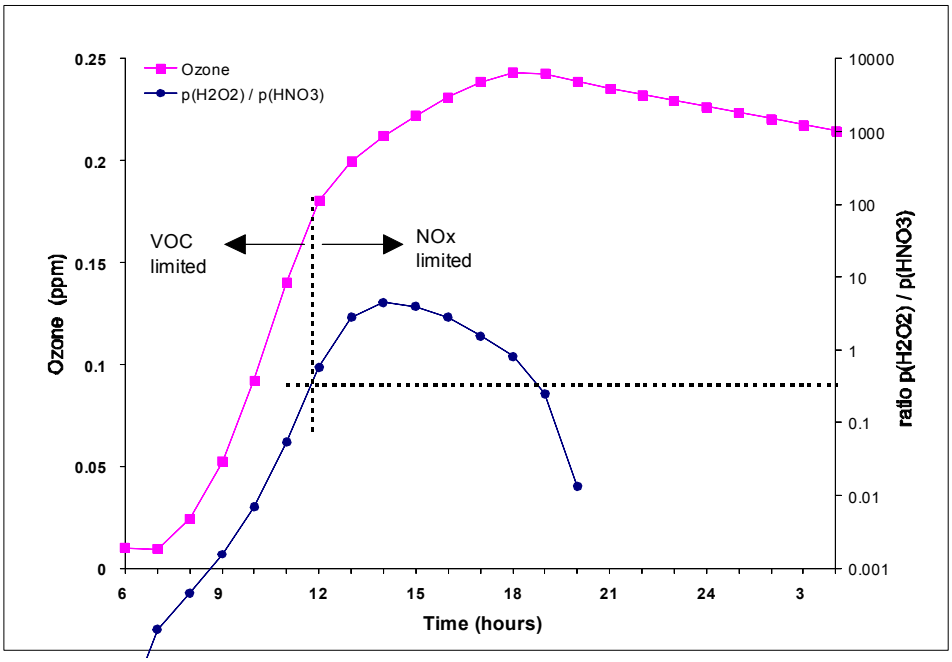

Figure 6-4. Box model simulation to evaluate P_{H202}/P_{HNO3} indicator for VOC vs. NOx limited ozone formation (see text). Ozone is plotted against the left axis, P_{H202}/P_{HNO3} is plotted against the right axis. For P_{H202}/P_{HN03} below 0.35 ozone formation is VOC limited. Thus, the transition form VOC to NOx limited ozone formation is predicted to occur about 12 noon. **Initial VOC/NOx = 10:1.**

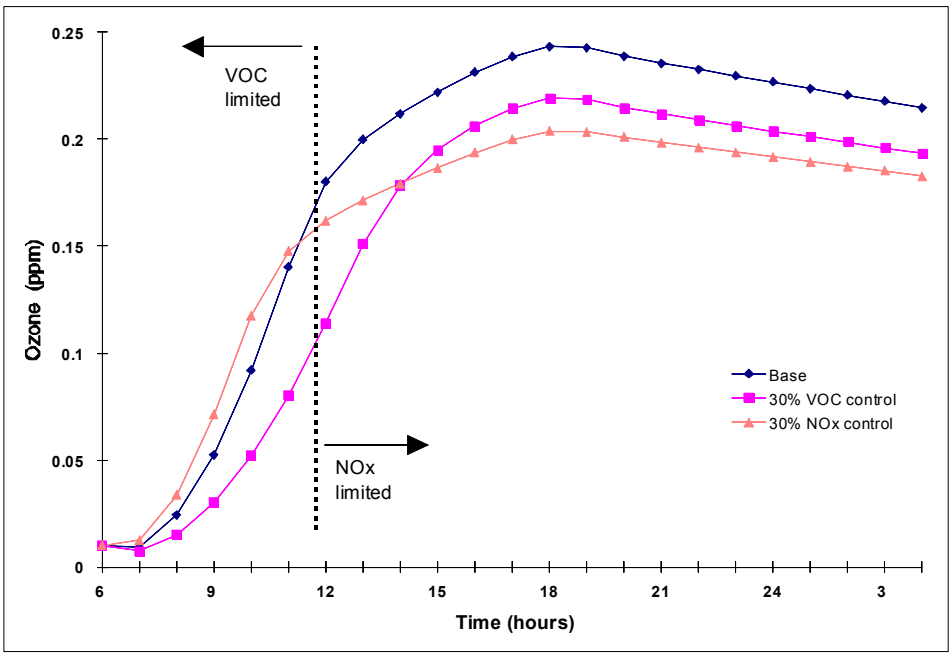

Figure 6-5. Effect on ozone of controlling VOC and NOx by 30 percent for the base scenario shown in Figure 6-4. The vertical dashed line shows the transition form VOC to NOx limited ozone formation for the base case derived in Figure 6-4. **Initial base case VOC/NOx = 10:1.**

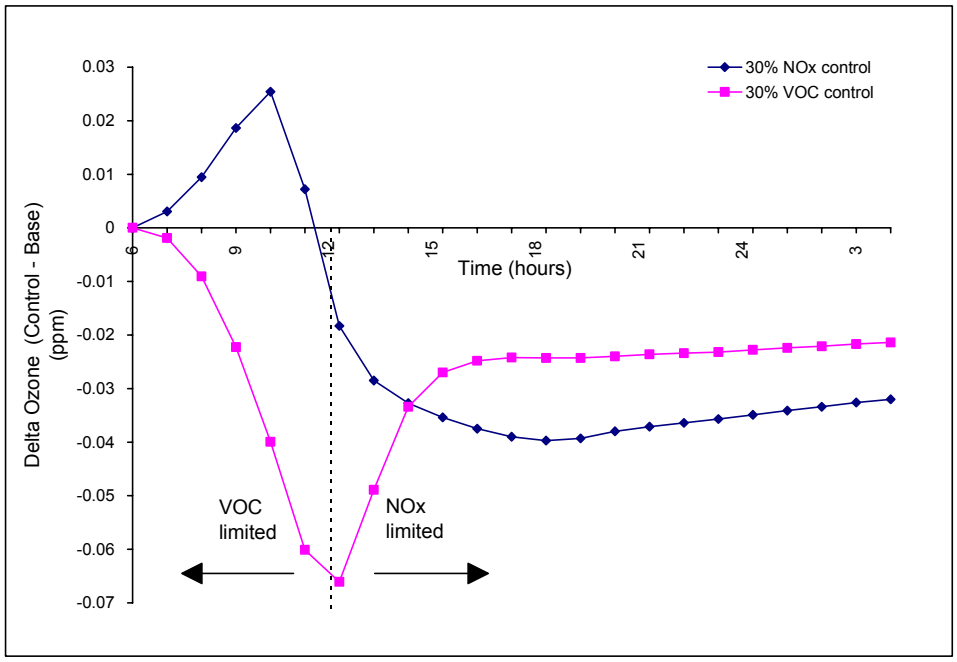

Figure 6-6. Change in ozone (control-base) for the VOC and NOx control scenarios shown in Figure 6-5. The vertical dashed line shows the transition from VOC to NOx limited ozone formation for the base case derived in Figure 6-4**. Initial base case VOC/NOx = 10:1.**

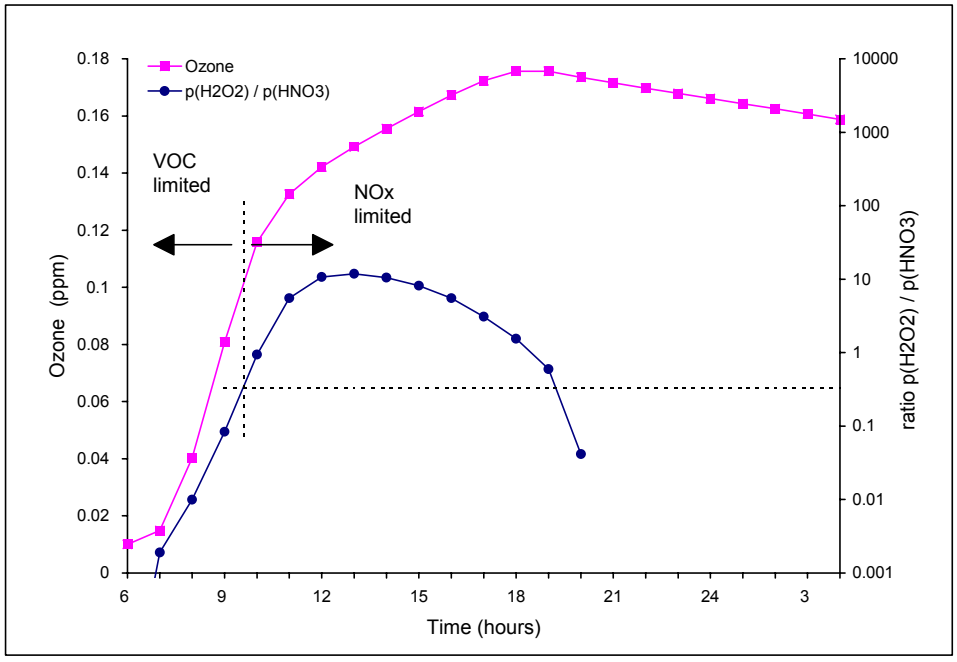

Figure 6-7a. As Figure 6-4, but for an **Initial VOC/NOx = 20:1.**

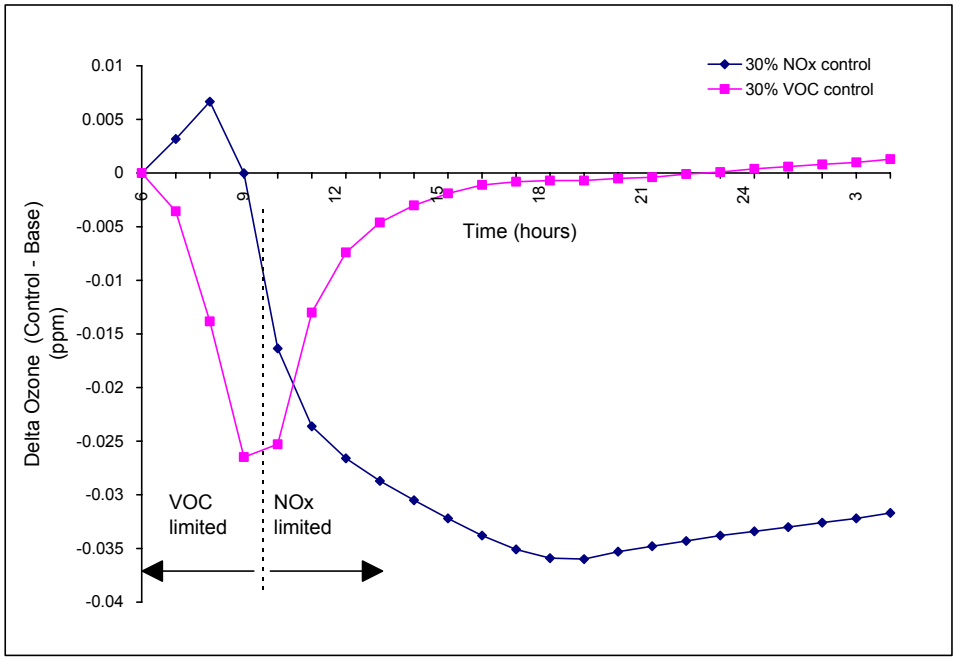

Figure 6-7b. As in Figure 6-6, but for an **Initial VOC/NOx = 20:1.**

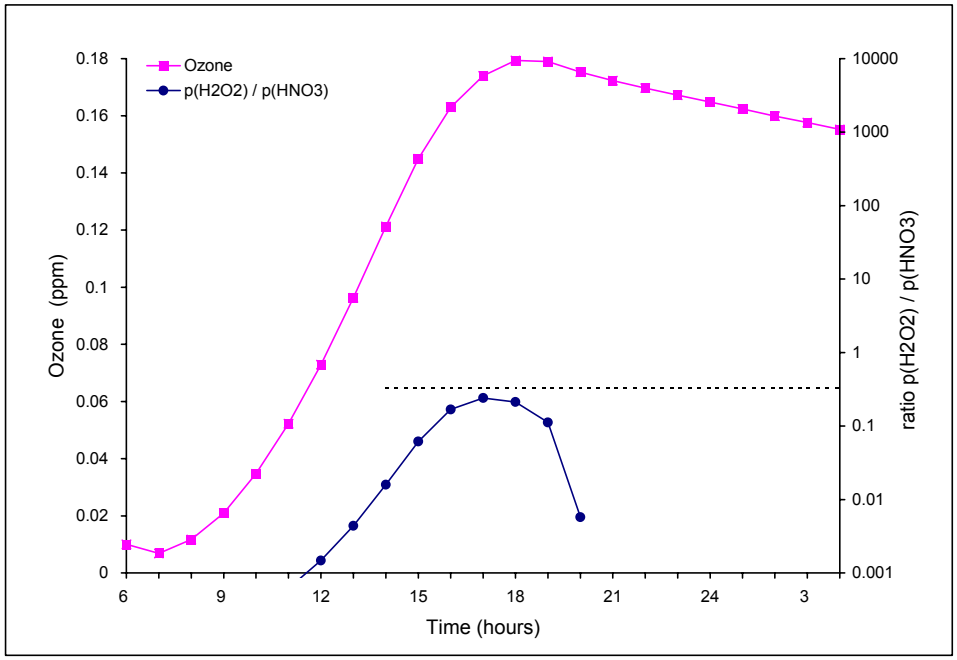

Figure 6-8a. As Figure 6-4, but for an **Initial VOC/NOx = 5:1.**

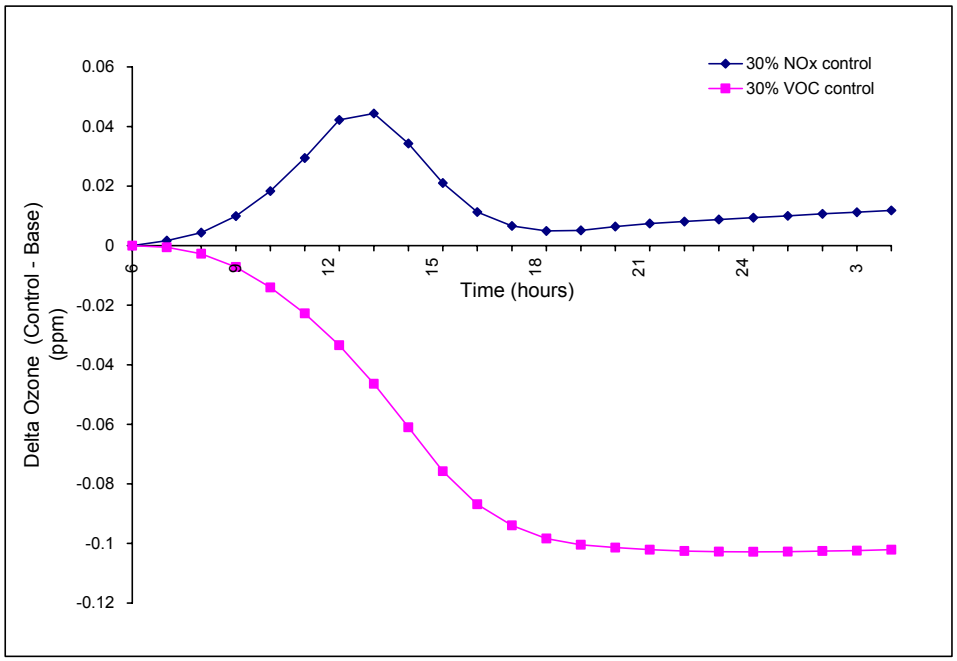

Figure 6-8b. As figure 6-6, but for an **Initial VOC/NOx = 5:1**

ozone formation is predicted to remain VOC-limited throughout the day. Figure 6-8b confirms this by showing no net benefit from NOx control throughout the day.

Alternative Chemical Apportionment Techniques

The formulation of OSAT described above was first methodology implemented into CAMx. Several variations on OSAT are now available that use different algorithms to attribute ozone contributions. One advantage of the coding framework for OSAT is that it allows for easy modification of the source attribution algorithm by modifying a single subroutine. The alternative methods currently available in CAMx are described below (other options are possible).

Geographic Ozone Assessment Technology (GOAT). GOAT does not attempt to trace ozone production back to the source of the precursors, but rather ozone formation is tracked based on the geographic location where it occurred. Thus ozone formation in a grid cell over "Area A" would be attributed to Area A even if the culpable emissions originated upwind in Area B. The disadvantage of GOAT is its simplistic assumption regarding the basis for ozone culpability. The advantages of GOAT are: (1) its freedom from assumptions about whether ozone formation is NOx or VOC limited; and (2) that its results may be more directly comparable to other emerging source attribution methodologies (e.g., trajectories, tracers, and possibly the spatial analysis component of Process Analysis).

Anthropogenic Precursor Culpability Assessment (APCA). APCA differs from OSAT in recognizing that certain emission groups are not controllable (e.g., biogenic emissions) and that apportioning ozone production to these groups does not provide information that is relevant to control strategies. To address this, in situations where OSAT would attribute ozone production to non-controllable (i.e., biogenic) emissions, APCA re-allocates that ozone production to the controllable portion of precursors that participated in ozone formation with the non-controllable precursor. In the case where biogenic emissions are the uncontrollable source category, APCA would only attribute ozone production to biogenic emissions when ozone formation is due to the interaction of biogenic VOC with biogenic NOx. When ozone formation is due to biogenic VOC and anthropogenic NOx under VOC-limited conditions (a situation in which OSAT would attribute ozone production to biogenic VOC), APCA re-directs that attribution to the anthropogenic NOx precursors present. The use of APCA instead of OSAT results in more ozone formation attributed to anthropogenic NOx sources and less ozone formation attributed to biogenic sources. APCA is not really a "source apportionment" technique because it expresses biases as to which sources should be implicated (i.e., those that are controllable), hence it is referred to as a "culpability assessment." The APCA ozone allocation scheme is described in more detail below.

The APCA Technique

OSAT identifies which emission source regions, categories, and species (VOC and NOx) that when reduced would have the greatest effect in reducing ozone concentrations. For the OTAG database, OSAT correctly identified biogenic VOC emissions as a major contributor to ozone formation, and if controlled, would result in efficient ozone reductions. However, biogenic emissions cannot be controlled; although scientifically and chemically correct, this information is irrelevant for the design of an ozone control strategy. The presence of a source category (biogenic emissions) that cannot be controlled requires special considerations when performing ozone source apportionment modeling for the purposes of aiding in the design of anthropogenic emission control strategies, or when performing an ozone precursor culpability analysis. (Note that some biogenic NOx emissions are soil NOx emissions, which are partly from fertilizers and thus are not truly "biogenic" in nature).

Biogenic versus anthropogenic ozone source apportionment, as a function of VOC and NOx precursor interactions, can be divided up into four ozone formation regimes as follows:

	Biogenic NOx	**Anthropogenic NOx**
Biogenic VOC	1	2
Anthropogenic VOC	3	4

Regime 1 involves ozone formation due to the interaction between biogenic VOC and biogenic NOx and is truly "biogenic ozone". Regime 4 is true "anthropogenic ozone" and the OSAT attribution scheme will provide control strategy relevant information by allocating ozone formed in Regime 4 to the proper anthropogenic ozone precursors (VOC or NOx). Difficulties arise in the mixed anthropogenic/biogenic regimes (Regimes 2 and 3) where precursors from both biogenic and anthropogenic sources participate in the ozone formation.

Much of the ozone in the OTAG modeling is formed under Regime 2, although Regime 1 may have some influence on ozone formation in high biogenic NOx regions (e.g., the corn belt). To design effective control strategies, an ozone allocation scheme is needed that accounts for the special status of biogenic emissions as being uncontrollable.

In the APCA technique, only the true "biogenic ozone" (i.e., ozone formed under Regime 1) would be attributed to biogenic emissions, while ozone formed in the remainder of the regimes (2-4) would be allocated to anthropogenic emissions. The standard OSAT approach is used to allocate ozone formed to anthropogenic VOC or NOx emissions when anthropogenic VOC and NOx emissions interact (i.e., Regime 4), and to allocate to biogenic VOC or NOx when these two precursors interact (Regime 1). However, when ozone forms due to the interaction of biogenic and anthropogenic emissions (i.e., Regimes 2 and 3), the APCA technique differs from OSAT by allocating ozone formed to anthropogenic emissions; the ozone increment is allocated to anthropogenic NOx (if VOC-limited) or anthropogenic VOC (if NOx-limited) precursors. Assuming that N and V are the NOx and reactivity-weighted VOC tracer concentrations in a grid cell from different source categories (e.g., biogenic sources and several anthropogenic emissions categories) that participated in the formation of an increment of ozone (O3), the APCA allocation scheme can be expressed mathematically as follows.

First, APCA defines the fraction of ozone formed due to the interaction of biogenic VOC with biogenic NOx, which will be attributed to biogenic emissions (Regime 1):

$$F_{bio} = \min\left(\frac{V_{bio}}{V_{total}}, \frac{N_{bio}}{N_{total}}\right)$$

under VOC-limited conditions, APCA attributes the fraction of ozone formed to biogenic VOC emissions (Regime 1):

$$O3V_{bio} = F_{bio} \cdot O_3$$

It then attributes the fraction of ozone increment to anthropogenic VOC source groupings due to the interaction of anthropogenic VOC with anthropogenic and biogenic NOx (Regime 4):

$$O3V^{i}_{anthro} = \left(\frac{V^{i}_{anthro}}{V_{total}}\right) \cdot O_3, \qquad i = 1,...,nanthro$$

Finally, the remainder of the ozone increment ($\Delta O3$), which would have been attributed to biogenic VOC in OSAT, is attributed to anthropogenic NOx (Regimes 2 and 3):

$$\Delta O3 = O_3 - O3V_{bio} - \sum_i O3V^{i}_{anthro}$$

$$O3N^{i}_{anthro} = \left(\frac{N^{i}_{anthro}}{N^{total}_{anthro}}\right) \cdot \Delta O_3, \qquad i = 1,...,nanthro$$

Under NOx-limited conditions, similar formulas are used, switching the N with V and O3N with O3V. Since it is expected that biogenic VOC precursors will almost always be greater than biogenic NOx precursors (i.e., $F_{bio} = N_{bio}/N_{total}$), then under NOx-limited conditions the APCA ozone allocation scheme will produce identical results to OSAT.

6.3 RUNNING CAMx WITH OSAT

CAMx Control File

OSAT and its derivatives are invoked similarly to the other Probing Tools within the CAMx control file. In the `&CAMx_Control` namelist module, the variable `Probing_Tool` must be set to "OSAT", "GOAT", or "APCA". An additional namelist module called `&SA_Control` must then be provided in the control file to configure the OSAT portion of the model. The additional namelist module is described below. The order of the variables follow the template available with the source code. Several examples of the OSAT portion of the CAMx run control file are shown in Figures 6-9(a-d).

Description of OSAT Control in the CAMx Run Control File

`&SA_Control`	Label for the Probing Tool namelist module that configures the OSAT option; it must begin in column 2
`&`	Flag ending a namelist module; it must be in column 2
`SA_Summary_Output`	Logical flag used to limit the species written to the tracer concentration file to a subset of the PSAT treated species. If set to true, the output will be restricted to the following species: O3N, O3V
`SA_File_Root`	Character root output path/filename
`SA_Master_Sfc_Output`	Logical flag for master grid surface output (TRUE=OSAT concentration file will be output for all tracers, FALSE=OSAT concentration file will not be output)
`SA_Nested_Sfc_Output`	Logical flag for nested grid surface output (TRUE=OSAT concentration file will be output for all tracers, FALSE=OSAT concentration file will not be output)
`SA_Stratify_Boundary`	Logical flag to stratify boundary types (TRUE=separate tracer types will be used for the N, S, E, W, and Top boundaries, FALSE=a single tracer type will be used for all 5 boundaries)
`SA_Number_of_Source_Regions`	Integer number of source regions for this run. This must be the same as the number of source areas defined in the `SA_Source_Area_Map` file.

SA_Number_of_Source_Groups	Integer number of emission groups for this run. Together with the Use_Leftover_Group flag, this determines the number of paired emission files that must be supplied (additional details below).
Use_Leftover_Group	Logical flag to define a "leftover" emissions group (TRUE= calculate a "leftover" emissions group from the difference between the sum of the emission group files and the regular CAMx emission files, FALSE=do not calculate a "leftover" emissions group)
Number_of_Timing_Releases	Integer number of timing tracer releases per 24 hour period (set to zero to turn off timing releases)
SA_Receptor_Definitions	Character input OSAT receptor definition path/filename. (This is an optional file).
SA_Source_Area_Map	Character array (by CAMx grid) input OSAT source area definition path/filename (required for master grid, optional for nested grids)
SA_Master_Restart	Character input master grid OSAT restart path/filename (ignored if Restart=FALSE)
SA_Nested_Restart	Character input nested grid OSAT restart path/filename (ignored if Restart=FALSE or Number_of_Grids=1)
SA_Points_Group	Character array (by source group) input OSAT elevated point source emissions path/filename (optional, ignored if Point_Emissions=FALSE)
SA_Emiss_Group_Grid	Character array (by source group, by CAMx grid) input OSAT gridded emissions path/filename (optional, ignored if Gridded_Emissions=FALSE)

Specifying Emission Groups

OSAT can apportion ozone and ozone precursor concentrations among several emission categories. To achieve this, the emissions for the separate groups must be supplied as sets of separate emissions files for each source group; a low level (gridded) file for each fine grid nest, and one elevated point source file. The additional emission files must be in the standard UAM emission file format (EPA, 1990), as described in Section 5. If the group being separated has no elevated emissions (e.g. biogenics), the point source file name for the group can be left blank. If the emission group being separated has no surface emissions (e.g. a utility), the surface file name for the group can be left blank for all grids. APCA requires two or more emissions categories, with the first category being biogenic emissions.

```
&SA_Control

 SA_File_Root              = '$TRACOUT/CAMx.OSAT.9507$today',

 SA_Master_Sfc_Output         = .true.,
 SA_Nested_Sfc_Output         = .true.,
 SA_Summary_Output            = .true.,
 SA_Stratify_Boundary         = .false.,
 SA_Number_of_Source_Regions  = 19,
 SA_Number_of_Source_Groups   = 1,
 Use_Leftover_Group           = .false.,
 Number_of_Timing_Releases    = 2,

 SA_Receptor_Definitions  = '$TRACIN/receptor.cities ',
 SA_Source_Area_Map(1)    = '$TRACIN/APCA.source.area.map',
 SA_Source_Area_Map(2)    = ' ',

 SA_Master_Restart        = ' ',
 SA_Nested_Restart        = ' ',

 SA_Points_Group(1)       = ' ',

 SA_Emiss_Group_Grid(1,1) = ' ',
 SA_Emiss_Group_Grid(1,2) = ' ',

 &
```

Figure 6-9a. An example of OSAT input records in the CAMx run control file. The options for this run are as follows: this is a two-grid run, master and nested grid surface concentrations are written to file, a single tracer type is to be used for all boundaries, 19 source regions, one emission group (i.e., zero additional emission files and no leftover group), and two timing tracer releases per day. This is the first day of the simulation (i.e., restart is false), so no OSAT restart files are supplied.

```
&SA_Control

 SA_File_Root              = '$TRACOUT/CAMx.OSAT.9507$today',

 SA_Master_Sfc_Output         = .true.,
 SA_Nested_Sfc_Output         = .true.,
 SA_Summary_Output            = .true.,
 SA_Stratify_Boundary         = .false.,
 SA_Number_of_Source_Regions  = 19,
 SA_Number_of_Source_Groups   = 1,
 Use_Leftover_Group           = .false.,
 Number_of_Timing_Releases    = 2,

 SA_Receptor_Definitions  = '$TRACIN/receptor.cities ',
 SA_Source_Area_Map(1)    = '$TRACIN/APCA.source.area.map',
 SA_Source_Area_Map(2)    = ' ',

 SA_Master_Restart        = '$TRACOUT/CAMx.OSAT.9507$yesterday.sa.inst.2',
 SA_Nested_Restart        = '$TRACOUT/CAMx.OSAT.9507$yesterday.sa.finst.2',

 SA_Points_Group(1)       = ' ',

 SA_Emiss_Group_Grid(1,1) = ' ',
 SA_Emiss_Group_Grid(1,2) = ' ',

 &
```

Figure 6-9b. As in Figure 6-9(a), but in this case the run is a continuation, and so the restart flag is set to TRUE and a "Tracer Restart" files are supplied.

```
&SA_Control

 SA_File_Root              = '$TRACOUT/CAMx.OSAT.9507$today',

 SA_Master_Sfc_Output        = .true.,
 SA_Nested_Sfc_Output        = .true.,
 SA_Summary_Output           = .true.,
 SA_Stratify_Boundary        = .false.,
 SA_Number_of_Source_Regions = 19,
 SA_Number_of_Source_Groups  = 3,
 Use_Leftover_Group          = .true.,
 Number_of_Timing_Releases   = 0,

 SA_Receptor_Definitions  = '$TRACIN/receptor.cities ',
 SA_Source_Area_Map(1)    = '$TRACIN/APCA.source.area.map',
 SA_Source_Area_Map(2)    = ' ',

 SA_Master_Restart        = '$TRACOUT/CAMx.OSAT.9507$yesterday.sa.inst.2',
 SA_Nested_Restart        = '$TRACOUT/CAMx.OSAT.9507$yesterday.sa.finst.2',

 SA_Points_Group(1)       = ' ',
 SA_Points_Group(2)       = '$PTSRCE/utilpt.ng.$todate-07.ag.07cem1A-run11',

 SA_Emiss_Group_Grid(1,1) = '$TRACEMS/bio2.cc.$todate-95',
 SA_Emiss_Group_Grid(1,2) = '$TRACEMS/bio2.ff.$todate-95.ne',
 SA_Emiss_Group_Grid(2,1) = '$TRACEMS/util.cc.$todate-07.ag.07cem1A-run11',
 SA_Emiss_Group_Grid(2,2) = '$TRACEMS/util.ff.$todate-07.ag.07cem1A-run11',

 &
```

Figure 6-9c. As in Figure 6-9(a), but in this case the run is a continuation day of a run with three emission groups. The three emission groups are defined by supplying two pairs of extra emission files for each grid (AREA group 1, AREA group 2, and POINT group 2), and setting the "Use_Leftover_Group" flag to TRUE for the model to calculate the third group internally. The POINT group 1 filename is blank because group 1 is a category with no point source emissions (e.g., biogenics).

```
&SA_Control

 SA_Master_Sfc_Output         = .true.,
 SA_Nested_Sfc_Output         = .true.,
 SA_Summary_Output            = .true.,
 SA_Stratify_Boundary         = .false.,
 SA_Number_of_Source_Regions  = 19,
 SA_Number_of_Source_Groups   = 3,
 Use_Leftover_Group           = .false.,
 Number_of_Timing_Releases    = 0,

 SA_Receptor_Definitions  = '$TRACIN/receptor.cities ',
 SA_Source_Area_Map(1)    = '$TRACIN/APCA.source.area.map',
 SA_Source_Area_Map(2)    = ' ',

 SA_Master_Restart        = '$TRACOUT/CAMx.OSAT.9507$yesterday.sa.inst.2',
 SA_Nested_Restart        = '$TRACOUT/CAMx.OSAT.9507$yesterday.sa.finst.2',

 SA_Points_Group(1)       = ' ',
 SA_Points_Group(2)       = '$PTSRCE/utilpt.ng.$todate-07.ag.07cem1A-run11',
 SA_Points_Group(3)       = '$PTSRCE/remain.ng.$todate-07.ag.07cem1A-run11',

 SA_Emiss_Group_Grid(1,1) = '$TRACEMS/bio2.cc.$todate-95',
 SA_Emiss_Group_Grid(1,2) = '$TRACEMS/bio2.ff.$todate-95.ne',
 SA_Emiss_Group_Grid(2,1) = '$TRACEMS/util.cc.$todate-07.ag.07cem1A-run11',
 SA_Emiss_Group_Grid(2,2) = '$TRACEMS/util.ff.$todate-07.ag.07cem1A-run11',
 SA_Emiss_Group_Grid(3,1) = '$TRACEMS/remain.cc.$todate-07.ag.07cem1A-run11',
 SA_Emiss_Group_Grid(3,2) = '$TRACEMS/remain.ff.$todate-07.ag.07cem1A-run11',

 &
```

Figure 6-9d. As in Figure 6-9(c) (i.e. a continuation day of a run with three emission groups), but in this case all three emission groups are defined explicitly by supplying extra emission files (AREA group 1, AREA group 2, POINT group 2, AREA group 3, and POINT group 3). Therefore, the "Use_Leftover_Group" flag is set to FALSE. The POINT group 1 filename is blank because group 1 is a category with no point source emissions (e.g., biogenics).

Imagine a case where the emission inventory is split into three groups. Three sets of emission files could be supplied that together have the same total emissions as the regular CAMx emissions files. Alternatively, two sets of files could be supplied and the third calculated from the "leftover" emissions (i.e., the regular CAMx emissions minus the two groups specified). Both approaches could be useful, depending upon the emissions files available to the user. Accordingly, OSAT reads an input flag "`Use_Leftover_Group`" that can be set true or false. If a leftover group is selected, the model verifies that the group is not too small to calculate within the numerical precision of the computer (this also traps cases where the flag was set true in error). If no leftover group is selected, the model verifies that the total emissions for the groups supplied are equal to the regular model emissions, i.e., that a leftover group is not needed. In both cases, if appropriate conditions are not met, the model stops with a descriptive error message.

The number of emission file sets that need to be supplied for different model configurations is summarized in Table 6-1. Table 6-1 also shows how the emissions groups are numbered, which is reflected in the tracer species names (defined below).

Table 6-1. Numbers of emission file sets (i.e., low level files and point source file) needed for different model configurations.

Number of Emission Groups	Use Leftover Group	Number of Emission File Sets Needed	Numbering of Emission Groups and Tracer Species
1	Not Applicable	0	0
n>1	False	n	1,2,3,...n
	True	n-1	1,2,3,...n

When specifying additional point source files to resolve source category groupings, the list of point sources on each file must be identical (i.e., same number of sources, same order) to the regular model point source file. This formal restriction is necessary to ensure that point sources are correctly cross-referenced within CAMx. Thus, a point source file for a specific source group may need to contain records for sources that are not in the group: these records should have zero emissions.

Geographic resolution is superimposed on emission group resolution using the source area map described below. The source area map is defined using master grid cells which may not adequately resolve point source locations. To provide finer control of point source assignments to geographic areas, the source area can be specified for any source by putting the source area index in the (unused) kcell value on the point source file (see file description in section 5). This feature is referred to as "point source override."

Running With Timing Tracers

Timing tracers will be released at hourly intervals according to the "`Number_of_Timing_Releases`" parameter. For example, 4 means a new release is started every six hours (hours 0, 6, 12 and 18). If the simulation is started in the middle of the

day (e.g. at hour 15), the first tracer release is time stamped with the model start time, subsequent releases occur on a schedule as if the start time were at hour zero.

OSAT can be run without timing tracers if the "`Number_of_Timing_Releases`" parameter is set to zero. Source apportionment of ozone and precursors is unaffected by this since these two functions of the model are independent. If timing tracers are omitted, the postprocessing software ("browser") described below will not report estimated release times for precursor emissions, nor will it estimate whether recirculation is likely to have occurred. Users may choose to run without timing tracers in situations where temporal resolution is not required. Omitting timing tracers reduces the number of tracer species employed and therefore may permit users to select relatively more geographic/emissions category resolution within the same computer memory limitations.

6.4 INPUT FILE FORMATS

Source Area Mapping

OSAT can apportion ozone and ozone precursor concentrations among several geographic regions within the modeling domain, as shown in Figure 6-1. The "source area mapping" file assigns each grid cell to a specific geographic source region. The format of the file is an array of integer numbers (i3) corresponding to the CAMx domain. Figure 6-10 shows the source area mapping file corresponding to Figure 6-1. Since the CAMx domain in Figure 6-1 has 63 rows and 64 columns of cells, the file shown in Figure 6-10 has 63 lines with 64 numbers on each line. The first number (top left) always corresponds to the Northwest corner of the domain. Note that the source area map is defined in terms of the master grid.

If desired, a source area map may be created for each nest. This provides for more finely resolved source areas within the nested domain. The source area map for a nest is in the same format as the master grid source area map described above, but contains a number of rows and columns corresponding to the nested grid, **including the boundary ("buffer") rows and columns**. Within a nest for which a nested grid source area map is supplied, the source areas as defined by this map will take precedence over the source areas defined by the master grid source area map. If a source area map is not provided for a specific nest the source area definition will be taken from the source area map of the parent grid.

Receptor Definition

Tracer concentrations for selected receptor locations are output to an ASCII file every hour. The receptors for each model run are defined in the "Receptor definition" input file. Three types of receptors are supported:

`POINT`	a point specified in the coordinate system of the CAMx grid. Concentrations at the point are determined by bi-linear interpolation of the surrounding four master grid surface cells.

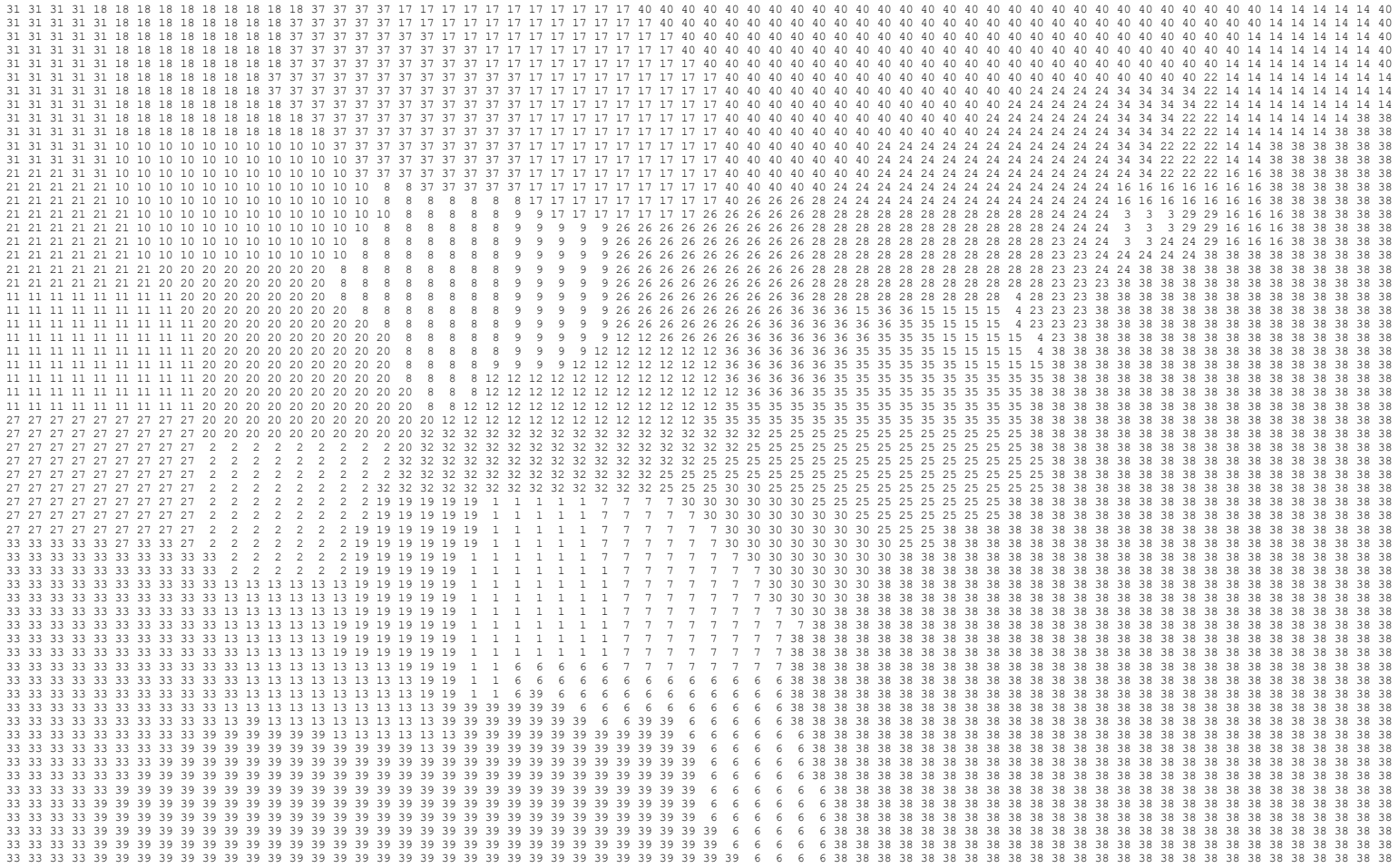

Figure 6-10. Example source area mapping file for the domain and source areas shown in Figure 6-1.

SINGLE CELL	a single surface grid cell identified by number.
CELL AVERAGE	a group of grid cells identified by number that are averaged together to provide multi-cell average tracer concentrations.
WALL OF CELLS	a group of grid cells defining a wall (i.e., a flux plane).

For the receptor types that are defined by grid cell it is necessary to specify the grid containing the receptor. This is done by including the grid number on the receptor definition record. Grid numbers are defined using the internal CAMx grid ordering. The grid numbering as defined by CAMx is shown in a table in the .diag file. Each receptor can be identified by a 10 character name. The formats for specifying each receptor type are given in Table 6-2. An example receptor file is shown below:

```
POINT               City 1      461.520  3762.040
SINGLE CELL         Cell 1          1        45        18
CELL AVERAGE        Region 10       2         8
       31        19
       32        19
       33        19
       34        19
       31        18
       32        18
       33        18
       34        18
WALL OF CELLS       Boundary1       2        10        20
                                            18        18
                                             1         5
```

6.5 OUTPUT FILE FORMATS

OSAT writes several output files that are in binary format, as described in Section 5. These include the master grid tracer instantaneous concentration files (.sa.inst.1 and .sa.inst.2) and the master grid surface tracer average concentration file (.sa.surf). The nested grid files for instantaneous and average surface concentrations are the same format as for the regular model species described in Section 5. In addition, OSAT writes out tracer concentrations for selected receptor locations to an ASCII file (.sa.receptor). The naming conventions for tracer species and the format of the receptor concentration file are discussed below.

Tracer Species Names

The names of tracer species uniquely identify the information carried by each species and, taken as a group, identify the model configuration in any run. Species names have less than ten characters, consistent with the UAM convention. The naming conventions are as follows:

Table 6-2. Format for the receptor definition file.

Receptor Type	Line	Columns	Data
POINT	1	1-15	The word "POINT"
	1	21-30	Receptor name
	1	31-40	X co-ordinate
	1	41-50	Y co-ordinate
SINGLE CELL	1	1-15	The word "SINGLE CELL"
	1	21-30	Receptor name
	1	31-40	Grid Number
	1	41-50	X cell number
	1	51-60	Y cell number
CELL AVERAGE	1	1-15	The words "CELL AVERAGE"
	1	21-30	Receptor name
	1	31-40	Grid number
	1	41-50	The number of cells to average (M)
	2-M	1-10	X cell number
	2-M	11-20	Y cell number
WALL OF CELLS	1	1-15	The words "WALL OF CELLS"
	1	21-30	Receptor name
	1	31-40	Grid number
	1	41-50	X-cell begin
	1	51-60	X-cell end
	2	41-50	Y-cell begin
	2	51-60	Y-cell end
	3	41-50	Z-cell begin
	3	51-60	Z-cell end

Timing Tracers

Inert Tracer **Idddhhrrr**
Decay Companion Tracer **Ddddhhrrr**

where:

ddd Julian day, e.g., 240
hh Hour tracer release started at, e.g., 12
rrr Region tracer released from, i.e., 001, 002, 003, etc

Examples: `I24012001, D24100012`

Ozone Reaction Tracers

Emission Sources **SSSeeerrr**

where:

SSS Species type, i.e., NOX, VOC, O3V or O3N
eee Emissions group:
Single group, always 000
Multiple groups, 001, 002, etc.
rrr Region tracer released from, 001, 002, 003, etc.

Initial/Boundary **SSSeeerrr**

where:

SSS Species type, i.e., NOX, VOC, O3V or O3N
eee Initial Concentrations: always 000
Boundary Concentrations not stratified by boundary: always 000
Boundary Concentrations stratified by boundary: WST, EST, STH, NTH, TOP indicating boundary of origin
rrr IC for Initial Concentrations, BC for Boundary Concentrations

Examples: `NOX000015, VOC002015, O3V000IC, O3NTOPBC`

Receptor Concentration File

Hourly average tracer concentrations at user specific receptor locations are output to the "receptor concentration" file. The file is in comma delimited ASCII format suitable for importing into a spreadsheet (a spreadsheet postprocessing tool is available to visualize the data in this file, as described below). An example output file is shown in Figure 6-11. Two header lines at the top of the file identify the model version and the date the run was performed. Next, two lines identify the time period covered by the file and the averaging interval (generally one hour, determined by the CAMx simulation control file). Next, three lines define the model configuration and seven lines specify the numbers of tracer species that result from this configuration. The names of each tracer species are given on six lines ordered

by tracer species type: the order in which species are listed here is the same as the order in which tracer concentrations are given later in the file.

The tracer species names are followed by the number of receptors and receptor names. Note that the first receptor (receptor 1) is always the location of the hourly peak ozone. Since the location of the hourly peak varies from hour to hour, the X and Y locations are left blank. Receptors 2 and higher are those specified in the "Receptor definition" file. The tracer concentrations are reported in blocks with a date and time stamp at the head of each block. Within each block, receptors are reported in numerical order. For each receptor, there are six lines of data for the tracer species identified at the heading "Tracer Names". All values are in CAMx units of ppm. At the bottom of the data block for each receptor are two lines with three numbers: these are the total tracer NOx, VOC, and ozone (first line) and regular CAMx NOx, VOC and ozone (second line).

6.6 POSTPROCESSING

The tracer concentrations in the gridded surface concentration files can be displayed using any post-processing software normally used for displaying UAM average file output formats.

The receptor concentration file contains information for all receptors and all hours within the model run that created the file. A post-processing tool is available to allow the user to "browse" through the information contained in this file and prepare displays like Figure 6-2. The "browser" is a Microsoft Excel Spreadsheet that is controlled by a graphical user interface (GUI) allowing you to rapidly visualize results for any receptor. To use this software, the user must have Microsoft Excel (version 5 or higher). The browser is comprised of three files:

O3TOOL.XLS	browser spreadsheet with displays for monochrome printers
O3TCOL.XLS	browser spreadsheet with color displays
ENVIRON.XLA	library of macro functions called by O3TOOL or O3TCOL

All three files should be placed in a single directory. To use the browser, open either O3TOOL.XLS or O3TCOL.XLS as you would any Excel spreadsheet.

Instructions for using the browser are given below. The browser is GUI driven (point and click) and easy to use. The following instructions assume some familiarity with Excel:

1. Open Excel and then File/Open o3tool.xls. When the browser is opening you will may be asked if you want to re-establish links, say no. If you say yes, the links will likely fail resulting in warnings that may be safely ignored.

2. Move to the front sheet (controls) of o3tool. Click the "Import File" button at top left and select the data file to be visualized. The selected data file is imported as a second spreadsheet.

3. When the data file is opened, all of the information on the controls sheet is updated for the new file (numbers of tracers, receptors, etc.). To begin viewing the data,

click the "Copy Receptor Data for Specified Time" button at top right to select the receptor (by number) and time to view the results. The user must also choose the method for rank ordering source contributions ("Sort by Sum" is a useful default choice). Click on "OK" to proceed. On the next dialog box, choose how many source areas you want to see results for. About 4 is a good default, this value can be changed later. Click on "OK" to proceed.

4. The browser now finds the data requested, calculates the values needed to plot the bar and pie charts (on the "Calcs" sheet) and moves to the "GraphWork" sheet to view the summary graphs and tables.

5. Use the buttons to the right of the display to change the number of sources, change the hour, or print the graph. The receptor or file can be changed from this page also.

The graphs and tables shown on the "Calcs" sheet are standard Excel graphics that may be customized using Excel commands and features.

```
CAMx, SOURCE APPORTIONMENT, VERSION -- 960315 ,
Mon Oct 26 10:37:34 1998               ,

 File Duration  ,     87238,     15.00,     87238,     24.00,
Average Interval ,    1.0000

Number of timing periods     ,         2
Number of source areas       ,        17
Number of emission groupings ,         1
Number of tracer species     ,       144
Number of NOx species        ,        19
Number of VOC species        ,        19
Number of O3N species        ,        19
Number of O3V species        ,        19
Number of INERT TIME species ,        34
Number of DECAY TIME species ,        34

Tracer Names,
NOX000IC ,NOX000BC ,NOX001001,NOX001002,NOX001003,NOX001004,NOX001005 ..
VOC000IC ,VOC000BC ,VOC001001,VOC001002,VOC001003,VOC001004,VOC001005 ..
O3N000IC ,O3N000BC ,O3N001001,O3N001002,O3N001003,O3N001004,O3N001005 ..
O3V000IC ,O3V000BC ,O3V001001,O3V001002,O3V001003,O3V001004,O3V001005 ..
I23815001,I23815002,I23815003,I23815004,I23815005,I23815006,I23815007 ..
D23815001,D23815002,D23815003,D23815004,D23815005,D23815006,D23815007 ..

Number of receptors ,         6
  No,   Name,    Type,    Xloc,      Yloc,
   1, HourlyPeak,    1,          ,          ,
   2, Rubidoux  ,    0,     461.5,     3762.0,
   3, Pasadena  ,    0,     396.4,     3778.5,
   4, Lennox    ,    0,     373.0,     3755.0,
   5, Peak      ,    1,        45,         18,
   6, Region 10 ,    8,        31,         19,
                               32,         19
                                  33,          19
                                  34,          19,
                                  31,          18,
                                  32,          18,
                                  33,          18,
                                  34,          18,

Time Varying Tracer Data,

 Data for Period,     87238,     15.00,     87238,     16.00,
  Receptor,    1,
1.3265E-02, 1.3544E-09, 1.0000E-16, 1.0974E-15, 1.0000E-16, 1.0000E-16 ..
1.2237E-01, 3.3869E-08, 1.0000E-16, 1.6165E-14, 1.0000E-16, 1.0000E-16 ..
8.7304E-02, 1.1926E-08, 1.0000E-16, 1.0000E-16, 1.0000E-16, 1.0000E-16 ..
9.0300E-02, 1.5269E-08, 1.0188E-16, 2.6997E-15, 1.0213E-16, 1.0162E-16 ..
1.0036E-16, 4.0640E-15, 1.0036E-16, 1.0036E-16, 1.0036E-16, 1.0029E-16 ..
1.0000E-16, 3.7563E-15, 1.0000E-16, 1.0000E-16, 1.0000E-16, 1.0000E-16 ..
1.4500E-02, 1.2663E-01, 1.7770E-01,
1.4500E-02, 1.2663E-01, 1.7770E-01,
  Receptor,    2,
(File continues with data for remaining receptors and hours)
```

Figure 6-11. Example Receptor Concentration File. Lines ending with ".." are truncated to fit the page, and the file would continue with data for additional receptors and hours in the same format.

7. PARTICULATE SOURCE APPORTIONMENT TECHNOLOGY

7.1 INTRODUCTION

Airborne particulate matter (PM) is widely recognized as an important pollution issue because it causes health problems and environmental degradation. In recent years the emphasis on controlling PM has shifted toward fine PM (or PM2.5, with particle diameter less than 2.5 μm) because it is more strongly associated with serious health effects than coarse PM. Knowing which sources contribute to PM2.5 is essential for developing effective control strategies. Many components of PM2.5 are secondary pollutants and so photochemical models are important tools for PM air quality planning. The Particulate Source Apportioning Technology (PSAT) has been developed for CAMx to provide PM source apportionment among specific geographic regions and source categories. PM source apportionment information from PSAT is useful for:

1) Understanding model performance and thereby improving model inputs/formulation;
2) Performing culpability assessments to identify sources that contribute significantly to PM pollution;
3) Designing the most effective and cost-effective PM control strategies.

Source apportionment for primary PM is relatively simple to obtain from any air pollution model because their source-receptor relationships are essentially linear. Gaussian steady-state models and Lagrangian puff models have been used extensively to model primary PM pollution from specific sources, which is a direct form of source apportionment. The Gaussian and Lagrangian approaches work for primary PM because the models can assume that emissions from separate sources do not interact. This assumption breaks down for secondary PM pollutants (e.g., sulfate, nitrate, ammonium, secondary organic aerosol) and so puff models may dramatically simplify the chemistry (to eliminate interactions between sources) so that they can be applied to secondary PM. Eulerian photochemical grid models are better suited to modeling secondary pollutants because they account for chemical interactions between sources. Grid models do not naturally provide source apportionment because the impact of all sources has been combined in the total pollutant concentration. PSAT has been developed to retain the advantage of using a grid model to describe the chemistry of secondary PM formation and also to provide source apportionment.

This section starts by reviewing several approaches to PM source attribution in grid models that were considered when PSAT was designed. Next, the PSAT algorithms are explained, and then example PSAT results are presented and compared to results from some other methods.

7.2 APPROACHES TO PM SOURCE ATTRIBUTION IN GRID MODELS

Several potential approaches were considered at the PSAT design stage and these are discussed below. The approaches considered fall into two general categories, which we have called sensitivity analysis and reactive tracers. The reactive tracer approaches also could be called tagged species approaches. This section concludes with a discussion of an important

fundamental difference between sensitivity analysis and source apportionment that explains why these two concepts should not be confused for secondary pollutants.

Sensitivity Analysis Methods

Sensitivity analysis methods measure the model output response to an input change, e.g., the change in sulfate concentration due to a change in SOx emissions. In general, sensitivity methods will not provide source apportionment if the relationship between model input and output is non-linear. For example, if sulfate formation is non-linearly related to SOx emissions, the sum of sulfate (SO4) sensitivities over all SOx sources will not equal the model total sulfate concentration. This concept is discussed in more depth later in this section.

Brute Force or Direct Method. The brute force method estimates first-order sensitivity coefficients (e.g., $\Delta SO4/\Delta SOx$) by making a small input change (ΔSOx) and measuring the change in model output ($\Delta SO4$). This method is simple and can be applied to any model, but is inefficient because a complete model run is required for each sensitivity coefficient to be determined. Accuracy also may be an issue for the brute force method because ideally the input change (ΔSOx) should be vanishingly small but for small input changes the output change may be contaminated by numerical precision or model "noise." For larger input changes, first-order sensitivities estimated by the brute force method may be distorted by non-linear chemical effects, e.g., a brute force coefficient ($\Delta SO4/\Delta SOx$) may be a mixture of first-order ($dSO4/dSOx$) and second-order ($d^2SO4/dSOx^2$) derivatives. Higher-order sensitivity coefficients also can be estimated by the brute force method.

Zero-Out Modeling. The zero-out method differs from the brute force method in that a specific emissions input is set to zero and the change in output measured. Zero-out modeling can be used with any model but is inefficient because a complete model simulation is required for each source. Accuracy also may be an issue if the zero-out method is applied to a small emissions source. This method has been used extensively for source attribution because it seems intuitively obvious that removing a source should reveal the source's impact. However, because zero-out modeling is a sensitivity method it does not provide source apportionment for non-linear systems because the sum of zero-out impacts over all sources will not equal the total concentration, as discussed in more depth later in this section.

Decoupled Direct Method (DDM). The DDM provides the same type of sensitivity information as the brute force method but using a computational method that is directly implemented in the host model (Dunker, 1981). The DDM has potential advantages of greater efficiency and accuracy relative to the brute force method (Dunker at al., 2002a) and the DDM implementation in CAMx (Dunker at al., 2002a,b) is currently being extended to PM species. Drawbacks of DDM are that the implementation is technically challenging, that using DDM for many sensitivities simultaneously requires large computer memory, and because DDM is a sensitivity method, it does not provide source apportionment for non-linear systems unless higher-order sensitivities are calculated.

Other Sensitivity Methods. There are other sensitivity methods that provide similar information to DDM such as adjoint methods (e.g., Menut at al., 2000; Elbern and Schmidt,

1999) and automatic differentiation in FORTRAN (ADIFOR). They have similar advantages and disadvantages as DDM but may be less computationally efficient (Dunker et al., 2002a).

Reactive Tracer Methods

Reactive tracers (or tagged species) are extra species added to a grid model to track pollutants from specific sources. For example, a standard grid model calculates concentrations for a species X that has many sources and so the concentration of X is the total concentration due to all sources. A reactive tracer (x_i) is assigned to for each source (i) with the intention that the sum of the reactive tracers will equal total concentration ($X = \Sigma x_i$). The challenge is to develop numerical algorithms for solving the reactive tracer concentrations that ensure that this equality is maintained. Depending upon the formulation of the tracer algorithms, it may be possible to model tracers for a single source of interest and omit tracers for all other sources, or it may be necessary to include tracers for all sources (as is the case for PSAT). Reactive tracers can potentially provide true source apportionment ($X = \Sigma x_i$), however the numerical value of the source apportionment will depend upon assumptions within the reactive tracer formulation. In particular, for any process that is non-linear in species concentrations (e.g., chemistry) there is no unique way to assign the total concentration change to the reactive tracers. This issue is discussed in more depth later in this section.

Source Oriented External Mixture (SOEM). Kleeman and Cass (2001) developed an approach called SOEM that tracks primary PM from different source categories/regions using tagged species that are considered to represent seed particles. Reactive tracers are added to track secondary PM and related gases from different source categories/regions, and source apportioned secondary PM condenses onto the seed particles. Chemical change for secondary PM and related gases is accounted for by expanding the chemical mechanism to treat different source regions/categories as separate precursor and product species. This requires thousands of chemical reactions and hundreds to thousands of chemical species, depending upon the number of source regions/categories. The main advantage of the SOEM method is that it is potentially accurate, and the main disadvantage is computational demand.

PSAT and TSSA. The PM Source Apportionment Technology (PSAT) uses reactive tracers to apportion primary PM, secondary PM and gaseous precursors to secondary PM among different source categories and source regions. The PSAT methodology is described below. PSAT was developed from the related ozone source apportionment method (OSAT) already implemented in CAMx (Dunker at al., 2002b). Tonnesen and Wang (2004) are independently developing a method very similar to PSAT called Tagged Species Source Apportionment (TSSA) in the Community Multiscale Air Quality (CMAQ) modeling system. Advantages of PSAT and TSSA are expected to be high efficiency and flexibility to study different source categories/regions. The accuracy of the PSAT (and TSSA) source apportionment results must be evaluated, as for any other method.

Source Apportionment and Source Sensitivity

Consider a chemical species X that has two sources A and B (so $X = x_A + x_B$) and which undergoes a second order self-reaction with rate constant k. The rate of chemical change is:

$$\frac{dX}{dt} = -kX^2$$

$$\frac{dX}{dt} = -k(x_A + x_B)^2$$

$$\frac{dX}{dt} = -kx_A^2 - kx_B^2 - 2kx_A x_B$$

The homogeneous rate terms kx_A^2 and kx_B^2 clearly describe chemical change for pollutants from sources *A* and *B* (x_A and x_B), but the inhomogeneous rate term $2kx_Ax_B$ is not uniquely associated with either source *A* or *B*. A reactive tracer (or tagged species) source apportionment method must deal with this inhomogeneous rate term either by developing rules to apportion the inhomogeneous term to sources *A* and *B* or by modifying the chemistry to eliminate the inhomogeneous term. For a sensitivity method, the homogeneous quadratic rate terms generate second-order homogeneous sensitivity coefficients (s_{AA} and s_{BB}) and the inhomogeneous rate term generates a second-order inhomogeneous sensitivity coefficient (s_{AB}). Consequently, the total concentration of *X* is incompletely described by the first-order sensitivity coefficients (s_A and s_B) that resemble source apportionments.

The example presented above is a simple case of a non-linear chemical system that illustrates why source apportionment and source sensitivity are not the same thing for nonlinear systems. The implications are:

1) There is no unique source apportionment for chemical species that depend upon nonlinear reactions, such as secondary PM species and ozone. Nonetheless, reasonable source apportionment schemes can be developed and are useful tools for achieving the objectives listed in the introduction.

2) Sensitivity coefficients are not source apportionments for chemical species that depend upon nonlinear reactions, such as secondary PM species and ozone. Sensitivity coefficients are most applicable for predicting the model response to an input change (e.g., control strategy) and are very useful for this purpose (within the range of linear model response), but sensitivity coefficients should be used with care for source apportionment or culpability assessment. Likewise, source apportionments should be used with care for predicting model response to input changes.

7.3 PSAT METHODOLOGY

PSAT is designed to source apportion the following PM species modeled in CAMx:

- Sulfate (SO4)
- Particulate nitrate (NO3)
- Ammonium (NH4)
- Particulate mercury (Hg(p))
- Secondary organic aerosol (SOA)
- Six categories of primary PM
    - Elemental carbon (EC)

- Primary organic aerosol (POA)
- Crustal fine
- Other fine
- Crustal coarse
- Other coarse

The PSAT "reactive tracers" that are added for each source category/region (*i*) are described below. In general, a single tracer can track primary PM species whereas secondary PM species require several tracers to track the relationship between gaseous precursors and the resulting PM. Particulate nitrate and secondary organics are the most complex species to apportion because the emitted precursor gases (NO, VOCs) are several steps removed from the resulting PM species (NO3, SOA). The PSAT tracers for each type of PM are listed below. There is a PSAT convention that tracer names for particulate species begin with the letter "P."

Sulfur

$SO2_i$	Primary SO_2 emissions
$PS4_i$	Particulate sulfate ion from primary emissions plus secondarily formed sulfate

Nitrogen

RGN_i	Reactive gaseous nitrogen including primary NOx (NO + NO_2) emissions plus nitrate radical (NO_3), nitrous acid (HONO) and dinitrogen pentoxide (N_2O_5).
TPN_i	Gaseous peroxyl acetyl nitrate (PAN) plus peroxy nitric acid (PNA)
NTR_i	Organic nitrates (RNO_3)
$HN3_i$	Gaseous nitric acid (HNO_3)
$PN3_i$	Particulate nitrate ion from primary emissions plus secondarily formed nitrate
$NH3_i$	Gaseous ammonia (NH_3)
$PN4_i$	Particulate ammonium (NH_4)

Secondary Organic

ALK_i	Alkane/Paraffin secondary organic aerosol precursors
ARO_i	Aromatic (toluene and xylene) secondary organic aerosol precursors
CRE_i	Cresol secondary organic aerosol precursors
TRP_i	Biogenic olefin (terpene) secondary organic aerosol precursors
$CG1_i$	Condensable gases from toluene and xylene reactions (low volatility)
$CG2_i$	Condensable gases from toluene and xylene reactions (high volatility)
$CG3_i$	Condensable gases from alkane reactions
$CG4_i$	Condensable gases from terpene reactions
$CG5_i$	Condensable gases from cresol reactions
$PO1_i$	Particulate organic aerosol associated with CG1
$PO2_i$	Particulate organic aerosol associated with CG2
$PO3_i$	Particulate organic aerosol associated with CG3
$PO4_i$	Particulate organic aerosol associated with CG4
$PO5_i$	Particulate organic aerosol associated with CG5

Mercury

- HG0$_i$ Elemental Mercury vapor
- HG2$_i$ Reactive gaseous Mercury vapor
- PHG$_i$ Particulate Mercury

Primary Particulate

- PEC$_i$ Primary Elemental Carbon
- POA$_i$ Primary Organic Aerosol
- PFC$_i$ Fine Crustal PM
- PFN$_i$ Other Fine Particulate
- PCC$_i$ Coarse Crustal PM
- PCS$_i$ Other Coarse Particulate

PSAT includes a total of 32 tracers for each source group (i) if source apportionment is applied to all types of PM. Since source apportionment may not always be needed for all species, the PSAT implementation is flexible and allows source apportionment for any or all of the chemical classes in each CAMx simulation (i.e. the SO4, NO3, NH4, SOA, Hg and primary PM classes listed above). For example, source apportionment for sulfate/nitrate/ammonium requires just 9 tracers per source group.

One fundamental assumption in PSAT is that PM should be apportioned to the primary precursor for each type of PM. For example, SO4 is apportioned to SOx emissions, NO3 is apportioned to NOx emissions, NH4 is apportioned to NH3 emissions, etc. As a source apportionment method, PSAT must account for all modeled sources of a PM species. Consider two model species A and B that are apportioned by reactive tracers a_i and b_i, respectively. Reactive tracers must be included for all sources of A and B including emissions, initial conditions and boundary conditions so that complete source apportionment is obtained, i.e., $A = \Sigma a_i$ and $B = \Sigma b_i$.

In PSAT, the general approach to modeling change over a model time step Δt is illustrated for a chemical reaction $A \rightarrow B$. The general equation for species destruction is:

$$a_i(t+\Delta t) = a_i(t) + \Delta A \frac{a_i}{\sum a_i}$$

Here, the relative apportionment of A is preserved as the total amount changes. This equation applies to chemical removal of A and also to physical removal of A by processes such as deposition or transport out of a specific grid cell.

The general equation for species production (e.g, chemical production by the chemical reaction $A \rightarrow B$) is:

$$b_i(t+\Delta t) = b_i(t) + \Delta B \frac{a_i}{\sum a_i}$$

Here, production of B inherits the apportionment of the precursor A. The same equation applies for "production" of B in a specific grid cell due to emissions or transport. For the

case where *B* increases due to emissions, a_i is the apportionment of the emissions inventory. For the case where *B* increases due to transport, a_i is the apportionment of the upwind grid cell.

In some cases, source category specific weighting factors (w_i) must be added to the equation for species destruction:

$$a_i(t+\Delta t) = a_i(t) + \Delta A \frac{w_i a_i}{\sum w_i a_i}$$

An example is chemical decay of the aromatic VOC tracers (ARO), which must be weighted by the average OH rate constant of each ARO_i. ARO tracers for different source groups have different average VOC reactivities because the relative amounts of toluenes and xylenes differ between source categories.

In some cases, source category specific weighting factors (w_i) must be added to the equation for species production:

$$b_i(t+\Delta t) = b_i(t) + \Delta B \frac{w_i a_i}{\sum w_i a_i}$$

An example is chemical production of condensable gases (CG1 or CG2) from aromatic VOC tracers, which must be weighted by aerosol yield weighting factors. The aerosol yield weighting factors depend upon the relative amounts of toluenes and xylenes in each source group.

Several aerosol reactions are treated as equilibria, $A \leftrightarrow B$. If *A* and *B* reach equilibrium at each time step, it follows that their source apportionments also reach equilibrium:

$$a_i(t+\Delta t) = [a_i(t)+b_i(t)]\left(\frac{A}{A+B}\right)$$

$$b_i(t+\Delta t) = [a_i(t)+b_i(t)]\left(\frac{B}{A+B}\right)$$

Examples are the equilibrium between gas phase nitric acid and aerosol nitrate, gas phase ammonium and aerosol ammonium, and condensable organic gases (CG) and secondary organic aerosols (SOA).

7.4 TESTING PSAT

Initial PSAT testing was conducted for primary PM species (e.g., fine crustal material) because these species are the most straightforward to implement and test (i.e., no chemistry). The results for primary PM species are not shown here but the tests were successful in that the sum of PSAT tracers over all source groups remained identical to the total model concentration ($A = \Sigma a_i$) for all grid cells and hours. The primary PM tests confirmed the proper implementation of PSAT for all CAMx algorithms except chemistry.

The next stage of PSAT testing included the chemistry algorithms and results are shown here for two different types of testing for sulfate and nitrate. Sulfate was tested by comparing PSAT to zero out results in full 3-D CAMx simulations. As discussed above, zero out results are not expected to agree perfectly with PSAT because zero out does not give true source apportionment in non-linear systems. However, non-linearity in sulfate formation chemistry is expected to be less important than for other secondary PM species making sulfate the best candidate for zero out testing.

The most complex PSAT chemistry algorithm is for nitrate. Zero out tests were not used for nitrate because the relationship between NO emissions and nitric acid may be highly non-linear. Therefore, 1-D (box model) tests were used to evaluate PSAT results for nitrate by comparing against the method used by Kleeman and Cass (2001) to track nitrate apportionment in the Source-Oriented External Mixture (SOEM) method, discussed above.

PSAT Sulfate Testing

The PSAT performance for sulfate was tested using a CAMx database developed by the Midwest RPO (MPRO) for PM and visibility modeling of the Eastern US. The modeling was conducted from June 18 to July 21, 2001 and used a 36-km modeling grid with meteorology developed using the mesoscale model version 5 (MM5). The modeling domain was sub-divided to geographic areas according to regional planning organizations (RPOs) responsible for developing regional visibility and PM control strategies in the U.S. The sub division of the modeling domain to RPOs is shown in Figure 7-1 and the RPOs are labeled by their respective acronyms (MRPO, MANE-VU, VISTAS, CERAP and WRAP). The state of Illinois (IL) was split out from the Midwest RPO (MPRO) to test the ability of PSAT to apportion the contribution from a single state. Four hypothetical point sources were added near the middle of the MRPO, MANE-VU, VISTAS and CENRAP areas (shown by the + symbols in Figure 1) to test the ability of PSAT to track contributions from singe sources. The hypothetical point sources were chosen to be generally representative of a large coal-fired electricity generating unit but do not represent actual sources at these locations. In total, sulfate was apportioned to 11 source regions, including a remainder area for Canada, Mexico and over water, plus initial and boundary conditions.

The sulfate impacts from the hypothetical MRPO point source are compared in Figure 7-2 at a single hour (hour 15) on 28 June 2001. The spatial distribution of sulfate impacts is very similar in the PSAT and zero out results as shown by the edge of the plume impacts (0.1 $\mu g/m^3$ level). There are differences in the areas of larger impacts (e.g. the 1 and 2 $\mu g/m^3$ levels) and these are due to the effects of non-linear chemistry in the zero out test. As discussed above, sensitivity methods such as zero out do not provide accurate source apportionments for non-linear processes. Sulfate formation can be limited by the availability of oxidants, especially hydrogen peroxide in aqueous-phase chemistry, which will tend to depress the maximum impact levels in zero out runs as well as shift impacts further downwind (to where oxidant availability is no longer limiting). The oxidant limiting effect on zero out sulfate impacts is most easily seen from the 2 $\mu g/m^3$ level extending further downwind over Lake Michigan in the zero out result than the PSAT source apportionment result.

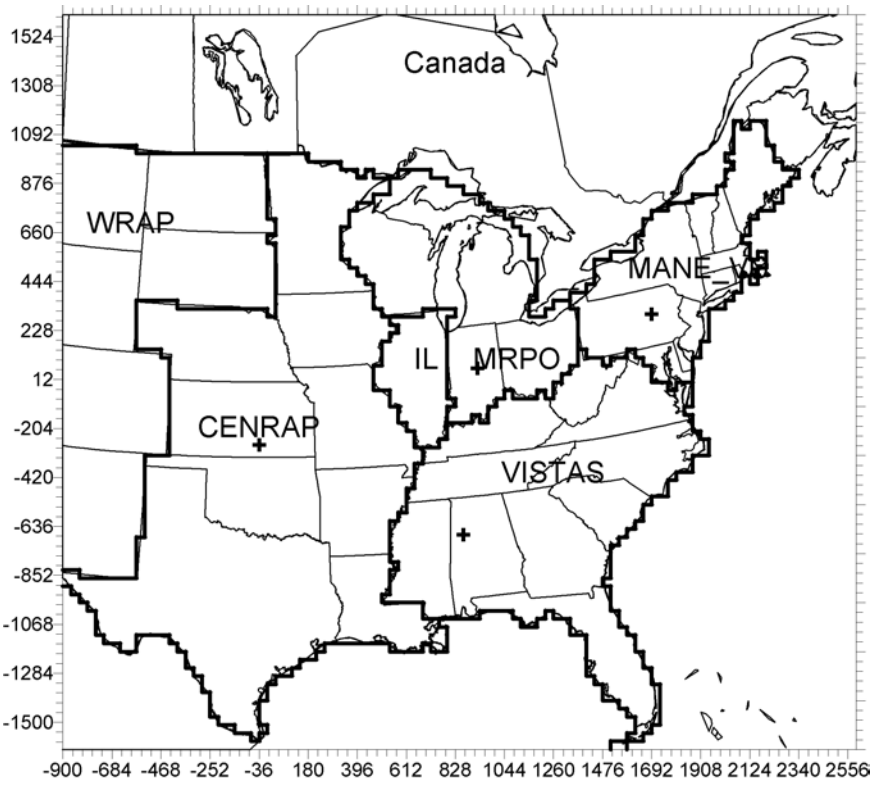

Figure 7-1. The CAMx modeling domain for PSAT testing showing sub-division to geographic areas and locations of four hypothetical point sources (+ symbols).

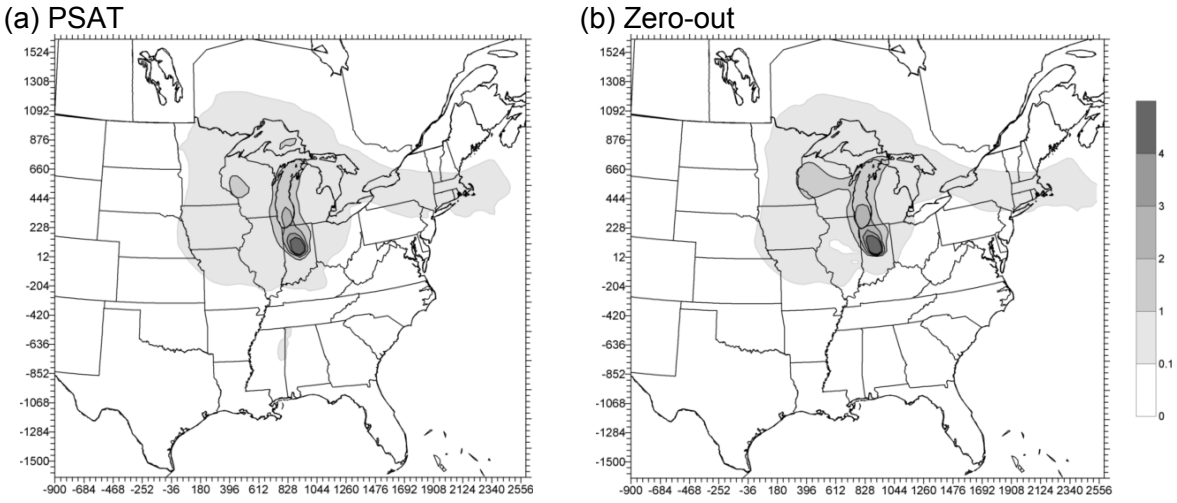

Figure 7-2. Comparison of sulfate contributions (μg/m^3) from the hypothetical MRPO point source on 28 June 2001 at hour 15: (a) PSAT result; (b) Zero-out result.

The episode average sulfate impacts from the hypothetical MRPO point source are compared in Figure 7-3 for the entire 28 June to July 21, 2001 modeling period. The spatial distribution of sulfate impacts is very similar in the PSAT and zero out results. The maximum impact occurs very close to the source and is higher in the PSAT result (2.2 $\mu g/m^3$) than the zero out result (1.8 $\mu g/m^3$) due to the effect of oxidant limitation on sulfate impacts determined by the zero out method.

The PSAT sulfate tests provided a comparison of the efficiency of the PSAT method compared to zero out modeling. Zero out modeling requires a new model run for each source contribution determined, so the incremental time for each "apportionment" is the same as for the model base case. In contrast, the marginal cost for each PSAT source apportionment was about 2% of the time required for the base case.

PSAT Nitrate Testing

The PSAT nitrate algorithms were tested using CAMx for a 1-D (box model) problem in order to focus upon the ability of the PSAT chemical algorithms to track nitrate apportionment. The box model problem was for summer conditions and PSAT was used to apportion nitrate between 20 ppb of initial NOx and 100 ppb of NOx emission injected continuously through the 24 hour run. The PSAT results were compared to the SOEM algorithm of Kleeman and Cass (2001) where the reactive nitrogen (NOy) reactions in the chemical mechanism are duplicated to provide two different types of NOy (think of them as "red" NOy and "blue" NOy). There was no ammonia in the box model so that nitric acid remained in the gas phase rather than forming PM nitrate.

The PSAT apportionment of NOy to initial conditions (ICs) and emissions during the 24 hour box model simulation is shown in Figure 7-4. The total NOy apportioned to ICs remains constant at 20 ppb throughout the simulation but the apportionment changes over time from NOx (RGN-IC) at the start to PAN (TPN-IC), organic nitrates (NTR-IC) and nitric acid (HN3-IC). The NOy apportioned to emissions increased linearly throughout the simulation and the apportionment also evolved as the NOx emissions (RGN-E) reacted. At the start of the simulation RGN (NOx) is dominated by ICs whereas late in the day (hour 18) RGN is dominated by emissions. The source apportionments shown in Figure 7-4 are reasonable and show necessary attributes (such as conserving the total 20 ppb of ICs).

The SOEM apportionment of NOy to ICs and emissions during the 24-hour box model simulation is shown in Figure 7-5. The time evolution of the source apportionments for the ICs and emissions is very similar for SOEM (Figure 7-5) and PSAT (Figure 7-4). It is not clear that either method is more "correct," or indeed that a correct source apportionment result exists for this test, but the consistency between the PSAT and SOME results is encouraging.

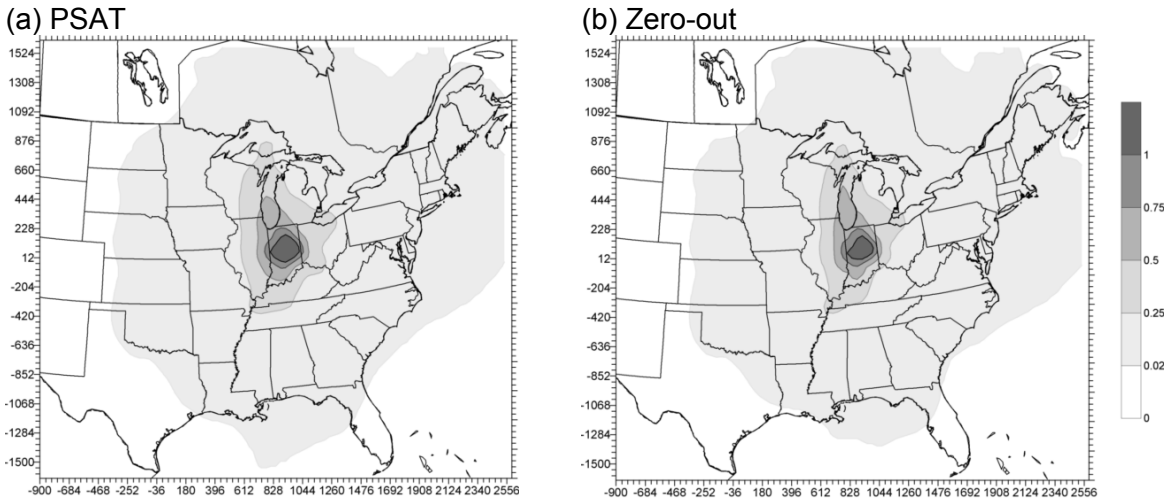

Figure 7-3. Comparison of episode average (June 18 to July 21, 2001) sulfate contributions (μg/m^3) from the hypothetical MRPO point source: (a) PSAT result; (b) Zero-out result.

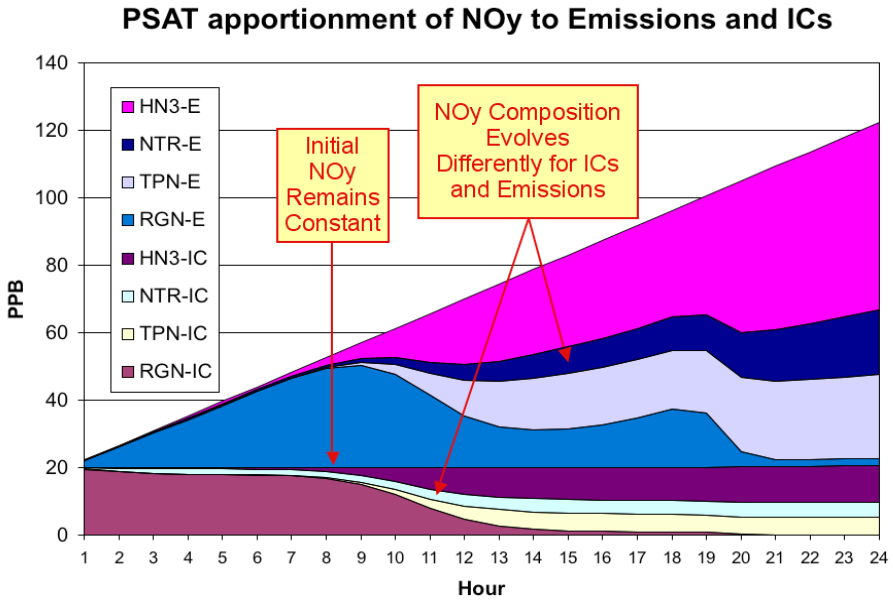

Figure 7-4. PSAT apportionment of reactive nitrogen (NOy) to initial conditions and emissions during a 24-hour box model simulation.

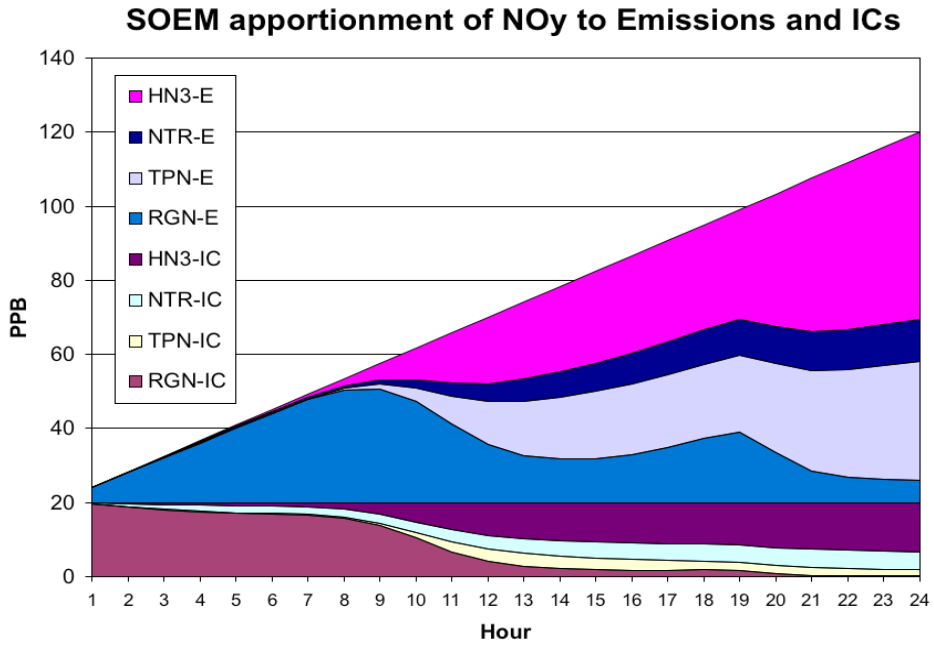

Figure 7-5. Source-Oriented External Mixture (SOEM) apportionment of reactive nitrogen (NOy) to initial conditions and emissions during a 24-hour box model simulation.

7.5 RUNNING CAMx WITH PSAT

CAMx Control File

PSAT is invoked similarly to the OSAT Probing Tool within the CAMx control file. In the `&CAMx_Control` namelist module, the variable `Probing_Tool` must be set to "PSAT". An additional namelist module called `&SA_Control` must then be provided in the control file to configure the PSAT portion of the model – note that this is identically the same module as used for OSAT. The PSAT/OSAT namelist module is described in Section 6; the additional variables needed for PSAT are described below. The order of the variables follow the template available with the source code. An example of the PSAT portion of the CAMx run control file is shown in Figure 7-6.

All other capabilities and I/O requirements for PSAT mirror those of OSAT. The only component that is not available for PSAT is the "Ozone Tool" Excel macro postprocessor. See Section 6 for a description of how to configure, set up, and run the Source Apportionment Probing Tools.

Description of PSAT Control in the CAMx Run Control File

`&SA_Control`	Label for the Probing Tool namelist module that configures the PSAT and OSAT options; it must begin in column 2
`&`	Flag ending a namelist module; it must be in column 2
`SA_Summary_Output`	Logical flag used to limit the species written to the tracer concentration file to a subset of the PSAT treated species. If set to true, the output will be restricted to the following species: O3N, O3V, PS4, PN3, PN4, PO1, PO2, PO3, PO4, PO5, PEC, POC, FCR, FPR, CCR, CPR, HG0, HG2, PHG
`PSAT_Treat_SULFATE_Class`	Logical flag to turn on the sulfate class of tracer species.
`PSAT_Treat_NITRATE_Class`	Logical flag to turn on the nitrate class of tracer species.
`PSAT_Treat_SOA_Class`	Logical flag to turn on the SOA class of tracer species.
`PSAT_Treat_PRIMARY_Class`	Logical flag to turn on the primary PM class of tracer species.
`PSAT_Treat_MERCURY_Class`	Logical flag to turn on the mercury class of tracer species.
`PSAT_Treat_OZONE_Class`	Logical flag to turn on the ozone class of tracer species.

```
&SA_Control

 SA_File_Root              = '$TRACOUT/CAMx.OSAT.9507$today',
 SA_Summary_Output         = .true.,

 SA_Master_Sfc_Output         = .true.,
 SA_Nested_Sfc_Output         = .true.,
 SA_Stratify_Boundary         = .false.,
 SA_Number_of_Source_Regions  = 19,
 SA_Number_of_Source_Groups   = 3,
 Use_Leftover_Group           = .false.,
 Number_of_Timing_Releases    = 0,
 PSAT_Treat_SULFATE_Class     = .true.,
 PSAT_Treat_NITRATE_Class     = .true.,

 SA_Receptor_Definitions  = '$TRACIN/receptor.cities ',
 SA_Source_Area_Map(1)    = '$TRACIN/APCA.source.area.map',
 SA_Source_Area_Map(2)    = ' ',

 SA_Master_Restart        = '$TRACOUT/CAMx.OSAT.9507$yesterday.sa.inst.2',
 SA_Nested_Restart        = '$TRACOUT/CAMx.OSAT.9507$yesterday.sa.finst.2',

 SA_Points_Group(1)       = ' ',
 SA_Points_Group(2)       = '$PTSRCE/utilpt.ng.$todate-07.ag.07cem1A-run11',
 SA_Points_Group(3)       = '$PTSRCE/remain.ng.$todate-07.ag.07cem1A-run11',

 SA_Emiss_Group_Grid(1,1) = '$TRACEMS/bio2.cc.$todate-95',
 SA_Emiss_Group_Grid(1,2) = '$TRACEMS/bio2.ff.$todate-95.ne',
 SA_Emiss_Group_Grid(2,1) = '$TRACEMS/util.cc.$todate-07.ag.07cem1A-run11',
 SA_Emiss_Group_Grid(2,2) = '$TRACEMS/util.ff.$todate-07.ag.07cem1A-run11',
 SA_Emiss_Group_Grid(3,1) = '$TRACEMS/remain.cc.$todate-07.ag.07cem1A-run11',
 SA_Emiss_Group_Grid(3,2) = '$TRACEMS/remain.ff.$todate-07.ag.07cem1A-run11',

 &
```

Figure 7-6. This figure follows from Figure 6-8(d): it is a continuation day of a 2-grid run with three emission groups, and all three emission groups are defined explicitly by supplying extra emission files (AREA group 1, AREA group 2, POINT group 2, AREA group 3, and POINT group 3). Therefore, the "Use_Leftover_Group" flag is set to FALSE. The POINT group 1 filename is blank because group 1 is a category with no point source emissions (e.g., biogenics). PSAT will trace PM sulfate and nitrate species only.

8. DECOUPLED DIRECT METHOD FOR SENSITIVITY ANALYSIS

Photochemical modelers have traditionally used sensitivity analysis both for model performance evaluation and emission control strategy design. The simplest approach to sensitivity analysis, often referred to as the "brute-force" approach, involves changing a model input parameter, rerunning the model, and then evaluating the change in model output. The change in output is quantified from the difference between the sensitivity case and base case. This approach requires a separate simulation for each parameter investigated. For example, a model performance evaluation may use sensitivity simulations to evaluate the impact of changing the initial conditions (ICs), boundary conditions (BCs), biogenic emissions, anthropogenic emissions, etc. Sensitivity analysis is also used to aid control strategy design. For example, across-the-board VOC and NO_x emission reductions are used to determine whether VOC and/or NO_x reduction strategies are the most effective path to reduce ozone.

The advantages of the "brute force" method for sensitivity analysis are:

- Applicable to any model input parameter;
- Results are conceptually easy to explain and interpret.

The limitations of the "brute force" method are:

- Computationally inefficient;
- Sensitivity depends upon the magnitude of the perturbation if the model response is non-linear;
- Sensitivity derived from small perturbations may contain significant levels of uncertainty (numerical noise).

The last two points bear further explanation. If the model response to an input parameter depends upon non-linear components within the model (e.g., chemistry), then the relative magnitude or even sign of the output response may change for perturbations of different sizes. An example is the response of ozone to NO_x reductions in a VOC-limited environment: smaller reductions in NO_x emissions increase ozone levels whereas larger NO_x reductions decrease ozone.

This situation can be illustrated mathematically. We define a "sensitivity coefficient" (s) which represents the change in concentration (c) with respect to some input parameter (λ), evaluated relative to the base state ($\lambda=\lambda_0$),

$$s = \left.\frac{\partial c}{\partial \lambda}\right|_{\lambda_o}$$

In general, λ can be a vector (denoted as $\underline{\lambda}$), which contains multiple parameters related to processes in the model (e.g., rate constants) or inputs to the model (e.g., emissions). The response of concentration to a change in $\underline{\lambda}$ can be represented by a Taylor series of sensitivity coefficients:

$$c(\underline{x},t;\underline{\lambda}) = c(\underline{x},t;\underline{\lambda}_0) + \sum_{i=1}^{n} \left.\frac{\partial c}{\partial \lambda_i}\right|_{\underline{\lambda}_o} (\lambda_i - \lambda_{i0}) + \frac{1}{2}\sum_{i=1}^{n}\sum_{j=1}^{n} \left.\frac{\partial^2 c}{\partial \lambda_i \partial \lambda_j}\right|_{\underline{\lambda}_o} (\lambda_i - \lambda_{i0})(\lambda_j - \lambda_{j0}) + \ldots$$

where n is the number of $\underline{\lambda}$ vector elements, $\underline{x}$ is the spatial dimension vector, and t is time. In the example above, the non-linear response of ozone to large NO_x emission reductions indicates that higher-order sensitivity coefficients are significant relative to the first order sensitivity. As the magnitude of the input perturbation tends to zero, the output response will become dominated by the first-order sensitivity. Therefore, very small changes in the input parameter may be required to use the "brute force" method to estimate the first-order (local) sensitivity. The practical limitation to this approach is that since the change in output must be determined from the difference between two simulations, small levels of numerical uncertainty (noise) in two very similar outputs will contaminate the sensitivity calculation.

An alternative methodology for evaluating model sensitivity was developed by Dunker (1980 and 1981) called the decoupled direct method (DDM). The DDM can be used to calculate the same type of sensitivity coefficient as is available from the "brute force" method. The difference is that with DDM, sensitivity coefficients are calculated explicitly by specialized algorithms implemented in the host model. Thus, the DDM offers several advantages over the brute force method:

- Improved computational efficiency;
- Improved accuracy since sensitivities need not be contaminated by numerical noise;
- Multiple sensitivities can be calculated simultaneously

The degree to which these advantages are realized depends upon how the method is implemented, i.e., the algorithms employed and their coding. Fortunately, the performance of the DDM can be evaluated quantitatively by careful comparison of DDM sensitivities against "brute-force" sensitivities.

The first implementation of the DDM into a three-dimensional air quality model used version II of the Urban Airshed Model (Dunker, 1981). This project demonstrated the accuracy and capabilities of the method, but application was restricted by the computing power available to the air quality modeling community at that time. Recently, Yang et al. (1997) described the implementation of the DDM into the California/Carnegie Institute of Technology airshed model, an application termed DDM-3D. The implementation of the DDM into CAMx was performed in a joint project between Dr. Alan Dunker and ENVIRON with sponsorship from the Coordinating Research Council (http://www.crcao.com). A rigorous analysis of the CAMx implementation of the DDM was performed as part of this project, and excellent agreement was demonstrated (manuscript in preparation).

8.1 IMPLEMENTATION

The implementation of DDM into CAMx has focused on the evaluation of first order sensitivity coefficients that relate predicted concentrations to pollutant sources (i.e., emissions, ICs and BCs). The DDM is theoretically applicable to the calculation of higher order sensitivity coefficients as well, but these are much more numerous than the first order coefficients and generally will be less useful. The DDM has also been applied in the past to the calculation of sensitivities to other model input parameters (e.g., chemical rate constants, meteorological parameters), but this was not attempted for the CAMx implementation because these sensitivities generally are less useful and because resources were limited. The CAMx implementation could be extended to other sensitivity parameters in the future.

The CAMx DDM permits the evaluation of sensitivity coefficients with respect to parameters related to emissions, BCs or ICs. The sensitivity to be evaluated may bear a simple relationship to the regular model input, such as scaling the ozone boundary concentration by a factor ($BC_{new} = \lambda \times BC_0$), or additively increasing the ozone boundary concentration by a constant amount everywhere ($BC_{new} = \lambda + BC_0$). To allow complete flexibility, the perturbations are specified by providing additional IC, BC, and/or emission input files with the same format as the regular model input files.

In mathematical terms, a regular model input file, for example the BC input file, represents some set of functions of space and time $f_i(\underline{x},t)$, where each chemical species can be defined by a unique function. An additional input file provided for the DDM represents another set of functions of space, time, and chemical species $g_i(\underline{x},t)$ that can be different from the regular input file. The scalar parameter λ_i is then defined by

$$F_i(\underline{x},t) \quad = \quad f_i(\underline{x},t) + \lambda_i \times g_i(\underline{x},t).$$

Here, $\lambda_i \times g_i(\underline{x},t)$ is the perturbation, and the user desires information on how the model would respond if the input $f_i(\underline{x},t)$ is replaced by the input $F_i(\underline{x},t)$. The DDM calculates the sensitivity $s_i(\underline{x},t)$ with respect to the scalar parameter λ_i. The Taylor series to first order then gives the estimate:

$$c_l(\underline{x},t;\lambda_i) \quad = \quad c_l(\underline{x},t;\lambda_i=0) + \lambda_i \times s_i(\underline{x},t)$$

where $c_l(\underline{x};t;\lambda_i)$ is the estimated model result for species l when $F_i(\underline{x},t)$ is used as input, and $c_l(\underline{x},t;\lambda_i=0)$ is the base case model result when $f_i(\underline{x},t)$ is used as input.

For example, to calculate the sensitivity of the predicted ozone concentration to scaling boundary ozone by a factor, CAMx would be provided with a DDM BC file that has the same ozone values as the regular model BC file. The sensitivity coefficient fields output by CAMx could then be used to estimate the resulting ozone concentration if the ozone BCs were increased by 20%, as follows:

$$c_{\lambda=0.2} \quad = \quad c_{\lambda=0} + 0.2 \times s$$

(For simplicity hereafter, the dependence on space, time, and chemical species will be omitted).

To calculate the sensitivity of the predicted ozone concentration to increasing boundary ozone by 10 ppb, CAMx would be provided with a DDM BC file that has a constant ozone value of 10 ppb. The sensitivity coefficient fields could be used to estimate the ozone concentration if the ozone BCs were increased by 10 ppb as follows:

$$c_{\lambda=1.0} = c_{\lambda=0} + 1.0 \times s$$

An alternative approach here would be to provide CAMx with a DDM BC file that has a constant ozone value of 1 ppb. This perturbation would be associated with a new parameter λ' and a new sensitivity coefficient s'. To estimate the ozone concentration if the ozone BC were increased by 10 ppb, one would use

$$c_{\lambda'=1.0} = c_{\lambda'=0} + 10.0 \times s'$$

This would give exactly the same estimate as the preceding approach in which CAMx is supplied with a DDM BC file that has an ozone value of 10 ppb everywhere because the two sensitivities are related by $s' = s \times 0.1$ (from the first to second approach, there has been only a change of the scalar variable from λ to λ').

These are examples of relatively simple sensitivities. A more complex example would be to calculate the sensitivity to morning (6-9 AM) NO_x emissions in specific group of grid cells. In this case you would provide CAMx with a DDM emissions file where all values are zero except for the NO_x emissions in the selected grid cells between 6 AM and 9 AM, which would have the same value as the regular emissions file. In this case the sensitivity coefficient for ozone might be interpreted as the increase (or decrease) in ozone concentration due to the selected emissions (however, caution is warranted because sensitivity coefficients are not directly equivalent to a source apportionment). More accurately, the sensitivity coefficient could be used to predict the concentration after a scalar change (λ) in the morning NOx emissions using the equation:

$$c_{\lambda} = c_{\lambda=0} + \lambda \times s$$

Any type of sensitivity perturbation can be described via an input file. However, the CAMx user interface also provides easy ways to define some sensitivities that are likely to be used frequently. For example, in the first example above the DDM BC file was described as having the "same ozone values as the regular model BC file." To make such a file you could copy the BC file and then remove (or zero out) all species but ozone. To avoid the effort of preparing an input file that is trivially different from the regular model file, the user interface allows you to select specific species from an input file to track - in this case ozone. It is possible to separately track the sensitivity to more than one species from the same file (e.g. ozone, and NO). It is also possible to track the combined sensitivity to a group of species, such as NO_x, VOC or ALL. The user interface also provides a simple way to track sensitivities to emissions from specific grid cells or groups of cells (sub-regions).

Tracking Sensitivity Coefficients Within CAMx

The conceptual approach in tracking DDM sensitivity coefficients is directly parallel to the way in which CAMx calculates three-dimensional concentration fields. The concentration fields are calculated by a series of code modules that operate sequentially to represent the

impact of different physical processes (emissions, advection, diffusion, chemistry, deposition, etc.) on the gridded concentrations. Sensitivity coefficients are calculated by a parallel set of modules which operate in step with the CAMx modules to calculate gridded sensitivity coefficients. For some processes (e.g., chemistry and horizontal advection), the sensitivity coefficient modules make use of information saved from the corresponding CAMx modules. The need to employ this approach arises in cases where the CAMx algorithm depends non-linearly upon species concentrations. In other cases, the sensitivity algorithm turns out to be identical to the CAMx algorithm (e.g., horizontal diffusion) and both concentrations and sensitivity coefficients can be processed by the single module. Finally, there are cases where the sensitivity algorithm turns out to be identical to the CAMx algorithm, but a specialized module has been written for the sensitivity coefficients to improve the computational efficiency (e.g., vertical advection).

Priorities in the DDM coding implementation were:

- Ensuring accuracy by using consistent numerical methods for the concentrations and sensitivities;
- Ensuring accuracy by calculating the concentrations and sensitivities using the same time steps;
- Optimizing the efficiency of the sensitivity coefficient calculations without compromising accuracy;
- Providing a flexible User Interface that allows calculation of sensitivities to all sources and precursors;
- Ensuring that the DDM algorithms have minimal impact on computer resource requirements (memory and CPU time) when the DDM is not being used.

Further details of the implementation of the DDM in CAMx will be published in the near future.

Horizontal Advection and Chemistry

Specialized modules were developed to calculate the effects of chemistry and horizontal advection upon DDM sensitivity coefficients. These DDM modules are exactly matched to the numerical methods employed in the corresponding CAMx modules. CAMx has three separate options for the horizontal advection solver (Smolarkiewicz, Bott and PPM) and two options for the gas phase chemistry solver (the CMC fast solver and an IEH solver). With the resources available, it was only possible to develop DDM implementations for one advection solver (Bott) and one chemistry solver (CMC). The DDM option in CAMx cannot be used with other solver options at the present time.

The implementation of DDM algorithms for the fast chemistry solver was integrated with the chemical mechanism compiler (CMC). Therefore, the DDM option is available for both the CB4 and SAPRC chemical mechanisms, and will be available for additional mechanisms implemented in CAMx in the future.

Plume-in-Grid and Aerosol Processes

Resource constraints did not permit implementation of DDM algorithms for the Plume-in-Grid (PiG) and aerosol chemistry options currently available in CAMx.

Source Code

The coding of DDM algorithms involved the creation of several new subroutines for CAMx. These subroutines are all grouped in a separate directory (called DDM) under the main CAMx source code directory. It was necessary to add additional code for DDM in several existing CAMx subroutines, and the new code is clearly marked by comments.

8.2 RUNNING CAMx WITH DDM

This section describes how to specify the sensitivity coefficients to be calculated and the additional input files that must be supplied. Since CAMx already contained a methodology for probing source-receptor relationships called OSAT (ozone source apportionment technology, see Section 6), the DDM user interface was designed along similar lines to the existing OSAT user interface. This makes it easier to learn how to use both options and promotes consistency in analyses performed using OSAT and DDM.

Inputs in the CAMx Control File

DDM is invoked similarly to the other Probing Tools within the CAMx control file. In the `&CAMx_Control` namelist module, the variable `Probing_Tool` must be set to "DDM". An additional namelist module called `&DDM_Control` must then be provided in the control file to configure the DDM portion of the model. The additional namelist module is described below. The order of the variables follow the template available with the source code. An example of the DDM portion of the CAMx run control file is shown in Figure 8-1.

Description of DDM Control in the CAMx Run Control File

`&DDM_Control`	Label for the Probing Tool namelist module that configures the DDM option; it must begin in column 2
`&`	Flag ending a namelist; it must be in column 2
`DDM_File_Root`	Character root output path/filename
`DDM_Master_Sfc_Output`	Logical flag for master grid surface output (TRUE=DDM file will be output for all sensitivities, FALSE=DDM file will not be output)

DDM_Nested_Sfc_Output	Logical flag for nested grid surface output (TRUE=DDM file will be output for all sensitivities, FALSE=DDM file will not be output)
DDM_Stratify_Boundary	Logical flag to stratify boundary types (TRUE=separate sensitivity types will be used for the N, S, E, W, and Top boundaries, FALSE=a single sensitivity type will be used for all 5 boundaries)
DDM_Number_of_Source_Regions	Integer number of source regions to be tracked. This must be the same as the number of source areas defined in the DDM_Source_Area_Map file. This value may be zero.
DDM_Number_of_Source_Groups	Integer number of emission groups to be tracked. This determines the number of emission files that must be supplied (additional details below). This value may be zero.
Number_of_IC_Species_Groups	Integer number of species or species groups in the initial conditions to be tracked. This number may be between zero and the number of species being simulated plus three (allowing for the three species groups VOC, NOX, ALL).
IC_Species_Groups	Character array (by IC group) names of the species or species groups in the initial conditions to be tracked. Allowed names are any species being simulated by the mechanism in use (e.g., O3, PAR, NO, etc.) plus the species groups NOX, VOC and ALL. It is permissible to specify both a species and a group containing that species, e.g., both NO and NOX. Each name may have up to 10 characters. Note that if you select a species that is not present on the IC file provided, the initial sensitivities for that species will be set to zero. This variable may be left blank if the number of initial condition species groups is zero.
Number_of_BC_Species_Groups	Integer number of species or species groups in the boundary conditions to be tracked. This number may be between zero and the number of species being simulated plus three (allowing for the three species groups VOC, NOX, ALL).
BC_species_Groups	Character array (by BC group) names of the species or species groups in the boundary conditions to be tracked. See description for IC_Species_Group above.
Number_of_EM_Species_Groups	Integer number of species or species groups in the emissions to be tracked. This number may be between zero and the number of species being simulated plus three (allowing for the three species groups VOC, NOX, ALL).
Emis_Species_Groups	Character array (by emissions group) names of the species or species groups in the emissions to be tracked. See description for IC_Species_Group above.

`DDM_Receptor_Definitions`	Character input DDM receptor definition path/filename
`DDM_Source_Area_Map`	Character array (by CAMx grid) input DDM source area definition path/filename (required for master grid, optional for nested grids). Source regions are defined using a map in the same format as an OSAT source area map (Section 6); however, DDM does not require that all parts of the modeling domain be tracked, therefore it is permissible to define an area numbered zero in the source area map (emissions from those areas will not be tracked). The non-zero source region numbers must be between 1 and the number of regions.
`DDM_Initial_Conditions`	The name of the sensitivity initial condition file. Leave the file name blank for restart days or if sensitivity to initial conditions is not being calculated.
`DDM_Boundary_Conditions`	The name of the sensitivity lateral boundary condition file. Leave the file name blank if sensitivity to boundary conditions is not being calculated.
`DDM_Top_Concentrations`	The name of the sensitivity top boundary condition file. Leave the file name blank if sensitivity to boundary conditions is not being calculated.
`DDM_Master_Restart`	Character input master grid DDM restart path/filename (ignored if `Restart=FALSE`)
`DDM_Nested_Restart`	Character input nested grid DDM restart path/filename (ignored if `Restart=FALSE` or `Number_of_Grids=1`)
`DDM_Points_Group`	Character array (by source group) input DDM elevated point source emissions path/filename (optional, ignored if `Point_Emissions=FALSE`)
`DDM_Emiss_Group_Grid`	Character array (by source group, by CAMx grid) input DDM gridded emissions path/filename (optional, ignored if `Gridded_Emissions=FALSE`)

```
&DDM_Control

 DDM_File_Root                 = '$DDM_OUT/CAMx.08jul95.runA',
 DDM_Master_Sfc_Output         = .true.,
 DDM_Nested_Sfc_Output         = .true.,
 DDM_Stratify_Boundary         = .false.,
 DDM_Number_of_Source_Regions = 4,
 DDM_Number_of_Source_Groups  = 2,

 Number_of_IC_Species_Groups = 1,
 IC_Species_Groups(1)         = 'ALL',
 Number_of_BC_Species_Groups = 1,
 BC_species_Groups(1)         = 'ALL',
 Number_of_EM_Species_Groups = 3,
 Emis_Species_Groups(1)       = 'NOX',
 Emis_Species_Groups(2)       = 'VOC',
 Emis_Species_Groups(3)       = 'ALL',

 DDM_Receptor_Definitions  = '$DDM_IN/receptor.cities',
 DDM_Source_Area_Map(1)    = '$DDM_IN/source_map.DDM.4areas',
 DDM_Source_Area_Map(2)    = ' ',

 DDM_Initial_Conditions    = ' ',
 DDM_Boundary_Conditions   = '$DDM_IN/BC.08jul95',
 DDM_Top_Concentrations    = '$DDM_IN/TC.08jul95',
 DDM_Master_Restart        = '$DDM_OUT/CAMx.07jul95.runA.sa.inst.2',
 DDM_Nested_Restart        = '$DDM_OUT/CAMx.07jul95.runA.sa.finst.2',

 DDM_Points_Group(1)       = ' ',
 DDM_Points_Group(2)       = '$DDM_PT/ptsr.ng.08jul95',

 DDM_Emiss_Group_Grid(1,1) = '$DDM_EMIS/bio.cc.08jul95',
 DDM_Emiss_Group_Grid(1,2) = '$DDM_EMIS/bio.ff.08jul95',
 DDM_Emiss_Group_Grid(2,1) = '$DDM_EMIS/anthro.cc.08jul95',
 DDM_Emiss_Group_Grid(2,2) = '$DDM_EMIS/anthro.ff.08jul95',

 &
```

Figure 8-1. Example input of DDM options and filenames via the CAMx control file. In this case, CAMx is run with two grids, and DDM is configure to track emissions from four source regions and two source groups (biogenic and anthropogenic). Initial and boundary conditions are tracked as a single sensitivity called "ALL", while emissions are tracked with three sensitivities called "NOx", "VOC", and "ALL". No source region map is provided for the nested grid (the region assignments on the nest are defined by the master grid). Initial condition sensitivity is not being tracked (no file provided), and only the group 2 point sources are tracked (no biogenic point sources are available).

8.3 APPROACHES TO DEFINE IC, BC AND EMISSIONS SENSITIVITIES

The description above shows how to specify the IC, BC and emissions files for DDM sensitivity calculations. The formats for each of these files are identical to the CAMx input files of these types. In many cases, users may choose to specify exactly the same file for a CAMx input file and a DDM input file. (Be aware that some computer systems do not allow a file to be opened twice by the same application. A work around for this problem is to copy or link the file "filename" to another file of different name, such as "filename.copy").

The user can perform many different sensitivity calculations in a single run according to the content of the DDM input files. Take initial conditions (ICs) as an example. If the same IC file is specified for both CAMx and DDM, the output sensitivity fields represent the sensitivity of the predicted concentrations to the ICs. Therefore, simply scaling the output sensitivity coefficients fields provides the incremental concentrations resulting from scaling the ICs.

As another example, if a DDM emissions file is supplied to CAMx that has a constant VOC emission rate everywhere, the sensitivity will correspond to a uniform absolute increase in the VOC emission rate rather than a percentage increase as described above. Another possibility would be a DDM emission file with a different spatial pattern than the CAMx input file. The sensitivity coefficient would then correspond to changing both the geographic distribution and magnitude of emissions. Still another possibility would be a DDM file that has zero emissions for all hours except midnight to 5 AM on the third simulated day. The program would then calculate the sensitivity to early morning emissions on the third day. In this case, just the concentrations could be simulated for the first two days and the DDM calculation begun on the third day, because sensitivities on the first two days are identically zero.

In short, the DDM input file can be arbitrary – different from the CAMx input file in the overall magnitude of concentrations or emissions, different in the geographic and temporal distribution, and different in the relative proportions of the chemical species. However, the user must understand what perturbations are being considered in order to properly interpret the resulting output sensitivity coefficient fields. Also, the user should recognize that as the size of perturbations increase, the second- and higher-order terms eventually become important, usually when the emissions are altered by more than 20-30%.

8.4 DDM OUTPUT FILES

The output file types for a DDM simulation are described in Table 8-1. These files have the same format as corresponding concentration output files, described in Section 5.

Table 8-1. DDM output file suffix names.

File Name Suffix	DDM File Type
.sa.inst.1	Master grid binary instantaneous sensitivity file for last odd simulation hour (used for restart), 3-D, all sensitivities, μmol m^{-3} $parameter^{-1}$ units.
.sa.inst.2	Master grid binary instantaneous sensitivity file for last even simulation hour (used for restart), 3-D, all sensitivities, μmol m^{-3} $parameter^{-1}$ units.
.sa.finst.1	Nested grid binary instantaneous sensitivity file for last odd simulation hour (used for restart), 3-D, all sensitivities, μmol m^{-3} $parameter^{-1}$ units.
.sa.finst.2	Nested grid binary instantaneous sensitivity file for last even simulation hour (used for restart), 3-D, all sensitivities, μmol m^{-3} $parameter^{-1}$ units.
.sa.surf	Master grid binary average sensitivity file, 2-D, surface layer sensitivities only for affected species requested in the CAMx average file, ppm $parameter^{-1}$ units.
.sa.fsurf	Nested grid binary average sensitivity file, 2-D surface layer sensitivities only for affected species requested in the CAMx average file, ppm $parameter^{-1}$ units.
.sa.receptor	Hourly average sensitivities at user specific receptor locations. This file is in comma delimited ASCII format suitable for importing into a spreadsheet.

8.5 DDM SENSITIVITY COEFFICIENT NAMES

Each DDM sensitivity coefficient tracks the influence of a species from a specific source (the *influencing species*) on a predicted concentration (the *affected species*). The sensitivity coefficient names are constructed to show this relationship, as follows:

{Affected Species}{Pollutant Source}{Influencing Species}

This is a lot of information to encode in a name that must conform to the ten character limit imposed by the binary I/O file formats. Because of this, two naming systems are used in CAMx:

- Long Names - these names are easy to read, but since they are more than ten characters in length they cannot be used in sensitivity coefficient binary output files. If an alternate I/O format is implemented in the future it may be possible to use the long names on sensitivity output files.

- Short Names - these convey the same information as the long names but require more practice to learn. They are used in the sensitivity coefficient binary output files.

At the start of each CAMx run a concordance of Long and Short sensitivity coefficient names is written to the diagnostic output file (.diag file). An example concordance is shown in Figure 8-2, and a detailed explanation of the naming convention follows.

Affected Species	Influencing Species	Source Type	Group	Region	Long Name	Short Name
NO	NO	EM	1	2	NO__EM0102NO__	01E0102001
NO2	NO	EM	1	2	NO2_EM0102NO__	02E0102001
O3	NO	EM	1	2	O3__EM0102NO__	03E0102001
PAN	NO	EM	1	2	PAN_EM0102NO__	04E0102001
NXOY	NO	EM	1	2	NXOYEM0102NO__	05E0102001
OLE	NO	EM	1	2	OLE_EM0102NO__	06E0102001
PAR	NO	EM	1	2	PAR_EM0102NO__	07E0102001
TOL	NO	EM	1	2	TOL_EM0102NO__	08E0102001
XYL	NO	EM	1	2	XYL_EM0102NO__	09E0102001
FORM	NO	EM	1	2	FORMEM0102NO__	10E0102001
ALD2	NO	EM	1	2	ALD2EM0102NO__	11E0102001
ETH	NO	EM	1	2	ETH_EM0102NO__	12E0102001
CRES	NO	EM	1	2	CRESEM0102NO__	13E0102001
MGLY	NO	EM	1	2	MGLYEM0102NO__	14E0102001
OPEN	NO	EM	1	2	OPENEM0102NO__	15E0102001
PNA	NO	EM	1	2	PNA_EM0102NO__	16E0102001
CO	NO	EM	1	2	CO__EM0102NO__	17E0102001
HONO	NO	EM	1	2	HONOEM0102NO__	18E0102001
H2O2	NO	EM	1	2	H2O2EM0102NO__	19E0102001
HNO3	NO	EM	1	2	HNO3EM0102NO__	20E0102001
ISOP	NO	EM	1	2	ISOPEM0102NO__	21E0102001
MEOH	NO	EM	1	2	MEOHEM0102NO__	22E0102001
ETOH	NO	EM	1	2	ETOHEM0102NO__	23E0102001
ISPD	NO	EM	1	2	ISPDEM0102NO__	24E0102001
NTR	NO	EM	1	2	NTR_EM0102NO__	25E0102001

Figure 8-2. Example concordance of long and short sensitivity coefficient names from the CAMx diagnostic output file.

Initial Condition Sensitivity Names

Long Name **NNNNIC____MMMM**

where:

- **NNNN** Affected species name with trailing underscore to pad blanks
- **IC** Indicates the sensitivity coefficient is for initial conditions
- ____ Four underscores to pad the name to 14 characters
- **MMMM** Influencing species name with trailing underscore to pad blanks

Examples:
```
FORMIC____VOC_
O3__IC____O3__
```

Short Name **nnI____mmm**

where:

- **nn** Affected species number
- **I** Indicates the sensitivity coefficient is for initial conditions
- _____ Four underscores to pad the name to 10 characters
- **mmm** Influencing species number or name of a species group (NOX, VOC or ALL).

Examples: `10I____VOC` (where FORM is species number 10)
`03I____003` (where O3 is species number 3)

Boundary Condition Sensitivity Names

Long Name **`NNNNBCRRR_MMMM`**

where:

`NNNN`	Affected species name with trailing underscore to pad blanks
`BC`	Indicates the sensitivity coefficient is for boundary conditions
`RRR`	NTH, STH, EST, WST or TOP if stratified by boundary; ALL if not stratified by boundary
`_`	Underscore to pad the name to 14 characters
`MMMM`	Influencing species name with trailing underscore to pad blanks

Examples: `FORMBCALL_VOC_`
`O3__BCTOP_O3__`

Short Name **`nnBRRR_mmm`**

where:

`nn`	Affected species number
`B`	Indicates the sensitivity coefficient is for initial conditions
`RRR`	NTH, STH, EST, WST or TOP if stratified by boundary; ALL if not stratified by boundary
`_`	Underscore to pad the name to 10 characters
`mmm`	Influencing species number or name of a species group (NOX, VOC or ALL)

Examples: `10BALL_VOC` (where FORM is species number 10)
`03BTOP_003` (where O3 is species number 3)

Emissions Sensitivity Names

Long Name **`NNNNEMGGRRMMMM`**

where:

`NNNN`	Affected species name with trailing underscore to pad blanks
`EM`	Indicates the sensitivity coefficient is for emissions
`GG`	Emissions group number
`RR`	Emissions region number
`MMMM`	Influencing species name with trailing underscore to pad blanks

Examples: `FORMEM0103VOC_`
`O3__EM020103__`

Short Name **nnEGGRRmmm**

where:

nn	Affected species number
E	Indicates the sensitivity coefficient is for emissions
GG	Emissions group number
RR	Emissions region number
mmm	Influencing species number or name of a species group (NOX, VOC or ALL)

Examples: `10E0103VOC` (where FORM is species number 10)
`03E0201003` (where O3 is species number 3)

9. PROCESS ANALYSIS

9.1 INTRODUCTION

Process Analysis (PA) is designed to provide in-depth analyses of the physical and chemical processes in an air quality model. Through PA, you can more fully understand the complex interactions of the different processes, explain simulation results within the context of model formulation, and improve the design of control strategies.

Most model photochemical grid model applications start off with a base case and then proceed to various sensitivity studies. The standard approach creates a particular set of meteorology inputs for the base-case episode. After the meteorology is fixed, various scenarios of emissions reduction, i.e., across the board emissions cuts, industry-specific, or source-specific emissions cuts, are applied to the emissions input files. In some cases, the combined effects of emissions reduction and variable meteorology are investigated. In general, regardless of the type of simulations performed, the results of these simulations are analyzed by examining the predicted concentrations, comparing predicted concentrations with observed concentrations, and calculating model performance statistics. While such comparisons are necessary to test the model's performance, they are far from sufficient for determining whether the model is adequately representing the real situation. This is because compensating errors among various processes in the model and the model inputs can result in a prediction that accurately agrees with limited observations but for the wrong reasons. Process Analysis can help prevent "getting the right answer for the wrong reasons" by providing details on how a model answer was obtained and thus opening the door to more fundamental evaluations of underlying model processes.

Three components of PA are implemented in CAMx:

1. Integrated Processes Rate (IPR) analysis. The IPR method provides detailed process rate information for each physical process in CAMx (i.e., advection, diffusion, deposition, emissions, chemistry, etc.) for selected grid cells and selected species. The IPR outputs can be analyzed to determine what processes governed the model-predicted concentrations at any time and place. IPR information has often been plotted as a time series of process contributions for specific cells or groups of cells. IPR outputs have also been used to check the mass balance in the host model, i.e., to determine whether model concentrations are fully explained by the diagnosed process information or whether unexpected artifacts are occurring. The IPR data are relatively easy to interpret and can be analyzed using simple tools such as spreadsheets.

2. Integrated Reaction Rate (IRR) analysis. The IRR method provides detailed reaction rate information for all reactions in the chemical mechanism for selected grid cells. The IRR data can be analyzed to determine how the chemical changes occurring in the model are related to the chemical mechanism. For example, by analyzing rate information over groups of reactions it is possible to quantify chemically meaningful attributes such as radical initiation rates, radical propagation efficiencies, chain lengths, etc. Since these analyses tend to be complex, IRR data generally require post-processing to be useful.

3. Chemical Process Analysis. CPA is closely related to the IRR method but is designed to be more user friendly and accessible. As mentioned above, IRR data are generally only useful after the data have been post-processed into chemically meaningful parameters. With CPA, a selection of useful parameters is calculated within CAMx and then output to gridded files. The gridded CPA files use the same format as the gridded concentration outputs, so the same post-processing tools can be used for CPA data as for concentration data.

9.2 IMPLEMENTATION OF PROCESS ANALYSIS IN CAMx

The main challenges in developing and implementing PA are:

- Extracting accurate process rate information for every process that affects model-predicted concentrations. The PA algorithms must be accurate to provide a useful description of how the model-predictions were obtained.

- Implementing the PA algorithms without changing the results from the underlying model.

- Providing a flexible interface for specifying what PA information to extract so that the volume of output is not overwhelming.

Integrated Process Rate Analysis

The Integrated Processes Rate (IPR) method provides detailed mass balance information for all of the transport, deposition, emissions, and chemistry processes within CAMx. The specific processes that are reported by IPR are listed in Table 9-1. This information is output for each chemical species selected for inclusion in the average concentration output file, and for each grid cell selected for analysis. The process rates are integrated across each model output time interval (normally hourly). Taken together, this information provides a complete description of how the species concentration changed across the output time interval (i.e., the final concentration minus the initial concentration) and the magnitude of all of the processes that caused this change. Information is output in the concentration units used internally within CAMx (μmole/m^3). A units conversion factor (ppm/μmole/m^3) specific to the grid cell/time period is also output to allow conversion to mixing ratio (ppm) for comparison with CAMx average concentration outputs. The grid cell volume also is output to allow aggregation across grid cells.

For most of the process rates listed in Table 9-1 the interpretation is straightforward, the rate is simply the concentration change caused by the named process across the output time interval. The sign convention followed is that a positive flux always tends to increase the cell concentration. Further explanation is provided for several processes below.

Table 9-1. Process information reported by the IPR option.

Order	Process Information	Units
1	Initial concentration	μmole/m^3
2	Gas phase chemistry	μmole/m^3
3	Area emissions	μmole/m^3
4	Point source emission	μmole/m^3
5	Plume-in-rid change	μmole/m^3
6	West boundary advection	μmole/m^3
7	East boundary advection	μmole/m^3
8	South boundary advection	μmole/m^3
9	North boundary advection	μmole/m^3
10	Bottom boundary advection	μmole/m^3
11	Top boundary advection	μmole/m^3
12	Dilution in the vertical	μmole/m^3
13	West boundary diffusion	μmole/m^3
14	East boundary diffusion	μmole/m^3
15	South boundary diffusion	μmole/m^3
16	North boundary diffusion	μmole/m^3
17	Bottom boundary diffusion	μmole/m^3
18	Top boundary diffusion	μmole/m^3
19	Dry deposition	μmole/m^3
20	Wet deposition	μmole/m^3
21	Heterogeneous chemistry	μmole/m^3
22	Final concentration	μmole/m^3
23	Units conversion	ppm/(μmole/m^3)
24	Average cell volume	m^3

Plume-in-Grid Change: The grid cell concentration change caused by plume-in-grid puffs that resided in the grid cell during the output time interval.

Point source emissions: Does not include point sources selected for PiG treatment as these are reported in Plume-in-Grid Change.

Dilution in the vertical: CAMx allows for layer interface heights to change over time which can lead to a "dilution" term for affected grid cells.

Boundary diffusion: In some cases this term will be zero by definition, namely: the bottom boundary of surface layer grid cells; the top boundary of top layer grid cells; any lateral boundary that coincides with a nest boundary.

Dry deposition: This term is zero by definition for all grid cells above the surface layer.

Integrated Reaction Rate Analysis

The Integrated Reaction Rate (IRR) method provides the integrated rate of each chemical reaction in ppm units for each grid cell selected for process analysis. Reaction rates are accumulated (integrated) within the chemistry solver at the time steps being used to solve the chemical equations, and output at the CAMx output time interval (usually 1 hour). Within the CMC fast solver the rate information can be accumulated at the exact time steps used by the solver and so the rates exactly correspond to the chemistry solution. The IEH solver uses the LSODE numerical integration package to obtain the solution for some species and it is difficult to obtain integrated rate information from the time steps used within LSODE. Therefore the rates are integrated around each call to LSODE by using the average of the initial and final concentrations. Thus, the integrated rates for the IEH solver do not exactly correspond to the chemistry solution.

Chemical Process Analysis

The reaction rate information provided by the IRR method is probably most useful when rates for several reactions are combined to describe chemically meaningful attributes of the chemical mechanism, such as radical initiation or termination rates. The Chemical Process Analysis (CPA) method builds some of this capability into CAMx by calculating a pre-determined set of parameters as listed in Table 9-2. The CPA parameters are calculated for all grid cells in either the surface layer or all layers. The selection between surface layer or all layer CPA outputs is determined by the "3-D average file" flag specified in the CAMx Control File (see Section 5). This is based on the premise that 3-D CPA information will be interpreted in conjunction with 3-D concentration fields.

9.3 RUNNING PROCESS ANALYSIS IN CAMx

Process analysis can be used with all of the physical options available in the CAMx model, e.g., different advection and chemistry solvers. However, PA cannot be used at the same time as the OSAT or DDM "probing tool" options because PA, OSAT and DDM share internal data structures to minimize the total memory resources required by CAMx.

PA is invoked similarly to the other Probing Tools within the CAMx control file. In the `&CAMx_Control` namelist module, the variable `Probing_Tool` must be set to "PA". An additional namelist module called `&PA_Control` must then be provided in the control file to configure the PA portion of the model. The additional namelist module is described below. The order of the variables follow the template available with the source code. An example of the PA portion of the CAMx run control file is shown in Figure 9-1.

Table 9-2. Chemical process analysis (CPA) outputs in CAMx with the CB4 and SAPRC99 mechanisms (mechanisms number 3 and 5).

Chemical Process Analysis (CPA) Parameters in CAMx		Chemical Mechanism	
Category and Description	**Name**	**CB4 (M3)**	**SAPRC99 (M5)**
Ox Budget			
Ox Chemical Production	OxProd	X	X
Ox Chemical Destruction	OxLoss	X	X
VOC Sensitive Ox Prod	POx_VOC	X	
NOx Sensitive Ox Prod	POx_NOx	X	
Net O3 Production	PO3_net	X	
Radical Initiation			
New OH from O1D+H2O	newOH_O1D	X	X
New OH from H2O2 & HONO	newOH_radres	X	
New OH from O3+HC	newOH_OXwVOC	X	
New OH from isoprene	newOH_isop	X	
New OH from other sources	newOHother		X
New HO2 from HCHO	nwHO2_HCHO	X	X
New HO2 from OLE & ETH	newHO2_OLE_ETH	X	
New HO2 Production (Total)	newHO2tot	X	X
New RO2 Production (Total)	newRO2tot	X	X
Total New HOx from isoprene	nHOx_isop	X	
Radical Propagation			
sum of OH+CO and OH+CH4 reactions	OHwCO_CH4	X	X
OH reacted with ISOP	ISOPwOH	X	X
isoprene reactions with O3, NO3 and O3P	ISOPwOx	X	X
OH reacted with OLE	OHw_OLE	X	
OH reacted with ETH	OHw_ETH	X	
OH reacted with PAR	OHw_PAR	X	
OH reacted with TOL	OHw_TOL	X	
OH reacted with XYL	OHw_XYL	X	
OH reacted with total VOC	OHw_all_HC	X	X
other OH propagation reactions	OHpropmisc	X	X
Total HO2 Production	HO2TotProd	X	X
Total RO2 Production	RO2TotProd	X	X
NO2 produced from reactions of HO2	HO2_to_NO2	X	
OH produced from reactions of HO2	HO2_to_OH	X	
Yield of OH per HO2	Y_OHperHO2	X	
NO2 produced from reactions of RO2	RO2_to_NO2	X	
Total OH production	OH_reacted	X	X
OH Chain length	HOx_CL	X	
HOx Chain length	OH_CL	X	
HCHO production from isoprene	HCHOp_isop	X	X
HCHO production total	HCHOp_Tot	X	X
Radical Termination			
OH termination	OHterm	X	X
HO2 termination	HO2term	X	X
RO2 termination	RO2term	X	X
NOx Termination (or Production)			

Chemical Process Analysis (CPA) Parameters in CAMx		Chemical Mechanism	
Category and Description	**Name**	**CB4 (M3)**	**SAPRC99 (M5)**
OH+NO2 → HNO3	HNO3_OHNO2	X	X
NO3+HC → HNO3	HNO3_NO3HC	X	X
N2O5+H2O → 2 HNO3	HNO3_N2O5	X	X
HNO3 reacted (to produce NOx)	HNO3reacte	X	
net PAN Prod	PANprodNet	X	X
net PAN Loss (source of NOx and a radical)	PANlossNet	X	X
HNO3 and RNO3 reacted to NO2	NOzreact		X
production of organic nitrates	RNO3_prod	X	
production of organic nitrates & XN	RNO3XNprod		X
Radical Concentrations			
OH radical concentration	OH	X	X
HO2 radical concentration	HO2	X	X
NO3 radical concentration	NO3	X	X
N2O5 concentration	N2O5	X	X
Total Number of CPA Variables		**49**	**31**

Description of PA Control in the CAMx Run Control File

&PA_Control	Label for the Probing Tool namelist module that configures the PA option; it must begin in column 2
&	Flag ending a namelist; it must be in column 2
PA_File_Root	Character root output path/filename
Number_of_PA_Domains	Integer number of PA analysis domains to be evaluated during the simulation.
Within_CAMx_Grid	Integer array (by PA domain) pointer into the CAMx grid within which the PA domain exists (1=master grid, etc.). Use the CAMx internal grid number reported in the *.diag file. Note that this may differ from the nest order provided by the user in the CAMx control file.
PA_Beg_I_Index	Integer array (by PA domain) grid column containing western edge of PA domain.
PA_End_I_Index	Integer array (by PA domain) grid column containing eastern edge of PA domain.
PA_Beg_J_Index	Integer array (by PA domain) grid row containing southern edge of PA domain.
PA_End_J_Index	Integer array (by PA domain) grid row containing northern edge of PA domain.
PA_Beg_K_Index	Integer array (by PA domain) grid layer containing bottom of PA domain.
PA_End_K_Index	Integer array (by PA domain) grid layer containing top of PA domain.

Rules for Defining Process Analysis Domains

1. A process analysis domain must be contained within a single CAMx grid.
2. A process analysis domain may not include cells that contain a nested grid.
3. A process analysis domain may contain as few as 1 grid cells.
4. A process analysis domain may contain up to all of the grid cells in the CAMx grid containing process analysis domain provided that this does not violate the second rule.

```
&PA_Control

 PA_File_Root         = 'CAMx.OTAG.950707.PA',

 Number_of_PA_Domains = 2,
 Within_CAMx_Grid(1)  = 1,
 PA_Beg_I_Index(1)    = 8,
 PA_End_I_Index(1)    = 12,
 PA_Beg_J_Index(1)    = 9,
 PA_End_J_Index(1)    = 13,
 PA_Beg_K_Index(1)    = 1,
 PA_End_K_Index(1)    = 5,

 Within_CAMx_Grid(2)  = 2,
 PA_Beg_I_Index(2)    = 107,
 PA_End_I_Index(2)    = 110,
 PA_Beg_J_Index(2)    = 78,
 PA_End_J_Index(2)    = 82,
 PA_Beg_K_Index(2)    = 1,
 PA_End_K_Index(2)    = 7,

 &
```

Figure 9-1. Example section of a CAMx control file specifying options for process analysis.

Process analysis grids may intersect or overlap. The same grid cell may be in several process analysis domains.

CAMx Process Analysis Test Problem

ENVIRON provides a test problem for CAMx based on the first two days of the OTAG July 1995 episode covering the eastern US. A simple demonstration of PA has been developed from this application and is available from the CAMx ftp server (see www.camx.com for ftp download instructions). The PA test case uses two PA regions as specified in Figure 9-1, the first covers the Houston area and the second covers the New York area. The PA test case is suitable only as a demonstration, not as a basis for air quality planning decisions, because the test case uses just the first two spin-up days of the OTAG July 1995 episode.

9.4 SETTING CAMx PARAMETERS FOR PROCESS ANALYSIS

Process analysis stores information in data structures that are dimensioned using FORTRAN parameter statements. These parameters must be large enough to accommodate the PA configuration specified in the CAMx control file. If one of these parameters is exceeded CAMx will stop with an error message stating that a parameter must be changed and the model recompiled. It is always a good idea to do a complete rebuild (use the Unix command

"make clean") when a parameter is changed. The parameters that may need to be changed are in two include files, "procan.com" and "tracer.com".

procan.com

MXPADOM – The maximum number of Process Analysis domains.

MXPACEL – The maximum number of Process Analysis cells over all domains

tracer.com

MXTRSP – This parameter defines gridded data structures that are used by several probing tools. For PA the data structures store chemical process analysis (CPA) variables, so MXTRSP must be set to at least the value of MXCPA (set in procan.com) which is 49.

9.5 OUTPUT FILE FORMATS

CAMx may output up to four files containing PA information according to the PA option selected (see Table 9-3). All of these files are in FORTRAN binary format to conserve disk space. Two files (the *.ipr and *.irr files) contain information for just the grid cells selected for PA. The formats for these files are not described here since two FORTRAN post-processor programs are provided to extract data from these files in a comma-delimited ASCII format. The files containing CPA information (the *.cpa.grid and *.cpa.fgrid files) are gridded files containing information for the same area as the regular model average files (*.avrg and *.favrg). The gridded CPA files have the same format as a regular model average file as described in Section 5.

Table 9-3. Process analysis keywords and associated CAMx output files.

Filename	Content	CAMx Key Word		
		PA	IRR	IPR
*.ipr	Integrated process rate (IPR) information for all selected cells	Yes	No	Yes
*.irr	Integrated reaction rate (IRR) information for all selected cells	Yes	Yes	No
*.grid.cpa *.fgrid.cpa	Chemical process analysis (CPA) parameters for the master and (optionally) nested grids	Yes	Yes	No

9.6 POSTPROCESSING

Two post-processors are provided to read the binary *.ipr and *.irr output files and extract PA data for further analysis. The CPA output files can be visualized directly.

IPR Output Files

The FORTRAN77 program "ext_ipr" extracts IPR data from one or more CAMx *.ipr binary files and reformats the data to comma delimited ASCII format (.csv) suitable for subsequent analysis (e.g., using spreadsheets). The "ext_ipr" program performs the following tasks:

- Reads and outputs the descriptive header of the *.ipr file.
- Optionally combines data from several consecutive *.ipr files to provide multi-day output.
- Selects data for an individual cell within a PA sub-domain or aggregates data over multiple cells within a PA sub-domain.
- Outputs the selected IPR data in .csv format in either ppb or molar units.

A sample script to run the "ext_ipr" program is provided with the source code, and the script includes a description of how to use the program. Also included is a spreadsheet macro that can read the .csv format and prepare several plots. This macro is described below. Both the "ext_ipr" program and the macro are provided with the CAMx PA example.

Aggregating Cells

The "ext_ipr" program can combine IPR information across several cells. This is useful for analyzing the contributions of model processes to a geographic area that spans multiple cells (e.g., an urban area). For simplicity, the multi-cell area must be defined as a rectangular box. The capability of aggregating IPR information across vertical layers is particularly important during the day because vertical columns of cells within the mixed layer become strongly coupled on time scales shorter than one hour. Thus, if the process contributions for a surface grid cell are analyzed during the day vertical diffusion will often completely dominate all other processes. In this situation, it is more informative to analyze a column of cells extending from the surface to the approximate height of the mixed layer.

When the "ext_ipr" program aggregates information across grid cells it accounts for differences in cell volume. If the output for aggregate cells is requested in ppb units, the output from CAMx in molar units is converted to ppb using the volume-weighted average units conversion factor for the cells being aggregated.

IPR Time Series Analysis

One useful approach to analyzing IPR data is to plot the contributions of several processes as a time series. Figures 9-2 and 9-3 show two examples of this approach based on data from the CAMx test case discussed above. The figures show process contributions to the ozone concentration in a multi-cell area around New York on July 7 and 8, 1995 and are intended solely as an illustration of how PA can be used. The figures were prepared using the "ext_ipr" program described above and the spreadsheet macro "process_analysis_macro.xls." The macro reads an output file from "ext_ipr" and prepares three charts:

1. Bar chart of the contribution from each process averaged over the duration of the PA data. This is useful to see which processes were important.

2. Bar chart showing the time series of contributions from all major processes. To reduce the number of processes being displayed, advection and diffusion information for each boundary is combined into a single transport term, and any series with zero contribution is excluded from the chart. An example of this chart is shown in Figure 9-3.

3. Bar chart showing the time series of contributions from major processes with lateral boundary transport shown as a single net term. An example of this chart is shown in Figure 9-2. For a small region lateral boundary transport often leads to large positive and negative terms that approximately cancel (e.g., inflow from the east and outflow to the west). This chart provides a comparison of the net effect of lateral boundary transport relative to other processes, whereas the second chart resolves the transport by boundary. Comparing Figures 9-2 and 9-3, based on the same data, shows the difference between these two analysis approaches.

The macro "process_analysis_macro.xls" used to prepare Figures 9-2 and 9-3 is provided with the CAMx PA example.

IRR Output Files

The FORTRAN77 program "ext_irr" extracts IRR data from one or more CAMx *.irr binary files and reformats the data for subsequent analysis. The "ext_irr" program performs the following tasks:

- Reads and outputs the descriptive header of the *.irr file.
- Optionally combines data from several consecutive *.irr files to provide multi-day output.
- Selects data for an individual cell or multiple cells within a PA sub-domain.
- Optionally, outputs the selected IRR data to a .csv format ASCII file.
- Optionally, outputs the selected IRR data to a UAM average format binary file.

The ASCII IRR data are suitable for subsequent analysis (e.g., using spreadsheets) but at this time there is no "pre-packaged" analysis available comparable to the macro for analyzing IPR data. The binary IRR output from "ext_irr" can be displayed using any post-processing software that can display CAMx average concentration outputs. The "ext_irr" program and a sample run script are included with the CAMx PA example.

CPA Output Files

The binary CPA output files have the same format as CAMx average concentration files and therefore can be visualized using any post-processing software that can display CAMx concentration outputs. Several example displays of CPA outputs from the CAMx test case characterizing the budget for the OH radical are shown in Figure 9-4. This figure is not intended to be a complete analysis of the CPA outputs from the test case, but rather to provide

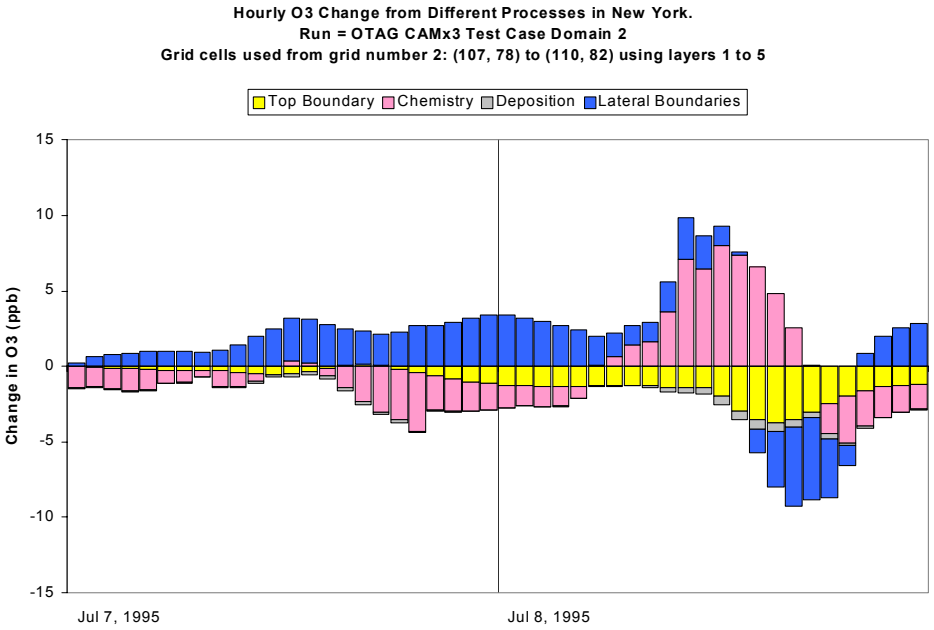

Figure 9-2. Example integrated process rate (IPR) time series analysis for ozone. The bars show the ppb change in ozone concentration in the analysis region caused by each named process. Lateral boundary inflow/outflow has been aggregated to a single net term.

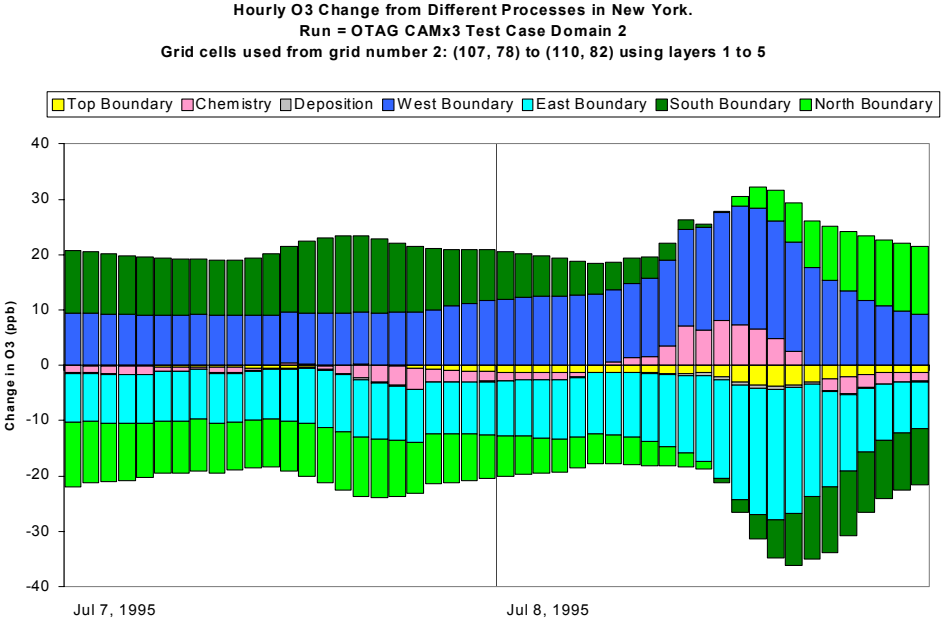

Figure 9-3. Example integrated process rate (IPR) time series analysis for ozone. The bars show the ppb change in ozone concentration in the analysis region caused by each named process. Lateral boundary inflow/outflow has not been aggregated, in contrast to Figure 9-2.

an illustration of the type of information that can be obtained. The results displayed in Figure 9-4 have the following significance:

NewOH_O1D – shows the production of "new" OH radicals (in ppb) from the photolysis of ozone to $O(^1D)$ atoms during hour 12 on July 8. The designation "new" indicates that this represents a new input to the radical pool, rather than a re-cycling of other radicals into OH.

NewOHother – shows the production of "new" OH radicals (in ppb) from sources other than the photolysis of ozone to $O(^1D)$ atoms. In the CB4 mechanism, these sources are photolysis of H_2O_2, HNO_3, HONO, reactions of ozone with alkenes and reactions of $O(^3P)$ atoms with organics.

HO2_to_OH – shows the production of OH radicals (in ppb) from the re-cycling of HO_2 radicals. In the CB4 mechanism this occurs by the reactions of HO_2 radicals with O_3, NO and C_2O_3 radicals.

OH_reacted – shows the amount of OH reacted (in ppb) which includes all termination and propagation reactions of OH.

OHterm – shows the loss of OH radicals (in ppb) through OH termination reactions. In the CB4 mechanism these include the reactions of OH with NO, NO_2, HONO, HNO_3, HO_2 and organics. For the OH organic reactions, only a fraction of the OH radical is considered terminated because there are radical products.

HNO3_OHNO2 – shows the loss of OH radical (in ppb) through termination with NO_2 to form HNO_3. In other words, this term is the integrated rate of a single reaction ($OH + NO_2 \rightarrow HNO_3$).

Comparison of the CPA displays in Figure 9-2 reveals the following:

- Ozone photolysis to $O(^1D)$ is a larger and more widespread source of "new" OH than other sources.
- New sources of OH are small compared to the source of OH represented by re-cycling of HO_2 to OH
- OH_reacted is much larger than OHterm indicating that most of the OH reacts by propagation to other radicals rather than termination. Since the magnitude of HO_2_to_OH is comparable to OH_reacted, many of the propagating OH radicals pass through HO_2 back into OH (a cycle).
- Reaction of OH with NO_2 is a large contributor to OH termination.

User's who are interested in better understanding the CPA outputs may look at how the CPA terms are calculated in the "cpamech3" subroutine for Mechanism 3 (the CB4 mechanism).

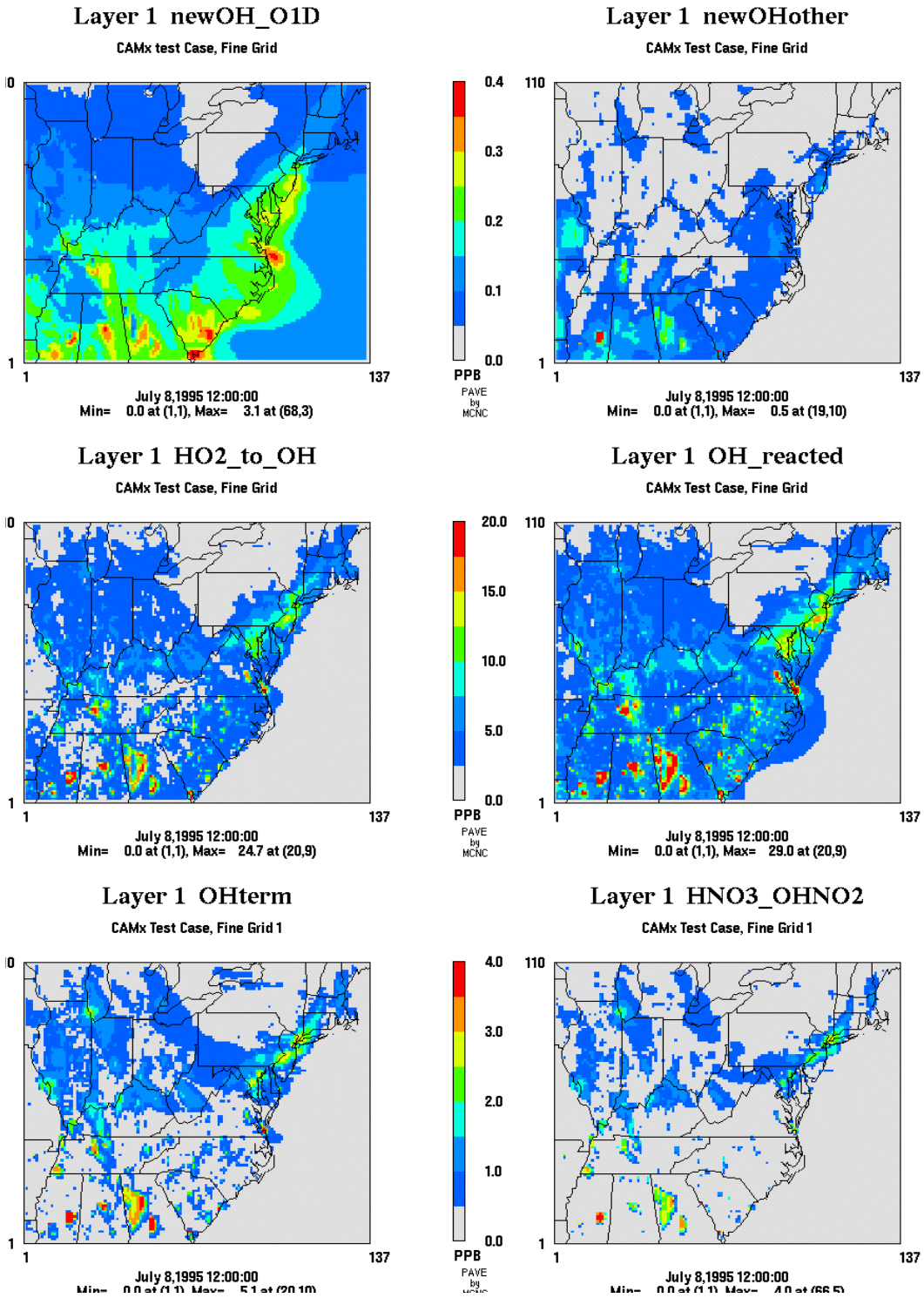

Figure 9-4. Example CAMx chemical process analysis (CPA) outputs describing the OH radical budget for the 12-km nested grid of the CAMx test case at noon on July 8, 1995.

9.7 CHEMICAL PROCESS ANALYSIS AND GRID NESTING

CAMx user's should already be aware that the horizontal and vertical resolution of CAMx grids can impact model results such as predicted concentrations. Such impacts may be considered modeling artifacts since they result from choices in modeling system design. These artifacts are rarely apparent in the course of a typical CAMx application because modeling grid design conventions have evolved that reduce grid resolution artifacts to acceptable levels (e.g., EPA guidance for 8-hour ozone modeling), and because grid resolution is usually held fixed throughout a modeling project. However, there are technical reasons why grid resolution artifacts are more likely to be apparent for process analysis (CPA and IRR) outputs than the normal CAMx concentration (average file) outputs. The purpose of this discussion is to alert users's to this situation and provide some technical background. An example is given below based on the CAMx test case, which uses OTAG model inputs.

The sensitivity of grid model concentrations to grid resolution depends upon competition between processes that tend to smooth out concentration gradients (i.e., horizontal and vertical mixing) and processes that tend to create concentration gradients (i.e., emissions, chemical reactions, deposition). Hence, long lived species with slow production and removal rates will tend to show little spatial variation in mixing ratio provided that some atmospheric mixing is occurring. For example, carbon monoxide mixing ratios tend to be spatially uniform in grid model simulations, except where there are large differences in emission strength between neighboring cells.

Many of the chemical process analysis (CPA) terms involve or describe radical concentrations. Radicals are distinguished from the state species in CAMx (i.e., the species that are listed in the chemistry parameters file and are available for output to average concentration file) by having very short lifetimes (sub-second). Short lifetime means that the radicals cannot be "transported" in the atmosphere since they react before they can travel farther than fractions of a centimeter. Consequently, CAMx does not transport radicals and there is no direct physical coupling between radical concentrations in neighboring grid cells. This suggests a greater potential for spatial variability in radical concentrations than exists for state species. However, the radical concentrations are determined by the state species concentrations in each grid cell, and since the concentrations of state species in neighboring cells are coupled by transport, the radical species concentrations in neighboring cells are indirectly coupled. Therefore, differences in radical concentrations between neighboring cells must reflect differences in the state species concentrations or differences in the steady state relationships between the radicals and the state species. The example below shows that these steady state relationships can show systematic dependencies on grid resolution that are directly visible in model outputs.

Vertical Nesting in the OTAG Modeling

The grid system developed for the OTAG modeling uses vertical nesting to economize on model resources in the master grid area. This means that the nested grid has seven layers but the master grid has only five layers. The vertical nesting is achieved by aligning the first two nested grid layers with the first master grid layer, and the third and fourth nested grid layers

with the second master grid layer. The surface layer in the master grid is 100 m deep whereas in the nested grid the surface layer is only 50 m deep.
The surface OH concentration is shown in Figure 9-5(a) for noon on July 8. This output was prepared from the master grid CPA output file, and so the hourly OH is the time weighted average of the mixing ratio at each sub-hourly time step. In the area occupied by the nested grid, the OH concentrations from 18 nested grid cells (i.e., a block of 3 by 3 by 2 cells) have been aggregated to the corresponding master grid cell using a volume weighted average. The area of the nested grid is clearly visible with a box shaped outline in Figure 9-5(a). The OH concentrations are systematically lower in the nested grid than the master grid. The area of the nested grid is also visible in other CPA outputs related to radical concentrations. Figure 9-6(a) shows the corresponding ozone distribution, and the area of the master grid cannot be distinguished.

A simple experiment shows that the difference in OH concentrations between the master and nested grids results from the vertical nesting. CAMx was run using a 5 layer nested grid (no vertical nesting) using the nested grid emissions but interpolating the meteorology from the master grid using the CAMx "flexi-nesting" capability. The surface OH concentration without vertical nesting is shown in Figure 9-5(b). Without vertical nesting, the area of the nested grid cannot be distinguished in the OH concentration field. This shows that the surface OH concentration is very sensitive to the thickness of the surface layer, much more so than ozone (Figure 9-6).

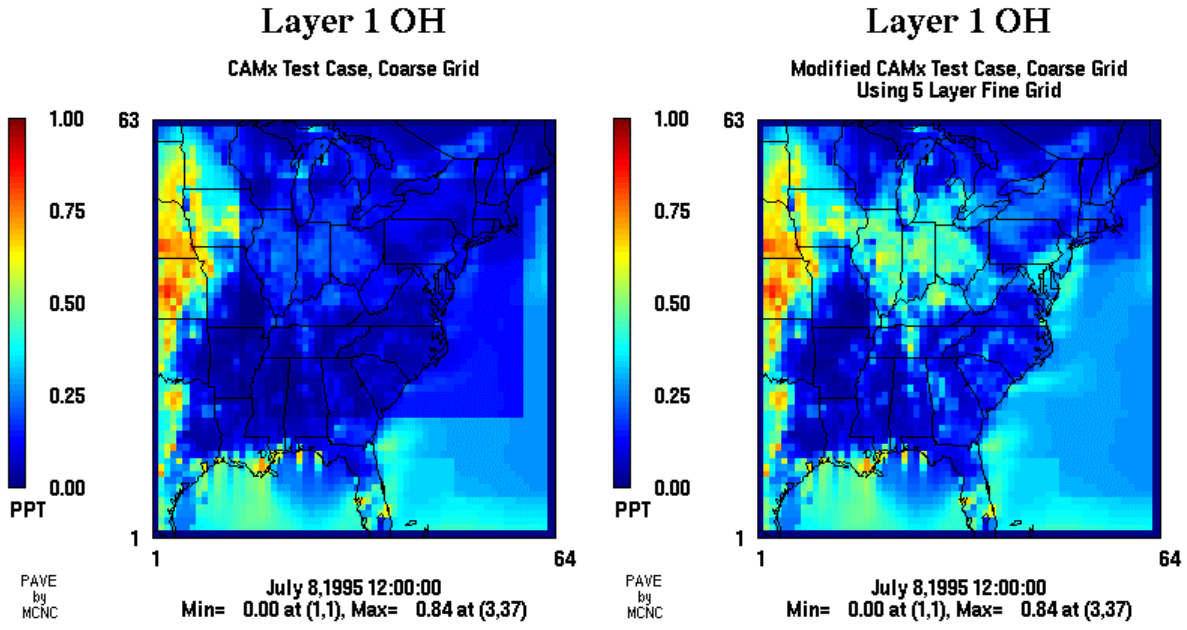

Figure 9-5. Surface OH concentrations for the OTAG master grid area with (a) and without (b) vertical nesting in the nested grid area.

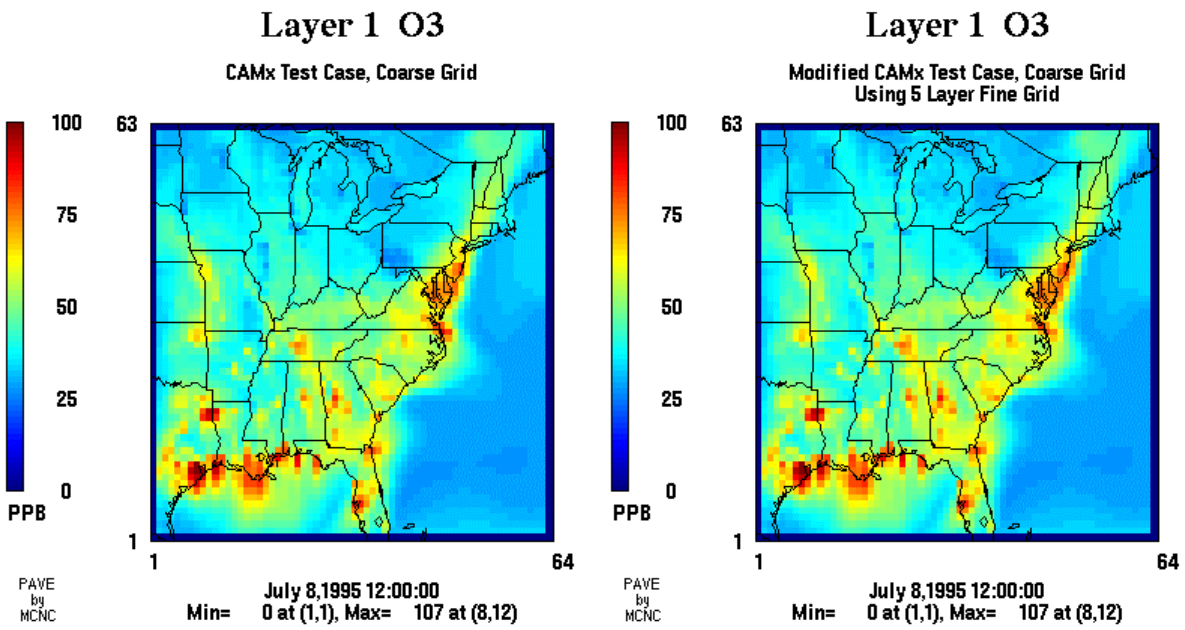

Figure 9-6. Surface ozone concentrations for the OTAG master grid area with (a) and without (b) vertical nesting in the nested grid area.

While results such as Figure 9-5(a) may appear "wrong" at first sight, a more considered response is a realization that CPA is simply providing new insight into relationships between modeling system design and function. Such information can be used to improve the design of a modeling system or to assist in the interpretation of model results. A modeler might conclude from these results that vertical nesting is undesirable in the surface layer because it provides relatively little saving in CPU and memory requirements at the cost of artifacts that are difficult to explain.

10. REACTIVE TRACERS

The CAMx reactive tracer (RTRAC) algorithm provides a flexible approach for simulating the emission, dispersion/transport, deposition, and chemistry of multiple gas and particulate tracers within the computational grid and the IRON PiG. Originally developed to model air toxics, RTRAC was extended to track a variety of organic and inorganic species. RTRAC is implemented as a CAMx "Probing Tool" and shares model data structures with other Probing Tools such as the Ozone Source Apportionment Technology (OSAT), Decoupled Direct Method (DDM) and Process Analysis. This streamlines the CAMx code and improves efficiency, but means that RTRAC cannot be used simultaneously with other Probing Tools.

RTRAC can be used to address a variety of issues, such as:

- Simulation of reactive and inert gaseous and particle air toxic compounds;
- Simulation of individual VOC compounds;
- Simulation of source-specific primary emitted inert and reactive compounds.

Tracers are defined for each CAMx run via an RTRAC chemistry parameters file similar to that used for the core model. The examples in Figure 10-1 and 10-2 illustrate an RTRAC air toxics application using the CB-IV and SAPRC99 chemical mechanisms, respectively (ENVIRON, 2002; Morris et al., 2003). The number and names of the tracers are arbitrary; i.e. information on the tracer species' chemical identities, structure, reaction pathways, and kinetics are kept separate from the core model. Consistent with the chemistry parameters files used for CB-IV and SAPRC99, the physical characteristics for each reactive tracer must be specified for deposition calculations and reaction pathways and rates must be defined. The structure of the RTRAC tracer definition provides complete flexibility in the selection of compounds/tracers to be included in each analysis. The user is able to easily alter or expand the compounds treated as needed.

The RTRAC calculations for emissions, transport, and deposition use the existing CAMx algorithms. The emissions are specified through an extra set of emission files (surface and/or point source) for the RTRAC tracer species. Emissions of gases are in moles per emission time period (normally moles/hour), whereas particles are in micro-grams per emission time period. The emissions file format is the same as for a regular CAMx emissions file (i.e., the UAM-IV format) as described in the Section 5.

For gas species, the required deposition parameters are the Henry's Law constant and a diffusivity parameter, $\sqrt{M_g / M_{H_2O}}$. The deposition calculation for gases that react in plant tissue also uses a reactivity parameter that describes whether a species reacts when dissolved inside leaf tissues (Wesely, 1989). This parameter is intended for modeling the deposition of reactive species, such as ozone, and should be set to zero for air toxics. The deposition calculation for gasses also uses an "Rscale" factor to adjust the surface resistance. This is used to set the surface resistance to zero for strong acids (e.g., HNO_3) and should be set to 1.0 for modeling air toxics.

```
CAMx Version       |VERSION4.2
Description        |MATES Toxics for CRC project A-42
No of gas tracers  |6
No of aero tracers |8
No photolysis rxns |4
No thermal rxns    |12
Gas Tracers
No.  Name      P/S   SNAM  lower bnd     H-law   T-fact    Diffrat  Reactvty
  1  PACET     PRIM         1.00E-12  6.30e+03    -6492.      1.56       0.0      1.0
  2  HCHO      PRIM         1.00E-12  6.30e+03    -6492.      1.29       0.0      1.0
  3  BENZ      PRIM         1.00E-12  1.80e-01        0.      2.08       0.0      1.0
  4  BUTA      PRIM         1.00E-12  1.00e-02        0.      1.73       0.0      1.0
  5  SACET     SEC   ALD2   1.00E-12  6.30e+03    -6492.      1.56       0.0      1.0
  6  SFORM     SEC   FORM   1.00E-12  6.30e+03    -6492.      1.29       0.0      1.0
Aero Tracers
No.  Name       lower bnd    Density   Low cut Upper cut
  7  DSLF        1.00E-09        1.5      0.10      2.50
  8  ECF         1.00E-09        1.5      0.10      2.50
  9  CRF         1.00E-09        1.5      0.10      2.50
 10  CR6F        1.00E-09        1.5      0.10      2.50
 11  DSLC        1.00E-09        1.5      2.50     10.00
 12  ECC         1.00E-09        1.5      2.50     10.00
 13  CRC         1.00E-09        1.5      2.50     10.00
 14  CR6C        1.00E-09        1.5      2.50     10.00
Photolysis reactions
Toxic      Rxn #    Factor
PACET        45       1.0
SACET        45       1.0
HCHO         39       1.6
SFORM        39       1.6
Thermal reactions and rates
Toxic     React A(ppm-1min-1)      Ea(K)          B      Tref
PACET     OH      8.2015E+03 -3.1099E+02       0.0     300.0
PACET     NO3     2.0689E+03  1.8599E+03       0.0     300.0
HCHO      OH      1.6699E+03 -6.4815E+02       2.0     300.0
HCHO      NO3     4.1377E+03  2.5161E+03       0.0     300.0
BENZ      OH      3.6944E+03  1.9978E+02       0.0     300.0
BUTA      OH      2.1871E+04 -4.4787E+02       0.0     300.0
BUTA      O3      4.8766E+01  2.5000E+03       0.0     300.0
BUTA      NO3     2.1871E+04  1.4890E+03       0.0     300.0
SACET     OH      8.2015E+03 -3.1099E+02       0.0     300.0
SACET     NO3     2.0689E+03  1.8599E+03       0.0     300.0
SFORM     OH      1.6699E+03 -6.4815E+02       2.0     300.0
SFORM     NO3     4.1377E+03  2.5161E+03       0.0     300.0
```

Figure 10-1. Example RTRAC chemistry input file for modeling the MATES toxic species using CB-IV as the host chemical mechanism.

```
CAMx Version       |VERSION4.2
Description        |Toxics for CRC project A-42 with SAPRC99 host mechanism
No of gas tracers  |14
No of aero tracers |0
No photolysis rxns |8
No thermal rxns    |28
Gas Tracers
No.  Name      P/S   SNAM  lower bnd     H-law   T-fact    Diffrat  Reactvty
  1  mPACET    PRIM         1.00E-12  6.30e+03    -6492.      1.56       0.0      1.0
  2  mPFORM    PRIM         1.00E-12  6.30e+03    -6492.      1.29       0.0      1.0
  3  mBENZ     PRIM         1.00E-12  1.80e-01        0.      2.08       0.0      1.0
  4  mBUTA     PRIM         1.00E-12  1.00e-02        0.      1.73       0.0      1.0
  5  SACET     SEC   CCHO   1.00E-12  6.30e+03    -6492.      1.56       0.0      1.0
  6  SFORM     SEC   HCHO   1.00E-12  6.30e+03    -6492.      1.29       0.0      1.0
  7  oPACET    PRIM         1.00E-12  6.30e+03    -6492.      1.56       0.0      1.0
  8  oPFORM    PRIM         1.00E-12  6.30e+03    -6492.      1.29       0.0      1.0
  9  oBENZ     PRIM         1.00E-12  1.80e-01        0.      2.08       0.0      1.0
 10  oBUTA     PRIM         1.00E-12  1.00e-02        0.      1.73       0.0      1.0
 11  pPACET    PRIM         1.00E-12  6.30e+03    -6492.      1.56       0.0      1.0
 12  pPFORM    PRIM         1.00E-12  6.30e+03    -6492.      1.29       0.0      1.0
 13  pBENZ     PRIM         1.00E-12  1.80e-01        0.      2.08       0.0      1.0
 14  pBUTA     PRIM         1.00E-12  1.00e-02        0.      1.73       0.0      1.0
Photolysis reactions
Toxic      Rxn #    Factor
mPACET      131       1.0
oPACET      131       1.0
pPACET      131       1.0
SACET       131       1.0
mPFORM      123       1.6
oPFORM      123       1.6
pPFORM      123       1.6
SFORM       123       1.6
Thermal reactions and rates
Toxic     React A(ppm-1min-1)      Ea(K)          B      Tref
mPACET    OH      8.2015E+03 -3.1099E+02        0.0     300.0
mPACET    NO3     2.0689E+03  1.8599E+03        0.0     300.0
oPACET    OH      8.2015E+03 -3.1099E+02        0.0     300.0
oPACET    NO3     2.0689E+03  1.8599E+03        0.0     300.0
pPACET    OH      8.2015E+03 -3.1099E+02        0.0     300.0
pPACET    NO3     2.0689E+03  1.8599E+03        0.0     300.0
mPFORM    OH      1.6699E+03 -6.4815E+02        2.0     300.0
mPFORM    NO3     4.1377E+03  2.5161E+03        0.0     300.0
oPFORM    OH      1.6699E+03 -6.4815E+02        2.0     300.0
oPFORM    NO3     4.1377E+03  2.5161E+03        0.0     300.0
pPFORM    OH      1.6699E+03 -6.4815E+02        2.0     300.0
pPFORM    NO3     4.1377E+03  2.5161E+03        0.0     300.0
mBENZ     OH      3.6944E+03  1.9978E+02        0.0     300.0
oBENZ     OH      3.6944E+03  1.9978E+02        0.0     300.0
pBENZ     OH      3.6944E+03  1.9978E+02        0.0     300.0
mBUTA     OH      2.1871E+04 -4.4787E+02        0.0     300.0
mBUTA     O3      4.8766E+01  2.5000E+03        0.0     300.0
mBUTA     NO3     2.1871E+04  1.4890E+03        0.0     300.0
oBUTA     OH      2.1871E+04 -4.4787E+02        0.0     300.0
oBUTA     O3      4.8766E+01  2.5000E+03        0.0     300.0
oBUTA     NO3     2.1871E+04  1.4890E+03        0.0     300.0
pBUTA     OH      2.1871E+04 -4.4787E+02        0.0     300.0
pBUTA     O3      4.8766E+01  2.5000E+03        0.0     300.0
pBUTA     NO3     2.1871E+04  1.4890E+03        0.0     300.0
SACET     OH      8.2015E+03 -3.1099E+02        0.0     300.0
SACET     NO3     2.0689E+03  1.8599E+03        0.0     300.0
SFORM     OH      1.6699E+03 -6.4815E+02        2.0     300.0
SFORM     NO3     4.1377E+03  2.5161E+03        0.0     300.0
```

Figure 10-2. Example RTRAC chemistry input file for modeling toxic species with SAPRC99 as the host chemical mechanism.

The deposition calculation for particles requires the particle density and size associated with each species. The particle size is calculated as the geometric mean of the lower and upper cut points (see Figure 10-1). If possible, the particle size and density should be based on the measured size of particles associated with each RTRAC species (e.g., for a toxic compound associated with soot particles, use a density and size representing the soot).

10.1 GAS-PHASE CHEMISTRY

The RTRAC chemistry calculations use a special RTRAC chemistry module. Chemistry may be modeled for primary and secondary gas species, meaning that tracers can be formed from the decay of primary tracers or from the decay of host model species (e.g., secondary formaldehyde). There is no chemistry for particulate tracers in this version of RTRAC.

The chemical decay of gaseous tracers can account for thermal reactions with ozone (O_3), hydroxyl radical (OH) and nitrate radical (NO_3), as well as photolysis. The algorithms are coded so that all chemical decay pathways are zero by default and only become non-zero if decay rates are explicitly specified in the input file (see Figure 10-1). The example RTRAC chemistry input file in Figure 10-1 shows how thermal reactions are specified by naming the tracer and oxidant, and providing reaction rate parameters. Note that the RTRAC chemical reaction rates depend on the rates and parameters provided in the RTRAC input file, and not the rates in the host model chemical mechanism; however the host model does provide the oxidizing species concentrations (i.e., O_3, OH, and NO_3).

Thermal Reactions

Thermal reactions with oxidants are modeled as second order reactions:

$$R = k[tracer][oxidant]$$

where R is the decay rate and the rate constant k is defined using the generalized temperature dependent rate expression:

$$k = A\left(\frac{T}{300}\right)^{B} \exp\left(\frac{-E_a}{T}\right)$$

The Arrhenius factor (A) must be in units ($ppm^{-1}min^{-1}$), the activation energy (E_a) must be Kelvin and B is dimensionless. This is the same as expression 3 in Table 5-4a. Oxidant concentrations for the decay calculation are obtained from the CAMx photochemical simulation for each grid cell at each time step. RTRAC can be used with either the CB-IV or SAPRC99 chemical mechanisms that are available in the current version of CAMx (see Section 3). Choosing between CB-IV and SAPRC99 mechanism will influence the RTRAC chemical decay rates by changing the oxidant concentrations in the host model.

Photolysis

Photolysis reactions are specified by naming the tracer undergoing photolysis and providing a ratio of the tracer photolysis rate to one of the photolysis reactions in the host photochemical mechanism (i.e., CB-IV or SAPRC99). For example, Figure 10-1 shows that there are both primary and secondary acetaldehyde reactive tracers (PACET and SACET) and the photolysis rate for both species is set equal to reaction 45. Reaction 45 in the CB-IV mechanism is photolysis of ALD2, which is based on acetaldehyde. Figure 10-1 also shows that there are two types of formaldehyde in the MATES toxics modeling (PFORM and SFORM). Modeling the photolysis of formaldehyde with RTRAC is complicated by the fact that the CB-IV mechanism includes two photolysis reactions for formaldehyde (reactions 38 and 39). The solution shown in Figure 10-1 is to model formaldehyde photolysis as 1.6 times the rate of CB-IV reaction 39. The CAMx host mechanisms are discussed in Section 3 and are defined by the ASCII chemistry parameters files and mechanism listings distributed with CAMx and available from the CAMx web page (www.camx.com).

Secondary Species

RTRAC allows for formation of secondary/daughter products related to the chemical decay of one of the primary tracers. Secondary species can also be subject to chemical decay, just like primary species, if the user desires. Therefore, the RTRAC chemistry module allows decay reactions (thermal and photolysis) to be specified for secondary species using the same method as for primary species. In this manner, concentrations of secondary species are determined by the balance between chemical production and destruction. RTRAC requires that any secondary daughter tracers must be specified after their parent tracer in the chemistry parameters input file.

RTRAC also allows tracers to be defined to track the secondary formation of any species that is included in the host chemical mechanism (CB-IV or SAPRC99). For example, in Figure 10-1 the species SFORM is used to track secondary formaldehyde, and so SFORM is defined as a secondary species and identified with the host species FORM. This means that the RTRAC chemistry module will identify the chemical production of FORM in each grid cell at each time step, and add this chemical production to the SFORM tracer. Since SFORM is intended to track only secondary formaldehyde, no primary emissions should be included for SFORM.

Example for Defining Chemical Rate Data

Reaction rate data for many gases can be found in rate constant compilations such as IUPAC (2001), JPL (2001) and Calvert et al. (2000, 2002). For the example rate constants for air toxics compounds in Figures 10-1 and 10-2, rate constants for the RTRAC air toxics chemistry were obtained from a study by Harley and Cass (1995) that modeled detailed VOCs for Los Angeles. Photolysis rates were calculated using the Tropospheric Ultra-violet Visible (TUV) model (Madronich, 2002) that is available as a CAMx pre-processor. TUV includes photolysis data (cross-sections and quantum yields) for many species and data for other species are included in IUPAC (2001), JPL (2001) and Calvert et al. (2002).

Chemical Decay Rates for Near-Source Modeling

The RTRAC methodology allows output of hourly chemical decay rates at user-specified locations for input to an external point-source dispersion model (e.g., a Gaussian or Langrangian plume/puff model). This methodology was developed for "fenceline" sub-grid scale air toxics modeling. The objective is to use the grid model (CAMx) to provide decay rate information to the plume-scale model. This approach provides flexibility in the selection of the external plume model.

If subgrid-scale near-source impacts are to be calculated, then the user inputs the locations of each of the near-source emission complexes using the CAMx Probing Tools receptor file input format. Figure 10-3 displays an example RTRAC receptor input file for the five point source complex locations for which subgrid-scale point source modeling as was used in a RTRAC air toxics applications (ENVIRON, 2002; Morris et al., 2003). At each grid cell, hourly decay rates for each air toxic compound and every vertical layer are output and can then be interfaced with the user-selected near-source plume model.

```
SINGLE CELL          Test Cell          1          42          44
SINGLE CELL          Test Cell          1          41          36
SINGLE CELL          Test Cell          1          39          36
SINGLE CELL          Test Cell          1          50          43
SINGLE CELL          Test Cell          1          34          48
```

Figure 10-3. Example RTRAC receptor input file identifying the grid cells with locations of point source complexes where hourly decay rates will be output for subgrid-scale point source modeling (see format for OSAT receptor file in Table 6-2).

10.2 SOURCE-RECEPTOR RELATIONSHIPS AND DOUBLE COUNTING

Separate families of RTRAC reactive tracer compounds can be simulated using separate emission inputs following the same procedures as used by OSAT (see Section 6). Simulating separate families of RTRAC tracers allows the calculation of source apportionment and can be used to avoid double counting when a subgrid scale plume model is used to obtain near-source impacts. For example, in the RTRAC air toxics example application discussed previously, separate air toxic emission inputs were provided to obtain source apportionment by on-road mobile sources, area plus non-road sources, point sources, and secondarily formed species (ENVIRON, 2002; Morris et al., 2003). Separate families of RTRAC air toxics tracers were also used for each point source complex being simulated by the subgrid-scale plume model so that the total air toxics impact near the point sources could include the plume model's local impact due to the local point source complex plus the regional grid model's impacts due to all emissions but those from the local point source complex.

10.3 RTRAC IN IRON PiG

RTRAC calculations for emissions and chemistry have been integrated into the IRON PiG algorithms. There are two ways in which RTRAC tracers may enter a PiG plume: as primary emissions from specifically flagged sources within the RTRAC point source file, or by formation of secondary species from decay of primary plume emissions. There is no entrainment of tracers from the grid to the plume as this is likely to result in negative tracer concentrations, especially if the entrained tracer is a secondary product of a host model species (e.g., secondary formaldehyde). Tracers are assumed to have negligible impact on PiG puff chemistry or oxidant levels. If the tracer concentration in the plume is high enough to enhance or suppress the plume oxidant levels, then the photochemical impacts of the tracer can be accounted for by separately adding the tracer emissions into the host model lumped emissions; e.g., for tracing high concentrations of propene and butene in a plume, one would track the propene/butene concentrations using RTRAC tracers but also add CB4-OLE or SAPRC99-OLE1 emissions to the plume to account for the oxidant impacts.

RTRAC checks to ensure that it is reading it's own input point source file. RTRAC and host model point source files must have the same number of sources in the same order; however, the list of species on each file may be different, and the sources flagged to receive the PiG treatment may vary. A pre-processor program was coded to help prepare consistent RTRAC and host model point source files.

Tracers released from PiG sources decay according to the oxidant and photolytic environment of the plume using user-supplied chemical rate parameters (as described earlier). Oxidant concentrations for the decay calculation are obtained from the CAMx PiG incremental photochemical simulation for each puff at each time step. RTRAC tracers in each puff reactor are updated based on the *total* oxidant concentrations for the reactor, i.e., puff increment plus puff ambient/background. RTRAC enforces a rule that no secondary tracer formation from the decay of host model species are allowed if IRON PiG is active (e.g., no secondary formaldehyde tracer formation is allowed with IRON PiG). Secondary tracer production from primary tracer decay is allowed.

Tracers are transferred from the PiG to the grid using the same approach as for any other host model species (see Section 4). Tracer concentrations at any point are the superposition of the grid concentration plus any collocated PiG puffs.

Integration of RTRAC Puff Sampling

RTRAC optionally employs surface-layer IRON puff sampling of tracers on a user-defined grid of arbitrary horizontal resolution, similarly to the way nested grids are defined. Sampling of core CB-IV or SAPRC99 species is not performed. Sampling grids are entirely passive, and intended to provide a display of the reactive tracer plume concentrations at scales much smaller than typically used for the finest computational grids (i.e., <1 km).

Given that the puffs constantly evolve via diffusive growth and reshaping due to deforming shears, the sampling procedure includes trigonometric calculations to define which sampling points are influenced by each puff. To determine this influence, puffs are assumed to exhibit a

two-dimensional Guassian shape in the horizontal, and are considered well-mixed in the vertical. The cross-puff σ_y defines the concentration variations in width, while a σ_x is diagnosed from the sum of puff length and σ_y to define the concentration variation in length. To include a sufficiently large percentage of mass across each puff for sampling, limits of $\pm 3\sigma$ in both horizontal dimensions are used to define the puffs' total elliptical area coverage.

Figure 10-4 shows an example plume of hypothetical tracer "TRAC1" emitted from a point source in the center of the image as displayed on a 1-km sampling grid. The finest core model computational mesh contains 4-km grid spacing and covers a much broader area than shown in the figure.

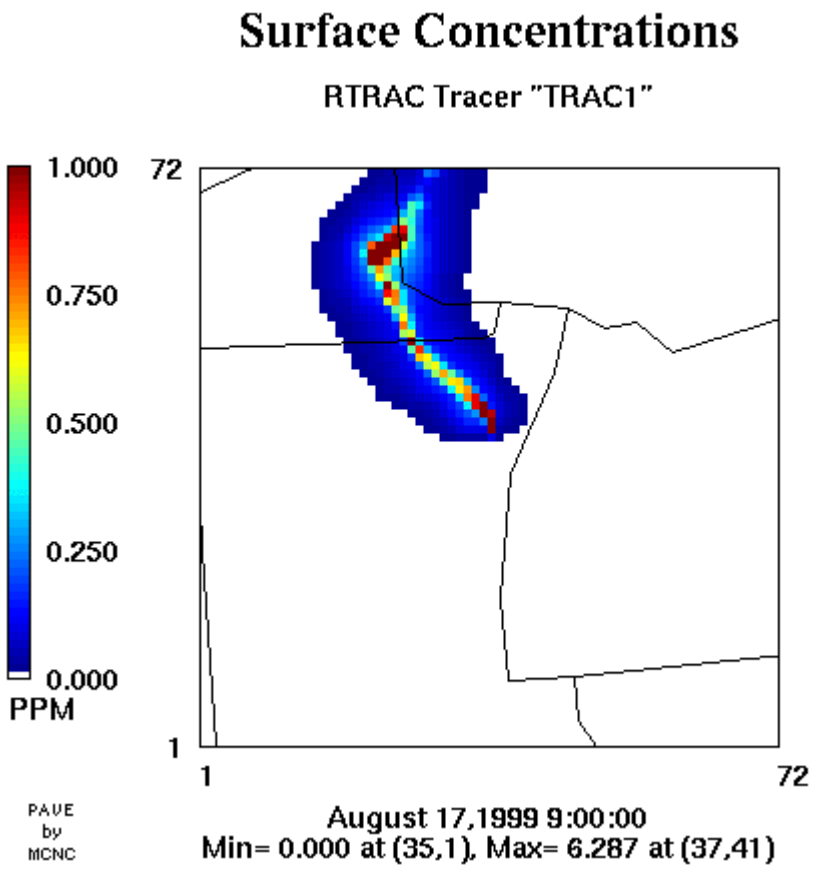

Figure 10-4. Example RTRAC tracer plume emanating from a large point source and displayed on a surface sampling grid with 1-km grid spacing. The figure illustrates the entire extent of the sampling grid.

10.4 RUNNING CAMx WITH RTRAC

CAMx Control File

RTRAC is invoked similarly to the other Probing Tools within the CAMx control file. In the `&CAMx_Control` namelist module, the variable `Probing_Tool` must be set to "RTRAC". An additional namelist module called `&RT_Control` must then be provided in the control file to configure the RTRAC portion of the model. The additional namelist module is described below. The order of the variables follow the template available with the source code.

Description of RTRAC Control in the CAMx Run Control File

`&RT_Control`	Label for the Probing Tool namelist module that configures the RTRAC option; it must begin in column 2
`&`	Flag ending a namelist; it must be in column 2
`RT_File_Root`	Character root output path/filename
`RT_Initial_Conditions`	Character input master grid RTRAC initial conditions path/filename (optional, ignored if `Restart=TRUE`)
`RT_Boundary_Conditions`	Character input master grid RTRAC boundary conditions path/filename (optional)
`RT_Top_Concentrations`	Character input master grid RTRAC top boundary conditions path/filename (optional)
`RT_Master_Restart`	Character input master grid RTRAC restart path/filename (ignored if `Restart=FALSE`)
`RT_Nested_Restart`	Character input nested grid RTRAC restart path/filename (ignored if `Restart=FALSE` or `Number_of_Grids=1`)
`Sampling_Grid`	Logical sampling grid flag for RTRAC IRON PiG output (TRUE=sampling grids are specified, FALSE=sampling grids will not be generated)
`Number_of_Sampling_Grids`	Integer number of sampling grids
`SG_Beg_I_Index`	Integer array (by sampling grid) master grid column containing western edge of sampling grid
`SG_End_I_Index`	Integer array (by sampling grid) master grid column containing eastern edge of sampling grid
`SG_Beg_J_Index`	Integer array (by sampling grid) master grid row containing southern edge of sampling grid

SG_End_J_Index	Integer array (by sampling grid) master grid row containing northern edge of sampling grid
SG_Mesh_Factor	Integer array (by sampling grid) cell size relative to master grid
RT_Chemistry_Parameters	Character input RTRAC chemistry parameters path/filename
RT_Receptor_Definitions	Character input RTRAC receptor definition path/filename
RT_Point_Sources	Character input RTRAC elevated point source emissions path/filename (optional, ignored if Point_Emissions=FALSE)
RT_Emiss_Grid	Character array (by CAMx grid) input RTRAC gridded emissions path/filename (optional, ignored if Gridded_Emissions=FALSE)

As with the output for the host model and other Probing Tools, a "root" file name is specified and suffixes are added depending upon the type of output produced. A separate root name for RTRAC (and other Probing Tools) allows the user to direct the output to a completely different path.

RTRAC/IRON PiG sampling grids are invoked in the RTRAC namelist by setting a logical flag. If set to TRUE, the user must provide the number of sampling grids and the grid parameters of each. Sampling grids are set identically to the way nested grids are specified for the host model, with one exception: there are no vertical levels to define (sampling grids are currently only 2-D surface fields). The same rules that apply for the specification of nested grids holds for the specification of all sampling grids (see Section 2 of the User's Guide). The "mesh factor" sets the resolution or cell size of the sampling grid relative to the master grid. In the example shown in Figure 10-5, the master grid contains 36-km cells, and a sampling grid meshing factor of 36 results in 1-km grid sampling cells. The CAMx diagnostic output file provides information on the location and size of each sampling grid to help ensure proper setup.

Once the RTRAC chemistry parameters file is established, the user should be sure that a sufficient allocation of memory is provided for this Probing Tool. This is done by examining the main Probing Tool parameter and common block file in /Inc/tracer.com. The parameter MXTRSP should be set to the total number of species defined in the chemistry parameters file. If sampling grids are to be used, the user should ensure that sufficient memory is available to define the size of sampling grid arrays. This is also set in /Inc/tracer.com. The parameters MXSAMPLE defines the number of sampling grids, while MXCOLS and MXROWS should be set to the maximum number of rows and columns expected among all sampling grids to be run (see Section 11).

```
&RT_Control

 RT_File_Root            = 'CAMx4.test.020614',

 RT_Initial_Conditions   = ' ',
 RT_Boundary_Conditions  = ' ',
 RT_Top_Concentrations   = ' ',
 RT_Master_Restart       = 'CAMx4.test.020613.rt.inst.2',
 RT_Nested_Restart       = 'CAMx4.test.020613.rt.finst.2',

 Sampling_Grid            = .true.,
 Number_of_Sampling_Grids = 1,
 SG_Beg_I_Index(1)        = 17,  ! Relative to master grid
 SG_End_I_Index(1)        = 18,
 SG_Beg_J_Index(1)        = 21,
 SG_End_J_Index(1)        = 22,
 SG_Mesh_Factor(1)        = 36., ! Cell size relative to master grid

 RT_Chemistry_Parameters = 'CAMx4.chemparam.rtrac_test',
 RT_Receptor_Definitions = 'receptor.rtrac.test',
 RT_Point_Sources        = 'pt.rtrac.test',
 RT_Emiss_Grid(1)        = 'emiss.rtrac.36km',
 RT_Emiss_Grid(2)        = 'emiss.rtrac.12km',
 RT_Emiss_Grid(3)        = 'emiss.rtrac.04km',

 &
```

Figure 10-5. Example input of RTRAC options and filenames via the CAMx control file.

11. THE CAMx MODELING SYSTEM

11.1 PROGRAM STRUCTURE

CAMx is written in ANSI standard Fortran 77/90, with compiler extensions (e.g., do/enddo loop definitions) that are commonly available on most workstation and PC platforms. The program is highly modular to allow for easy substitution of alternate routines for specific processes. Each subroutine is well documented to describe the tasks performed, the input/output arguments, a history of modifications, the routine(s) from which it is called, and the routine(s) that it calls.

The Fortran source code is arranged in several directories, grouped according to function. The main source directory contains the main driver program, compile utilities, and various release notes, while sub-directories contain core model and ancillary routines according to the following:

`/CAMx`	Source code for the core model routines.
`/Inc`	"Include" files, consisting of parameters to define array dimensions and the various memory common blocks.
`/IO_bin`	Source code for Fortran binary (unformatted) I/O.
`/IO_vfm`	Source code for RAMS "VFM" output format.
`/CF_AERO`	Source code for inorganic aerosol chemistry (aqueous and thermodynamic partitioning) for the CF scheme.
`/CMU_AERO`	Source code for inorganic aerosol chemistry (aqueous and thermodynamic partitioning) for the CMU scheme.
`/SOAP`	Source code for secondary organic aerosol thermodynamic partitioning.
`/PiG`	Source code for the Plume-in-Grid sub-model, consisting of I/O and core routines that are unique to PiG.
`/CMC`	Source code for the various chemical mechanism routines.
`/HG`	Source code for the mercury chemistry routines.
`/Osat`	Source code for the OSAT Probing Tool, consisting of I/O and core routines that are unique to OSAT.
`/DDM`	Source code for the DDM Probing Tool, consisting of I/O and core routines that are unique to DDM.

/PA	Source code for the Process Analysis Probing Tool, consisting of I/O and core routines that are unique to PA.
/Rtrac	Source code for the Reactive Tracer Probing Tool, consistent of I/O and core routines that are unique to RTRAC.

Figure 11-1 provides a general flow diagram of the basic process stream during CAMx execution. The diagram notes the processes that are optional and selected by the user at run-time. The diagram does not list the flow through the hundreds of individual sub-routines.

Memory Management

All of the model's large multi-dimensional variable fields are carried as single-dimension vectors. This approach makes the best use of available computer memory by alleviating the large fraction of reserved yet unused variable space that can occur with the use of multi-dimensional arrays. This dramatically reduces memory requirements when several nested grids of different shape and/or size are used.

Since the model is written almost entirely in Fortran 77, variable arrays are not dynamically allocated during runtime. All dimension declarations are static and defined in the common block include files that reside within the /Inc sub-directory. Therefore, before model compilation, the user should tailor CAMx to the specific memory requirements for the given application. This is easily accomplished by setting various parameters in the camx.prm, section.inc, section_aq.inc, and tracer.com files within the /Inc sub-directory. The parameters that the user would typically need to modify are listed below.

camx.prm

Parameters for grid dimensions:

To make best use of available memory, change the following parameters to correspond to the dimensions of each simulation grid. Set these parameters to 0 for unused grid numbers. CAMx currently allows up to 10 grids to be defined.

MXCOLn	number of columns in grid n
MXROWn	number of rows in grid n
MXLAYn	number of layers in grid n

The parameters below must be set to the maximum values among the numbered set above.

MXCOLA	maximum number of columns among all grids
MXROWA	maximum number of rows among all grids
MXLAYA	maximum number of layers among all grids
MX1D	maximum number of cells in any direction in any grid

Parameters for point source data:

MXPTSRC	maximum number of point sources
MXPIG	maximum number of PiG puffs

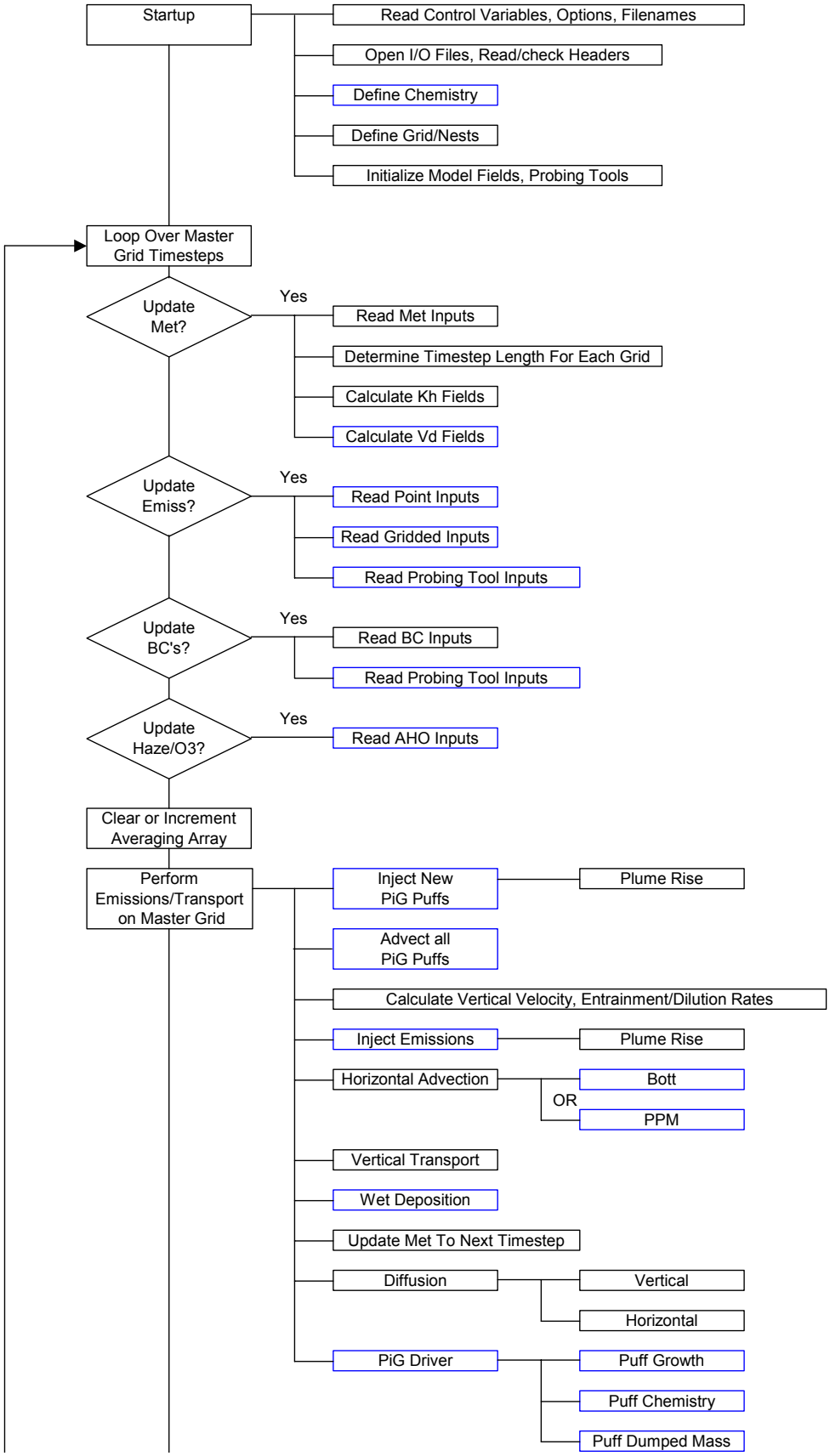

Figure 11-1. Flow diagram of the basic CAMx process stream. Optional components are shown in blue.

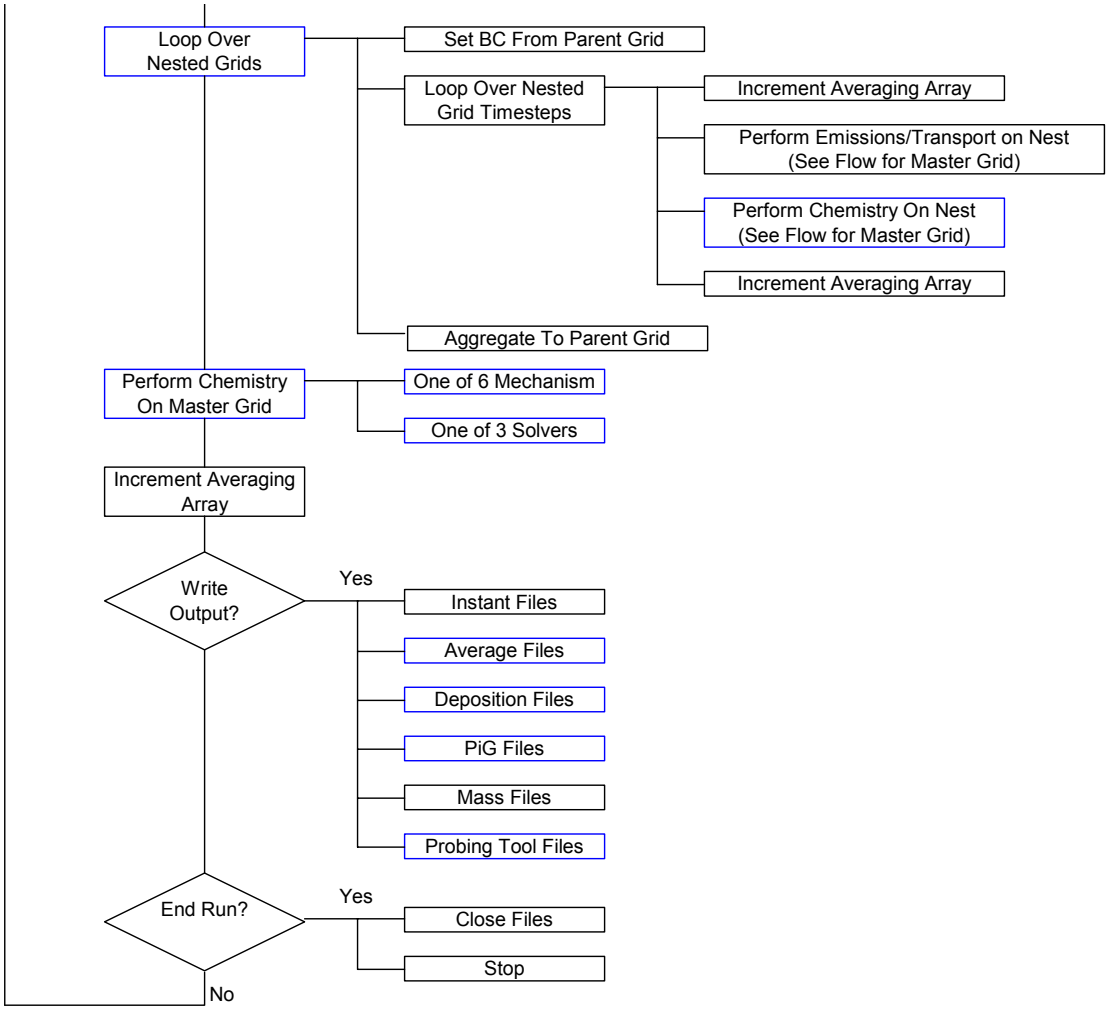

Figure 11-1. (Concluded).

Parameters for chemistry:

MXSPEC maximum number of total simulated species (gases + aerosols)
If the multi-section CMU aerosol scheme is to be run, the following formula must be used to determine this value:
MXSPEC = ngas + naero*nsec, where the value of each parameter is defined in the chemistry parameters file.

section.inc

Parameters for the CMU aerosol scheme:

NSEC number of aerosol size sections

section_aq.inc

Parameters for the RADM aqueous chemistry algorithm:

NSECT number of aerosol size sections

tracer.com

Parameter for number of tracer species used by the "Probing Tools": OSAT, DDM, PA, and RTRAC:

MXTRSP The value of this parameter greatly affects the amount of memory required by the model. Read the instructions in tracer.com to see how to set this parameter. For a simulation without "Probing Tools", set MXTRSP=1.

Parameters for RTRAC IRON PiG sampling grids:

MXSAMPLE Maximum number of RTRAC sampling grids
MXCOLS Maximum number of RTRAC sampling grid columns
MXROWS Maximum number of RTRAC sampling grid rows

All of the above parameters can be determined before starting a simulation except for MXPIG. A value of 10,000 is usually sufficient for most applications. If this parameter is exceeded during a simulation, the model will halt. Simply increase MXPIG, recompile the model executable, and restart the simulation if this happens. The other parameters in these files will not normally need to be changed and are not discussed further. If you encounter limits in other parameters, consider sending email to camxusers@environ.org for help.

11.2 COMPILING CAMx

A single "Makefile" script is provided in the main source directory. The Makefile will compile the CAMx Fortran source code into an executable program for a number of Unix and Linux computer platforms, including: DEC, Sun, SGI, HP, IBM, and Linux PC (Portland Group or Intel compilers). CAMx is compiled by issuing the following command at a shell prompt within the main source directory:

make *platform* <DOMAIN=*domain_name*>

where the text within the brackets "<>" is optional, and *platform* is one of the following:

dec
sun
hp
ibm
sgi or sgiomp
pg_linux or pg_linuxomp (Portland Group compiler)
i_linux or i_linuxomp (Intel compiler)

These keywords inform the Makefile of the type of machine being used to compile and run the model, so that the Makefile can invoke the proper compiler-specific commands and flags. The "omp" options are discussed in the sub-section on parallel processing below.

The optional *domain_name* allows the CAMx executable program to be labeled for a specific domain configuration as defined within the CAMx parameters file described above. The Makefile will search for a CAMx parameters file in the /Inc sub-directory called

camx.prm.domain_name.

If the variable "DOMAIN" is not defined on the Makefile command line, the Makefile uses the default label "mrpo.36.12", and will compile CAMx using the parameters file that defines the MRPO test case domain configuration. The MRPO parameters file is supplied with the source code so that the model may be run using the test case inputs that are distributed with the model.

The Makefile will generate a CAMx executable program named

CAMx.*domain_name.platform*

which will reside in the main source directory.

All chemistry mechanisms (1 through 5) and solvers are compiled together into the model executable from the /CMC sub-directory. The choice of which chemistry mechanism and solver to use is selected at model run-time as defined in the chemistry parameters and run control files, respectively. Similarly, all OSAT, DDM, Process Analysis, and RTRAC source are compiled into the model executable from their respective sub-directories. The choice of which (or none) of these "Probing Tools" to use is selected at model run-time in the run control file.

Parallel Processing

There are two main approaches to parallel processing: (1) OpenMP (OMP) for "shared-memory" or "symmetric multi-processing" machines (multiple CPUs on a single motherboard sharing common memory, such as a dual-processor PC); and (2) Message Passing Interface

(MPI) for distributed-memory computers (multiple networked CPU nodes operating with their own memory, such as a multi-node cluster of PCs).

Currently, the CAMx multi-processor capability uses OMP compiler directives (www.openmp.org). The code was developed and tested on dual-processor Linux machines using Portland Group and Intel compilers. The code has also been successfully tested on an SGI workstation for up to 16 processors. Tests on a Sun workstation in mid-2001 found that the Sun FORTRAN compiler did not support OMP, but that third-party software from Kuck and Associates (www.kai.com) did enable CAMx to run on a dual-processor Sun. The current CAMx Makefile includes platform options for `linuxomp` and `sgiomp` that have been tested. Consult the CAMx release notes for guidance on setting shell variables for OMP at run time.

The capability to use CAMx on distributed-memory computer clusters using MPI will be available in a future release.

A Note on Binary Input/Output Files

Certain CAMx input and output files are written as Fortran "unformatted" (binary) files. This means that the data are written directly to the output unit as represented in memory, without translation from binary to the ASCII character set. This reduces file volume and improves read/write speed. However, there are two ways to represent machine-level formats for storing binary information in memory: IEEE "big endian" and "little endian". The difference between these is essentially the order of the bits in a word, and which order is used depends on the computer platform and its operating system. The native format for many Unix workstations is big endian, and this includes Sun, SGI, HP, and IBM. Exceptions are DEC and Linux PCs, which use little endian by default.

In general, CAMx can be run on machines that use either the big or little endian binary formats, as long as the model and all of its pre- and post-processors are consistently run on the same type of platform. If any component of the modeling system is run on a different platform using the opposite binary representation, I/O files will not be properly read and will likely lead to a program crash.

In practice, user's should begin by using the same binary format as the CAMx MRPO test problem that is distributed with the model. The test problem is in IEEE big endian format. To run the CAMx test case, therefore, you must compile the source code for the big endian format (this is the default for Sun, SGI, HP, and IBM workstations). For Unix DEC workstations, this requires the compiler option "`-convert big_endian`," and this is built into the CAMx Makefile. For Linux PCs, the only compilers known to support big endian are the Portland Group and Intel compilers. Therefore, you cannot use the GNU compiler with the test case. The Portland Group compiler option is "`-byteswapio`", whereas the Intel compiler option is "`-convert big_endian`"; both of these are built into the CAMx Makefile. Therefore, use of the CAMx Makefile on any of the supported platforms will by default result in the model reading and writing big endian binary files.

A typical run-time error message from using the wrong binary format is "input record too long," so if you get this error message, check for consistency between your binary files and compiler options.

Running CAMx with Namelist Input

The CAMx control file (CAMx.in) changed to a Fortran Namelist format with the release of CAMx v4.20. A description of the format and contents of this file is provided in Section 5 (core model) and Sections 6 through 10 (Probing Tools). Therefore, job scripts and control files developed for previous versions of CAMx ***will not work with v4.20 and later***. To facilitate migration of existing applications to v4.20, we have provided two new files in the source directory:

`CAMx.namelist.template`
This file contains a complete list of the namelist variables needed to configure the model and to choose various in CAMx options. Use this as a reference when creating your CAMx control file by scratch.

`convert.camxin.prl`
This is a PERL script that will convert an existing control file from a previous version of CAMx to the current namelist format. Use this to create your application-specific template, or alternatively, use this conversion script within your existing CAMx job script. Please be aware that this script will not work with any control file in which probing tools have been activated. The syntax is:

```
perl convert.camxin.prl CAMx.in.myapp
```

This will create a namelist-style control file called "`CAMx.in.myapp.namelist`" with all of the appropriate variables assigned to the values defined in the previous control file "`CAMx.in.myapp`".

Common Errors When Creating a Namelist

Fortran programs ingest the entire contents of namelist files using a single READ statement. If the program experiences an error reading the namelist, it echoes a simple error message like "error reading namelist" and stops. It is therefore difficult to determine why the read of the namelist has caused an error, especially if the namelist is lengthy and contains a variety of data types. When experiencing an error reading the CAMx control file namelist, you must carefully inspect the file for any syntax errors. These errors can be subtle and difficult to spot. Here are a few of the common reasons an error occurs when reading a namelist:

- *Mistyped variable name*:
  All variables to be assigned within a namelist must be recognized as a declared namelist variable within the reading program. If a variable is mispelled or an unknown variable is assigned a value, a read error will occur.

- *Incorrect data type for the assigned variable*:
  If the data type of the value assigned to a namelist variable does not match the variable's declared data type within the reading program, an error will occur. Some compilers will allow real type variables to be assigned to integer values, but not the converse.

- *Missing period around a logical value*:
  The logical values `.true.` and `.false.` must be surrounded by a period.

- *Missing quotes around a character variable*:
  Any character data type must be surrounded by quotes.

- *Overflow when assigning values to an array*:
  The values in an array can be assigned using array index notation. If the index used to assign an array value exceeds the declared dimension of the array, a read error occurs.

- *Wrong number of dimensions when assigning values to a multi-dimensional array*:
  When assigning values to an array using array index notation, the number of subscripts in the assignment must match the declared dimensions of the array (e.g., assignments to an array dimensioned `var(i,j)` must be referenced using two indices).

- *Missing comma following a variable definition*:
  A comma must be the last character in a "`variable = value,`" assignment. A comment may be placed after the comma (delimited using the "`!`" symbol, see below) on the same file record. This restriction on the use of commas is ignored on some compilers.

- *Too many commas following a scalar variable definition*:
  More than one comma following a scalar variable assignment will result in a read error.

- *Too many commas following the variable assignment list for an array*:
  The entire contents of an array can be assigned using a single statement by listing the values of each element separated by commas. The read will fail if there are more commas than the dimension of the array.

- *Comment does not begin with !*:
  The character that delimits a comment in a namelist is the exclamation point. Comments can appear anywhere within the namelist. However, all text in the namelist must either be part of a namelist variable assignment or part of an identified comment.

Benchmarking Model Run Times

Table 11-1 provides some example CAMx configurations and associated system requirements when run on a dual-processor Linux PC (with and without OMP). All of these tests utilized the CMC fast solver for the CB-IV gas-phase mechanism.

Table 11-1. Example of computer requirements for several CAMx configurations on a dual-processor Athlon 2800+ (2.1Ghz) PC.

Configuration	Memory	Disk Usage	CPUs	Execution Time
1 grid MRPO domain (97 x 90 x 14) ~123,000 grid cells Mechanism 3 (25 species)	112 mB	564 mB/episode day	1	24 min/ episode day
1 grid MRPO domain (97 x 90 x 14) ~123,000 grid cells Mechanism 3 (25 species)	112 mB	564 mB/episode day	2	16 min/ episode day
2 grids MRPO domain (97 x 90 x 14) and (119 x 134 x 14) ~ 346,000 grid cells Mechanism 3 (25 species)	248mB	960 mB/epidode day	2	1 hr/ epsiode day
2 grids MRPO domain (97 x 90 x 14) and (119 x 134 x 14) ~ 346,000 grid cells Mechanism 4 CF (50 species)	306 mB	1.2 gB/epidode day	1	2.5 hrs/ epsiode day
2 grids MRPO domain with OSAT (97 x 90 x 14) and (119 x 134 x 14) ~ 346,000 grid cells Mechanism 3 (25 species) 16 OSAT source regions 2 OSAT source groups Total OSAT tracers = 136	506 mB	1.6 gB/episode day	2	4 hrs/ episode day
2 grids VISTAS domain (148 x 112 x 19) and (170 x 179 x 19) ~ 608,000 grid cells Mechanism 4 CMU (4 sections, 86 total species)	1 gB	2.3 gB/episode day	1	8 hrs/ episode day

11.3 CAMx AS PART OF A MODELING SYSTEM

CAMx comprises the core component of an overall air quality modeling system, as illustrated in Figure 11-2. Model inputs are developed using other modeling and processing tools that characterize meteorology, emissions, and various other environmental characteristics (land cover, radiative/photolysis properties, and initial/boundary conditions). Interface programs are often needed to translate the products of each model into the specific input fields and formats required by CAMx. After the air quality simulation is completed, additional programs are used to process/format concentration fields, develop model performance statistics and measures, process Probing Tool output into various reportable formats, and further translate raw results into forms necessary for regulatory purposes (e.g., reporting 8-hour RRF design value scaling measures to demonstrate attainment). While third-party visualization software and models for emissions and meteorology are not distributed with CAMx, ENVIRON does provide many of the necessary interface programs, pre-processors, and post-processors on the CAMx web site (www.camx.com). A brief description of these is provided below.

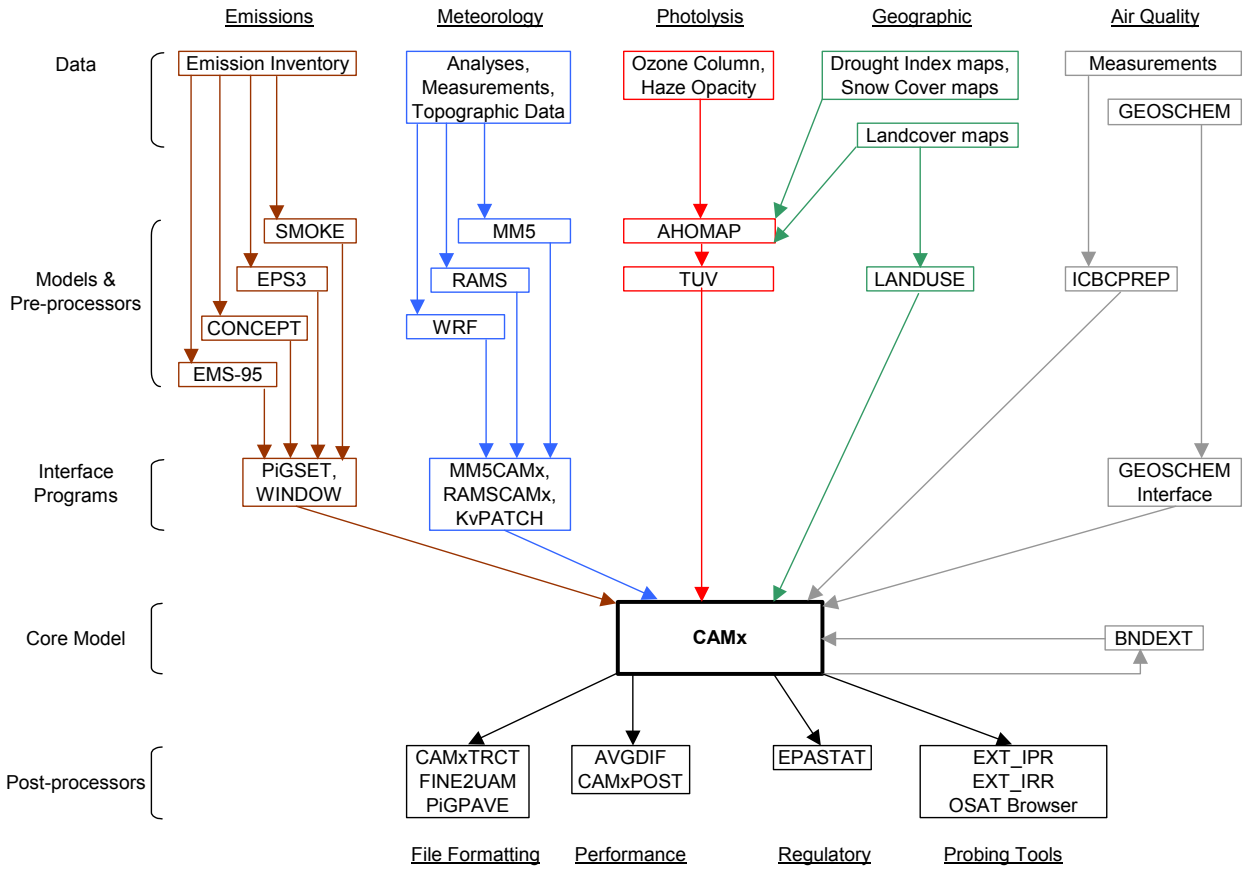

Figure 11-2. Schematic diagram of the CAMx modeling system. See Table 5-1 for a detailed list of specific model input requirements for the five major data classes shown at the top of the figure. Certain pre- and post-processor programs shown in the figure are described in the Section 11 text. Third-party models and preprocessors for emissions, meteorology, and the GEOSCHEM interface are not described in this User's Guide and are not distributed with CAMx. CAMx does not include graphics software in its distribution, nor does ENVIRON promote the use of any particular visualization applications. Common third-party graphics packages used with CAMx include PAVE, Surfer®, and Grads.

CAMx Pre- and Post-Processors

This section describes a variety of CAMx pre- and post-processors that we have made available to the user community. These programs are distributed by ENVIRON as free software. As such, they contain notices like this in the source code:

```
ccccccccccccccccccccccccccccccccccccccccccccccccccccccccccccccccccccccc
c Copyright (C) 2003  ENVIRON
c
c This program is free software; you can redistribute it and/or
c modify it under the terms of the GNU General Public License
c as published by the Free Software Foundation; either version 2
c of the License, or (at your option) any later version.
c
c This program is distributed in the hope that it will be useful,
c but WITHOUT ANY WARRANTY; without even the implied warranty of
c MERCHANTABILITY or FITNESS FOR A PARTICULAR PURPOSE.  See the
c GNU General Public License for more details.
c
c To obtain a copy of the GNU General Public License
c write to the Free Software Foundation, Inc.,
c 59 Temple Place - Suite 330, Boston, MA  02111-1307, USA.
ccccccccccccccccccccccccccccccccccccccccccccccccccccccccccccccccccccccc
```

ENVIRON occasionally posts updates for certain widely-used programs when necessary, but does not actively support or maintain every one. Users can e-mail questions, comments, suggestions or improvements to camx@environ.org.

Emissions

Most emission models (those shown in Figure 11-2) can provide speciated, temporally-allocated, gridded and point source emission input files in the CAMx-ready format. Further processing may be required, however, to select point sources for the PiG treatment, translate the point source files from a common ASCII text format to CAMx-ready binary files, or to refine the domain size/resolution for gridded emissions. There are two interface programs that perform these operations.

PIGSET: This program allows the user to select and set certain point sources for the Plume-in-Grid (PiG) treatment in a CAMx simulation. It also converts ASCII point source files commonly generated by emission models to CAMx-ready binary format. See the source code for more information, and the sample job for usage. Also see Section 4 for guidance in selecting PiG point sources and manipulating day-specific point source files.

WINDOW: This program is used to "window" out a sub-section of the surface emissions grid for use on a smaller CAMx grid. It can also be used to aggregate or interpolate surface emissions to coarser or finer resolution, respectively. See the sample job for usage.

Meteorology

The recommended approach to develop meteorological inputs for CAMx is through the use of prognostic meteorological models. Currently, the most common of these is MM5 and RAMS, and ENVIRON provides interface programs for these specific models. This does not

necessarily preclude other meteorological models to be used, but users will need to develop interface programs on their own.

MM5CAMx: This program generates CAMx v4 meteorological input files from MM5 v3 output files. See the README in the archive for a description of the program and how it is applied.

RAMSCAMX: This program generates CAMx v4 meteorological input files from RAMS v4 output files. See the README in the archive for a description of the program and how it is applied.

KVPATCH: This program applies minimum Kv values to layers below 100 m based on an input landuse grid. Minimum Kv's are determined from a weighted average of landuse for each cell, where each landuse is assigned a Kv value. See the source code for more information. Use of this program to adjust Kv inputs is entirely optional.

Photolysis Rates

The development of photolysis rate inputs for CAMx is crucial for the photochemical mechanisms, but is not needed for inert or simple chemistry (e.g., Mechanism 10) applications. Two programs are available to assist the user in developing photolysis and albedo/haze/ozone input files.

AHOMAP: This program prepares albedo/haze/ozone column input files for CAMx, and must be run prior to running the TUV model as it defines the albedo, haze, and ozone column intervals based on input data. A CAMx-ready landuse file and TOMS ozone column data files (http://jwocky.gsfc.nasa.gov/) must be supplied as input. The program assumes a constant haze turbidity value for the entire grid. NOTE: gaps in day-specific TOMS data at low latitudes, and high latitudes during winter, may result in zero ozone column values over portions of the modeling grid (see Figure 11-3). This results from the inability of polar-orbiting satellite platforms to cover the entire globe on a daily basis. The user may instead use seasonal-average TOMS input files (no data gaps); alternatively, AHOMAP provides an option to fill these day-specific gaps with an average determined from valid data processed for the extraction domain. See the Readme file and job script in the archive for usage.

TUV: This program develops photolysis rate inputs for all CAMx CB-IV and SAPRC99 photochemical mechanisms via a delta-Eddington radiative transfer model. TUV originates from UCAR (http://acd.ucar.edu/~siri/tuv.html). The program uses the albedo, ozone column, and haze turbidity intervals defined in AHOMAP. See the sample.job in the archive for usage.

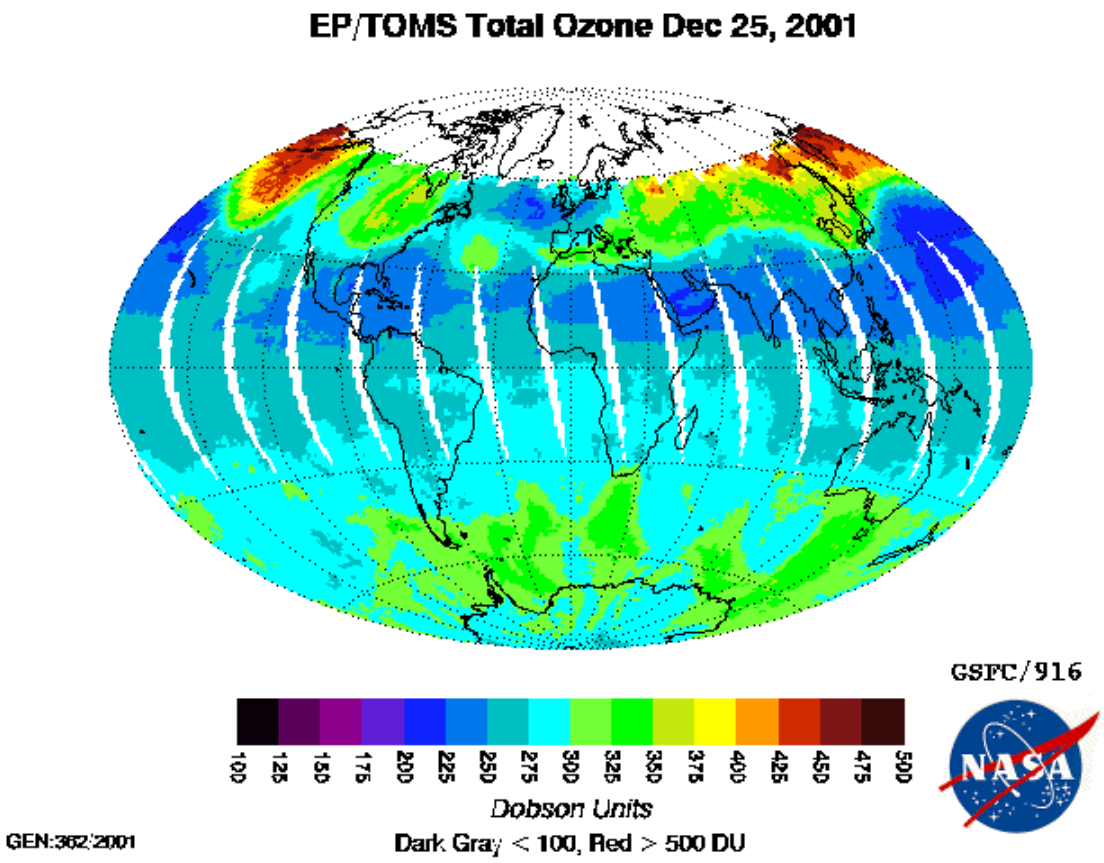

Figure 11-3. An example of global ozone column from the Earth Probe TOMS platform. White areas denote missing data. From http://jwocky.gsfc.nasa.gov/.

Air Quality

There are numerous approaches for defining initial, boundary, and top concentration inputs for CAMx. The level of possible detail ranges from time- and space-constant values for all pollutants, to specific time and space profiles for each. The level of detail depends on available measurements, focus and detail of the modeling exercise, and scale considerations (e.g., local vs. continental domains). ENVIRON provides one simple program, as described below. Another approach gaining popularity is to extract initial and boundary conditions for large regional applications from global-scale chemical transport models, such as GOESCHEM. Interface programs have been developed for this purpose, but are not distributed by ENVIRON. Users will need to develop their own programs if they choose an alternative methodology to generate initial/boundary conditions.

ICBCPREP: This program prepares CAMx initial condition (IC) and boundary condition (BC) files. Values are constant in space and time, but unique values may be specified for each chemical species to be modeled; they are defined by the CAMx ASCII top concentration file. See the file sample.job in the archive for usage.

Landuse

Approaches for developing landuse/landcover inputs for CAMx (and for AHOMAP) are about as varied as they are for initial/boundary conditions. Popular approaches have included: (1) translating gridded spatial allocation surrogates developed during emissions processing into the CAMx categories described in Section 5; (2) translating the gridded landuse/landcover fields from the meteorogical model; or (3) separately developing landuse input fields from raw data (such as from USGS) using GIS or other programs. The advantages of (1) are consistency with input emissions estimation methodologies, and the fact that land cover processing is done just once. The advantages of (2) are similar consistency with the meteorological modeling and one-time processing, but most models assign a single dominant landuse to each grid cell, which may not be representative for coarse-resolution grids (CAMx allows a distribution of multiple land cover types per cell). The third option is generally not performed much anymore. ENVIRON offers a single simple program for the third option, as described below.

LANDUSE: This program reads USGS 1:250,000 quad maps of 200 m pixel landuse/ landcover, and converts to CAMx landuse input format. See the source code for more information.

Post-processors

Most of the CAMx post-processors provided by ENVIRON provide some manner of concentration file manipulation, either to extract certain information from the raw output files, to re-format for use in other programs and applications, to concatenate files, etc. A few others are provided to assist in evaluating Probing Tool output. As stated above, ENVIRON does not provide any visualization or graphics software other than a few Excel® spreadsheet macros.

AVGDIF: This program is used to compare two UAM-IV format files and print a table of differences. This is useful for checking differences between CAMx runs on different machines or different compile options for the test case. Note that the CAMx master grid output file is in UAM-IV format, but the nested grid output file needs to first be translated into that format before AVGDIF can be used (see FINE2UAM below). See the file sample.job in the archive for usage.

BNDEXTR: Use this program to extract boundary conditions for a nested grid when you apply CAMx in one-way nesting mode. One-way nesting means that CAMx is run successively for each grid, with BNDEXTR as the interface between each run. This program is not needed when CAMx is run in the more standard two-way nesting mode, where all grids are run in a single simulations. See the example job for usage.

CAMxPOST: This is a suite of post-processing utilities designed to facilitate the evaluation of model performance. It is used to combine observations and predictions, calculate statistics, and plot time series. See the README file in the archive for usage.

CAMxTRCT: This program extracts specified chemical species for specified grids from the output average concentration and deposition files, and from input emission files. All

output from this program is written in the standard UAM-IV format (master grid output format). It also has the capability to convert units. See the file sample.job in the archive for usage.

EXT_IPR: This program extracts IPR data from one or more CAMx IPR Process Analysis output files and reformats the data to comma delimited ASCII format (.csv) suitable for subsequent analysis (e.g. using spreadsheets).

EXT_IRR: This program extracts IRR data from one or more CAMx IRR Process Analysis output files and reformats the data to comma delimited ASCII format (.csv) suitable for subsequent analysis (e.g. using spreadsheets).

FINE2UAM: This program converts nested grid output files (e.g., *.favrg) to master grid (e.g., *.avrg) format. This is useful for post-processing (e.g., bypasses the need for PAVE metafiles). See the sample.job in the archive for usage.

12. REFERENCES

Anthes, R.A. and T.T. Warner. 1978. Development of Hydrodynamic Models Suitable for Air Pollution and Other Mesometeorological Studies. *Mon. Wea. Rev.*, **106**, 1045-1078.

Ariya, P.A., A. Khalizov and A. Gidas. 2002. Reactions of gaseous mercury with atomic and molecular halogens: kinetics, product studies, and atmospheric implications. *J. Phys. Chem.*, **106**, 7310-7320.

Bott, A. 1989. A Positive Definite Advection Scheme Obtained by Nonlinear Renormalization of the Advective Fluxes. *Mon. Wea. Rev.,* **117**, 1006-1015.

Calvert, J.G., R. Atkinson, J.A. Kerr, S. Madronich, G.K. Moortgat, T.H. Wallington and G. Yarwood. 2000. *The Mechanisms of Atmospheric Oxidation of the Alkenes*. Oxford University Press, New York, New York.

Calvert, J.G., R. Atkinson, K.H. Becker, R.M. Kamens, J.H. Seinfeld, T.H. Wallington and G. Yarwood. 2002. *The Mechanisms of Atmospheric Oxidation of the Aromatic Hydrocarbons*. Oxford University Press, New York, New York.

Carter, W.P.L. 1996. Condensed Atmospheric Photooxidation Mechanisms for Isoprene. *Atmos. Environ.,* **30**, 4275-4290.

Carter, W.P.L. 2000. Programs and Files Implementing the SAPRC-99 Mechanism and its Associates Emissions Processing Procedures for Models-3 and Other Regional Models. January 31, 2000. http://pah.cert.ucr.edu/~carter/SAPRC99.htm

Chang, J.S., R.A. Brost, I.S.A. Isaksen, S. Madronich, P. Middleton, W.R. Stockwell, and C.J, Walcek. 1987. A Three-dimensional Eulerian Acid Deposition Model: Physical Concepts and Formulation. *J. Geophys. Res.*, **92**, 14,681-14,700.

Chock, D.P., S.L. Winkler, and P. Sun. 1994. Comparison of stiff chemistry solvers for air quality models. *Environ. Sci. Technol.*, **28**, 1882-1892.

Clever, H., S.A. Johnson and E.M. Derrick. 1985. The solubility of mercury and some sparingly soluble mercury salts in water and aqueous solutions. *J. Phys. Chem. Ref. Data*, **14**, 631-680.

Colella, P., and P.R. Woodward. 1984. The Piecewise Parabolic Method (PPM) for Gas-dynamical Simulations. *J. Comp. Phys.*, **54**, 174-201.

Dunker, A. M. 1980. The response of an atmospheric reaction-transport model to changes in input functions. *Atmos. Environ.*, **14**, 671-679.

Dunker, A.M. 1981. Efficient calculations of sensitivity coefficients for complex atmospheric models. *Atmos. Environ.* **15**, 1155-1161.

Dunker A.M., G. Yarwood, J.P. Ortmann, G.M. Wilson. 2002a. The decoupled direct method for sensitivity analysis in a three-dimensional air quality model – implementation, accuracy and efficiency. *Environ. Sci. Technol.*, **36,** 2965-2976.

Dunker A.M., G. Yarwood, J.P. Ortmann, G.M. Wilson. 2002b. Comparison of source apportionment and source sensitivity of ozone in a three-dimensional air quality model. *Environ. Sci. Technol.*, **36,** 2953-2964.

Edgerton, E.S., B.E. Hartsell and J.J. Jansen. 2001. Atmospheric mercury measurements at a rural and urban site near Atlanta, GA, USA. *6th International Conference on Mercury as a Global Pollutant*, 15-19 October 2001, Minamata, Japan.

Elbern, H. and H. Schmidt. 1999. *J. Geophys.Res.*, ***104***, 18583-18598.

ENVIRON. 2002. Development, Application, and Evaluation of an Advanced Photochemical Air Toxics Modeling System. Prepared for the Coordinating Research Council, Alpharetta, GA, and the U.S. Department of Energy, Office of Heavy Vehicle Technologies (September 27, 2002). Available from www.crcao.com.

EPA. 1990. User's Guide for the Urban Airshed Model-Volume I; User's Manual for UAM(CB-IV). U.S. Environmental Protection Agency, Research Triangle Park, NC, EPA-450/4-90-007a.

EPA. 1998. User's Guide for the AERMOD Meteorological Preprocessor (Revised Draft). Prepared by the U.S. Environmental Protection Agency, Research Triangle Park, NC (November, 1998).

EPRI. 2000. SCICHEM Version 1.2: Techical Documentation. Final Report prepared by ARAP/Titan Corporation, Princeton, NJ, for EPRI, Palo Alto, CA. December 2000 (1000713).

Fahey, K.M. and S.N. Pandis. 2001. Optimizing model performance: variable size resolution in cloud chemistry modeling. *Atmos. Environ.* **35**, 4471-4478.

Gardfeldt, K. and M. Johnson. 2003. Is bimolecular reduction of Hg(II)-complexes possible in aqueous systems of environmental importance? *J. Phys. Chem.*, in press.

Gear, C.W. 1971. *Numerical Initial Value Problems in Ordinary Differential Equations*. Prentice-Hall, Englewood Cliffs, NJ.

Gery, M.W., G.Z. Whitten, J.P. Killus, and M.C. Dodge. 1989. A Photochemical Kinetics Mechanism for Urban and Regional Scale Computer Modeling. *J. Geophys. Res.*, **94**, 925-956.

Gillani, N. V. and J. E. Pleim. 1996. Sub-grid-scale Features of Anthropogenic Emissions of NOx and VOC in the Context of Regional Eulerian Models. *Atmos. Environ.,* **30**, 2043-2059.

Guthrie P.D., G. Yarwood, S.B. Shepard and M.P. Ligocki. 1995. Fast UAM: An Example of an Adaptive Approximation Solver for Atmospheric Chemistry Problems. Presented at SciCADE95, Stanford University, March 28 - April 1, 1995.

Hall, B. 1995. The gas-phase oxidation of elemental mercury by ozone. *Water Air Soil Pollut.*, **80**, 301-315.

Hall, B. and N. Bloom. 1993. Report to EPRI, Palo Alto, CA.

Harley R. A., and G. R. Cass. 1995. Modeling the Atmospheric Concentrations of Individual Volatile Organic Compounds. *Atmos. Environ.* **29**, No. 8, 905-922.

Herman, J.R. and E. A. Celarier. 1997. Earth surface reflectivity climatology at 340-380 nm from TOMS data. *J. Geophys. Res.*, **102**, No. 23.

Hesstvedt, E., Hov, O., and Isaksen, I. S. A. 1978. Quasi-steady state approximation in air pollution modeling: comparison of two numerical schemes for oxidant prediction. *Int. J. Chem. Kin.*, 10, 4148-4156.

Hindmarsh, A.C. 1983. ODEPACK, a Systematized Collection of ODE Solvers. In *Numerical Methods for Scientific Computation,* **55**, R.S. Stepleman, Ed., North-Holland, New York.

IUPAC. 1992. Evaluated Kinetic and Photochemical Data for Atmospheric Chemistry. Supplement IV. IUPAC Subcommittee on Gas Kinetic Data Evaluation for Atmospheric Chemistry (R. Atkinson, D.L. Baulch, R. A. Cox, R. F. Hampson, Jr., J. A. Kerr, and J. Troe). *Journal of Physical and Chemical Reference Data,* **21**, No. 6, 1125-1568.

IUPAC. 2001. Evaluated kinetic and photochemical data for atmospheric chemistry. IUPAC Subcommittee for Gas Kinetic Data Evaluation. Available at http://www.iupac-kinetic.ch.cam.ac.uk/index.html. December, 2001.

Jacob, D.J. 2000. Heterogeneous chemistry and tropospheric ozone. *Atmos. Environ.*, **34**, 2131-2159.

Jaegle, L., D.J. Jacob, W.H. Brune and P.O. Wennberg. 2001. Chemistry of HOx radicals in the upper troposphere. *Atmos. Environ.*, **35**, 469-489.

JPL. 2001. Chemical Kinetics and Photochemical Data for Stratospheric Modeling -- Evaluation 13. NASA Jet Propulsion Laboratory publication 00-3. Available at http://jpldataeval.jpl.nasa.gov. February, 2001.

Kleeman, M.J. and G.R. Cass. 2001. A 3D Eulerian source-oriented model for an externally mixed aerosol. *Environmental Science and Technology*, **35,** 4834-4848.

Koo, B., A.S. Ansari, and S.N. Pandis. 2003. Integrated Approaches to Modeling the Organic and Inorganic Atmospheric Aerosol Components. *Atmos. Environ.*, **37**, 4757-4768.

Kumar, N., F.W. Lurmann, A.S. Wexler, S. Pandis, and J.H. Seinfeld. 1996. Development and Application of a Three Dimensional Aerosol Model. Presented at the A&WMA Specialty Conference on Computing in Environmental Resource Management, Research Triangle Park, NC, December 2-4, 1996.

Kumar, N. and A. G. Russell. 1996. Development of a Computationally efficient, Reactive Sub-Grid-Scale Plume Model and the Impact in the Northeastern United States Using Increasing Levels of Chemical Detail. *J. Geophys. Res.,* **101**, 16,737-16,744.

Landis, M.S. and G. Keeler. 2002. Atmospheric mercury deposition to Lake Michigan during the Lake Michigan Mass Balance Study. *Environ. Sci. Technol.,* **36**, 4518-4524.

Lambert, J. D. 1973. *Computational Methods in Ordinary Differential Equations*. John Wiley and Sons Ltd. New York.

Lin, C.J. and S.O. Pehkonen. 1997. Aqueous-free radical chemistry of mercury in the presence of iron oxides and ambient aerosol. *Atmos. Environ.*, **31**, 4125-4137.

Lin, C.J. and S.O. Pehkonen. 1998. Oxidation of elemental mercury by aqueous chlorine ($HOCl/OCl^-$): Implications for tropospheric mercury chemistry. *J. Geophys. Res.*, **103**, 28093-28102.

Lindqvist, O. and H. Rodhe. 1985. Atmospheric mercury - a review. *Tellus*, **37B**, 136-159.

Louis, J.F. 1979. A Parametric Model of Vertical Eddy Fluxes in the Atmosphere. *Bound. Lay. Meteor.* **17**, 187-202.

Madronich, S. 1993. UV radiation in the natural and perturbed atmosphere, in *Environmental Effects of UV (Ultraviolet) Radiation* (M. Tevini, ed.), Lewis Publisher, Boca Raton, pp. 17-69.

Madronich, S. 2002. The Tropospheric Visible Ultra-violet (TUV) model web page. National Center for Atmospheric Research, Boulder, CO. http://www.acd.ucar.edu/TUV/.

Mentel, Th.F., D. Bleilebens and A. Wahner. 1996. A Study of Nighttime Nitrogen Oxide Oxidation in a Large Reaction Chamber -- The Fate of NO_2, N_2O_5, and O_3 at Different Humidities. *Atmos. Environ.,* **30**, 4007–4020.

Menut L., R. Vautard, M. Beekmann, C. Honoré. 2000. Sensitivity of Photochemical Pollution using the Adjoint of a Simplified Chemistry-Transport Model. *Journal of Geophysical Research – Atmospheres,* **105,** (D12) 15,379-15,402.

Morris, R.E., S. Lau, and G. Yarwood. 2003. "Development and Application of an Advanced Air Toxics Hybrid Photochemical Grid Modeling System." Presented at 96th Annual Conference and Exhibition of the A&WMA, San Diego, California (June 2003).

Munthe, J. 1992. The aqueous oxidation of elemental mercury by ozone. *Atmos. Environ., Part A*, **26**, 1461-1468.

NASA. 1997. Chemical Kinetics and Photochemical Data for Use in Stratospheric Modeling, *JPL Publication 97-4.* Jet Propulsion Laboratory, California Institute of Technology, Pasadena, California. January 15.

Nenes, A, C. Pilinis, and S.N. Pandis. 1998. ISORROPIA: A New Thermodynamic Model for Multiphase Multicomponent Inorganic Aerosols. *Aquatic Geochemistry*, 4, 123-152.

Nenes, A, C. Pilinis, and S.N. Pandis. 1999. Continued Development and Testing of a New Thermodynamic Aerosol Module for Urban and Regional Air Quality Models. *Atmos. Environ.* 33, 1553-1560.

Novelli, P.C., P.M. Lang, K.A. Masarie, D.F. Hurst, R. Myers, and J.W. Elkins. 1999. Molecular hydrogen in the troposphere: global distribution and budget. *J. Geophys. Res.*, **104**, 30: 427-30,444.

Odman, M. T. and Ingram, C. L. 1993. Multiscale Air Quality Simulation Platform (MAQSIP): Source Code Documentation and Validation. Technical report, 83 pp., ENV-96TR002, MCNC–North Carolina Supercomputing Center, Research Triangle Park, North Carolina, 1996.

Pandis, S.N., A.S. Wexler, and J.H. Seinfeld. 1993. Secondary organic aerosol formation and transport, II, Predicting the ambient secondary organic aerosol size distribution. *Atmos. Environ.,* **27A**, 2403-2416.

Pehkonen, S.O. and C.J. Lin. 1998. Aqueous photochemistry of divalent mercury with organic acids. *J. Air Waste Manage. Assoc.*, **48**, 144-150.

Russell, L.M., S.N. Pandis, and J.H. Seinfeld. 1994. Aerosol production and growth in the marine boundary layer. *J. Geophys. Res.,* **99**, 20989-21003.

Ryaboshapko, A., R. Bullock, R. Ebinghaus, I. Ilyin, K. Lohman, J. Munthe, G. Petersen, C. Seigneur and I. Wängberg. 2002. Comparison of mercury chemistry models. *Atmos. Environ.*, **36**, 3881-3898.

Sanemasa, I. 1975. The solubility of elemental mercury vapor in water. *Bull. Chem. Soc. Jpn.*, **48**, 1795-1798.

Schroeder, W.H. and J. Munthe. 1998. Atmospheric mercury – An overview. *Atmos. Environ.*, **32**, 809-822.

Scott, B.C. 1978. Parameterization of sulfate removal by precipitation. J. Appl. Meteor., 17, 1375-1389

Sehmel, G.A. 1980. Particle and Gas Deposition, a Review. *Atmos. Environ.,* **14**, 983-1011.

Seigneur, C., H. Abeck, G. Chia, M. Reinhard, N.S. Bloom, E. Prestbo and P. Saxena. 1998. Mercury adsorption to elemental carbon (soot) particles and atmospheric particulate matter. *Atmos. Environ.*, **32**, 2649-2657.

Seigneur, C., P. Karamchandani, K. Lohman, K. Vijayaraghavan and R.-L. Shia. 2001a. Multiscale modeling of the atmospheric fate and transport of mercury. *J. Geophys. Res.*, **106**, 27795-27809.

Seigneur, C., P. Karamchandani, K. Lohman and J. Jansen. 2001b. Modeling of mercury in power plant plumes. *6th International Conference on Mercury as a Global Pollutant*, 15-19 October 2001, Minamata, Japan.

Seigneur, C., K. Vijayaraghavan, K. Lohman and P. Karamchandani. 2003a. Modeling the atmospheric fate and transport of mercury over North America. *Fuel Processing Technol.*, in press.

Seigneur, C., P. Karamchandani, K. Vijayaraghavan, K. Lohman and G. Yelluru. 2003d. *Scoping Study for Mercury Deposition in the Upper Midwest.* AER Report CP149-03-01a, prepared for the Midwest Regional Planning Organization, Des Plaines, IL.

Seinfeld, J.H., and S.N. Pandis. 1998. *Atmospheric Chemistry and Physics, From Air Pollution to Climate Change*. John Wiley and Sons, Inc., NY.

Sillen, G.L. and A.E. Martell, (Eds.). 1964. Stability constants of metal ion complexes, *Spec. Publ. Chem. Soc.*, **17**, 754.

Sillman, S. 1995. The Use of NO_y, H_2O_2, and HNO_3 as Indicators for Ozone - NO_x-Hydrocarbon Sensitivity in Urban Locations. *J. Geophys. Res.*, **100**, 14,175-14,188.

Slinn S.A. and W.G.N. Slinn. 1980. Predictions for particle deposition on natural waters. *Atmos. Environ.*, **24**, 1013-1016.

Smagorinsky, J. 1963. General Circulation Experiments with the Primitive Equations: I. The Basic Experiment. *Mon. Wea. Rev.*, **91**, 99-164.

Smolarkiewicz, P.K. 1983. A Simple Positive Definite Advection Scheme with Small Implicit Diffusion. *Mon. Wea. Rev.*, **111**, 479-486.

Sommar, J., K. Gårdfeldt, D. Strömberg and X. Feng. 2001. A kinetic study of the gas-phase reaction between the hydroxyl radical and atomic mercury. *Atmos. Environ.*, **35**, 3049-3054.

Strader, R., C. Gurciullo, S.N. Pandis, N. Kumar, and F.W. Lurmann. 1998. Development of gas-phase chemistry, secondary organic aerosol, and aqueous-phase chemistry modules for PM modeling. Final report for CRC Project A21-1 prepared for the Coordinating Research Council, Atlanta, GA by Sonoma Technology, Inc., Petaluma, CA, STI-97510-1822-FR, October.

Strader, R., F. Lurmann, and S.N. Pandis. 1999. Evaluation of secondary organic aerosol formation in winter. *Atmos. Environ.,* **33**, 4849-4863.

Sun, P., D.P. Chock, and S.L. Winkler. 1994. An Implicit-Explicit Hybrid Solver for a System of Stiff Kinetic Equations. *J. Comp. Phys.,* **115**.

Tanaka, P.L., D.T. Allen, E.C. McDonald-Buller, S. Chang, Y. Kimura, C.B. Mullins, G. Yarwood, J.D. Neece. 2000. Development of a chlorine mechanism for use in the carbon bond IV chemistry model. *Journal of Geophysical Research*. Vol. 108(D4), 4145.

Tokos, J.J.S., B. Hall, J.A. Calhoun and E.M. Prestbo. 1998. Homogeneous gas-phase reaction of Hg^0 with H_2O_2, O_3, CH_3I, and $(CH_3)_2S$: Implications for atmospheric Hg cycling. *Atmos. Environ.*, **32**, 823-827.

Tonnesen G. and B. Wang. 2004. CMAQ Tagged Species Source Apportionment, July 22, 2004; http://www.wrapair.org/forums/aoh/meetings/040722/UCR_tssa_tracer_v2.ppt.

van Loon, L., E. Mader and S.L. Scott. 2000. Reduction of the aqueous mercuric ion by sulfite: UV spectrum of $HgSO_3$ and its intramolecular redox reactions. *J. Phys. Chem.*, **104**, 1621-1626.

van Loon, L.L., E.A. Mader and S.L. Scott. 2001. Sulfite stabilization and reduction of the aqueous mercuric ion: kinetic determination of sequential formation constants. *J. Phys. Chem.*, **105**, 3190-3195.

Warneck, P. 1989. *The Chemistry of the Natural Atmosphere*. Academic Press, New York, NY.

Wesely, M.L. 1989. Parameterization of Surface Resistances to Gaseous Dry Deposition in Regional-Scale Numerical Models. *Atmos. Environ.*, **23**, 1293-1304.

Whitten, G., H.P. Deuel, C.S. Burton, and J.L. Haney. 1996. Memorandum to OTAG Participants "Overview of the Implementation of an Updated Isoprene Chemistry Mechanism in CB4/UAM-V." (Revised Memorandum, July 22).

Yamartino, R. 2000. Refinement of Horizontal Diffusion in Photochemical Grid Models. Presented at the American Meteorological Society 11th Joint Conference on the Applications of Air Pollution Meteorology with the Air and Waste Management Association, Long Beach, CA, January 9-13.

Yang, Y.J., J.G. Wilkinson and A.G. Russell, 1997: Fast direct sensitivity analysis of multidimensional photochemical models, *Environ. Sci. Technol.*, **31**, 2859-2868.

Yarwood, G., R.E. Morris, M.A. Yocke, H. Hogo and T. Chico. 1996. Development of a Methodology for Source Apportionment of Ozone Concentration Estimates from a Photochemical Grid Model. Presented at the 89th AWMA Annual Meeting, Nashville TN, June 23-28.

Yarwood, G., T.E. Stoeckenius, G. Wilson, R.E. Morris, and M.A. Yocke. 1996. Development of a Methodology to Assess Geographic and Temporal Ozone Control Strategies for the South Coast Air Basin. Prepared for South Coast Air Quality Management District, Diamond Bar, CA.

Zaveri, R.A. and L. K Peters. 1999. A new lumped structure photochemical mechanism for large-scale applications. *J. Geophys. Res.*, **104**, 30: 387-30,415.